NASA CR-135073

NASA

HIGH-TEMPERATURE, LOW-CYCLE FATIGUE OF COPPER-BASE ALLOYS FOR ROCKET NOZZLES; PART II - STRAINRANGE PARTITIONING AND LOW-CYCLE FATIGUE RESULTS AT 538°C.

by: J.B.Conway, R.H. Stentz and J.T. Berling

MAR-TEST INC.

Cincinnati, Ohio

August, 1976

prepared for

NATIONAL AERONAUTICS AND SPACE ADMINISTRATION

NASA Lewis Research Center
Contract NAS3-19720
G.R.Halford, Project Manager

1. Report No.	2. Government Accession No.	3. Recipient's Catalog No.
NASA CR-135073		

4. Title and Subtitle	5. Report Date
High-Temperature, Low-Cycle Fatigue of Copper-Base Alloys for Rocket Nozzles; Part II - Strainrange Partitioning & Low-Cycle Fatigue Results at 538°C	August, 1976
	6. Performing Organization Code

7. Author(s)	8. Performing Organization Report No.
J.B. Conway, R.H. Stentz and J.T. Berling	MTI-RC84-3-2
	10. Work Unit No.

9. Performing Organization Name and Address	11. Contract or Grant No.
Mar-Test Inc. 45 Novner Drive Cincinnati, Ohio 45215	NAS3-19720

12. Sponsoring Agency Name and Address	13. Type of Report and Period Covered
National Aeronautics & Space Administration Lewis Research Center - 21000 Brookpark Rd. Cleveland, Ohio 44135	Contractor Report Nov.1975 through July,1976
	14. Sponsoring Agency Code

15. Supplementary Notes

Project Manager - Dr. G. Halford, NASA-Lewis Research Center, Cleveland, Ohio

16. Abstract

Low-cycle fatigue tests of ½ Hard AMZIRC Copper and NARloy Z were performed in argon at 538°C to determine partitioned strainrange versus life relationships for the strainrange components $\Delta\varepsilon_{cc}$, $\Delta\varepsilon_{cp}$ and $\Delta\varepsilon_{pc}$ over the range from about 1.0% to 4.0%. These relationships are shown to be quite effective in predicting fatigue life values for hold-time tests and for tests involving slow-fast and fast-slow cycling.

Strain-controlled low-cycle fatigue tests of a Zr-Cr-Mg copper-base alloy were performed at 538°C in argon using a frequency of 30 cpm. Strain ranges, lower than those employed in previous tests, were imposed in order to extend the fatigue life curve out to approximately 400,000 cycles.

Short-term tensile and low-cycle fatigue tests of an experimental copper alloy and an experimental silver alloy were performed to provide screening information for both compositions. Tensile tests were performed in air at room temperature and in argon at 538°C using a strain rate of 2×10^{-3} sec^{-1}. Strain-controlled low-cycle fatigue tests were performed at 538°C in argon to define the fatigue life over the regime from 300 to 3000 cycles. For the experimental silver alloy three additional heat treatments were introduced and a limited evaluation of the short-term tensile and low-cycle fatigue behavior at 538°C was performed.

17. Key Words (Suggested by Author(s))	18. Distribution Statement
Strainrange Partitioning, Fatigue, Creep-Fatigue, Tensile, Copper-Base Alloys, Silver-Base Alloy	Unclassified - Unlimited

19. Security Classif. (of this report)	20. Security Classif. (of this page)	21. No. of Pages	22. Price*
Unclassified	Unclassified		

For sale by the National Technical Information Service, Springfield, Virginia 22151

TABLE OF CONTENTS

		Page No.
I -	SUMMARY	1
II -	INTRODUCTION	2
III -	MATERIAL AND SPECIMENS	5
IV -	TEST RESULTS AND DISCUSSION OF RESULTS	
	Part I - Determination of Partitioned Strainrange Life Relationships for R-2 and R-24 Alloys	9
	Part II - Determination of High-Cycle Fatigue Behavior of R-9 Alloy	44
	Part III - Tensile and Low-Cycle Fatigue Evaluation of R-27 and R-28 Alloys	48
	Part IV - Short-Term Tensile and Low-Cycle Fatigue Behavior of R-30, R-31 and R-32 Alloys	55
	Part V - Plots of Load Range versus Cycles for Low-Cycle Fatigue Tests	59
	Part VI - Typical Hysteresis Loops for Low-Cycle Fatigue Tests	114
	Part VII - Values of N_5 and N_f for Low-Cycle Fatigue Tests of Section IV	148
V -	CONCLUSIONS	151
VI -	REFERENCES	153
VII -	DISTRIBUTION LIST FOR THIS REPORT	154

I - SUMMARY

This report describes the test results obtained in the Part II portion of this program which involved four different types of evaluations. These were as follows:

1. Determination of Partitioned Strainrange versus Life Relationships for AMZIRC (½ Hard) and NARloy Z at 538°C (R-2 and R-24)

2. Determination of High-Cycle Fatigue Behavior of Zr-Cr-Mg Copper-Base Alloy at 538°C (R-9)

3. Tensile and Low-Cycle Fatigue Evaluation of an Experimental Copper-Base Alloy and an Experimental Silver-Base Alloy at Room Temperature and at 538°C (R-27 and R-28)

4. An Evaluation of the Effect of Different Heat Treatments on the Tensile and Low-Cycle Fatigue Behavior of an Experimental Silver Alloy at 538°C (R-30, R-31 and R-32).

In the determination of the partitioned strainrange versus life relationships for both the R-2 and R-24 compositions some difficulty was encountered in the identification of the pure $\Delta\varepsilon_{pp}$ component of strain. At the test temperature and stress levels involved, very high creep rates were exhibited by these materials and it was found that experimental limitations on the available extensometry made it impossible to employ high enough cyclic rates to completely eliminate a creep component of inelastic strain. This complication, in turn, precluded a direct calculation of the $\Delta\varepsilon_{cc}$ component of inelastic strain by the usual method of partitioning a hysteresis loop to separate out the PP component. As a result, it was found necessary to analyze the fatigue life results at various strain rates and estimate the saturation limits in the low and high strain rate regimes. This analysis furnished N_{pp} and N_{cc} values along with corresponding $\Delta\varepsilon_{pp}$ and $\Delta\varepsilon_{cc}$ information. Then, slow-fast and fast-slow cycling was performed at several strain-ranges to provide the necessary information to allow the N_{cp}-$\Delta\varepsilon_{cp}$ and N_{pc}-$\Delta\varepsilon_{pc}$ relationships to be determined.

Tests of the R-9 alloy were performed in argon at 538°C to extend the previously measured fatigue curve for this material into the cyclic regime beyond 100,000 cycles. A cyclic frequency of 30 cpm was employed and strain-ranges from 0.8% to 0.3% were selected to enable the fatigue behavior to be defined out to approximately 400,000 cycles. These results were found to yield a fairly smooth extension of the fatigue curve established in the previous tests in the higher strain ranges.

An experimental copper alloy (R-27) and an experimental silver alloy (R-28) were evaluated. Short-term tensile tests were performed in duplicate at room temperature in air and at 538°C in argon. Low-cycle fatigue tests were performed at 538°C in argon to define the fatigue life over the range from 300 to 3000 cycles. Data for both materials are compared with previously reported results for electroformed copper and pure silver.

Three different heat treatments were applied to the R-28 (experimental silver alloy) material to yield the R-30, R-31 and R-32 alloy designations. A limited evaluation was made of the effect of these heat treatments on the tensile and fatigue behavior at 538°C in argon.

II - INTRODUCTION

Regeneratively-cooled, reusable-rocket nozzle liners such as found in the engines of the Space Shuttle, Orbit-to-Orbit Shuttle, Space Tug, etc., undergo a severe thermal strain cycle during each firing. To withstand the severe cycles, the liner material must have a proper combination of high thermal conductivity and high low-cycle fatigue resistance. Copper-base alloys possess these desirable qualities and for this reason a broad-based NASA-Lewis/Mar-Test program was initiated in 1972 to evaluate several candidate alloys by generating the material property data that are required for the design and life prediction of rocket nozzle liners.

This report deals with a portion of the overall program that focused on providing a more detailed evaluation of three copper-base alloys studied previously and a limited evaluation of two new experimental alloys. The materials investigated in this portion of the program were as follows: AMZIRC (½ Hard), R-2; NARloy Z, R-24; Zr-Cr-Mg Copper, R-9; experimenta. copper alloy, R-27; and experimental silver alloy,R-28. Specimen blank material was supplied by NASA-Lewis Research Center and the responsibility was assigned to Mar-Test Inc. for having the desired number and type of test specimens machined.

The material evaluations specified for this Task II effort were as follows:

1. Conduct strain-controlled, low-cycle fatigue tests in high-purity argon at 538°C to determine partitioned strainrange versus life relationships for the R-2 and R-24 compositions.

2. Determine the high-cycle fatigue behavior of the R-9 alloy at 538°C in high-purity argon using a frequency of 30 cpm and strain ranges of 0.8% and lower to define the fatigue life out to approximately 400,000 cycles.

3. Study the tensile and low-cycle fatigue behavior of the R-27 and the R-28 compositions; perform tensile tests in air at room temperature and in argon at 538°C using a strain rate of 2×10^{-3} sec^{-1}; also, perform low-cycle fatigue tests at 538°C in argon at a strain rate of 2×10^{-3} sec^{-1} to define the cyclic life over the range from 300 to 3000 cycles.

4. Perform a limited evaluation of the tensile and low-cycle fatigue behavior of three different heat treatments of the R-28 alloy; tests to be performed at 538°C in argon using a strain rate of 2×10^{-3} sec^{-1}.

All the tensile and fatigue tests were performed using hourglass-shaped specimens. A servo-controlled, hydraulically actuated fatigue testing machine (see NASA CR-134627 for complete description) was used in

all these evaluations and the threaded test specimens were mounted in the holding fixtures of the test machine using special threaded adaptors. Elevated temperature tests were performed in high-purity (guaranteed 99.999% purity) argon gas with 3000 ppm of hydrogen added to provide a slightly reducing environment for additional protection of the specimens. In order to perform these tests in this argon environment (oxygen content less than 0.01 percent by volume) a cylindrical containment vessel made of pyrex was positioned between the holding fixtures of the fatigue machine and neoprene low-force bellows at either end provided the seal to enable the desired gas purity levels to be maintained throughout the test. Side outlets (with appropriate seals) on this containment vessel provided entrance ports to accommodate the extensometer arms and similar side outlets provided entrance ports for the copper tubing leads to the induction coil. In addition, special ports near the bottom of the containment vessel enabled the thermocouples, used for specimen temperature measurement, to be routed out to the temperature control system. Specimen test temperatures were attained using induction heating and this was provided by positioning a specially designed induction coil around the test specimen (see Figure 1).

All force measurements were made using a load cell mounted within the loading train of the fatigue machine and specimen strains were measured by using a high temperature diametral extensometer. A test procedure, developed previously (see NASA CR-134627) was used to allow the short-term tensile tests to be performed at a constant strain rate which was maintained throughout the test. In the fatigue tests an analog strain computer was employed which allowed the diametral strain signal to be used in conjunction with the load signal so as to provide an instantaneous value for the axial strain which was then the controlled variable (see NASA CR-134627 for complete description of test procedure).

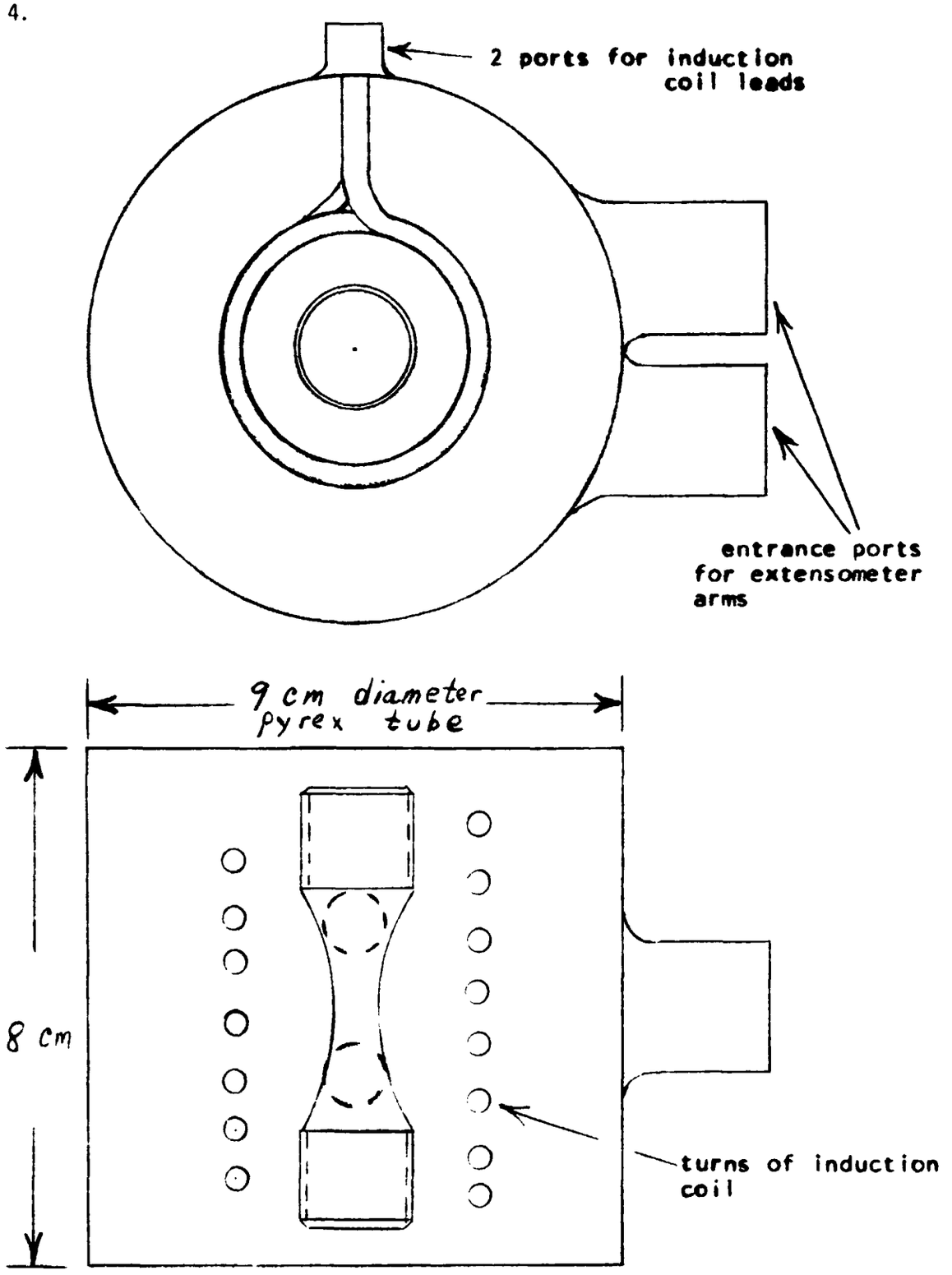

Figure 1 - Schematic of Pyrex Environmental Chamber

III - MATERIAL AND SPECIMENS

Specimen material for use in this portion of the program was supplied by NASA-Lewis Research Center, Cleveland, Ohio. A brief description of the five materials evaluated within this effort is given in Table 1. Using the specimen design shown in Figure 2 the following specimens were machined:

R-2	16 specimens (includes 2 spares)
R-24	18 specimens (includes 2 spares)
R-27	12 specimens (includes 2 spares)
R-28	12 specimens (includes 2 spares)
R-9	8 specimens (includes 1 spare)
R-30	3 specimens
R-31	3 specimens
R-32	3 specimens

In addition, several spare specimens of the R-24 alloy that were machined in conjunction with a previous program were on hand and were used in the present testing effort.

After being machined, all specimens were wrapped in soft tissue paper and placed in individual hard plastic cylinders (about 9 cm in length and 2.2 cm inside diameter). The ends of these cylinders were then sealed with masking tape and the specimen code number was written on the external surface of the cylinder. These cylinders were used for storage before and after test.

In preparing for a test, each specimen was subjected to the following:

1) the specimen was washed with Freon to remove any surface oils which might have remained after machining;
2) a small quantity of dilute phosphoric acid was applied by hand to the complete surface of the specimen; this removed any surface oxides and any machining oil not removed by the cleaning with Freon; this operation was completed within 15 seconds;
3) the specimen was rinsed in warm water and dried using soft absorbent tissue;
4) the specimen was then subjected to a final cleaning with Freon.

Table 1 - Description of the Materials Evaluated in this Effort

Code No.	Material	Description
R-2	AMZIRC Copper, ½ Hard	Billet size of 20.3 cm diameter by 63.5 cm (8" x 25") in length; extrusion temperature of 960°C; extruded to 2.7 cm (1.06") diameter rod and water quenched after extrusion; drawn to 50% hard in two passes to 2.2 cm (0.87") and then 1.9 cm (0.75") diameter; stress relief by springing; aged at 420°C in cracked natural gas atmosphere and then straightened and cut to 91 cm (36") lengths.
R-24	NARloy Z	A copper-base alloy developed by North American Rockwell and was furnished in centrifugally cast form and had been hot-rolled, solution annealed and aged. Material was furnished in the form of a rectangular bar, 23.2 cm long x 5.1 cm x 4.1 cm (9.12" x 2" x 1.6").
R-9	Zr-Cr-Mg Copper	Billet size of 20.3 cm diameter by 63.5 cm (8" x 25") in length supplied to NASA by United States Metals Refining Co.; extruded to 3.2 cm (1.25") diameter; solution heat treated at 1006°C (1850°F) in neutral (barium chloride) salt and quenched in water, cold drawn to 2.12 cm (0.837") diameter, aged at 482°C (900°F) for 2.5 hours and finish drawn to 1.9 cm (0.75") diameter.
R-27	Experimental Copper Alloy	Electroformed copper cylinder (copper sulfate solution) ; 23.6 cm long x 17.3 cm OD x 13 cm ID (9.3" x 6.8" x 5.1").

- continued -

Table 1 - Description of the Materials Evaluated in this Effort (continued)

Code No.	Material	Description
R-28	Experimental Silver Alloy	0.5 wt.% Zirconium (Reactor Grade) alloyed with fine silver; vacuum melted and cast; cold reduced to 2.86 cm (1.125") diameter bar; annealed and then cold reduced to 2.22 cm (0.875") diameter bars; final reduction corresponds to a 37% cold reduction in cross-sectional area, which can be considered as the ½ hard condition for this alloy
R-30	Heat-treated R-28	Aged R-28 at 482°C (900°F) for two hours by canning the material in stainless steel, sealing the can, then heating in an air furnace to desired temperature; air cooled
R-31	Heat-treated R-28	Solution annealed R-28, 899°C (1650°F) for one hour in salt bath; water quenched
R-32	Heat-treated R-28	Aged R-28 at 593°C (1100°F) for two hours; canned as above for R 30

Figure 2

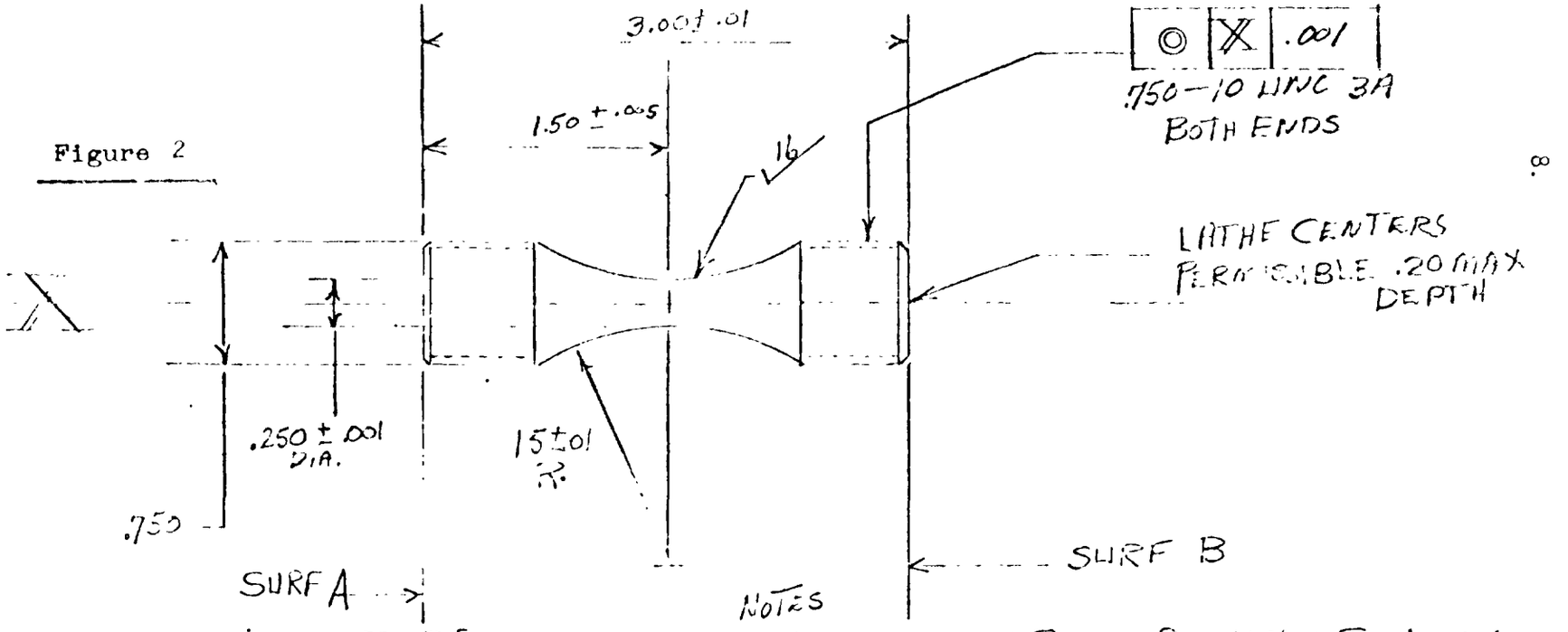

NOTES

1- SURFACES A, & B TO BE PARALLEL WITHIN .001
2- SURFACES A & B TO BE PERPENDICULAR TO CENTER LINE OF SPECIMEN WITHIN .000 5 TIR
3- CONTOURED PORTION OF SPECIMEN TO HAVE A 16 FINISH OR BETTER. FINISHING SHOULD BE IN THE AXIAL DIRECTION USING LOW STRESS LAPPING OR POLISHING OPERATION
4- ~~ALL DIA'S TO BE CONCENTRIC WITHIN .001 T.I.R.~~
5- SCREW THREADS TO BE AS LISTED IN NBS HAND BOOK H 28

UNLESS OTHERWISE SPECIFIED DIMENSIONS ARE IN INCHES TOLERANCES ON FRACTIONS ± DECIMALS ± ANGLES ± ALL SURFACES 32	DRAWN	SPECIMEN Low Cycle Fatigue	Mar-Test inc. CINCINNATI, OHIO
	DATE		
	APPD		
	ISSUED		
MATERIAL GOVT. OR COML To BE SPECIFIED	APPROVED ENGR SJC	DATE 4-12-71	SIZE MTI-1002
	MFG		
	MATL	SCALE 1/1 WT CALC ACTUAL	CONT ON SHEET SH NO.

IV - TEST RESULTS AND DISCUSSION OF RESULTS

PART I - DETERMINATION OF PARTITIONED STRAINRANGE LIFE RELATIONSHIPS FOR R-2 AND R-24 ALLOYS

Low-cycle fatigue data for these two alloys were reported previously in NASA CR-121259,-121260,-121261 and -134627. In order to extend the range of the available fatigue data for these two compositions, some additional tests were performed at 538°C (1000°F) in high-purity argon with the objective of determining partitioned strainrange versus life relationships.

In initiating the evaluations of the R-2 and R-24 materials, two continuous cycling fatigue tests were performed using conditions (in argon at 538°C and a strain rate of 2×10^{-3} sec^{-1}) identical to those used in some of the previously reported tests. The results of these tests are summarized in Table 2 and (see below) served to establish that the fatigue characteristics for the materials involved in the present program were comparable to those previously determined for these same compositions at the same test conditions. It was important to establish this material similarity since a lot of the previously reported results had to be used in identifying the partitioned strainranges in the current program.

A summary of the previously reported continuous cycling fatigue results obtained at a strain rate of 2×10^{-3} sec^{-1} for the R-2 and R-24 alloys is presented in terms of total and inelastic strainrange in Figures 3 through 6. Also shown in these plots are the two data points referred to above. These comparisons are seen to identify material behavior that is very similar to that previously reported. In making these comparisons it was also noted, based on a study of hysteresis loops, that a significant creep component was always present in the inelastic strainrange of all the continuous cycling tests.

R-2 ALLOY

In planning the first few tests to evaluate partitioned strainranges, the CC type of cycle (References 1 and 2) was employed. As shown in Figure 7, this involves the rapid application (in load control) of a tensile stress along AB and a hold at this stress level until a preset amount of inelastic strain is accumulated along BC. When the desired inelastic strain limit is reached, the direction of the stress is rapidly reversed along CD and a constant compressive stress level is maintained until a preset inelastic strain limit is reached along DA. At point A, the tensile stress is rapidly reapplied along AB to repeat the cycle.

One of the experimental difficulties associated with the use of the CC type of cycle with the R-2 material involved the extensive amount of cyclic softening that was exhibited (see NASA CR-134908). In the first cycle, for example, a tensile stress lev was imposed to provide a reasonable time period for the accumulation o the preset inelastic strain limit. However, the very extensive strain softening that occurred during this portion of the cycle, along with the Bauschinger effect, caused the material to strain very rapidly as the load was being reversed. As a matter of fact, the strain

Table 2 - Low-Cycle Fatigue Test Results Obtained in Argon at 538°C
Using a Strain Rate of 2×10^{-3} sec^{-1}

R-2 Series
AMZIRC Copper,
½ Hard

and

R-24 Series
NARloy Z Alloy
(cent. cast, hot-rolled,
solution annealed and aged)

Axial Strain Control
A-ratio of infinity

Spec. No.	Poisson's Ratio	Total Strain Range, %	Freq. cpm	Stress Range at Start, MN/m^2	at $N_f/2$			N_f, Cycles to Failure	Remarks
					$\Delta\varepsilon_{inel.}$ %	$\Delta\varepsilon_e$ %	$\Delta\sigma$ MN/m^2		
				R-2 alloy; E = 80.7 x 10^3 MN/m^2					
R-2-107	0.35	1.7	3.5	344.0	1.56	0.14	113.7	5760*	Softened
R-2-108	0.35	3.0	2.0	323.0	2.86	0.14	115.9	1310	Softened
				R-24 alloy; E = 98.6 x 10^3 MN/m^2					
R-24-101	0.35	1.0	6.0	259.5	0.75	0.25	242.9	1948	Slight initial hardening
R-24-102	0.35	2.0	3.0	284.4	1.72	0.28	277.3	535	followed by softening

* Excessive barrelling of specimen caused termination of test.

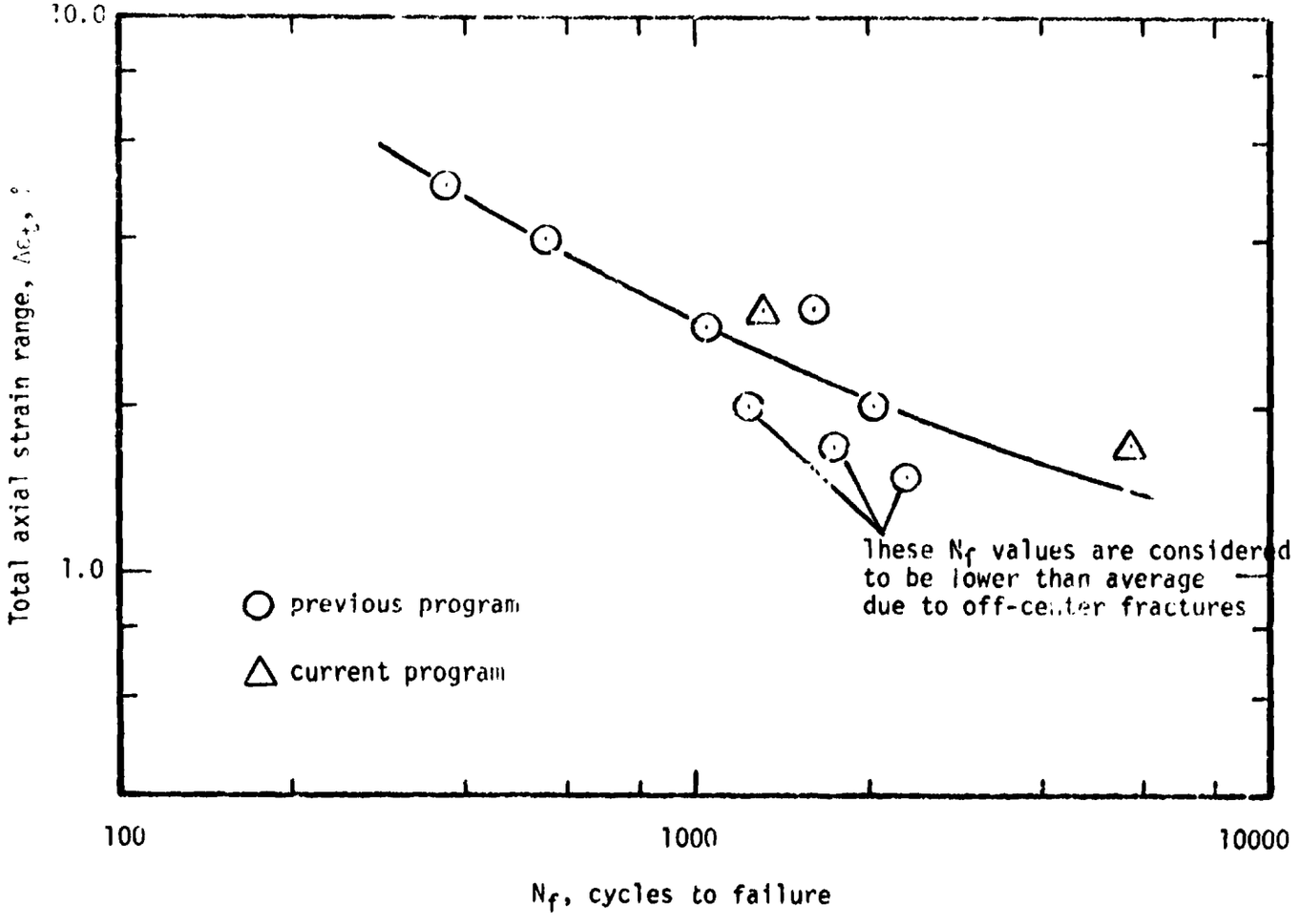

Figure 3 - Low-cycle fatigue life as a function of total axial strain range for R-2 alloy at 538°C in argon and a strain rate of 2×10^{-3} sec^{-1}

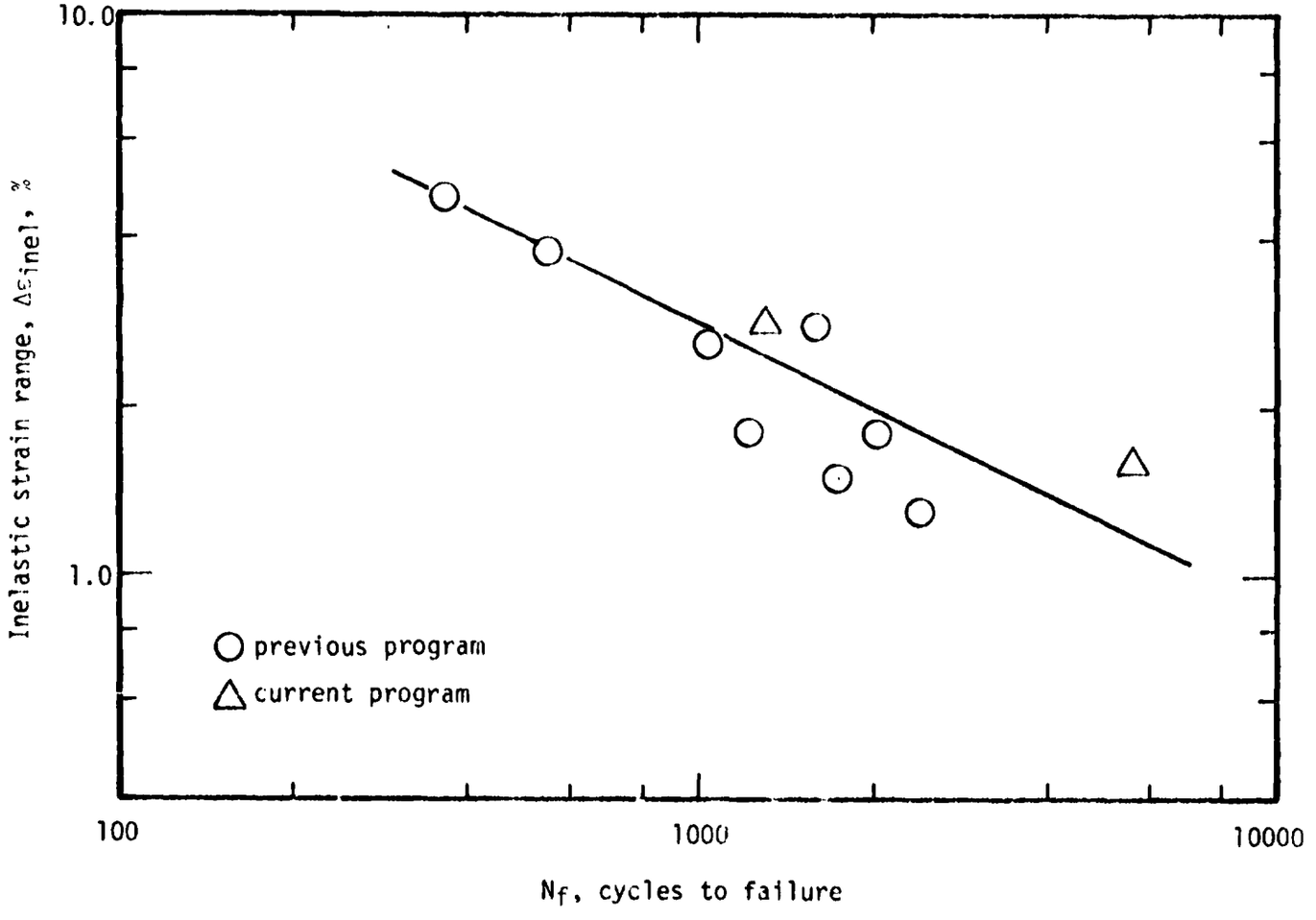

Figure 4 - Low-cycle fatigue life as a function of inelastic strain range for R-2 alloy at 538°C in argon and a strain rate of 2×10^{-3} sec^{-1}

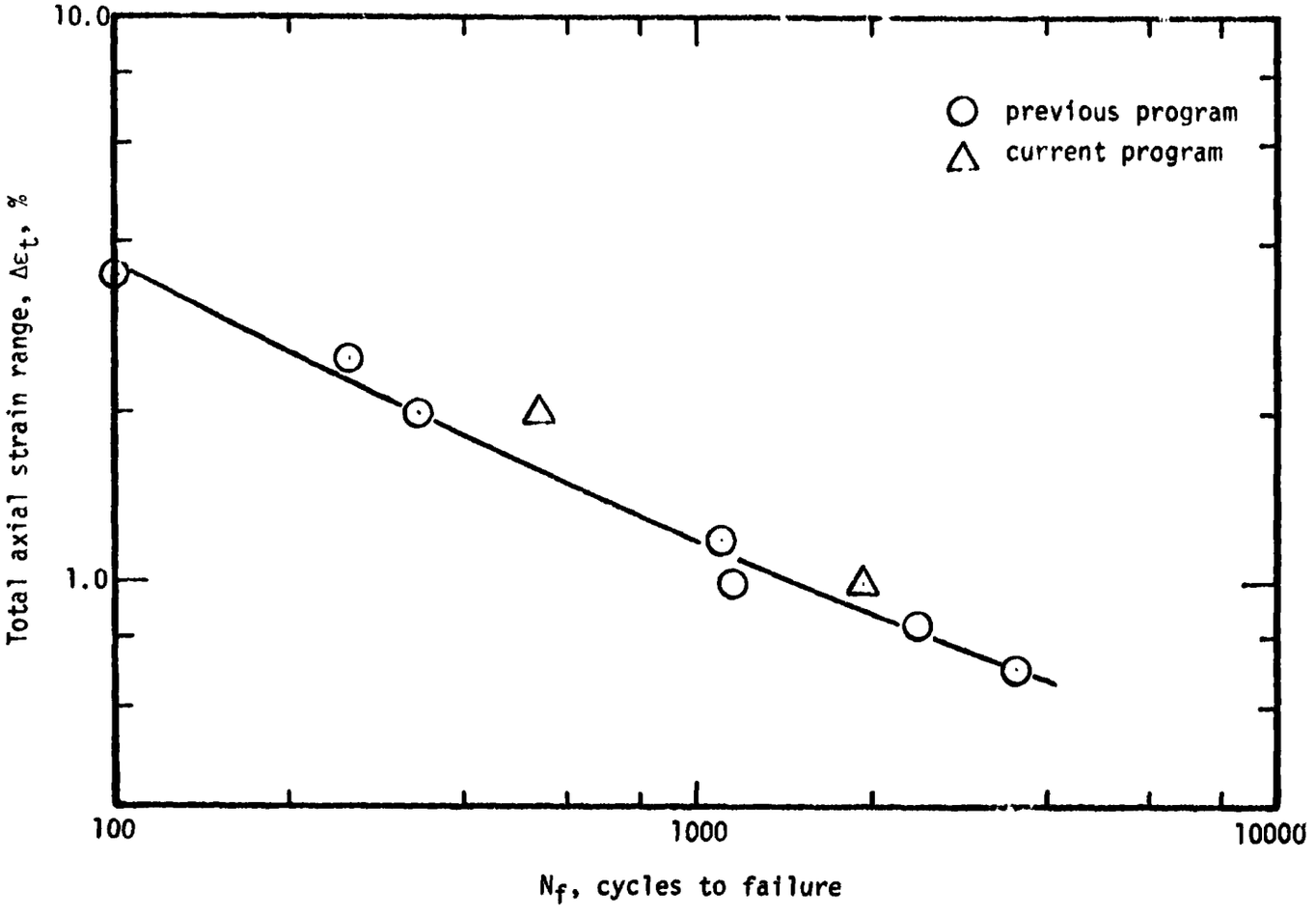

Figure 5 - Low-cycle fatigue life as a function of total axial strain range for R-24 alloy at 538°C in argon and a strain rate of 2×10^{-3} sec^{-1}

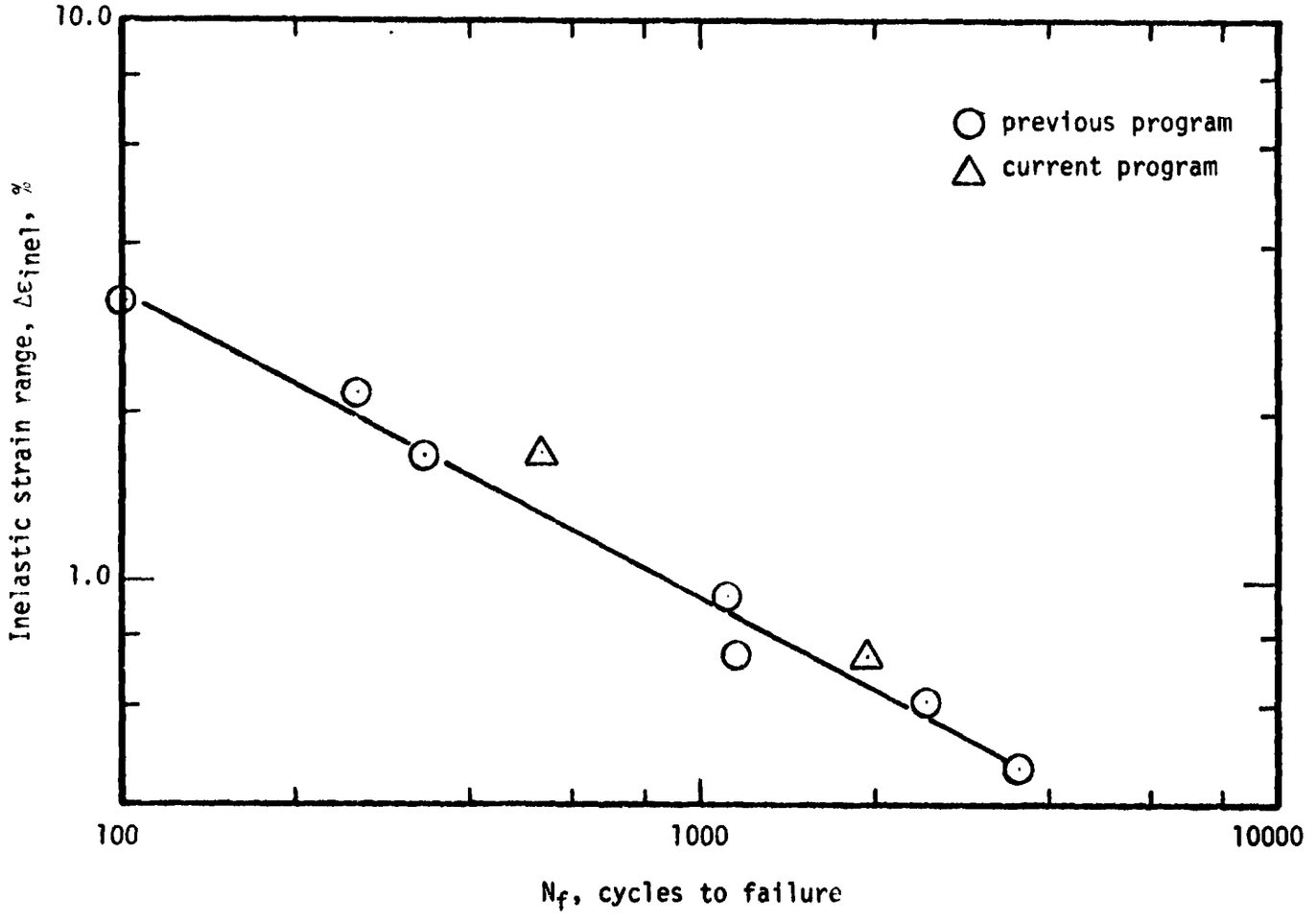

Figure 6 - Low-cycle fatigue life as a function of inelastic strain range for R-24 alloy at 538°C in argon and a strain rate of 2×10^{-3} sec^{-1}

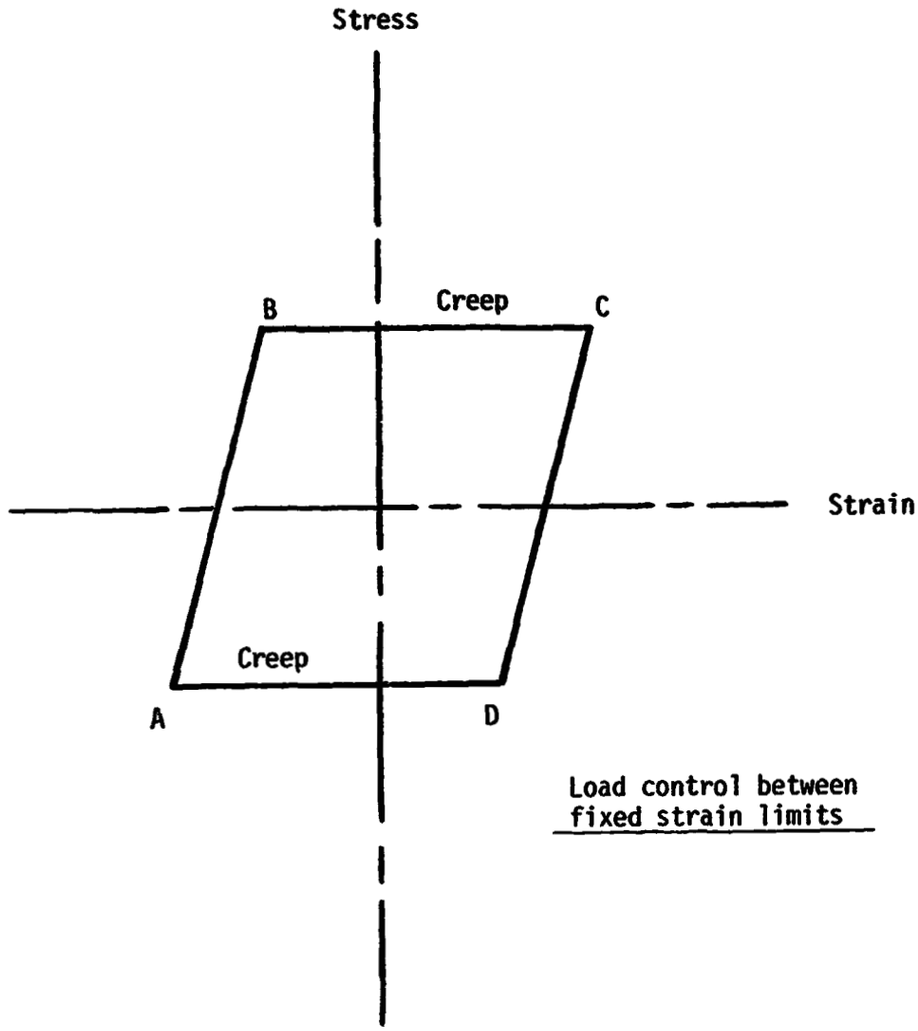

Figure 7 - Idealized CC Type Cycle (Ref. 1)

rates involved were so high that the extensometer readout always lagged the instantaneous strain value and, as a result, the compressive strain limit would be exceeded even before the desired stress level was attained. Because of this problem, it was decided to begin the test in strain control and subject the material to something less than 100 completely reversed strain cycles (always less than 10% of the fatigue life corresponding to the strainrange employed). A strainrange was imposed that was close to that corresponding to the actual inelastic strainrange to be employed in the CC type cycle and the number of strain cycles applied was sufficient to encompass the initial period during which extensive cyclic strain softening was exhibited. This approach proved to be very effective in that the subsequent material response was fairly stable and the CC type cycling in load control between fixed strain limits could be initiated quite easily and complete control of the initial loadings was achieved.

A summary of the results obtained in the CC type of testing is presented in Table 3. These data are shown graphically in Figure 8 in a comparison with the continuous cycling data reported previously for this alloy. It is seen that in terms of inelastic strainrange the CC type of cycling gave essentially the same behavior as that observed in strain-controlled fatigue tests. This supports the contention expressed above that the inelastic strainrange data established in a previous program contain a substantial creep component. It is not possible, therefore, to employ the continuous cycling data in Figure 4 as PP type information. In view of this fact, it is not possible to partition the loops obtained in the tests of Table 3 to yield the CC strainrange.

In order to establish a PP strainrange versus life relationship for the R-2 material a study was made of all previously reported strain rate data for this alloy. A summary of these data is presented in Figure 9 and some slight tendency toward a saturation fatigue life in both the low and high strain rate regimes is suggested in accordance with previously reported observations (See Ref. 2 and 3). Some thought was given to the performance of some additional tests at these strainranges to provide a more accurate determination of these saturation limits, but it was decided that this was not practical. The response characteristics of the extensometer used in these tests are such that the highest strain rate (5×10^{-2} sec^{-1}), used in the generation of the data in Figure 9, is considered to be the upper limit for these types of strain-controlled evaluations. Another problem was envisioned in this consideration to extend the range of data for this alloy. In the lower strain rate regime the long test durations involved lead to severe barrelling of the specimen. These limitations led to the conclusion that a reasonable estimate of the two saturation limits could best be obtained by using some judgement in extending the curve that was defined by the existing data points. Such an extension is shown in Figure 9. Then, in accordance with the strainrange partitioning concept (1,2)*the saturation values for fatigue life in the low and high strain rate regimes were considered to be N_{cc} and N_{pp} respectively. Corresponding values of $\Delta\varepsilon_{cc}$ and $\Delta\varepsilon_{pp}$ were not directly obtainable since, for a given strainrange, the inelastic strainrange changed slightly in going from the low to the high strain rate regime.

*Numbers in parentheses apply to references in Section VI.

Table 3 - Load Control Testing Between Fixed Strain Limits at 538°C in Argon

R-2 Series
AMZIRC Copper,
½ Hard

Load Control;
essentially completely
reversed

Specimen Number	Ramp Stress Rate, $MN/m^2/sec.$	Tensile Force, newtons	Compressive Force, newtons	Inelastic Strain Limits, %		N_f, cycles	Remarks
				Tension	Compression		
R-2-104	99.7	1535	1624	1.0	1.0	603	Extensive barrelling caused extensometer to move from the min.diameter point and specimen was pulled to failure leading to low N_f value.
R-2-105	100.0	1612	1557	1.5	1.5	1031	
R-2-106	99.7	1579	1579	2.0	2.0	450	

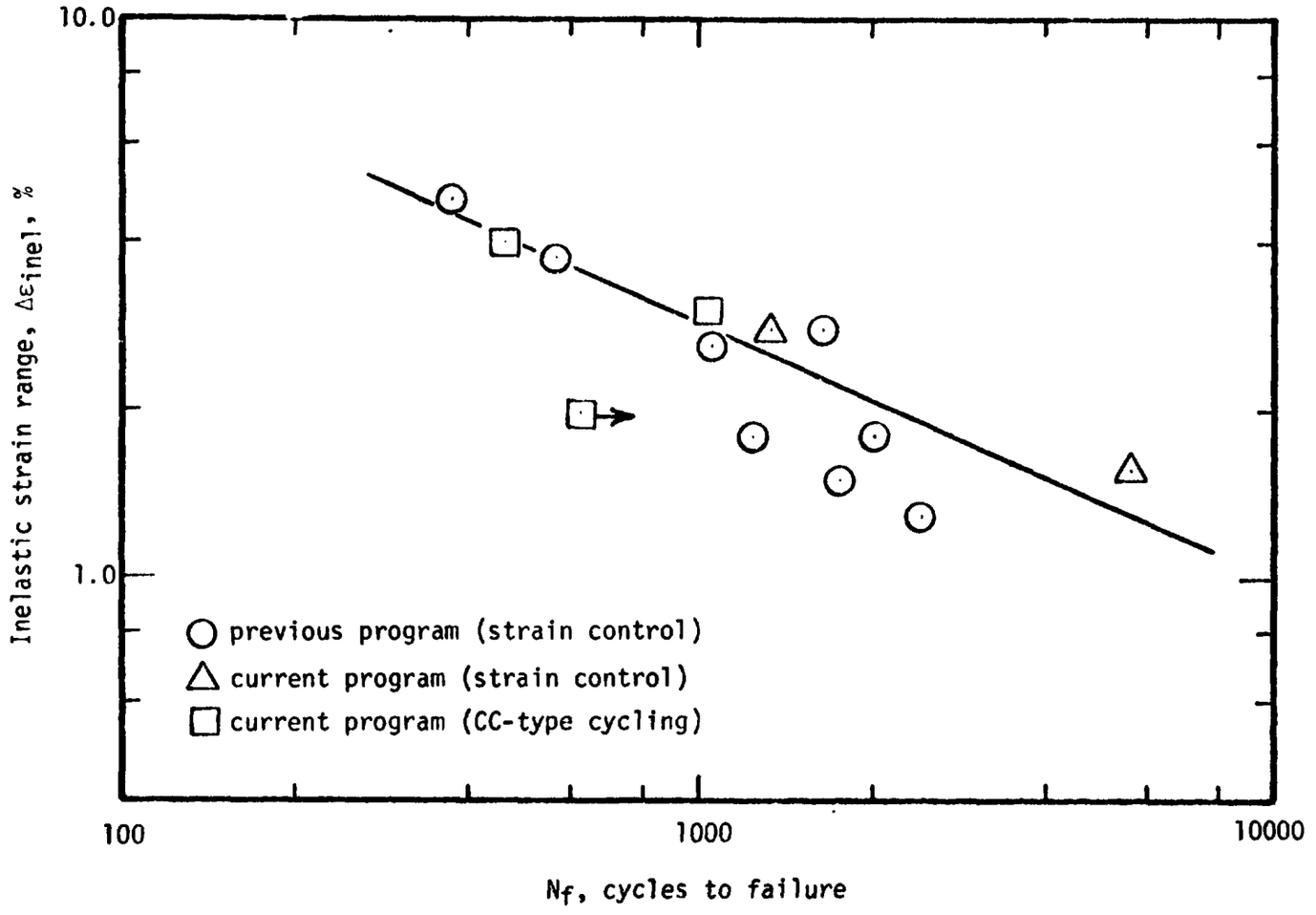

Figure 8 - Comparison of strain-controlled with CC-type results for R-2 alloy tested in argon at 538°C

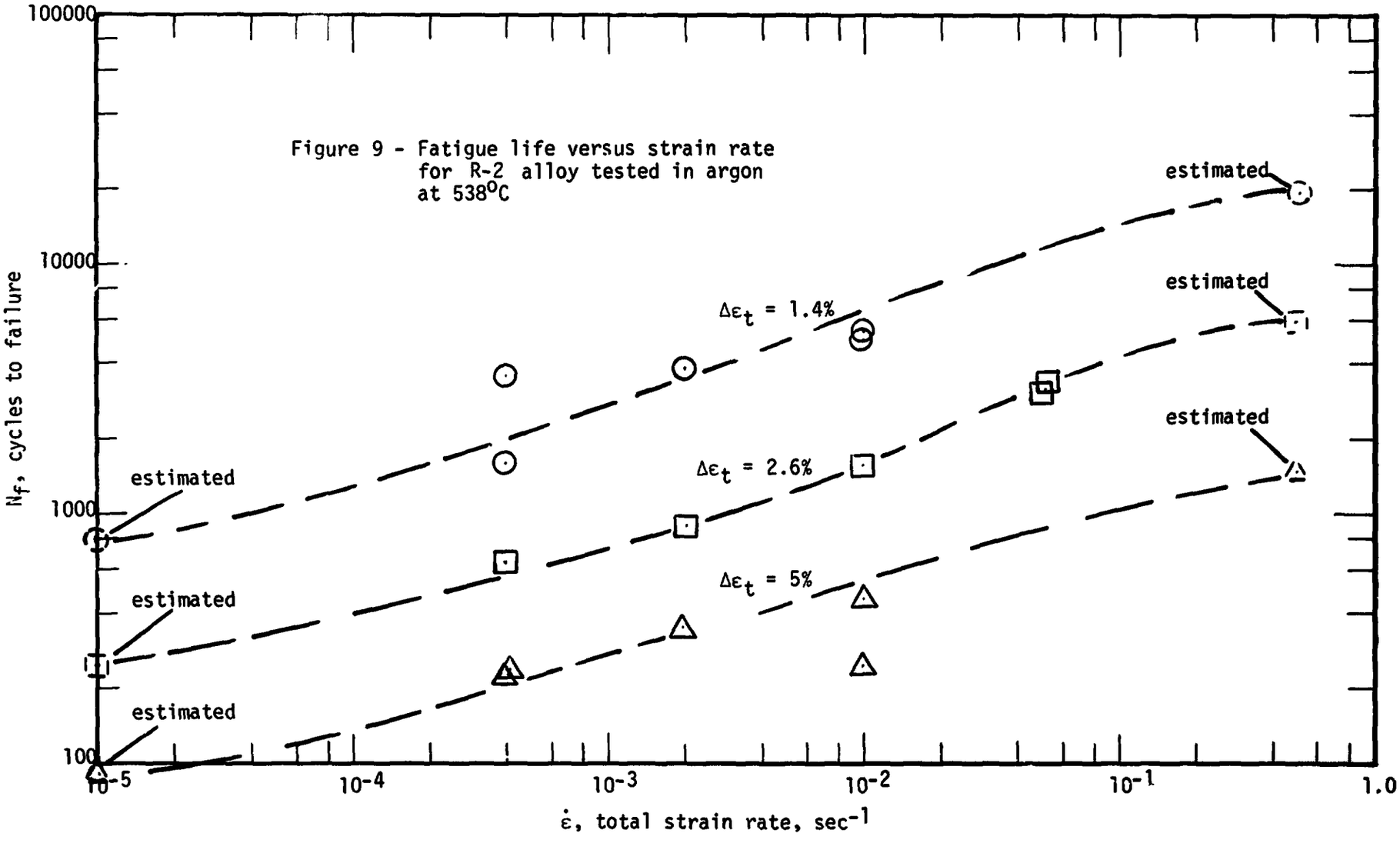

Figure 9 - Fatigue life versus strain rate for R-2 alloy tested in argon at 538°C

Rather then estimate these values or pick some average value, it was decided to select the value of the total strainrange for the values of $\Delta\varepsilon_{cc}$ and $\Delta\varepsilon_{pp}$ in preparing the strainrange partitioning plots. These results were then used to position the PP and CC lines for the R-2 alloy as shown in Figure 10.

Slow-fast and fast-slow strain cycling, in accordance with the strain profiles shown in Figure 11, was employed to establish the CP and PC partitioned strainrange versus life relationships. During the slow straining portion of the cycles a strain rate of 4×10^{-4} sec^{-1} was employed while a strain rate of 1×10^{-2} sec^{-1} was used during fast straining. A summary of the results obtained in these tests is presented in Table 4 to indicate that the slow-fast cycling is much more detrimental than the fast-slow cycling. In addition, it can be noted that a mean compressive stress develops during slow-fast cycling while a mean tensile stress is seen to exist in the fast-slow cycle.

In order to partition the strainranges involved in the slow-fast and fast-slow cycling, the creep and plastic strain components in each half cycle had to be determined. This was accomplished using Figure 9. For a given strainrange, the saturation values for N_f were noted and used for N_{pp} and N_{cc} in the Interaction Damage Rule (2):

$$\frac{F_{pp}}{N_{pp}} + \frac{F_{cc}}{N_{cc}} = \frac{1}{N_f} \qquad (1)$$

$$\frac{F_{pp}}{N_{pp}} + \frac{(1-F_{pp})}{N_{cc}} = \frac{1}{N_f} \qquad (2)$$

Then for each strain rate involved (4×10^{-4} sec^{-1} and 1×10^{-2} sec^{-1}) the N_f value was obtained from Figure 9 and used to solve equation (2) for the corresponding F_{pp} and F_{cc} fractions for the continuous cycling tests. These fractions, for the individual strain rates, were then assumed to apply within the appropriate half-cycle of the slow-fast and fast-slow tests. For example, at a strainrange of 2.6% and a strain rate of 1×10^{-2} sec^{-1} the N_f value from Figure 9 for continuous cycling is 1600. This, together with N_{pp}=6000 and N_{cc}=250, yields F_{pp}=0.88 and F_{cc}=0.12. Similar values for F_{pp} and F_{cc} at a strain rate of 4×10^{-4} sec^{-1} are 0.61 and 0.39. Applying these results to the test of R-2-109 from Table 4, and dealing in terms of total strainrange, since this was the basis for Figures 9 and 10, gives:

$$\Delta\varepsilon_{inelastic} = 2.60\%$$

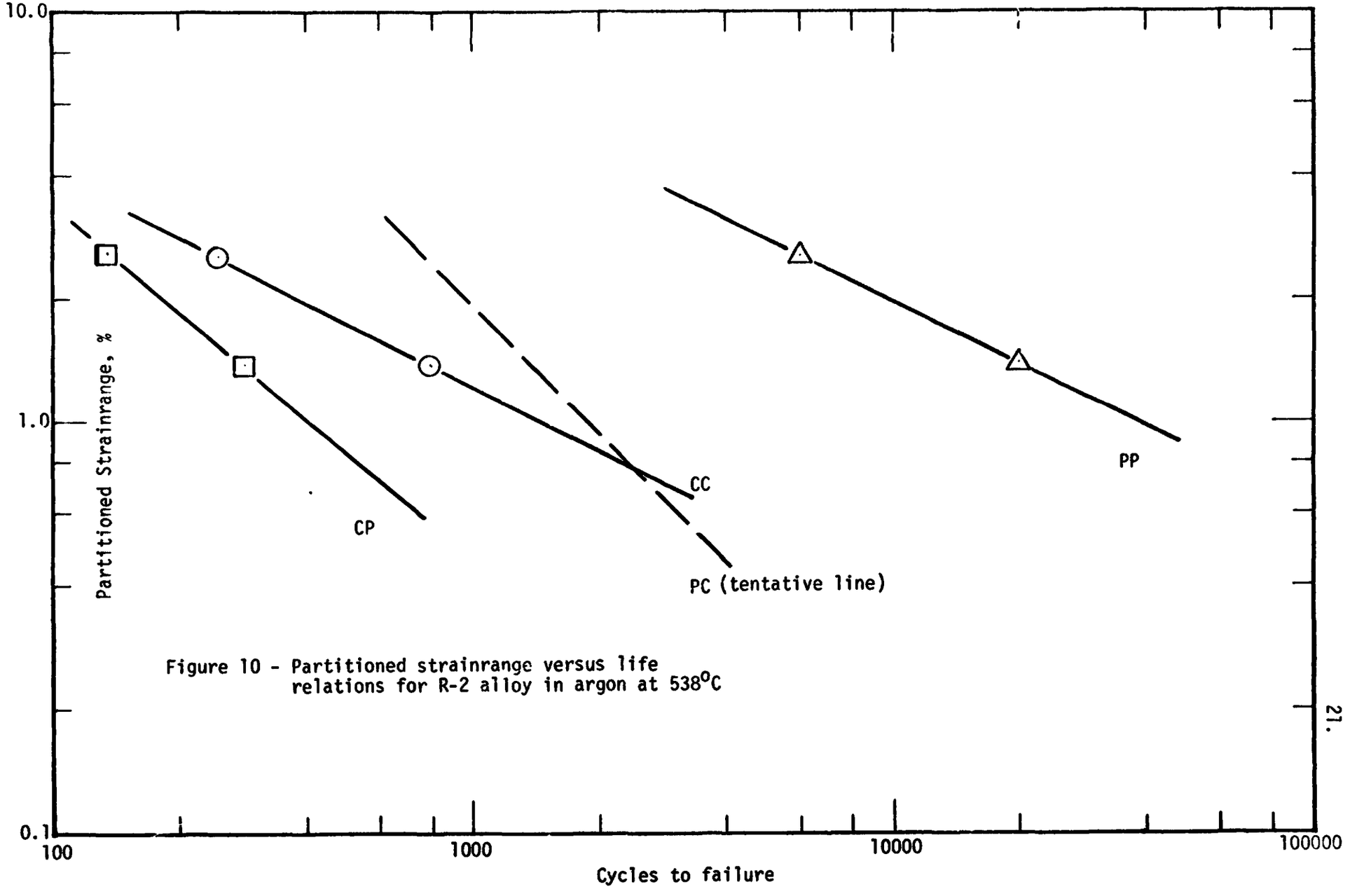

Figure 10 - Partitioned strainrange versus life relations for R-2 alloy in argon at 538°C

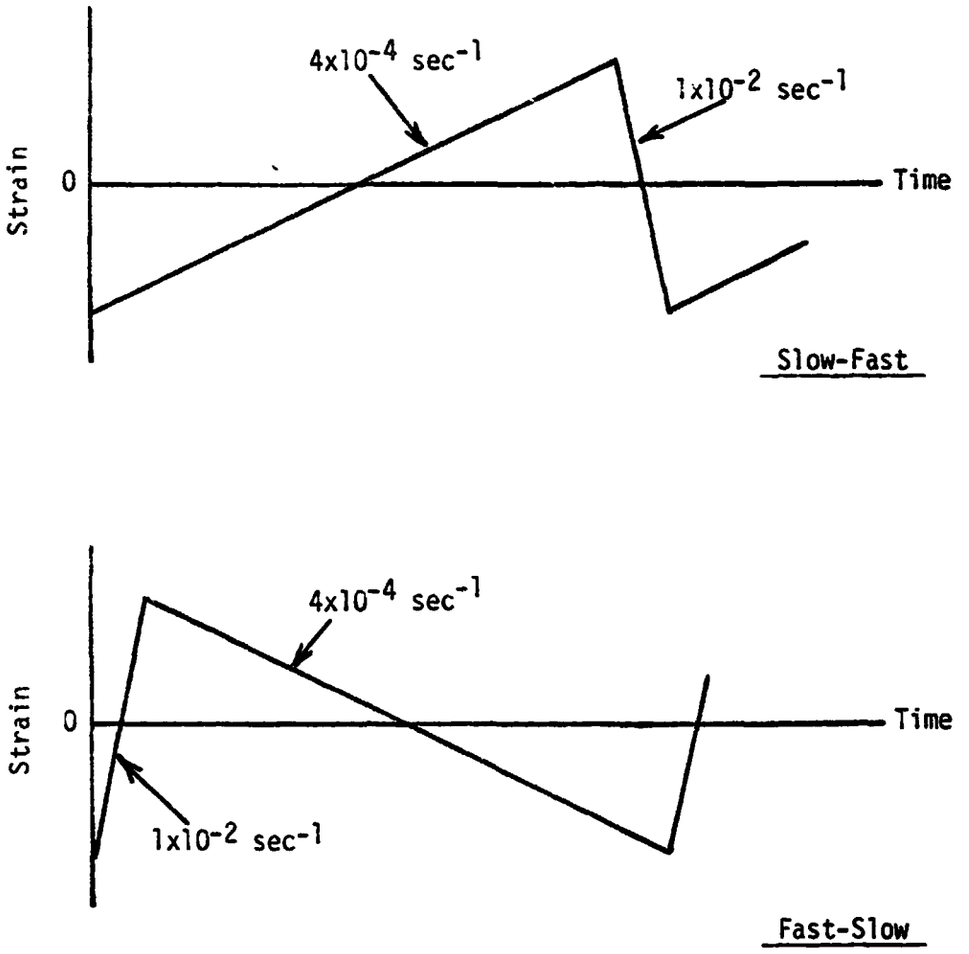

Figure 11 - Strain profiles for slow-fast and fast-slow cycling using $4x10^{-4}$ sec^{-1} and $1x10^{-2}$ sec^{-1}

Table 4 - Low-Cycle Fatigue Test Results Obtained in Argon at 538°C
Using Fast-Slow and Slow-Fast Cycling

R-2 Series
AMZIRC Copper,
½ Hard

Axial Strain Control
A-ratio of infinity
$E = 8.07 \times 10^4$ MN/m^2

Spec. No.	Poisson's Ratio	Total Strain Range, %	Time(1) for t/c half of cycle, sec.	Stress Range at Start, MN/m^2	at $N_f/2$			N_f, Cycles to Failure	Remarks
					$\Delta\varepsilon_{inel.}$ %	$\Delta\varepsilon_e$ %	$\Delta\sigma$(2) MN/m^2		
		1×10^{-2} sec^{-1} in tension and 4×10^{-4} sec^{-1} in compression							Softened; severe barrelling caused instability at extensometer contact point
R-2-111	0.333	2.6	2.6/65	369	2.45(3)	0.15(3)	118(3) (63.2/54.8)	1314(4)	
R-2-112	0.333	1.4	1.4/35	379	1.26	0.14	113 (61.1/51.9)	3239	Softened; severe barrelling
		4×10^{-4} sec^{-1} in tension and 1×10^{-2} sec^{-1} in compression							
R-2-109	0.333	2.6	65/2.6	367	2.43	0.17	133.4 (56.9/76.5)	387	Softened
R-2-110	0.333	1.4	35/1.4	374	1.24	0.16	126.4 (56.9/69.5)	1006	Softened

(1)-time for tension/compression going portion of cycle
(2)-(tensile stress/compressive stress)
(3)-at 650 cycles
(4)-test terminated; no failure

Slow cycling portion of cycle:

$$\Delta\varepsilon_p = 1.59\%$$

$$\Delta\varepsilon_c = 1.01\%$$

Fast cycling portion of cycle:

$$\Delta\varepsilon_p = 2.29\%$$

$$\Delta\varepsilon_c = 0.31\%$$

Then for the overall portion of the cycle:

$$\Delta\varepsilon_{p,} = 1.59\%$$

$$\Delta\varepsilon_{cc} = 0.31\%$$

$$\Delta\varepsilon_{cp} = 0.70\%$$

These data enable F_{pp}, F_{cc} and F_{cp} to be calculated and using N_f=387 for this test, the Interaction Damage Rule can be solved for N_{cp}; thus:

$$\frac{F_{pp}}{N_{pp}} + \frac{F_{cc}}{N_{cc}} + \frac{F_{cp}}{N_{cp}} = \frac{1}{387}$$

Simil.. alculations led to the determination of the N_{cp} and N_{pc} versus parti.. ed strainrange values as shown plotted in Figure 10.

..ause of the dimensional stability (barrelling) problem encountered with tne R-2 material, it was decided to limi.. the number of tests performed to define the partitioned strainrange versus life relationships over a broad range. For this reason, the life relationships shown in Figure 10 are probably not as precisely defined as they might be. However, they are considered reasonable and are capable to providing meaningful information. For example, these partitioned strainranges were used to estimate the N_f values for the hold-time tests of the R-2 material reported in NASA CR-121260. For hold periods in compression, the estimated N_f values were in good agreement with the measured values. However, for hold periods in tension the estimated results were approximately twice the measured values.

An interesting comparison of all the R-2 data generated to date is presented in Figure 12. The load control tests between strain limits, the fast-slow strain cycling and the compression hold-time results all yield

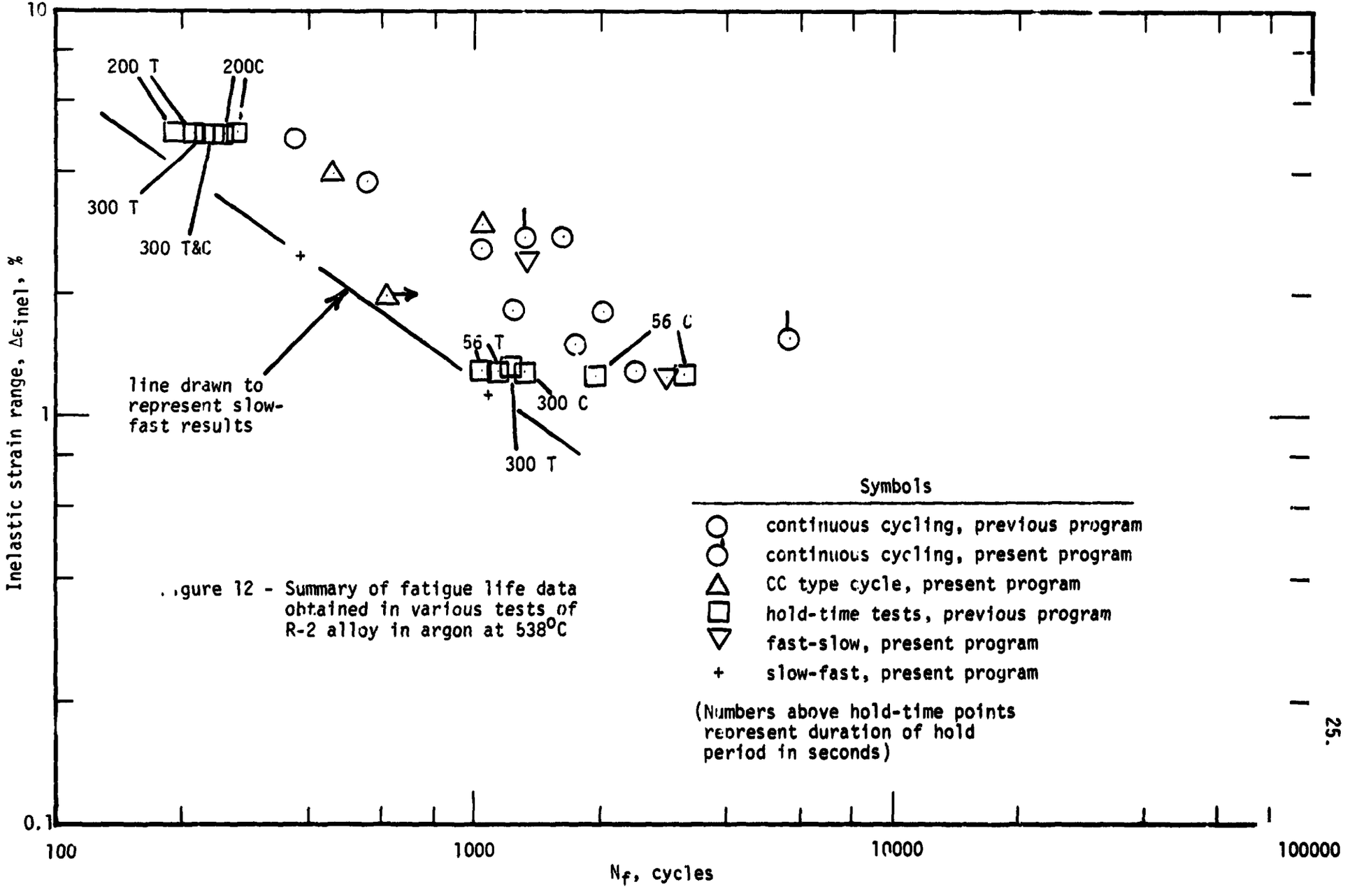

Figure 12 - Summary of fatigue life data obtained in various tests of R-2 alloy in argon at 538°C

N_f values that are close to the continuous cycling results. However, the detrimental effect of hold periods in tension is definitely noticeable, as is the even more detrimental effect of the slow-fast strain cycling. In connection with the slow-fast tests it is to be noted (see Table 4) that the tension-going times are 35 and 65 seconds for the 1.4% and 2.6% strainranges respectively. In other words, more damage is encountered in the slow-fast tests even though the tension-going times are much less than the hold-period durations in the tension hold-time tests. Admittedly, the difference in fatigue life is not large and some of it is probably due to a hold-time saturation effect in the hold-time evaluations. An interesting point here relates to whether or not a similar saturation effect exists as the tension-going strain rate is decreased in the slow-fast strain cycling tests.

R-24 ALLOY

An evaluation of this alloy was initiated by performing a study of strain rate effects. Strain rates of $4x10^{-5}$ sec^{-1}, $4x10^{-4}$ sec^{-1} and $1x10^{-2}$ sec^{-1} were employed to yield the results summarized in Table 5. These data are presented graphically in terms of total strainrange and inelastic strainrange in Figures 13 and 14 to indicate a very interesting effect. As the strainrange is increased at a strain rate of $1x10^{-2}$ sec^{-1} the fatigue life gradually comes closer and closer to that observed at a strain rate of $4x10^{-4}$ sec^{-1}. At a strainrange near 3.0% the fatigue life at a strain rate of $1x10^{-2}$ sec^{-1} is essentially identical to that observed at this same strainrange at the lower strain rate. This behavior pattern suggests that more and more of a creep effect is introduced at the higher strain rate as the strainrange is increased. This effect is supported by the fact that the stress range is increasing noticeably as the higher strainranges are imposed. For example, at the 3.0% strainrange the stress range (at half-life) is 325 MN/m^2 compared to 241 MN/m^2 at this same strainrange at the lower strain rate. So that even though the cycle time is much shorter at a strain rate of $1x10^{-2}$ sec^{-1}, the stress level attained is high enough to introduce substantial creep damage.

A similar evaluation of strain rate effects was reported in NASA CR-134627 for the R-24 alloy and these results are reproduced in Figure 15 for comparison. It is to be noted that this behavior pattern is somewhat different from that discussed above since the duplicate tests in Figure 15 appeared to warrant definite separations of the three strain rate curves and hence no tendency toward a saturation effect in the higher strainrange regime was identified. This difference is emphasized here for it indicates some lack of similarity in the strain rate response for the R-24 material tested in the two evaluations. Actually, though, it might be that in Figure 15 too much emphasis was given to the reproducible results observed in the duplicate tests. For example, if these previous data are viewed along with the current results (see Figure 16) a single trend behavior can be established within a reasonable scatter of the data. There is good reason for accepting the interpretation in Figure 16 in view of the fact that the test points at 0.70% and 3.0% at $1x10^{-2}$ sec^{-1} were obtained using specimens that remained from the previous program.

Table 5 - Low-Cycle Fatigue Test Results Obtained in Argon at 538°C for Several Strain Rates

R-24 Series
NARloy Z Alloy
(cent. cast, hot-rolled, solution annealed and aged)

Axial Strain Control
A-ratio of infinity

$E = 98.6 \times 10^3$ MN/m^2

Spec. No.	Poisson's Ratio	Total Strain Range, %	Freq. cpm	Stress Range at Start, MN/m^2	at $N_f/2$			N_f, Cycles to Failure	Remarks
					$\Delta\varepsilon_{inel.}$ %	$\Delta\varepsilon_e$ %	$\Delta\sigma$ MN/m^2		
				1×10^{-2} sec^{-1}					
R-24-103	0.35	1.0	30	252	0.75	0.25	252	5022	Slight hardening & then slight softening
R-24-47	0.33	0.7	43	272	0.46	0.24	235	14194	
R-24-105	0.35	2.0	15	286	1.69	0.31	309	673	"
R-24-35	0.34	3.0	10	310	2.67	0.33	325	165	"
				4×10^{-4} sec^{-1}					
R-24-104	0.35	1.0	1.2	252	0.80	0.20	200	1266	Softened
R-24-106	0.35	2.0	0.6	269	1.76	0.24	234	351	Softened
R-24-112	0.35	3.0	0.4	276	2.76	0.24	241	154	Softened
				4×10^{-5} sec^{-1}					
R-24-117	0.35	0.9	0.13	249	0.72	0.18	173	787	Softened
R-24-118	0.35	2.6	0.046	232	2.42	0.18	177	116	Softened

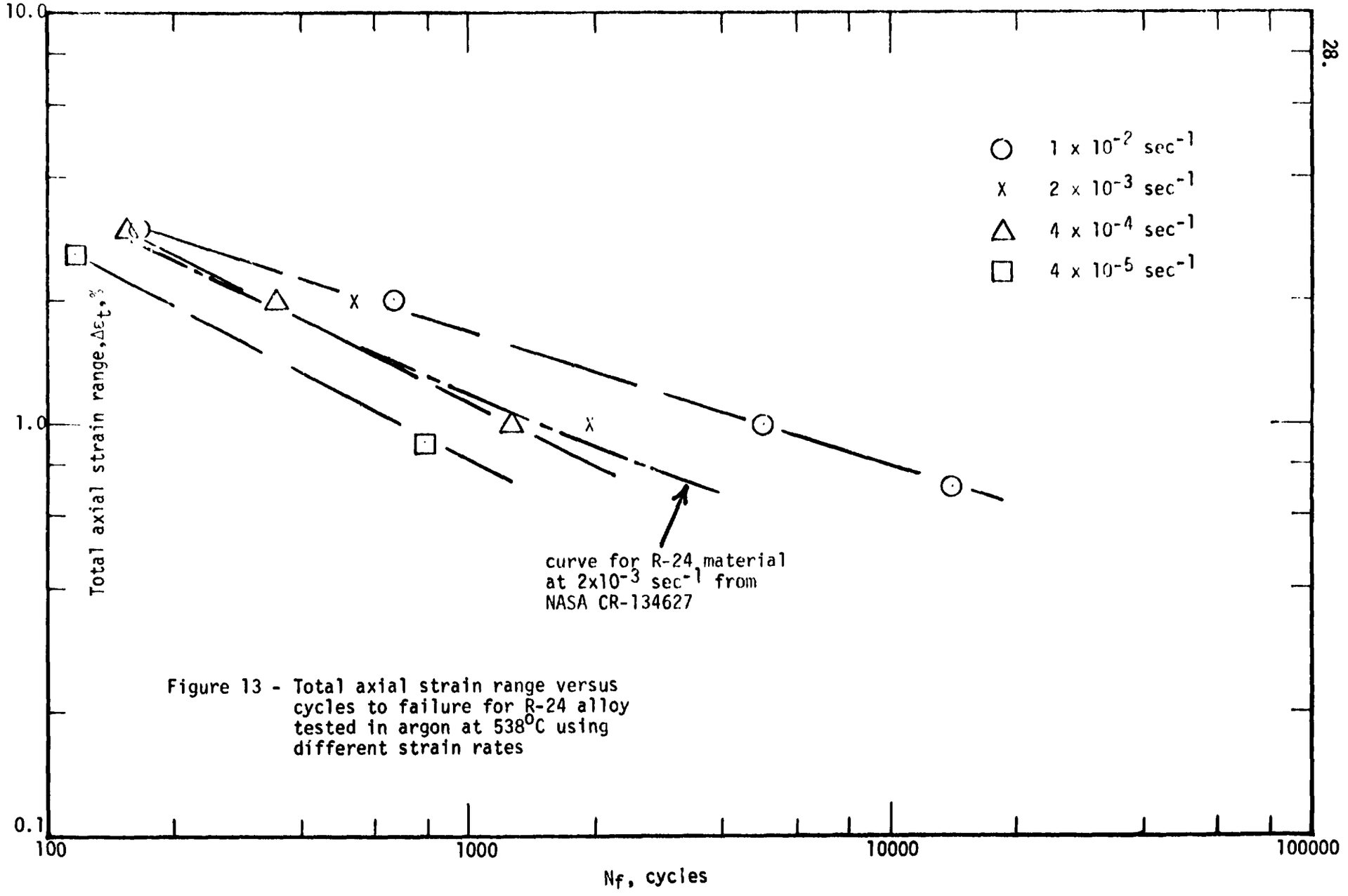

Figure 13 - Total axial strain range versus cycles to failure for R-24 alloy tested in argon at 538°C using different strain rates

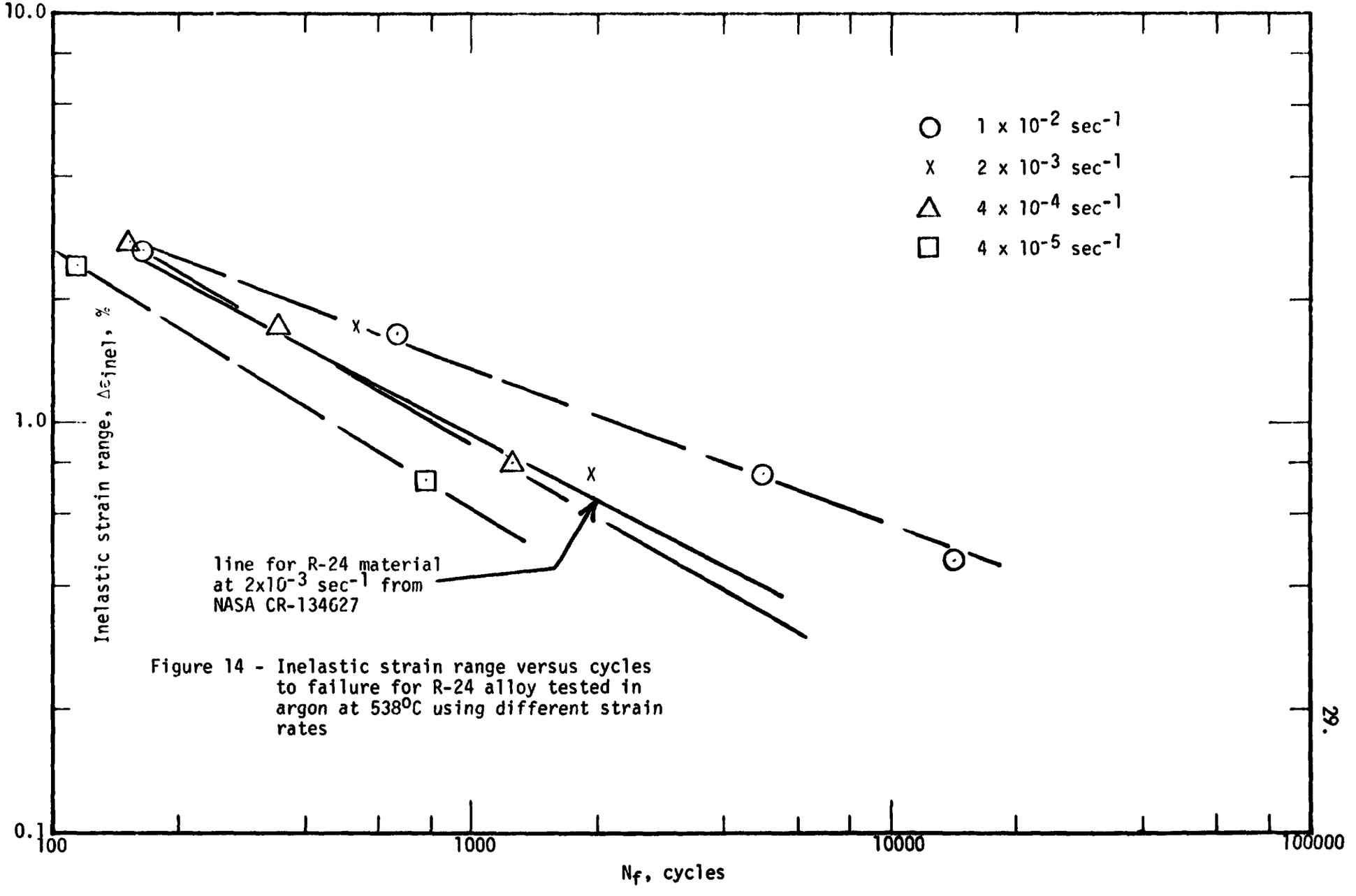

Figure 14 - Inelastic strain range versus cycles to failure for R-24 alloy tested in argon at 538°C using different strain rates

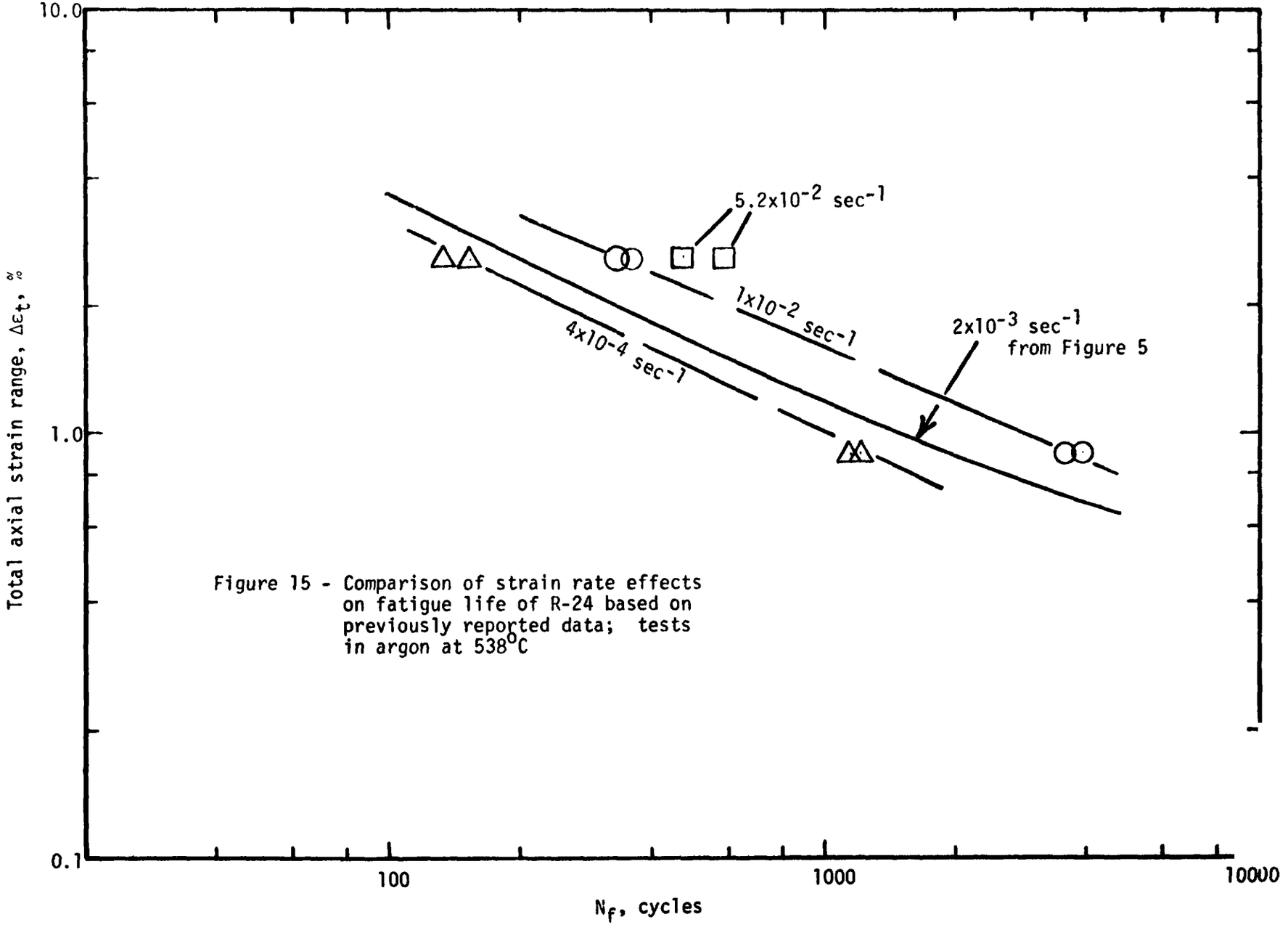

Figure 15 - Comparison of strain rate effects on fatigue life of R-24 based on previously reported data; tests in argon at 538°C

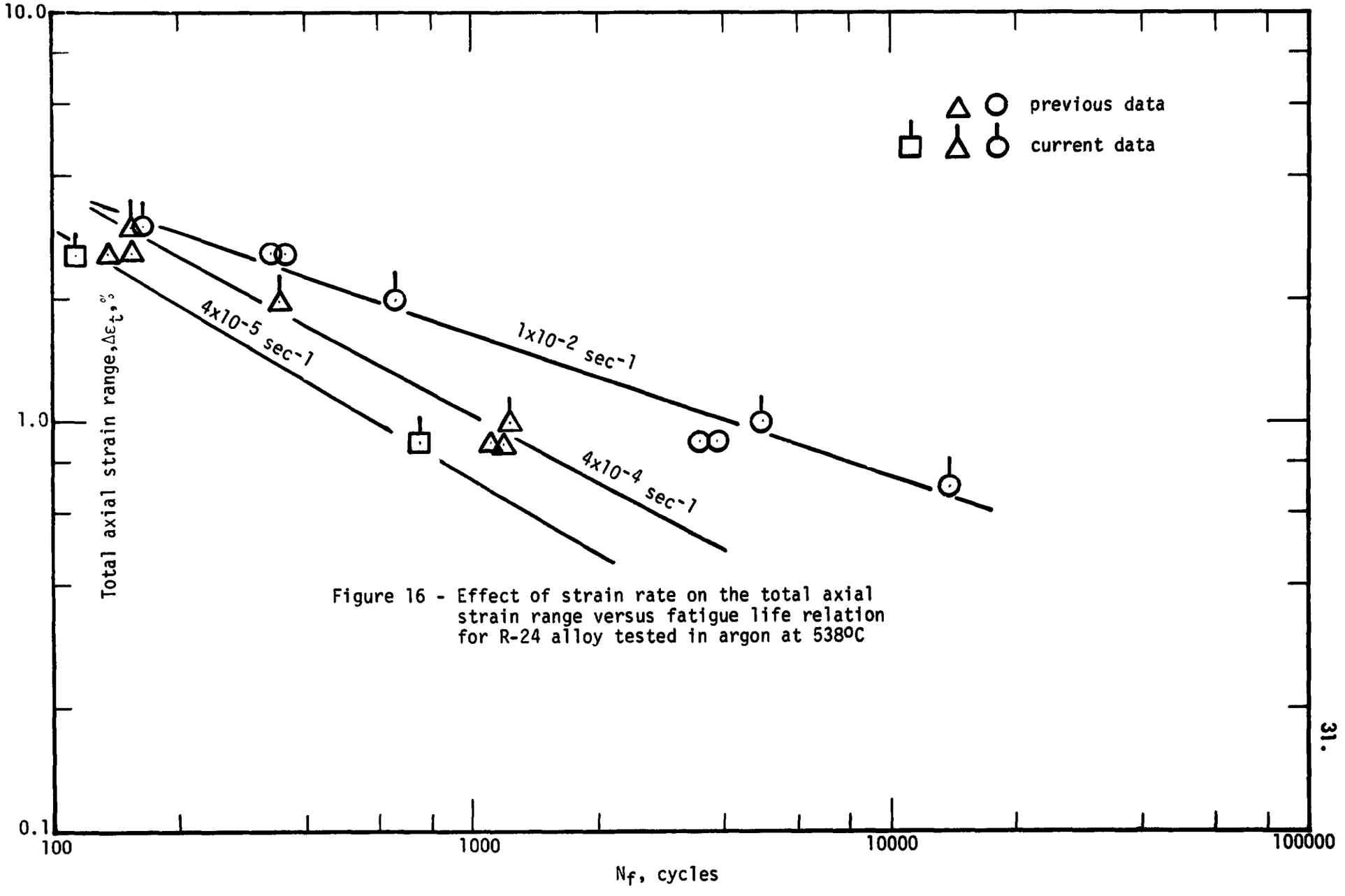

Figure 16 - Effect of strain rate on the total axial strain range versus fatigue life relation for R-24 alloy tested in argon at 538°C

The next portion of this evaluation of the R-24 alloy was devoted to the identification of partitioned strainrange versus life relationships for this material at 538°C. Initially, an evaluation was made of the continuous cycling results in order to identify the N_{pp} and N_{cc} values along with the corresponding strainrange components. It was concluded that the test results obtained at a strain rate of $2x10^{-3}$ sec^{-1} contained a substantial creep component so that these data could not be used in the identification of N_{pp}. Tests at higher strain rates were performed but, as pointed out above, some creep component was felt to be involved in most of these tests. Since the response characteristics of the extensometer were such that testing at higher frequencies was not possible, an indirect determination of N_{pp} was adopted. Using data from the previous program (see NASA CR-134627) as well as the test results from the current program a plot was made of the cycles to failure, at a given strainrange, versus strain rate and is shown in Figure 17. At each strainrange an evaluation of the data trend was made to identify the saturation fatigue life in the high strain rate regimes. A value was selected as the maximum fatigue life for a given strainrange as a value of N_f that would not be increased by any further increases in strain rate. This value was adopted as N_{pp} and was associated with the total strainrange involved (see description of R-2 alloy) which was taken to be $\Delta\varepsilon_{pp}$. A similar construction in the lower strain rate regime led to N_{cc} and $\Delta\varepsilon_{cc}$ values. A plot of these results is presented in Figure 17 for these strainrange components and, admittedly, involves some judgement in identifying the saturation limits (a strain rate of $1x10^{-7}$ sec^{-1} was chosen to define the extrapolation limit to obtain the N_{cc} values). However, some verification was obtained by referring these estimates and the subsequent CP and PC lines to an estimation of the previously reported (NASA CR-134627) hold-time results. Since the agreement between measured and predicted fatigue life was found to be excellent (see below), the approach outlined in Figure 17 appears to have yielded meaningful results.

In order to identify the N_{cp} and N_{pc} data, tests were performed that involved slow-fast and fast-slow cycling of the type described above for the R-2 material. Data obtained using strain rates of $4x10^{-4}$ sec^{-1} and $1x10^{-2}$ sec^{-1} in the same cycle (see Figure 11) are summarized in Table 6 and were used to establish the N_{cp}-$\Delta\varepsilon_{cp}$ and N_{pc}-$\Delta\varepsilon_{pc}$ relationships using the approach described previously. These relations are shown in Figure 18 to describe the various strainrange versus life relationships at 538°C for this material.

In some additional slow-fast testing of the R-24 alloy, the strain rate of $1x10^{-2}$ sec^{-1} was maintained for the fast portion of the cycle while rates of $4x10^{-5}$ sec^{-1} and $7x10^{-6}$ sec^{-1} were employed in the tension-going slow straining portion of the cycle. These evaluations led to the results summarized in Table 6 and presented graphically in Figures 19 and 20. These interesting comparisons highlight several important considerations. One is the fact that slow-fast cycling of this material at the conditions employed is much more detrimental than fast-slow cycling. Another is the fact that the fast-slow exposure leads to a fatigue life that is not significantly different from that observed in the continuous cycling tests at the fast ($1x10^{-2}$ sec^{-1}) strain rate. In other words, the introduction of a strain rate of $4x10^{-4}$ sec^{-1}

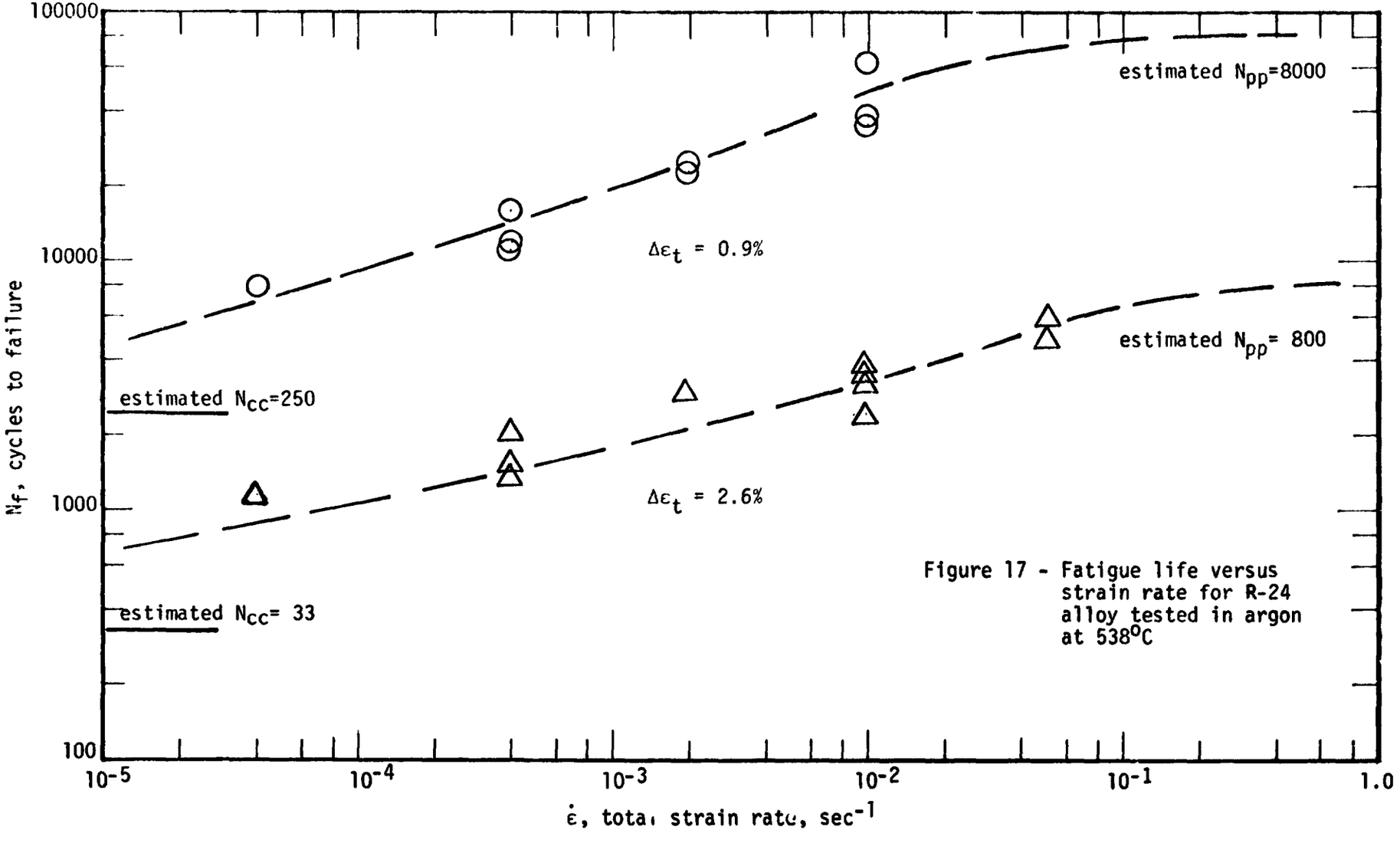

Figure 17 - Fatigue life versus strain rate for R-24 alloy tested in argon at 538°C

Table 6 - Low-Cycle Fatigue Test Results Obtained in Argon at 538°C Using Fast-Slow and Slow-Fast Cycling

R-24 Series
NARloy Z Alloy
(cent. cast, hot-rolled, solution annealed and aged)

Axial Strain Control
A-ratio of infinity

$E = 98.6 \times 10^3$ MN/m^2

Spec. No.	Poisson's Ratio	Total Strain Range, %	Time[1] for t/c half of cycle, sec.	Stress Range at Start, MN/m^2	at $N_f/2$			N_f, Cycles to Failure	Remarks
					$\Delta\varepsilon_{inel.}$ %	$\Delta\varepsilon_e$ %	$\Delta\sigma$[2] MN/m^2		
		1×10^{-2} sec^{-1} in tension and 4×10^{-4} sec^{-1} in compression							
R-21-108	0.35	1.0	1/25	262	0.72	0.28	276 (148/128)	2091	Slight hardening
R-24-110	0.35	2.0	2/50	272	1.71	0.29	283 (166/117)	451	Slight hardening
		4×10^{-4} sec^{-1} in tension and 1×10^{-2} sec^{-1} in compression							
R-24-107	0.35	1.0	25/1	259	0.73	0.27	262 (121/141)	238	Slight hardening
R-24-109	0.35	2.0	50/2	283	1.70	0.30	296 (133/163)	66	Slight hardening
R-24-111	0.35	3.0	75/3	303	2.68	0.32	312 (139/173)	35	Slight hardening
R-24-113	0.35	0.5	12.5/0.5	258	0.27	0.23	223 (105/118)	1156	Slight softening

(1)-time for tension/compression going portion of cycle (2)-(tensile stress/compressive stress)

Table 6 - Low-Cycle Fatigue Test Results Obtained in Argon (cont.) at 538°C Using Fast-Slow and Slow-Fast Cycling

R-24 Series
NARloy Z Alloy
(cent. cast, hot-rolled, solution annealed and aged)

Axial Strain Control
A-ratio of infinity

$E = 98.6 \times 10^3$ MN/m^2

Spec. No.	Poisson's Ratio	Total Strain Range, %	Time(1) for t/c half of cycle, sec.	Stress Range at Start, MN/m^2	at $N_f/2$			N_f, Cycles to Failure	Remarks
					$\Delta\varepsilon_{inel.}$ %	$\Delta\varepsilon_e$ %	$\Delta\sigma$(2) MN/m^2		
		4×10^{-5} sec^{-1} in tension and 1×10^{-2} sec^{-1} in compression							
R-24-115	0.35	0.5	125/0.5	239	0.28	0.22	212 (93/119)	300	Slight initial hardening & then slight softening
R-24-114*	0.35	3.0	707/12	281	2.73	0.27	269 (114/155)	16	Slight softening
		7×10^{-6} sec^{-1} in tension and 1×10^{-2} sec^{-1} in compression							
R-24-116	0.35	0.5	720/0.5	232	0.26	0.24	200 (81/119)	115	Slight softening

*Strain rates actually used were 4.2×10^{-5} sec^{-1} in tension and 2.5×10^{-3} sec^{-1} in compression
(1)-time for tension/compression going portion of cycle (2)-(tensile stress/compressive stress)

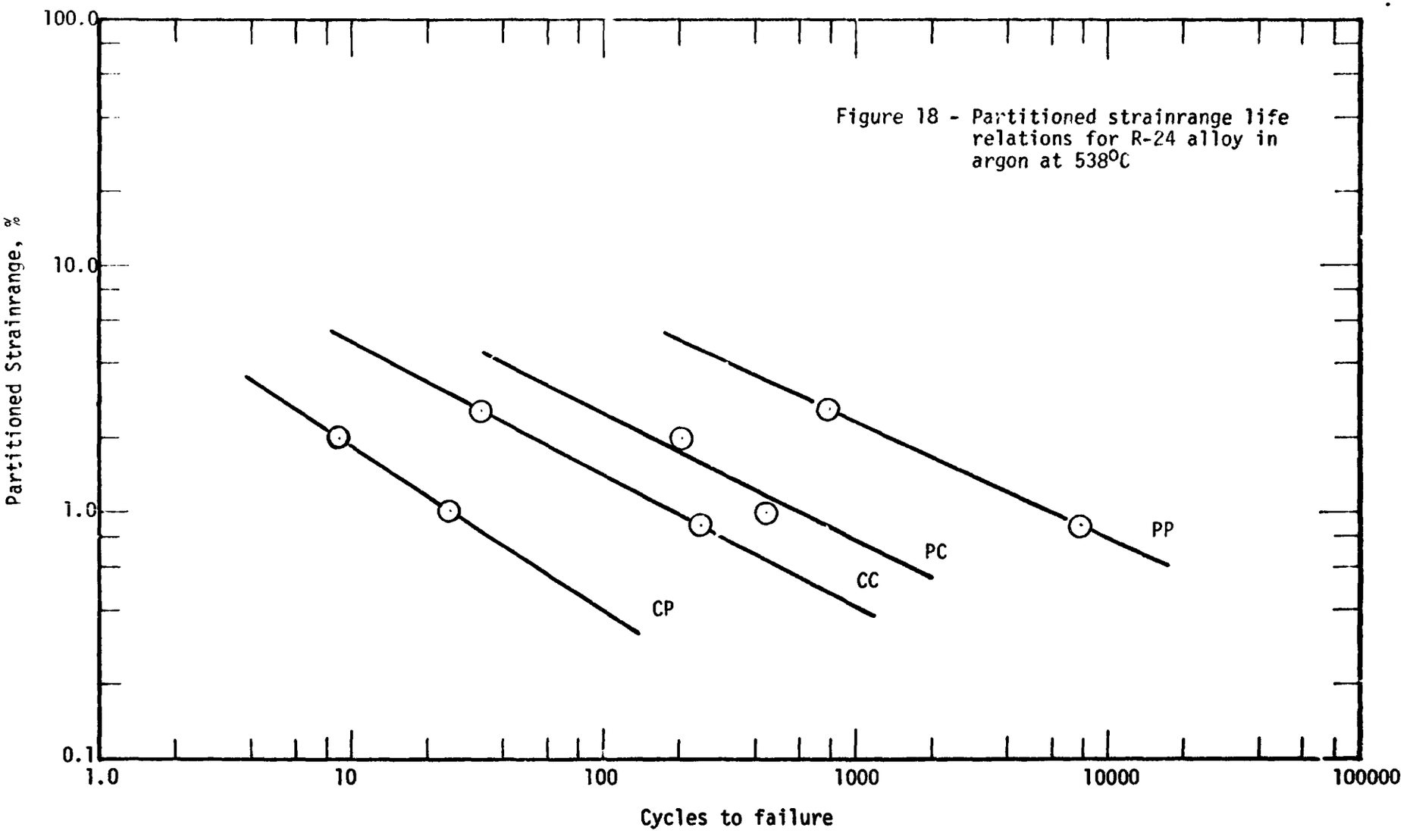

Figure 18 - Partitioned strainrange life relations for R-24 alloy in argon at 538°C

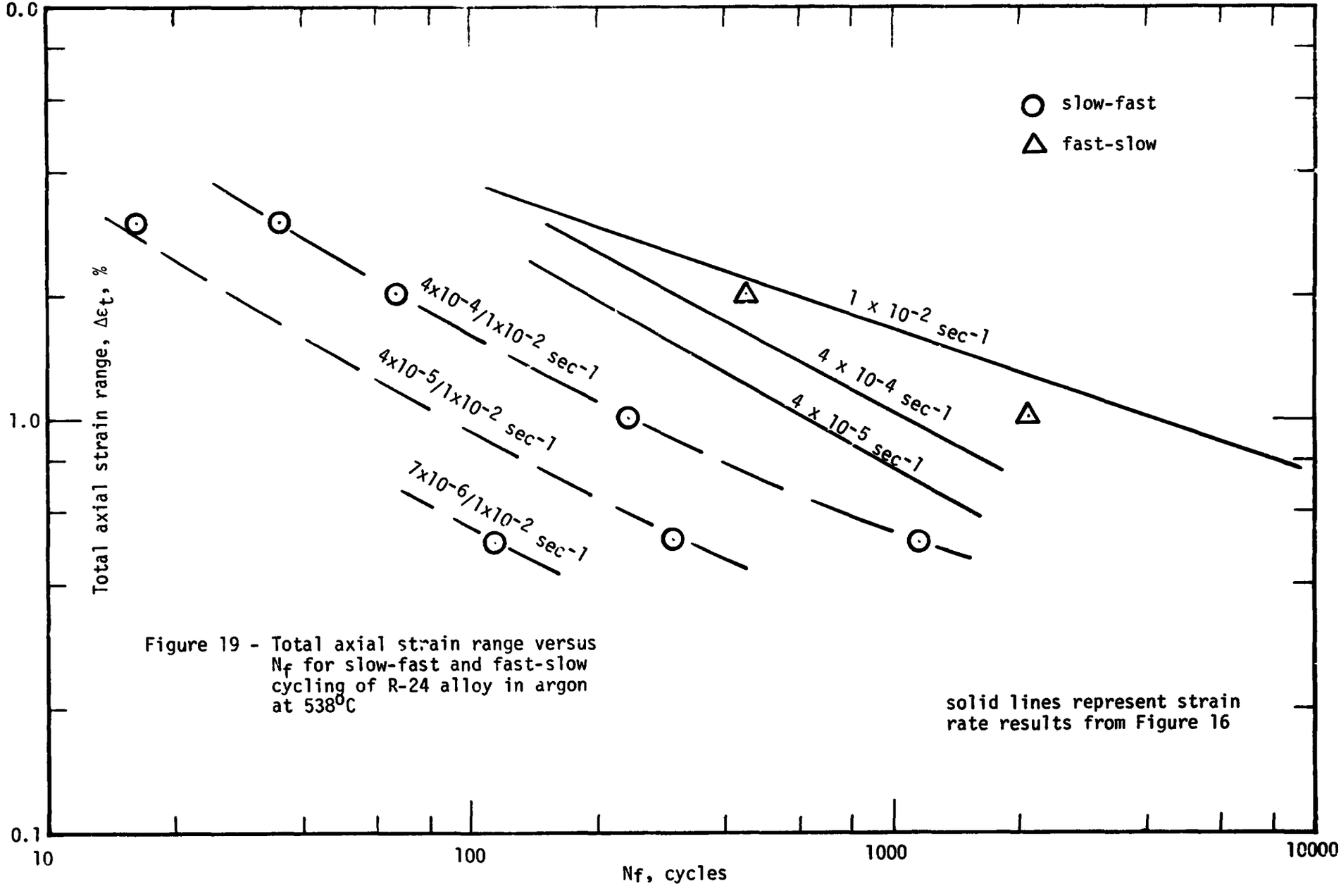

Figure 19 - Total axial strain range versus N_f for slow-fast and fast-slow cycling of R-24 alloy in argon at 538°C

Figure 20 - Inelastic strain range versus N_f for slow-fast and fast-slow cycling of R-24 alloy in argon at 538°C

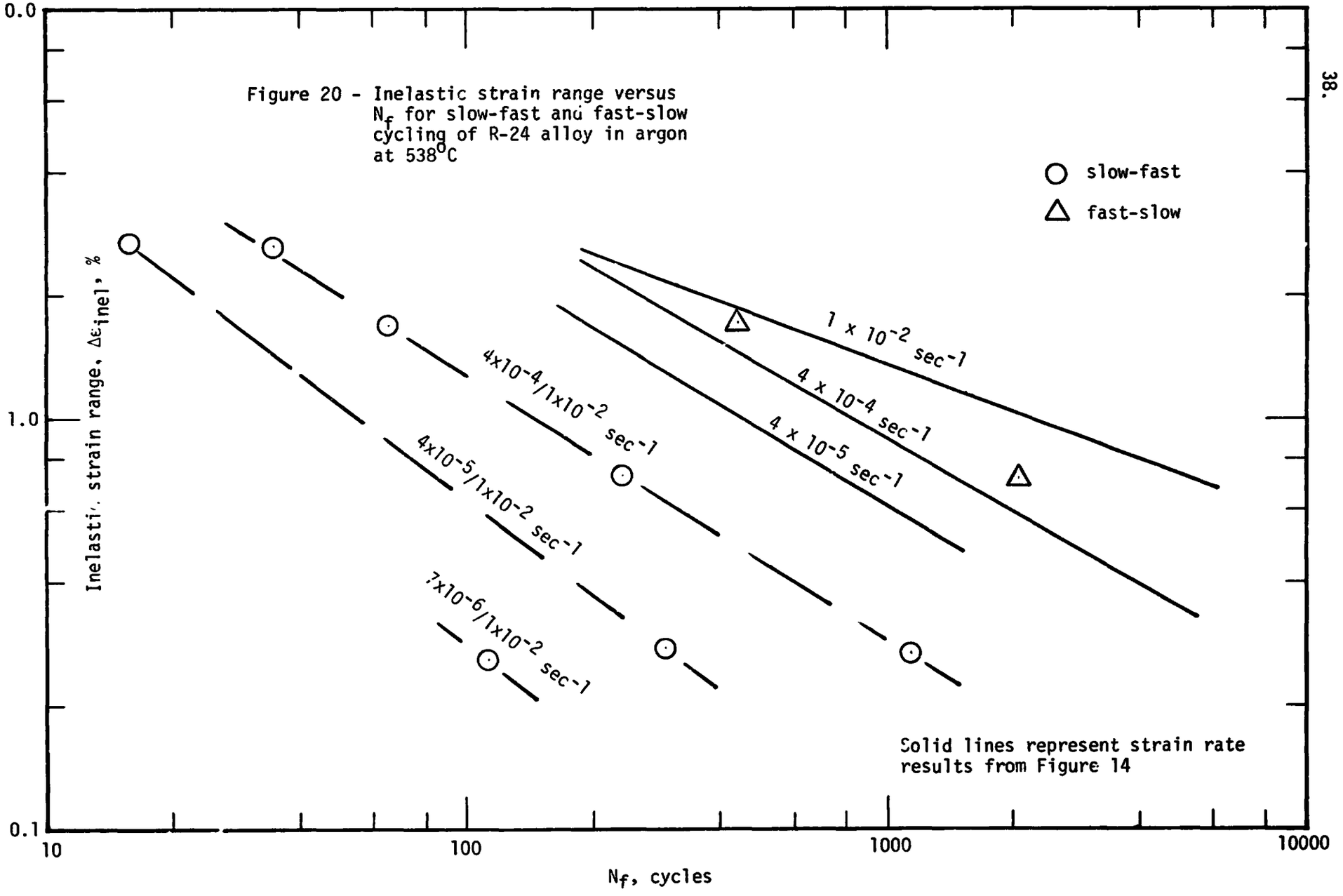

into the compression going portion of the cycle led to a small but not significant reduction in the fatigue life. The third observation made in connection with Figures 19 and 20 relates to the continual reduction in fatigue life as the tension-going strain rate is decreased. Based on a strain range of 0.50%, the introduction of a tension-going strain rate of $7x10^{-6}$ sec^{-1} leads to a fatigue life reduction of more than two orders of magnitude based on the use of a strain rate of $1x10^{-2}$ sec^{-1} throughout the cycle.

A further assessment of the data presented in Figures 19 and 20 involved the application of the strainrange partitioning lines of Figure 18 to a prediction of the slow-fast and fast-slow results. A summary of this study is presented in Table 7 to indicate a very impressive agreement. These results along with a similar comparison (see Table 8) based on previously reported (NASA CR-134627) hold-time results establish the validity of the strainrange partitioning lines of Figure 18 and the approach used in the positioning of these lines.

In a different type of analysis of the slow-fast and fast-slow test results, the correlation shown in Figure 21 was derived. This logarithmic plot reveals a fairly well-defined linearity between σ_t (measured at $N_f/2$) and the total tension-going time encountered throughout the test. It is particularly impressive that the fast-slow results also fall along the line established by the slow-fast results. This linearity is represented by the following:

$$\sigma_t = \text{constant}\left(\frac{N_f \Delta\varepsilon_t}{\dot{\varepsilon}}\right)^{-m}$$

where m is about 0.16.

The line established in Figure 21 has been positioned in Figure 22 to show another interesting result. All the continuous cycling fatigue data involving strain rates from $4x10^{-5}$ sec^{-1} to $1x10^{-2}$ sec^{-1} also appear to correlate well with the line established in the slow-fast and fast-slow analysis. It is also to be noted that the compression-hold fatigue results (see NASA CR-134627) are also in excellent agreement with this method of data presentation. However, when the tension-hold fatigue results are considered, some decision must be made as to the appropriate value to use for σ_t. If the tensile stress at the beginning of the hold period is employed the points will fall much above the line in Figure 22 while the reverse is true if the tensile stress at the end of the hold period is employed. If an average σ_t is used the results shown in Figure 22 are obtained to indicate fairly good agreement.

It seems reasonable to conclude, therefore, that the fatigue characteristics of the R-24 alloy at 538^0C are all summarized in the linear relation in Figure 21. And once a given exposure is considered and the value of σ_t is established for this exposure, a fairly reliable value for the fatigue life can be obtained from Figure 21.

Table 7 - A Comparison of Measured and Predicted Fatigue Life Values for Slow-Fast and Fast-Slow Tests of R-24 Alloy at 538°C

Type of Test	$\Delta\varepsilon_t$, %	N_f Predicted by Strainrange Partitioning	N_f Measured
$4x10^{-5}$ sec^{-1}/$1x10^{-2}$ sec^{-1}	0.50	209	300
$4x10^{-5}$ sec^{-1}/$1x10^{-2}$ sec^{-1}	0.90	69	110*
$7x10^{-6}$ sec^{-1}/$1x10^{-2}$ sec^{-1}	0.50	74	110
$7x10^{-6}$ sec^{-1}/$1x10^{-2}$ sec^{-1}	0.90	37	40*

*not a measured value; estimated from line in Figure 19.

Table 8 - A Comparison of Measured and Predicted Fatigue Life Values for the Hold-Time Tests of the R-24 Alloy at 538°C

$\Delta\varepsilon_t$, %	Hold Period, seconds	N_f Predicted by Strainrange Partitioning	N_f Measured
2.6	300 T	105	102
2.6	300 T	105	75
2.6	300 C	219	353
2.6	300 C	219	337
0.9	300 T	318	262
0.9	300 T	318	317
0.9	300 C	2052	2981
0.9	300 C	2052	3392

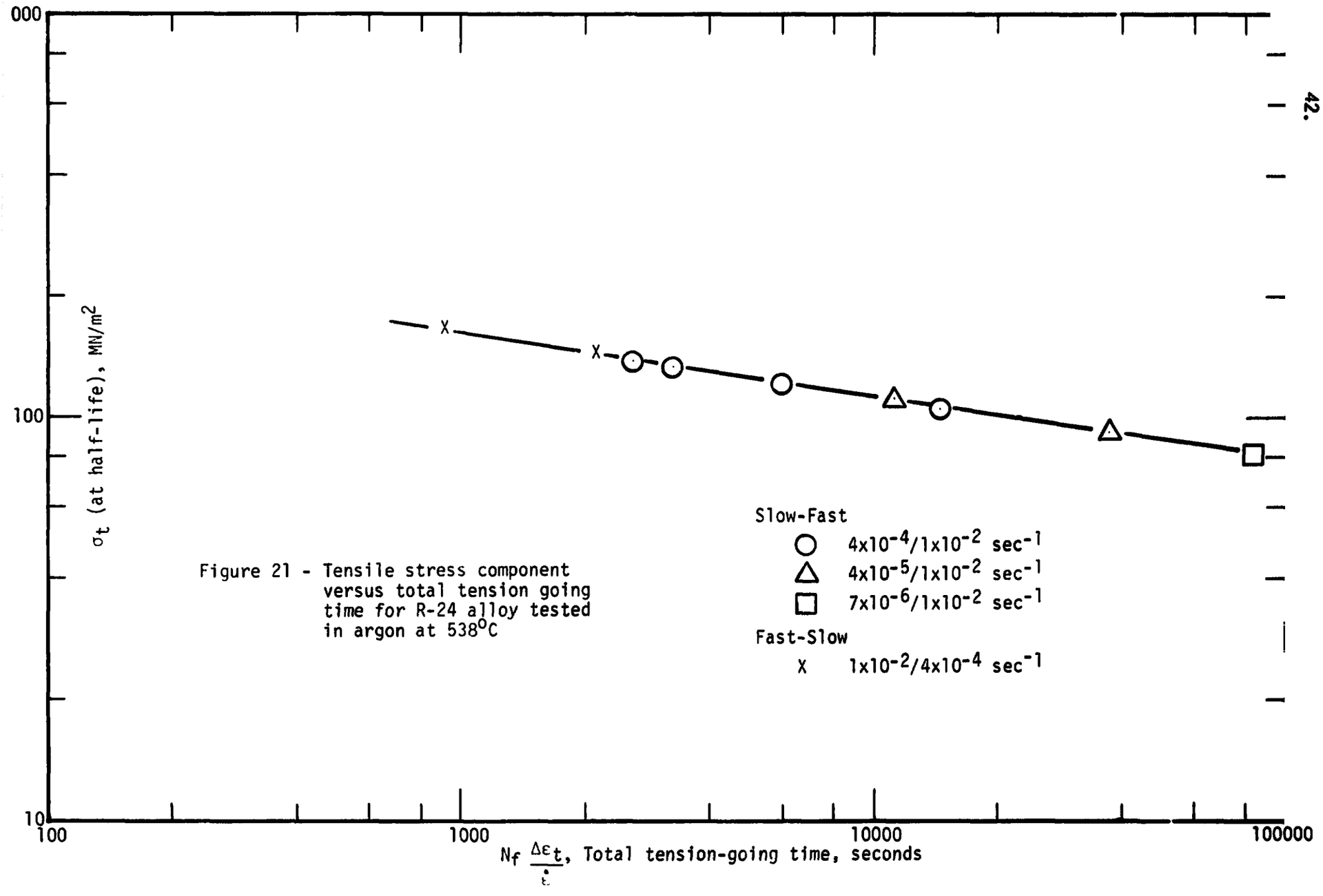

Figure 21 - Tensile stress component versus total tension going time for R-24 alloy tested in argon at 538°C

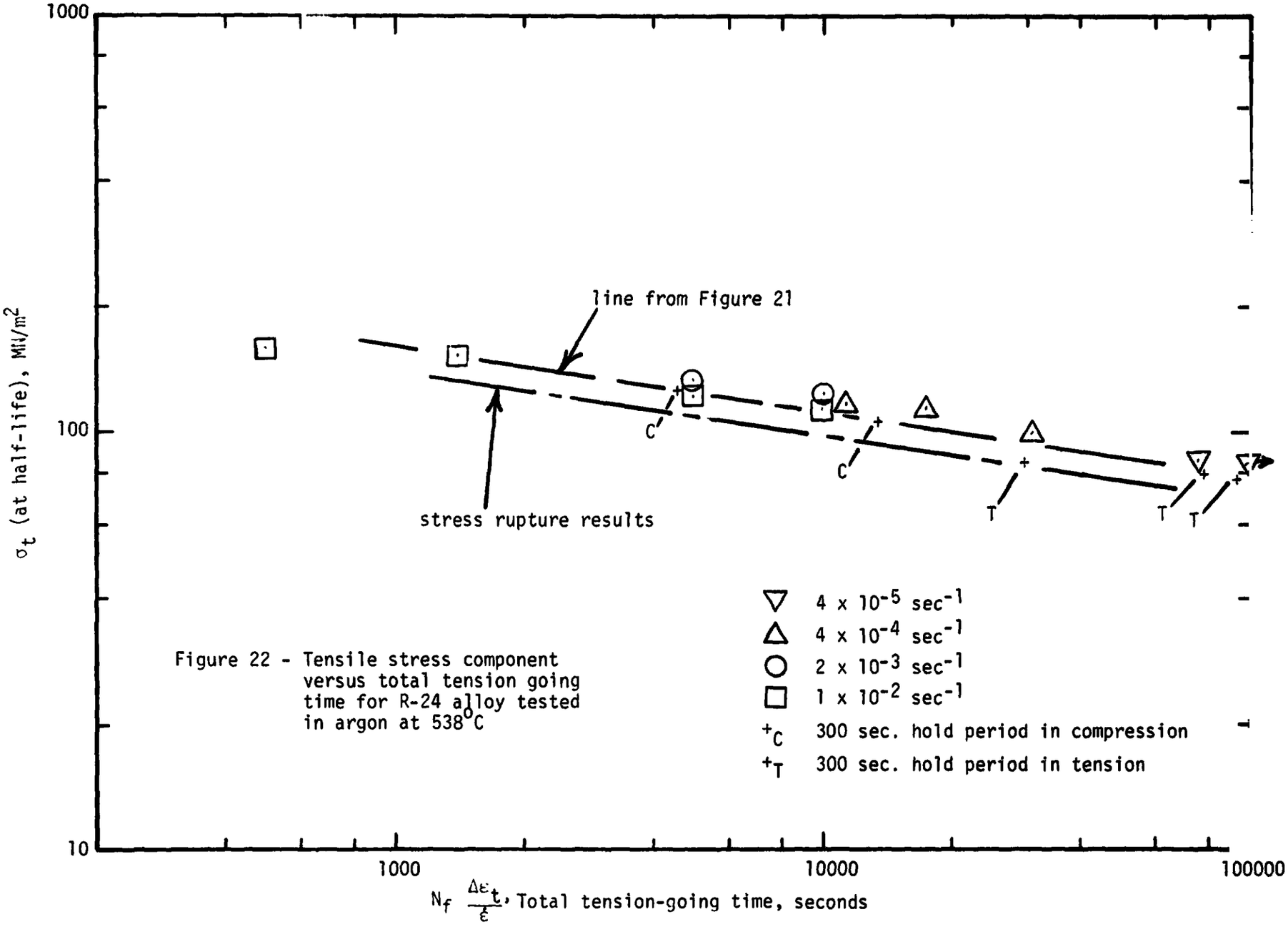

Figure 22 - Tensile stress component versus total tension going time for R-24 alloy tested in argon at 538°C

Another impressive result involves the comparison of the data in Figure 22 with the stress-rupture results for R-24 material at 538°C (AFRPL-TR-73-10, Volume 1). A dashed line has been positioned in Figure 22 to indicate essentially the same stress dependency for the two types of data. Since the σ_t value for the fatigue data does not exist for the entire cycle the use of some average stress value for the cycle could bring these data into closer coincidence with the stress-rupture data. Some additional study of the type of correlation shown in Figure 21 appears to be warranted.

PART II - DETERMINATION OF HIGH-CYCLE FATIGUE BEHAVIOR OF R-9 ALLOY

Seven strain controlled fatigue tests of the R-9 alloy were performed at 538°C (1000°F) in high-purity argon using a test frequency of 0.5 Hz (30 cpm). Total axial strain ranges between 0.30% and 0.80% were employed to extend the fatigue curve, established in previous tests (see NASA CR-121259), into the high-cycle regime. The results obtained in these tests are summarized in Table 9 and are presented graphically in Figure 23 in comparison with the previously reported data for this alloy. It is noted that a fairly smooth extension of the previously reported fatigue curve is obtained to define the fatigue characteristics over the range from about 300 to 400,000 cycles. There is, however, some tendency for the fatigue curve to bend downward in the cyclic life range beyond 10^5 cycles to suggest a gradual trend toward a reduced fatigue resistance compared to that expected by the usual extension of the curve defined by the test data in the regime to 10^5 cycles. This change in the curvature is an interesting result and is associated with a notable shift in stress-strain characteristics. In the region near 10^5 cycles a noticeable compressive stress bias develops and becomes more pronounced as the strain range decreases. At a strain range of 0.30%, for example, the half-life compressive stress is almost twice the tensile stress. Also, of interest, is the fact that near 10^5 cycles a definite change of slope is indicated in the elastic strain range plot (see Figure 24). A corresponding change in the plastic strain range behavior is also observable. While there is no clear explanation for this behavior pattern displayed by the R-9 material it is possibly related to some time-dependent metallurgical change taking place at the long exposure times or to some localization of plastic strain developing in the low strain range regime.

Table 9 - Low-Cycle Fatigue Test Results Obtained in Argon at 538°C
Using a Frequency of 30 cpm

R-9 Series
Zr-Cr-Mg Copper,
SA,CW and Aged

Axial Strain Control
A-ratio of infinity
$E = 6.895 \times 10^4$ MN/m^2

Spec. No.	Poisson's Ratio	Total Strain Range, %	Freq. cpm	Stress Range at Start, MN/m^2	at $N_f/2$			N_f, Cycles to Failure	Remarks
					$\Delta\varepsilon_{inel.}$ %	$\Delta\varepsilon_e$ %	$\Delta\sigma$ MN/m^2		
R-9-101	0.35	0.80	30	488	0.26	0.54	372	12543(1)	Softened
R-9-102	0.34	0.72	30	449	0.20	0.52	358	18746	Softened
R-9-103	0.33	0.50	30	323	0.11	0.39	268	83751	Softened
R-9-104	0.33	0.60	30	379	0.15	0.45	314	50010	Softened
R-9-106	0.32	0.50	30	318	0.11	0.39	267	101210	Softened
R-9-107	0.323	0.40	30	260	0.11	0.29	204	141447	Softened
R-9-108	0.315	0.30	30	200.1	0.07	0.23	162	382769	Softened

(1)-System did not shut down after last cycle; as a result a compressive load was applied to the specimen after the last cycle.

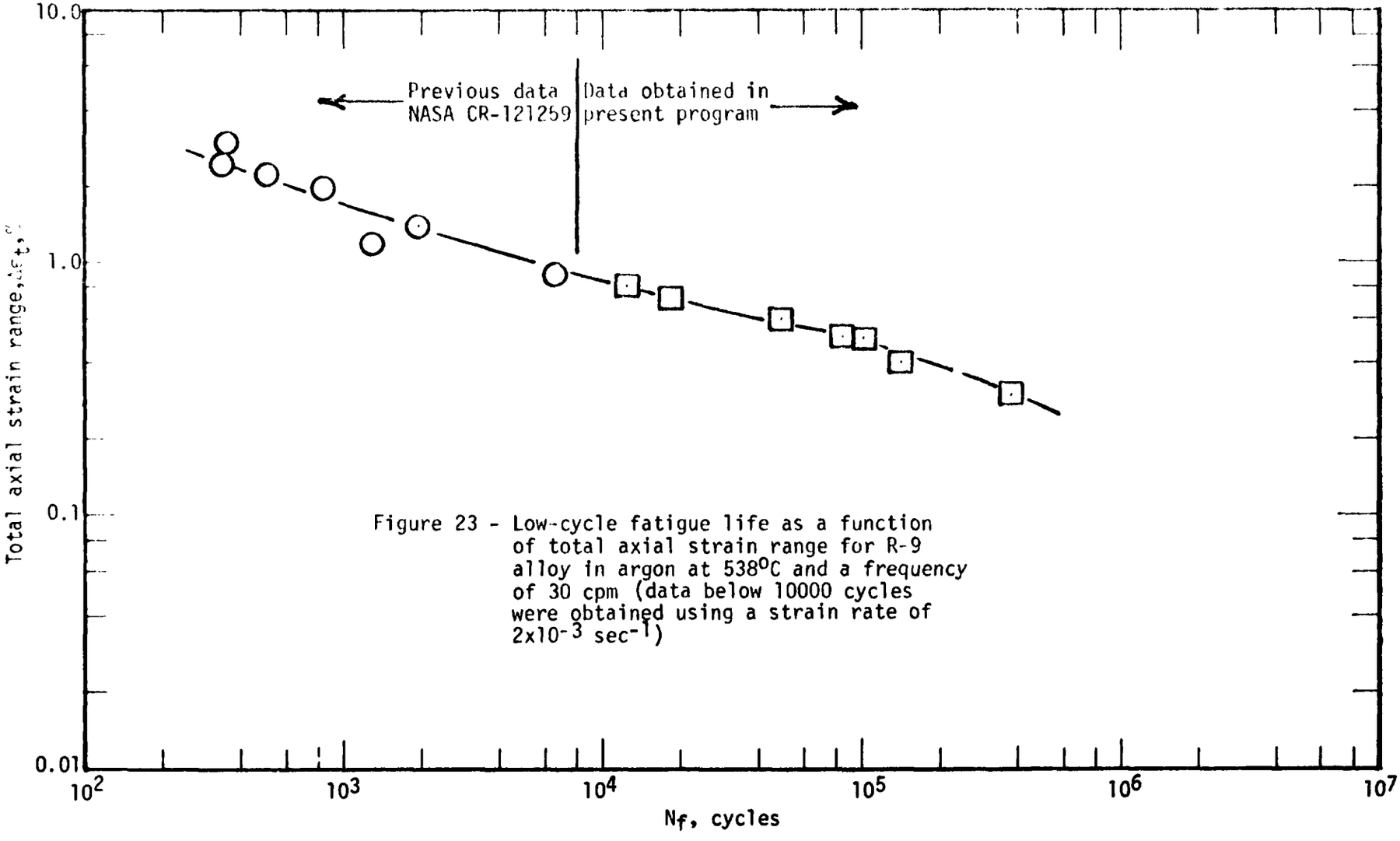

Figure 23 - Low-cycle fatigue life as a function of total axial strain range for R-9 alloy in argon at 538°C and a frequency of 30 cpm (data below 10000 cycles were obtained using a strain rate of 2×10^{-3} sec^{-1})

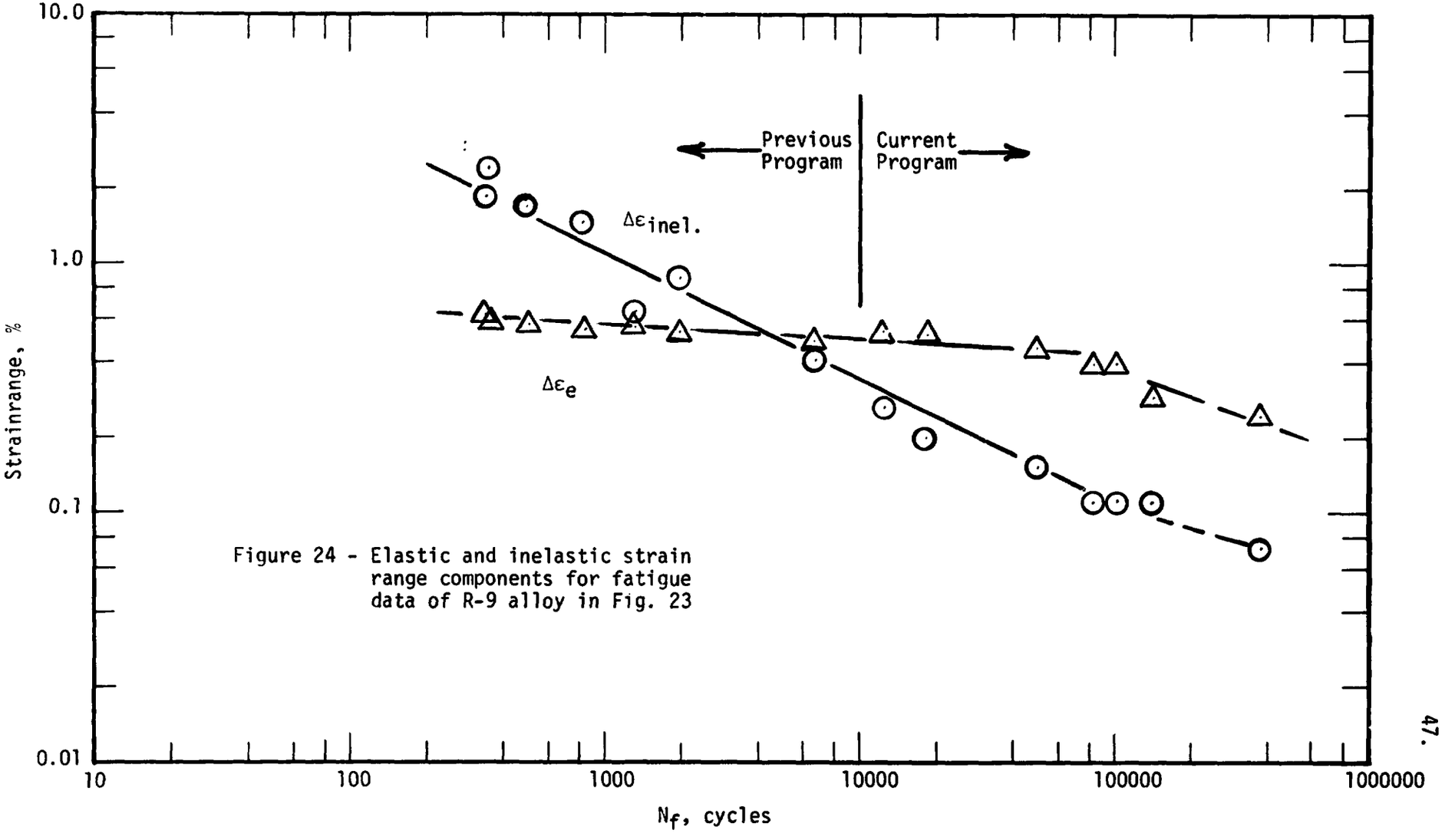

Figure 24 - Elastic and inelastic strain range components for fatigue data of R-9 alloy in Fig. 23

PART III - TENSILE AND LOW-CYCLE FATIGUE EVALUATION OF R-27 AND R-28 ALLOYS

Short-term tensile tests of these two alloys were performed in duplicate at room temperature and at 538°C using a strain rate of 2×10^{-3} sec^{-1}. The tests at room temperature were performed in air while those at 538°C were performed in high-purity argon. A summary of the data generated in these tests is presented in Tables 10 and 11.

At room temperature the R-27 composition is seen to exhibit a much lower yield strength (about 60 MN/m^2 compared to 110 MN/m^2) and a slightly lower (190 MN/m^2 compared to 230 MN/m^2) ultimate strength than the R-10 alloy reported in NASA CR-121259. At 538°C the R-27 alloy exhibited about the same ultimate strength as the R-10 material although the yield strength of R-27 was still lower (about 22 MN/m^2 compared to 35 MN/m^2) than that of the R-10 alloy. Some slight ovality was noted in the fracture surfaces for all the R-27 tensile tests.

In the case of the R-28 alloy the yield and ultimate strengths at room temperature were just slightly higher (about 300 and 400 MN/m^2 compared to 280 and 290 MN/m^2) than those of the R-8 material (pure silver) reported in NASA CR-121259. However, at 538°C a pronounced difference in strength was exhibited. For the R-28 material the yield and ultimate strengths were about 135 MN/m^2 and 145 MN/m^2 respectively and these compare to 16 MN/m^2 and 35 MN/m^2 for the R-8 material. An impressive increase in strength is seen to result from the addition of the 0.5% zirconium in the R-28 alloy.

Tensile data generated by NASA-Lewis at room temperature and at liquid nitrogen temperature are included in Table 11 for comparison.

Low-cycle fatigue tests of the R-27 alloy were performed in argon at 538°C using a strain rate of 2×10^{-3} sec^{-1} and strain ranges selected to define the fatigue life over the range from 300 to 3000 cycles. A summary of the results of these tests is presented in Table 12. In addition, a graphical presentation of the fatigue life in terms of N_f and N_5 (see Part VII) is shown in Figure 25. These results are also compared in Figure 25 with the N_5 data for the R-10 alloy reported previously. Slightly longer fatigue life is seen to be exhibited for the R-27 alloy.

It was noted in the R-27 tests that cracks developed very early in the test. For this reason the usual half-life information in Table 12 has been replaced with data at 10% of the fatigue life.

Low-cycle fatigue tests of the R-28 alloy were performed in argon at 538°C using a strain rate of 2×10^{-3} sec^{-1} and strain ranges selected to define the fatigue life over the range from 300 to 3000 cycles. A summary of the results of these tests is presented in Table 13. These results are presented graphically in Figure 26. Considerable data scatter is exhibited when the results are plotted in terms of N_f due to the large variation exhibited in the crack propagation period. However, a smoother curve is obtained by plotting the results in terms of the life value, N*, defined in NASA CR-121259. The load versus time traces were studied and failure was chosen as that point at which the length of the cusp in the compression portion of the load trace was 10 percent of the length of the compressive load trace.

The fatigue results for the R-28 alloy are just slightly lower than those obtained previously (NASA CR-121259) for pure silver (R-8 Series).

Table 10 - Short-Term Tensile Properties of Experimental Copper Alloy, R-27

Diametral Extensometer		Hourglass-Shaped Specimens			
Specimen Number	Temp. °C	Strain Rate, sec^{-1}	0.2% Offset Yield Strength, MN/m^2	Ultimate Tensile Strength, MN/m^2	Reduction in Area,(1) %
R-27-9	R.T.(2)	2×10^{-3}	65	190	48
R-27-12	R.T.(2)	2×10^{-3}	56	190	54
R-27-10	538 (3)	2×10^{-3}	21	44	33
R-27-11	538 (3)	2×10^{-3}	24	40	20

(1)-Slight ovality was noted in the fractured surfaces.
(2)-Tested in air. (3)-Tested in argon.

Table 11 - Short-Term Tensile Properties of Experimental Silver Alloy, R-28

Diametral Extensometer			Hourglass-Shaped Specimens		
Specimen Number	Temp. °C	Strain Rate, sec^{-1}	0.2% Offset Yield Strength, MN/m^2	Ultimate Tensile Strength, MN/m^2	Reduction in Area, %
R-28-8	R.T.(1)	2×10^{-3}	310	411	84
R-28-11	R.T.(1)	2×10^{-3}	280	380	82
R-28-9	538 (2)	2×10^{-3}	135	141	42
R-28-10	538 (2)	2×10^{-3}	139	146	45
R-28-21	R.T.(3)	2×10^{-3}	-	388	81
R-28-20	-196(4)	2×10^{-3}	-	508	67

(1)-Tested in air. (2)-Tested in argon. (3)-Tested in air, NASA-Lewis.
(4)-Tested in liquid nitrogen, NASA-Lewis.

Table 12 - Low-Cycle Fatigue Test Results Obtained in Argon at 538°C
Using a Strain Rate of 2×10^{-3} sec^{-1}

R-27
Experimental Copper;
electroformed

Axial Strain Control
A-ratio of infinity

$E=6.895 \times 10^4$ MN/m^2

Spec. No.	Poisson's Ratio	Total Strain Range, %	Freq. cpm	Stress Range at Start, MN/m^2	at $N_f/10$			N_f, Cycles to Failure	Remarks
					$\Delta\varepsilon_{inel}$ %	$\Delta\varepsilon_e$ %	$\Delta\sigma$ MN/m^2		
R-27-1	0.333	1.0	6	49.1	0.90	0.10	67.4	6107 (1)	Initial hardening; cracks developed in specimens after a few loading cycles
R-27-2	0.333	3.86	1.5	87.0	3.74	0.12	80.0	361	
R-27-3	0.333	1.2	5	47.7	1.09	0.11	75.8	1834	
R-27-4	0.333	2.8	2.14	67.4	2.68	0.12	83.0	608	
R-27-5	0.333	1.5	4	64.6	1.39	0.11	75.8	1904	
R-27-6	0.333	2.0	3	64.6	1.88	0.12	85.0	577	
R-27-7	0.333	1.2	5	63.2	1.10	0.10	67.4	5155 (2)	
R-27-8	0.333	2.0	3	64.6	1.91	0.09	63.2	6192 (3)	

(1) Tensile load was below 100 pounds during the last 3100 cycles of the test.
(2) Tensile load was below 100 pounds during the last 2200 cycles of the test.
(3) Tensile load was below 100 pounds during the last 3700 cycles of the test.

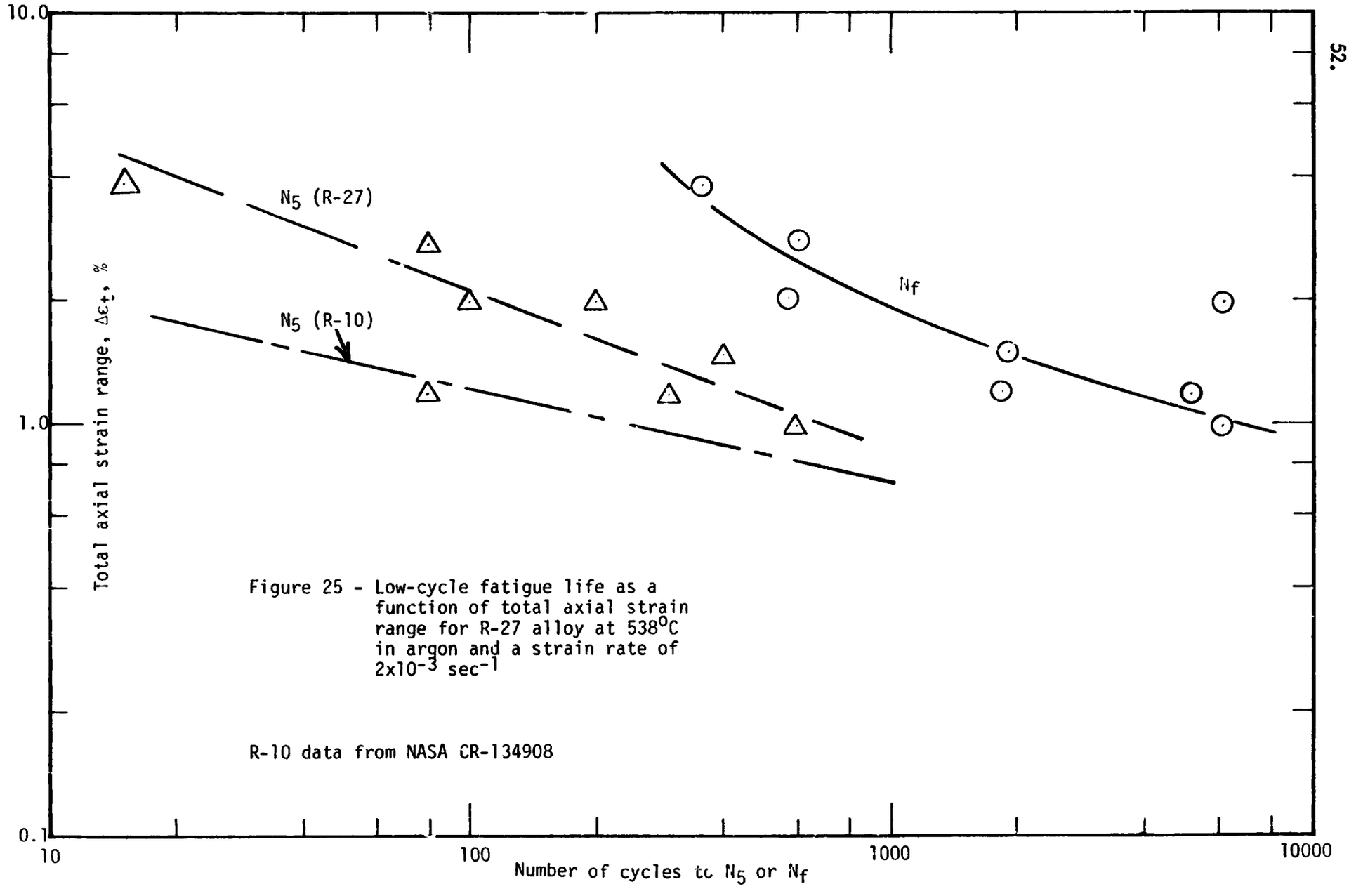

Figure 25 - Low-cycle fatigue life as a function of total axial strain range for R-27 alloy at 538°C in argon and a strain rate of 2×10^{-3} sec^{-1}

R-10 data from NASA CR-134908

Table 13 - Low-Cycle Fatigue Test Results Obtained in Argon at 538°C Using a Strain Rate of 2×10^{-3} sec^{-1}

R-28
Experimental Silver Alloy
0.5% Zr

Axial Strain Control
A-ratio of infinity
$E = 4.34 \times 10^4$ MN/m^2

Spec. No.	Poisson's Ratio	Total Strain Range, %	Freq. cpm	Stress Range at Start, MN/m^2	at $N_f/2$			N_f, Cycles to Failure (1)	Remarks
					$\Delta\varepsilon_{inel.}$ %	$\Delta\varepsilon_e$ %	$\Delta\sigma$ MN/m^2		
R-28-1	0.333	1.0	6	211	0.72	0.28	123	1066 (2)	Softened
R-28-2	0.333	4.0	1.5	277	3.69	0.31	135	307 (3) (195)	
R-28-3	0.333	1.0	6	233	0.75	0.25	107	4046 (2300)	
R-28-4	0.333	2.8	2.14	281	2.38	0.42	182	261 (245)	
R-28-5	0.333	1.2	5	268	0.81	0.39	168	1038 (1030)	
R-28-6	0.333	2.0	3	284	1.62	0.38	166	648 (350)	
R-28-7	0.333	1.5	4	298	1.06	0.44	190	667 (530)	

(1) N* values given in parentheses. (2) Appears to be premature failure.
(3) Experienced high compressive load on failure.

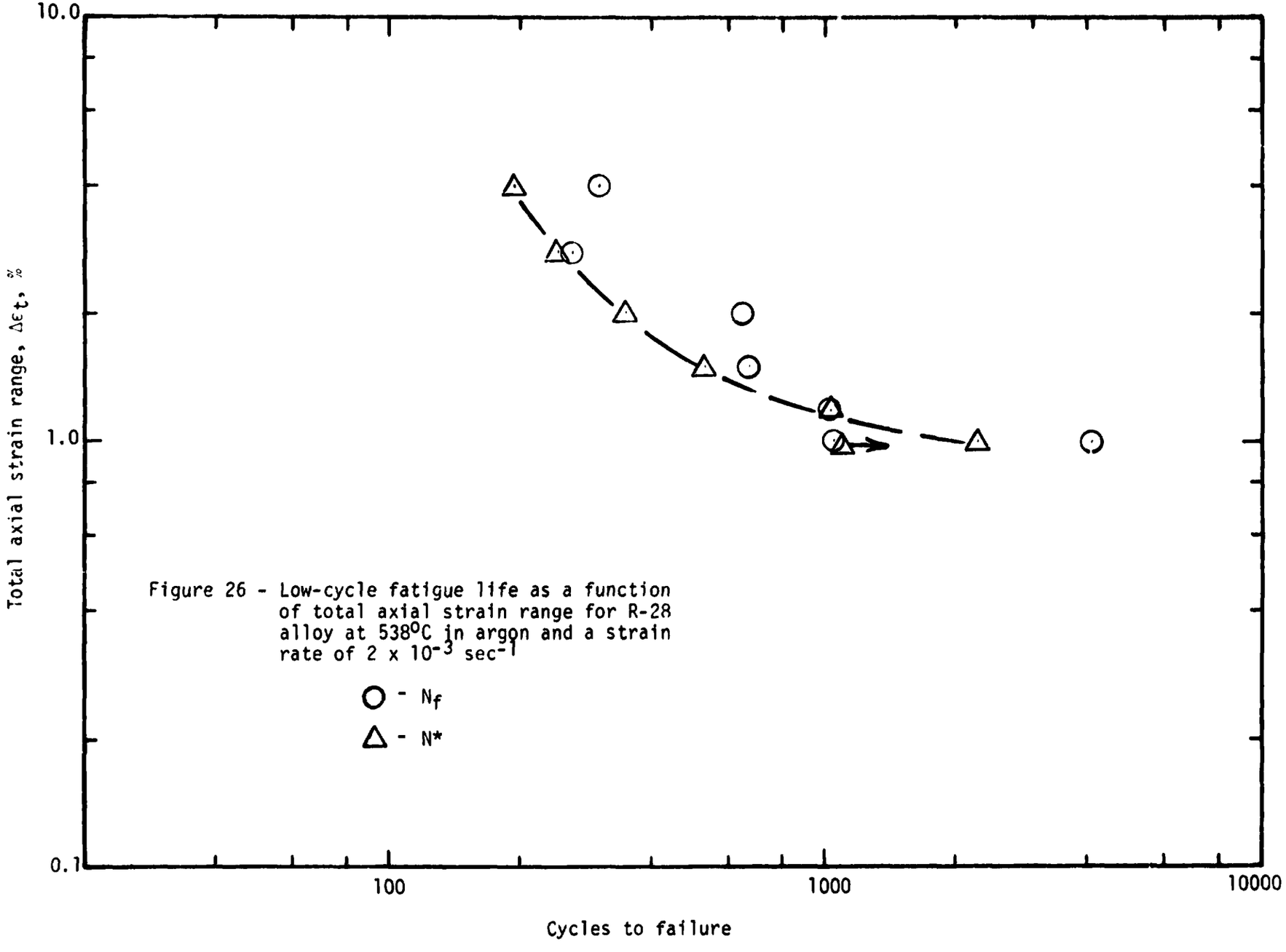

Figure 26 - Low-cycle fatigue life as a function of total axial strain range for R-28 alloy at 538°C in argon and a strain rate of 2×10^{-3} sec^{-1}

○ - N_f

△ - N*

PART IV - SHORT-TERM TENSILE AND LOW-CYCLE FATIGUE BEHAVIOR OF R-30, R-31 AND R-32 ALLOYS

Three different heat treatments of the R-28 alloy (see Table 1) were evaluated to a limited extent in short-term tensile and low-cycle fatigue tests at 538°C in argon. A summary of the short-term tensile results is presented in Table 14 to indicate slightly reduced yield and ultimate strengths for the R-30 and R-31 alloys compared to R-28. In the case of R-32 a significant reduction in strength was observed compared to the R-28 alloy. In terms of ductility (reduction in area) R-32 was comparable to R-28, R-31 exhibited about one-half the value for R-28, while the R-31 alloy exhibited a significant reduction below the R-28 value.

Tensile data generated by NASA-Lewis at room temperature and at liquid nitrogen temperature are included in Table 14 for comparison.

A summary of the low-cycle fatigue results for the R-30, R-31 and R-32 alloys is presented in Table 15. These data are compared in Figure 27 to indicate comparable behavior for the R-28, R-30 and R-32 alloys. In the case of the R-31 alloy, a noticeably lower fatigue life is exhibited compared to the other alloys. This appears to be consistent with the much lower ductility exhibited by the material (see Table 14).

Table 14 - Short-Term Tensile Properties of R-30, R-31 and R-32 Alloys

Diametral Extensometer				Hourglass-Shaped Specimens	
Specimen Number	Temp. °C	Strain Rate, sec^{-1}	0.2% Offset Yield Strength, MN/m^2	Ultimate Tensile Strength, MN/m^2	Reduction in Area, %
R-30-3	538 (1)	2×10^{-3}	125	130	54
R-31-3	538 (1)	2×10^{-3}	105	114	12
R-32-3	538 (1)	2×10^{-3}	58	64	72
R-30-5	R.T. (2)	2×10^{-3}	-	316	89
R-31-5	R.T. (2)	2×10^{-3}	-	201	85
R-32-5	R.T. (2)	2×10^{-3}	-	219	90
R-30-4	-196 (3)	2×10^{-3}	-	472	75
R-31-4	-196 (3)	2×10^{-3}	-	313	82
R-32-4	-196 (3)	2×10^{-3}	-	368	74

(1)-Tested in argon. (2)-Tested in air at NASA-Lewis. (3) Tested in liquid nitrogen at NASA-Lewis.

Table 15 - Low-Cycle Fatigue Results for R-30, R-31 and R-32 Alloys Tested in Argon at 538°C Using a Strain Rate of 2×10^{-3} sec^{-1}

R-30, R-31 and R-32 Alloys

Axial Strain Control
A-ratio of infinity
$E = 4.34 \times 10^4$ MN/m^2

Spec. No.	Poisson's Ratio	Total Strain Range, %	Freq. cpm	Stress Range at Start, MN/m^2	at $N_f/2$			N_f, Cycles to Failure (1)	Remarks
					$\Delta\varepsilon_{inel}$ %	$\Delta\varepsilon_e$ %	$\Delta\sigma$ MN/m^2		
R-30-1	0.333	2.0	3	256	1.6	0.4	173	290 (290)	Softened
R-30-2	0.333	1.0	6	256	0.63	0.37	161	1123 (1000)	↓
R-31-1	0.333	2.0	3	207	1.56	0.44	193	56 (40)	
R-31-2	0.333	1.0	6	218	0.62	0.38	163	381 (240)	
R-32-1	0.333	1.0	6	96	0.78	0.22	94	2971 (1700)	Slight hardening and then slight softening
R-32-2	0.333	2.0	3	111	1.76	0.24	104	1074 (600)	

(1) N* values in parentheses.

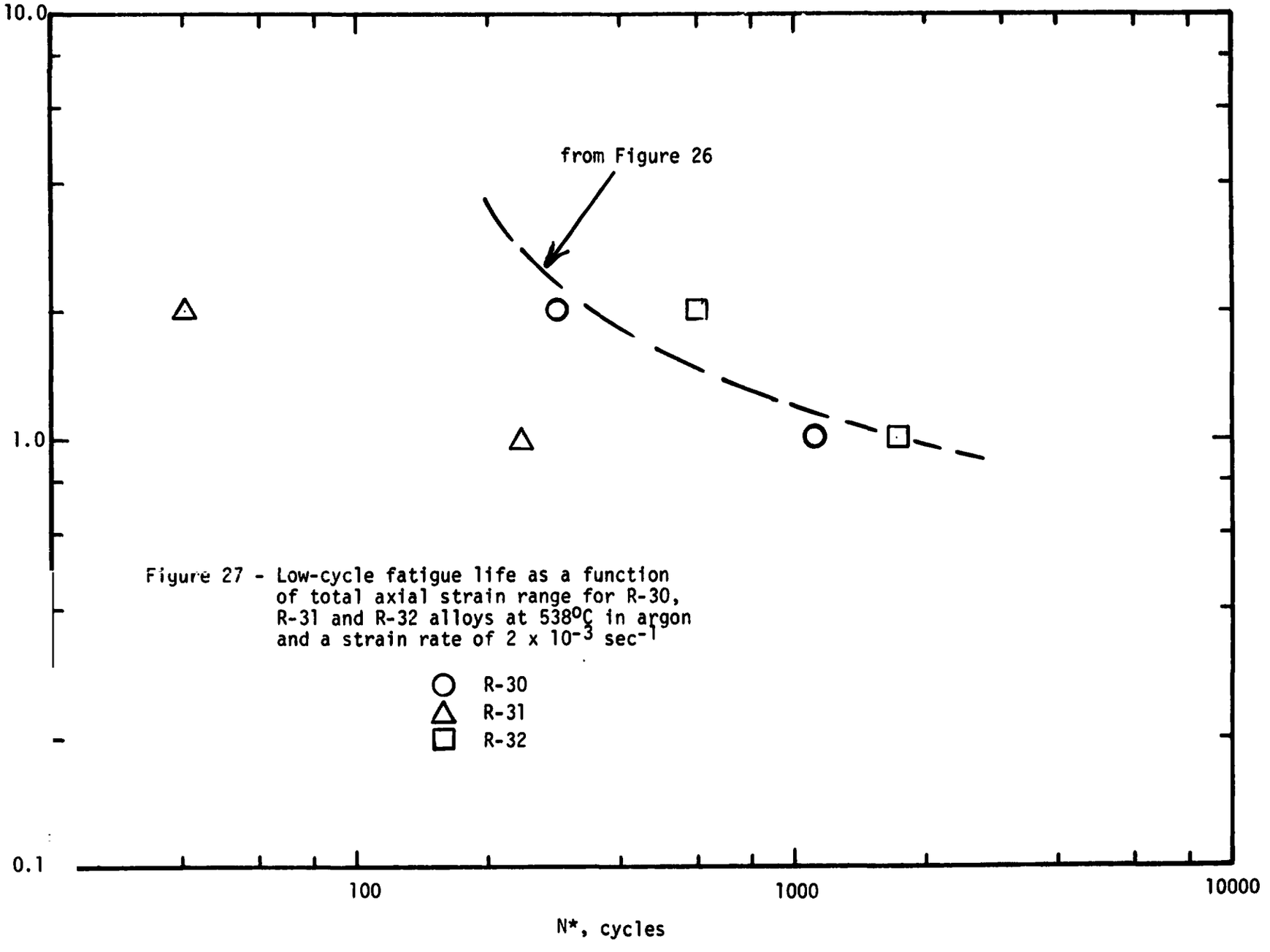

Figure 27 - Low-cycle fatigue life as a function of total axial strain range for R-30, R-31 and R-32 alloys at 538°C in argon and a strain rate of 2×10^{-3} sec^{-1}

PART V - PLOTS OF LOAD RANGE VERSUS CYCLES FOR LOW-CYCLE FATIGUE TESTS

For each test, the continuous load records were analyzed to yield plots of load range as a function of the number of cycles throughout the test. In general, the first and second cycle information was read from the x-y traces (stress-strain hysteresis loops) and these points were plotted. Then this plotting was continued for subsequent cycles using load range information as read from the strip-chart recordings. A sufficient number of data points was selected throughout the fatigue life to define a fairly smooth pattern for the plot of load range versus cycles. Such plots are presented in this section for the following:

Material	No. of Tests
R-2	6
R-24	20
R-9	7
R-27	8
R-28	7
R-30	2
R-31	2
R-32	2

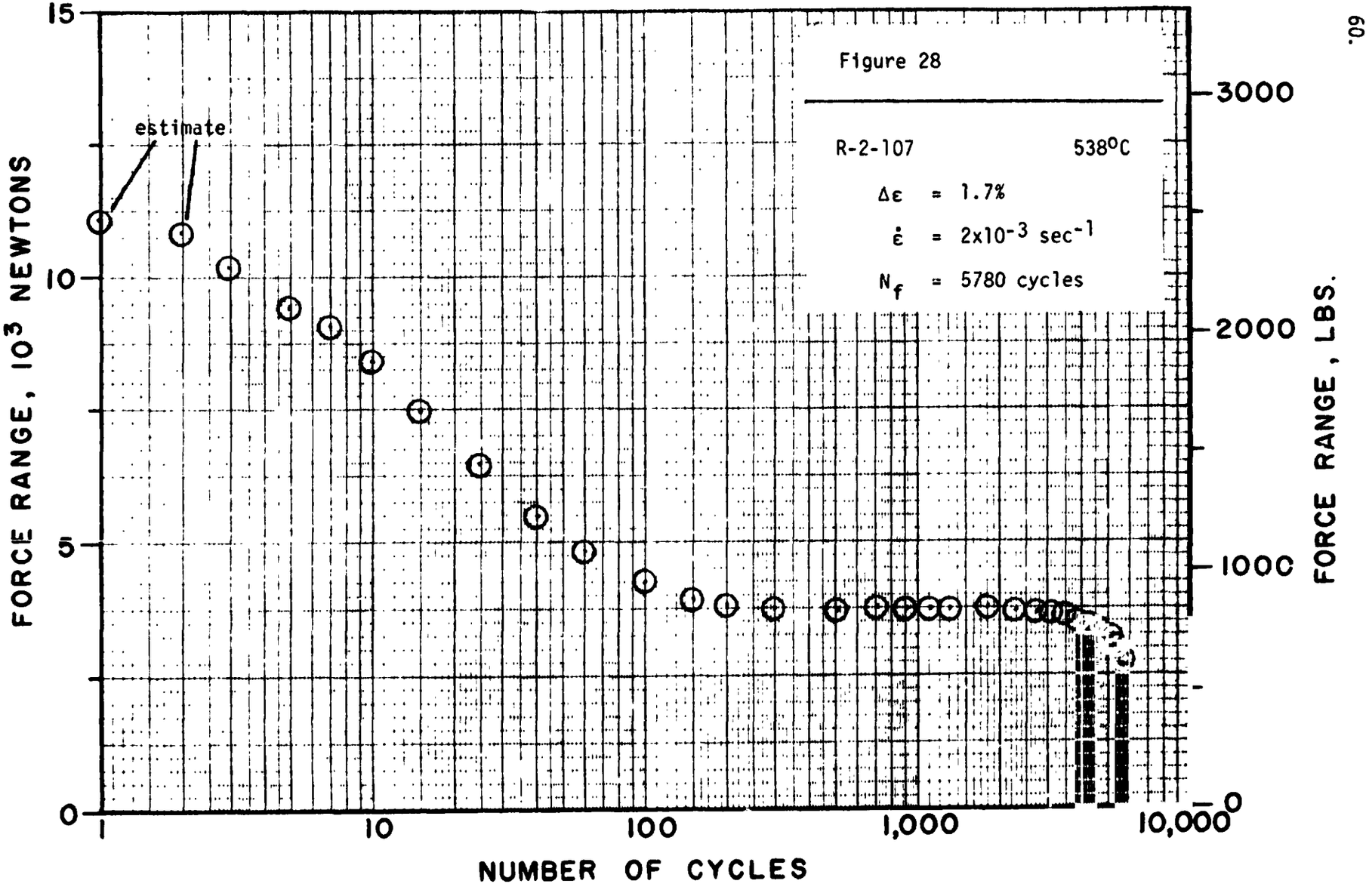
Figure 28
R-2-107
538°C
Δε = 1.7%
ε̇ = 2x10-3 sec-1
Nf = 5780 cycles
estimate
FORCE RANGE, 10³ NEWTONS
FORCE RANGE, LBS.
NUMBER OF CYCLES
15
10
5
0
3000
2000
1000
0
1
10
100
1,000
10,000

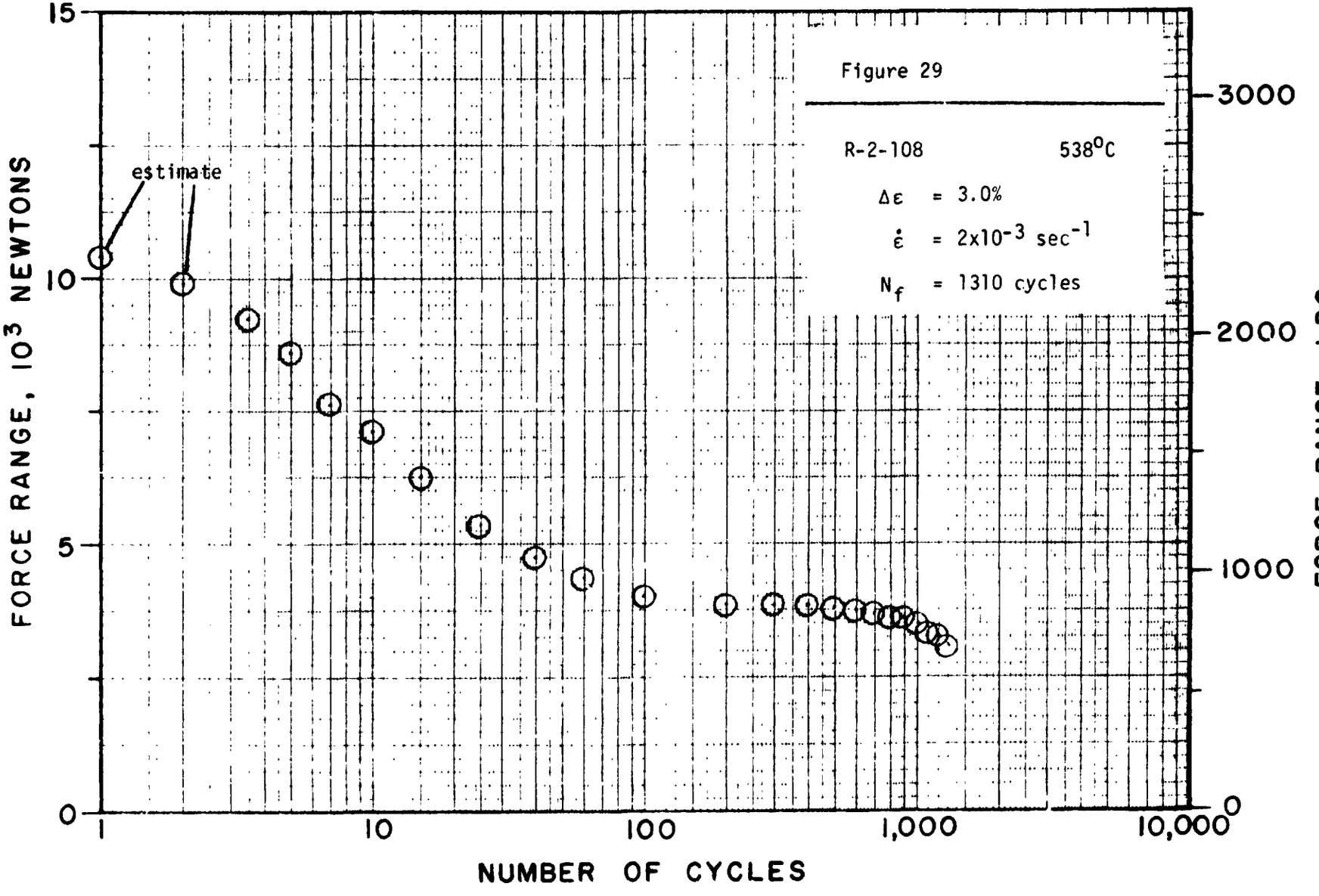
Figure 29
R-2-108
538°C
Δε = 3.0%
ε̇ = 2x10-3 sec-1
Nf = 1310 cycles
estimate
FORCE RANGE, 10³ NEWTONS
FORCE RANGE, LBS.
NUMBER OF CYCLES
15
10
5
0
3000
2000
1000
0
1
10
100
1,000
10,000

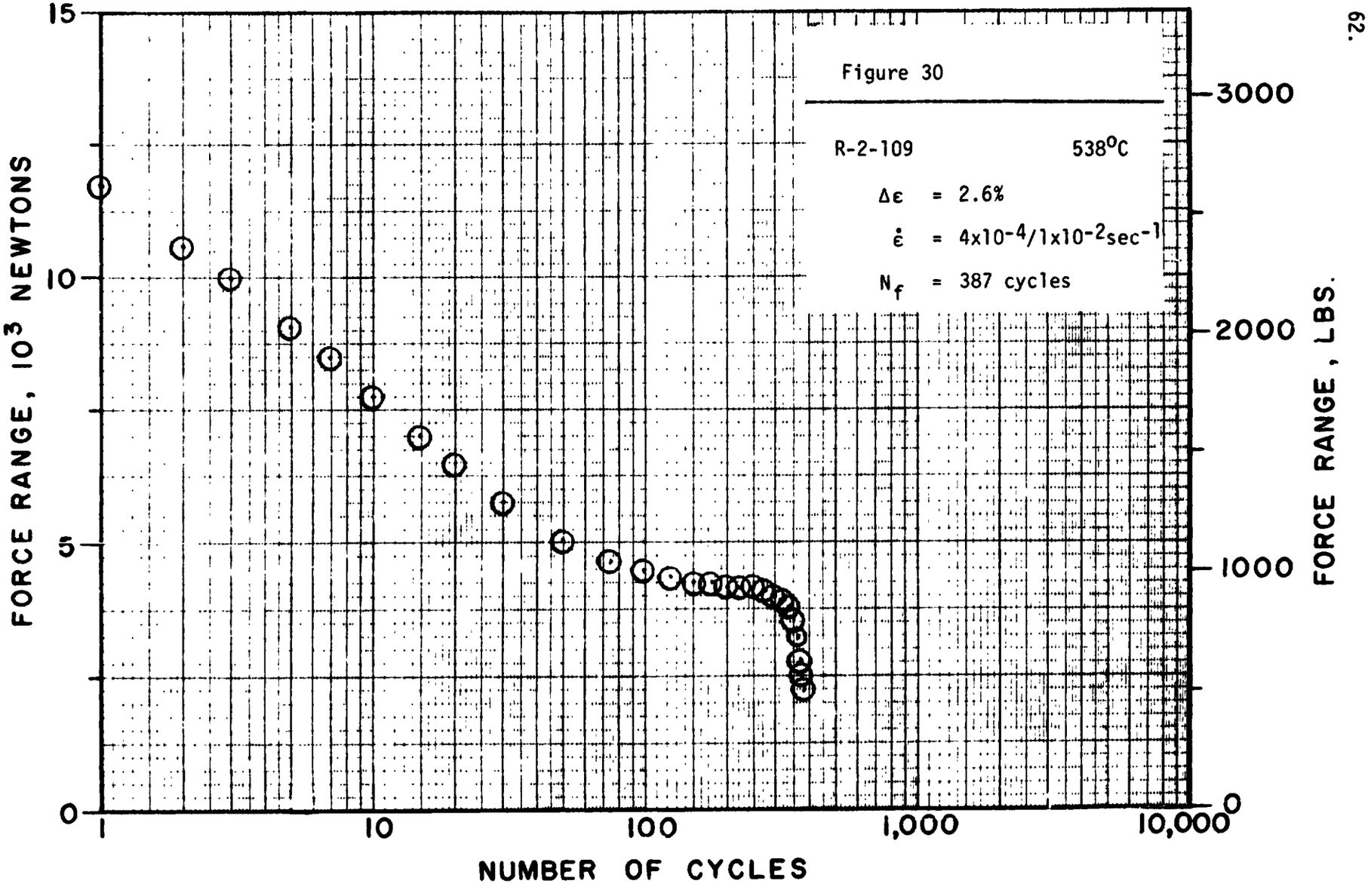
Figure 30
R-2-109
538°C
Δε = 2.6%
ε̇ = 4x10-4/1x10-2sec-1
Nf = 387 cycles
FORCE RANGE, 10³ NEWTONS
FORCE RANGE, LBS.
NUMBER OF CYCLES
15
10
5
0
3000
2000
1000
0
1
10
100
1,000
10,000

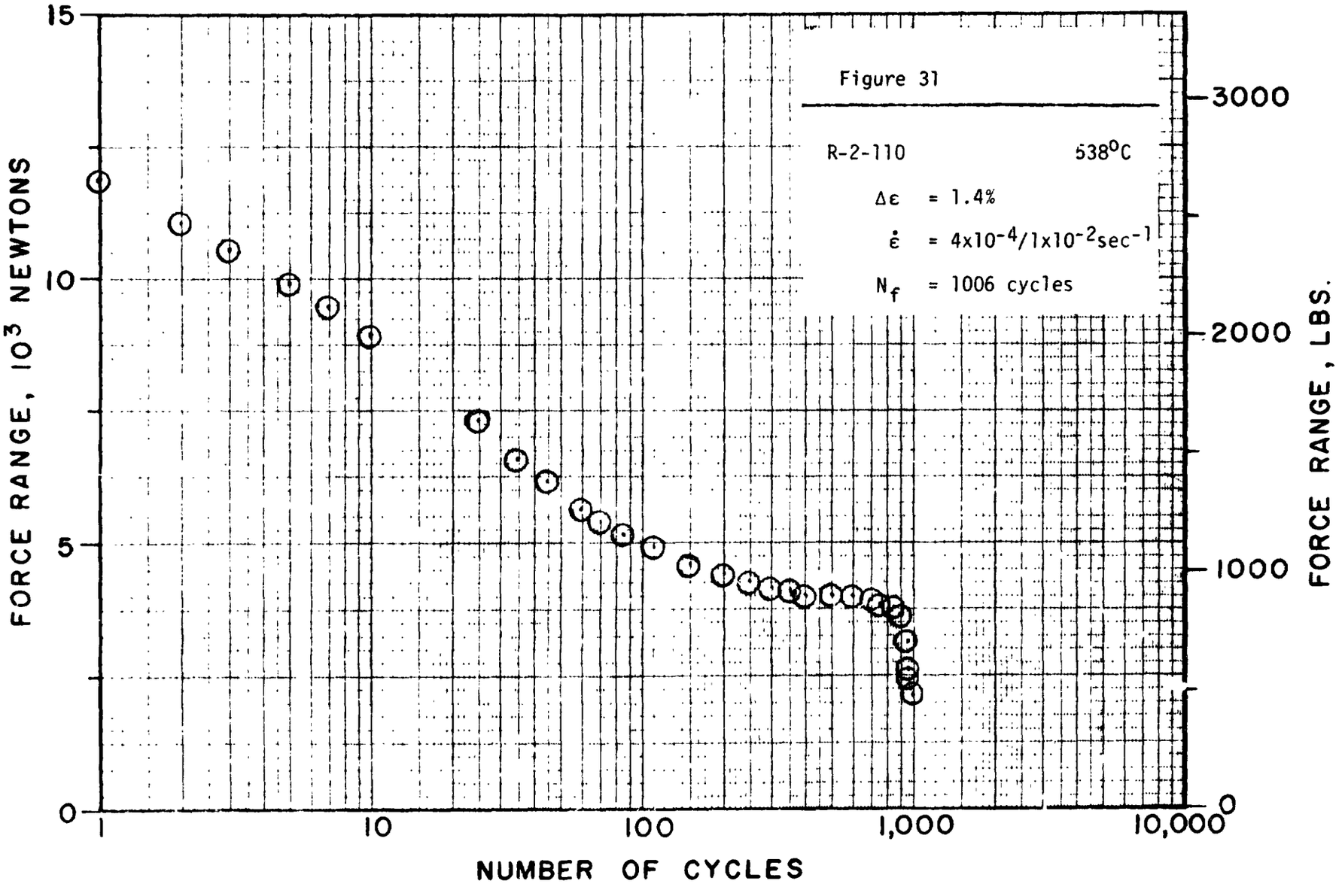
Figure 31
R-2-110
538°C
Δε = 1.4%
ε̇ = 4x10-4/1x10-2sec-1
Nf = 1006 cycles
FORCE RANGE, 10³ NEWTONS
FORCE RANGE, LBS.
NUMBER OF CYCLES
15
10
5
0
3000
2000
1000
0
1
10
100
1,000
10,000

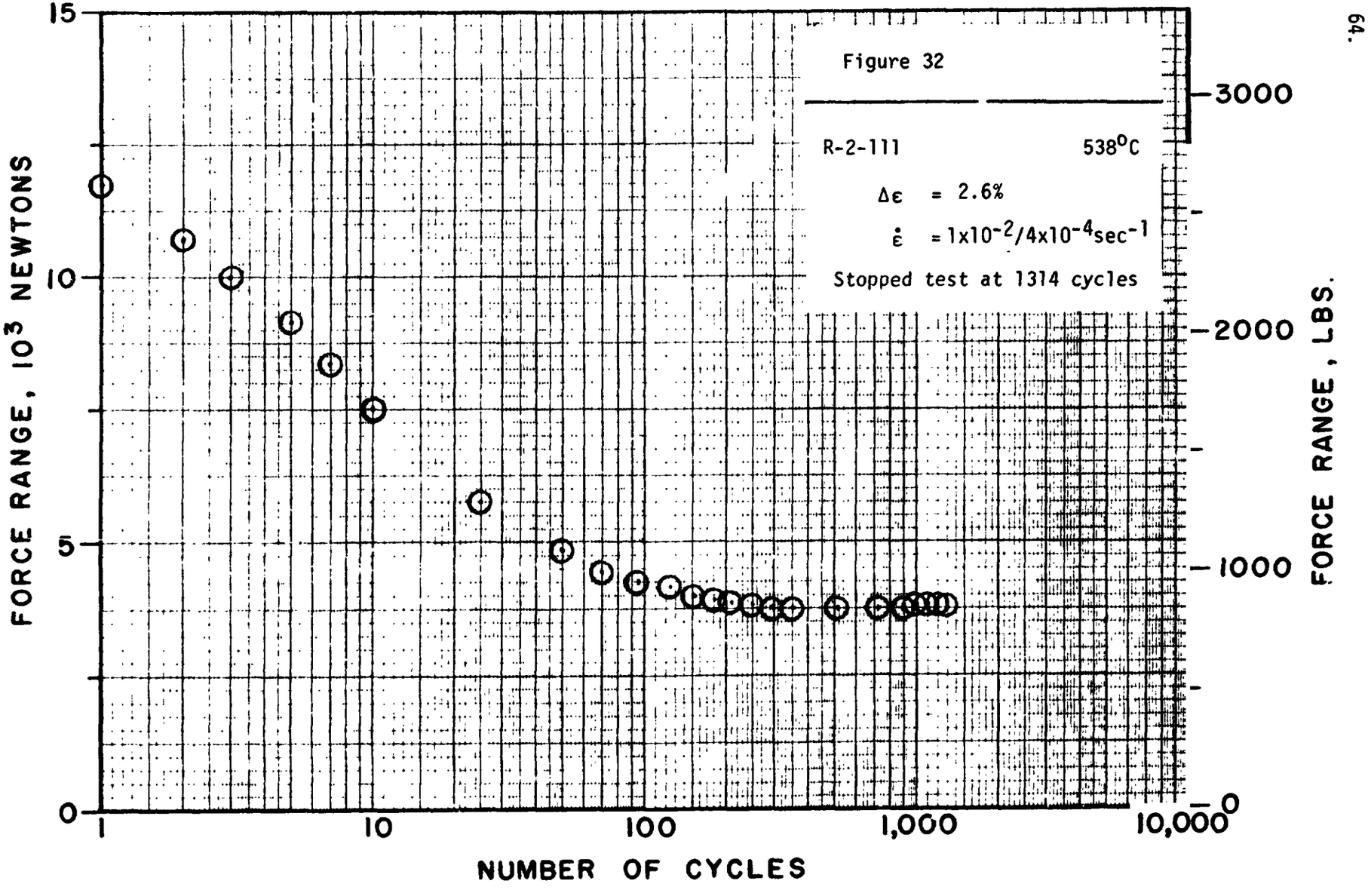
Figure 32
R-2-111
538°C
Δε = 2.6%
ε̇ = 1x10-2/4x10-4sec-1
Stopped test at 1314 cycles
FORCE RANGE, 10³ NEWTONS
FORCE RANGE, LBS.
NUMBER OF CYCLES
15
10
5
0
3000
2000
1000
0
1
10
100
1,000
10,000

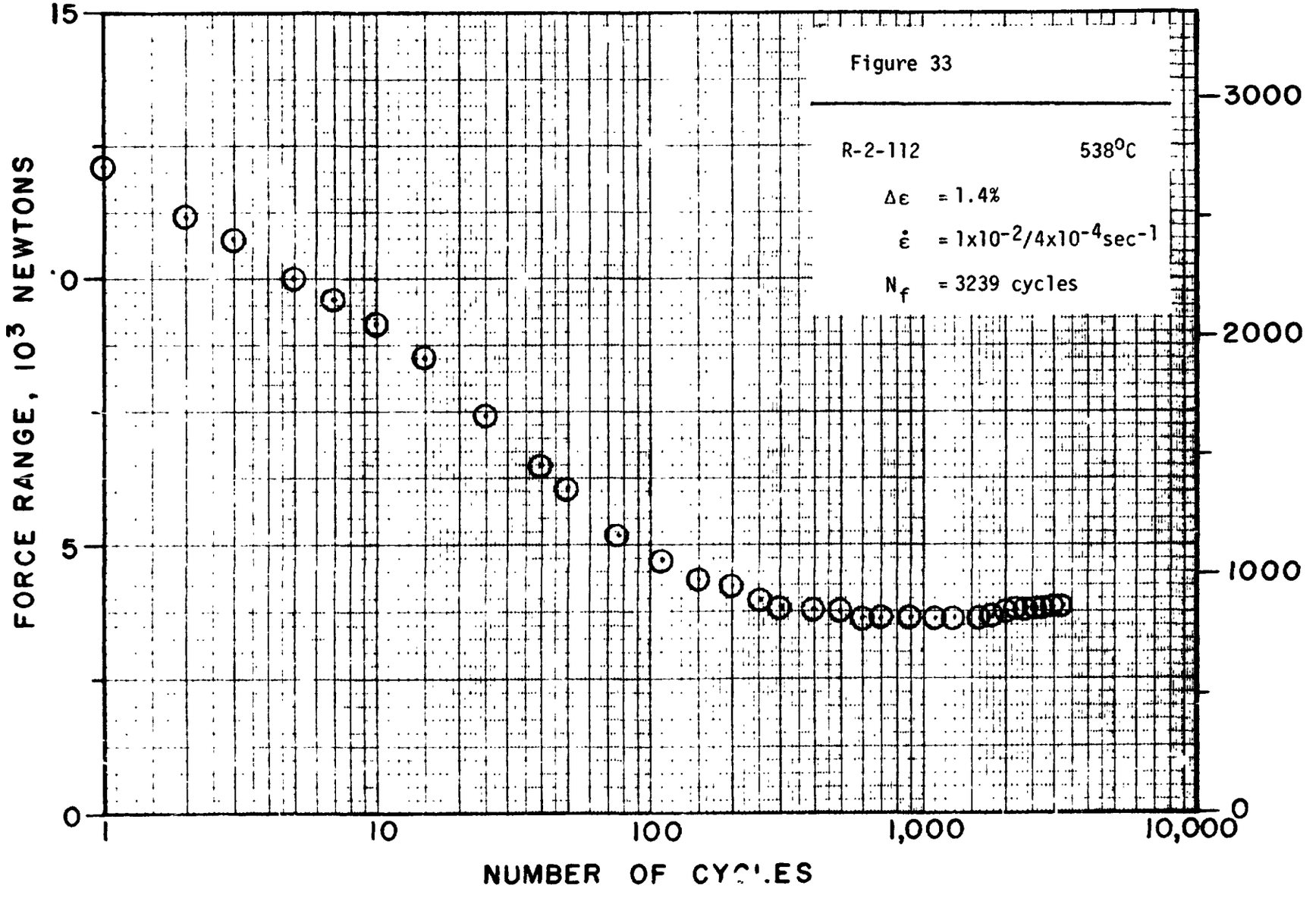
Figure 33
R-2-112
538°C
Δε = 1.4%
ε̇ = 1x10-2/4x10-4sec-1
Nf = 3239 cycles
FORCE RANGE, 10³ NEWTONS
FORCE RANGE, LBS.
NUMBER OF CYCLES
15
0
5
0
1
10
100
1,000
10,000
3000
2000
1000
0

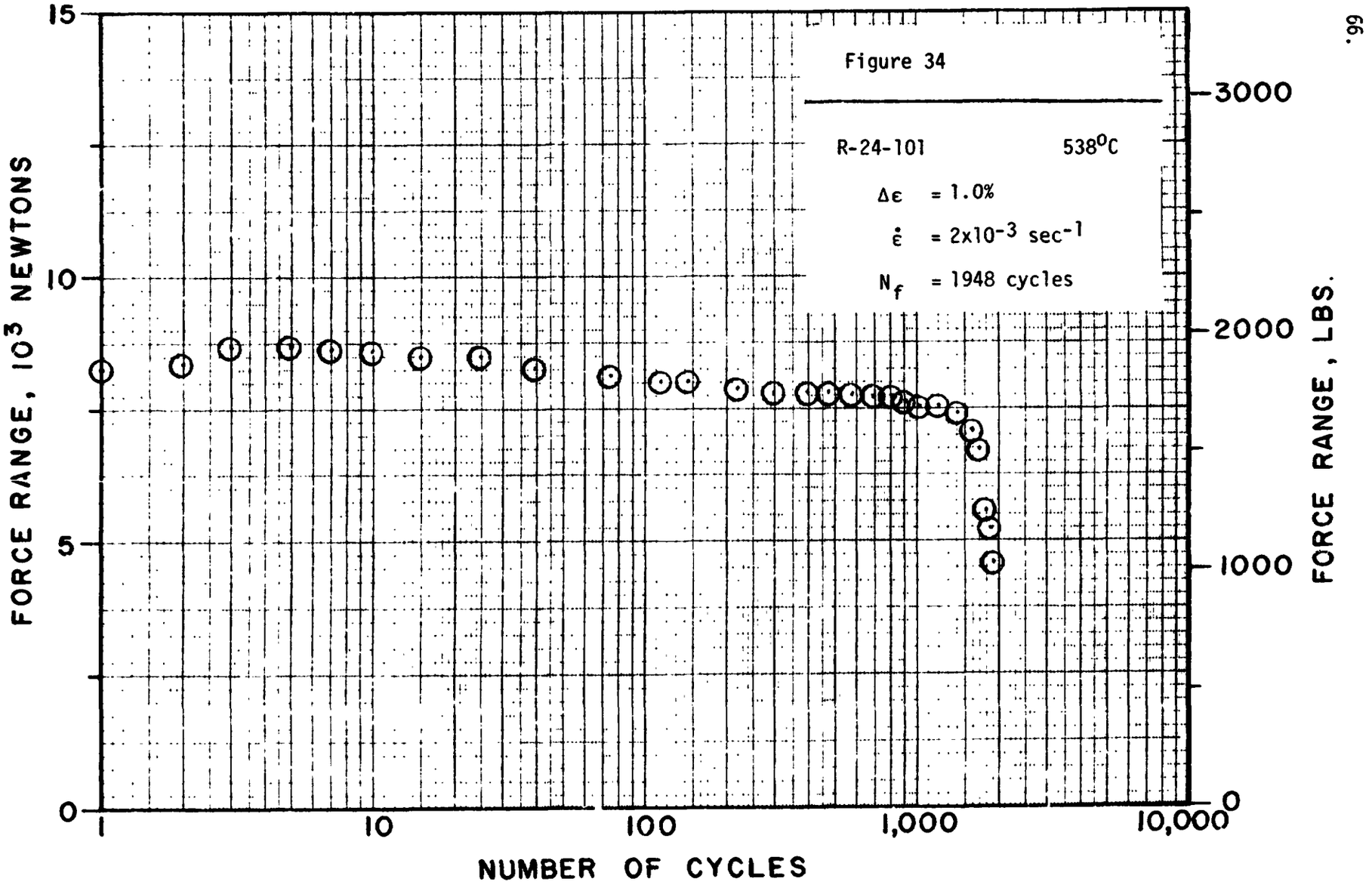
Figure 34
R-24-101
538°C
Δε = 1.0%
ε̇ = 2x10-3 sec-1
Nf = 1948 cycles
FORCE RANGE, 10³ NEWTONS
FORCE RANGE, LBS.
NUMBER OF CYCLES
15
10
5
0
3000
2000
1000
0
1
10
100
1,000
10,000

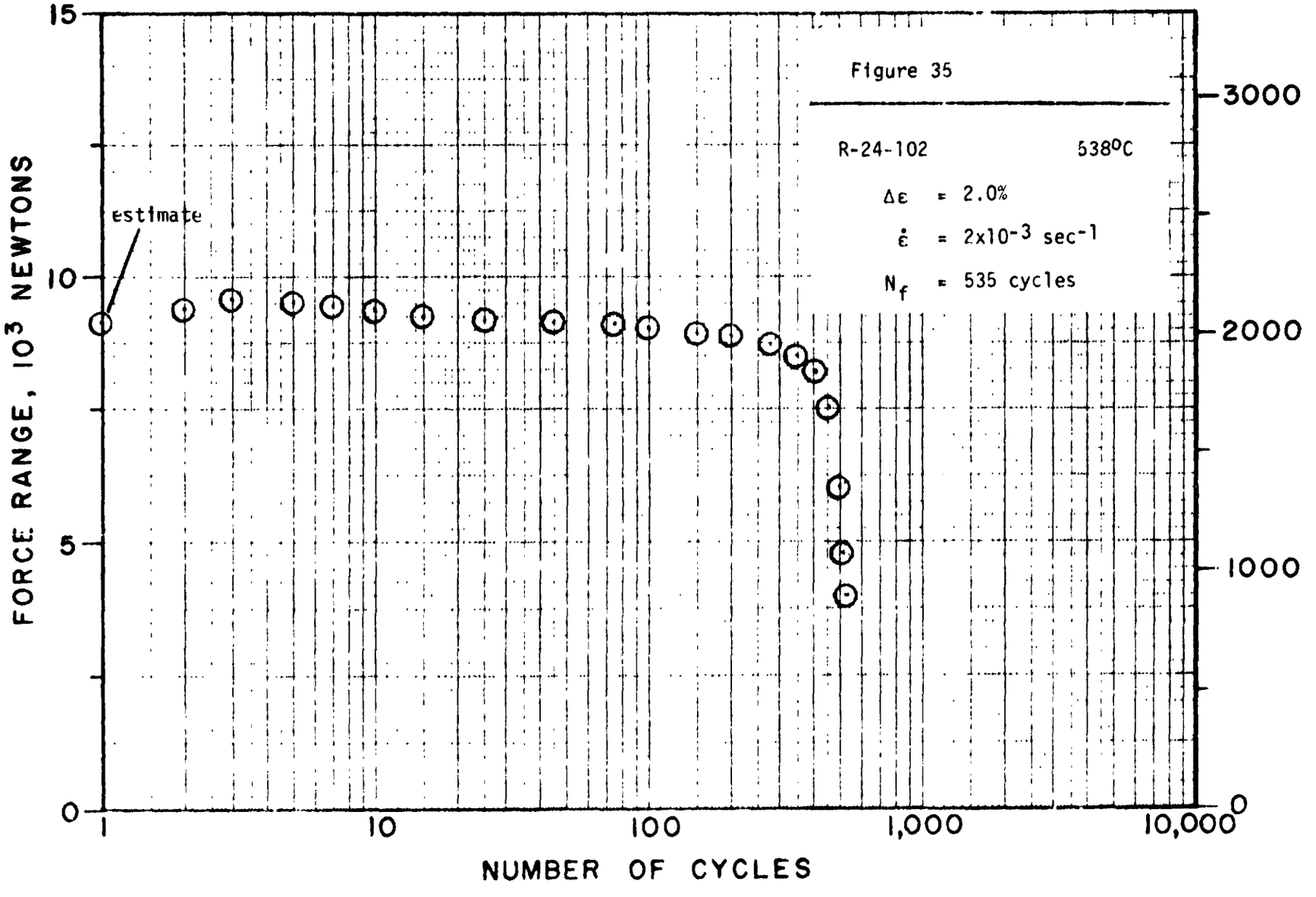
Figure 35
R-24-102
538°C
Δε = 2.0%
ε̇ = 2x10-3 sec-1
Nf = 535 cycles
estimate
FORCE RANGE, 10³ NEWTONS
FORCE RANGE, LBS.
NUMBER OF CYCLES
15
10
5
0
3000
2000
1000
0
1
10
100
1,000
10,000

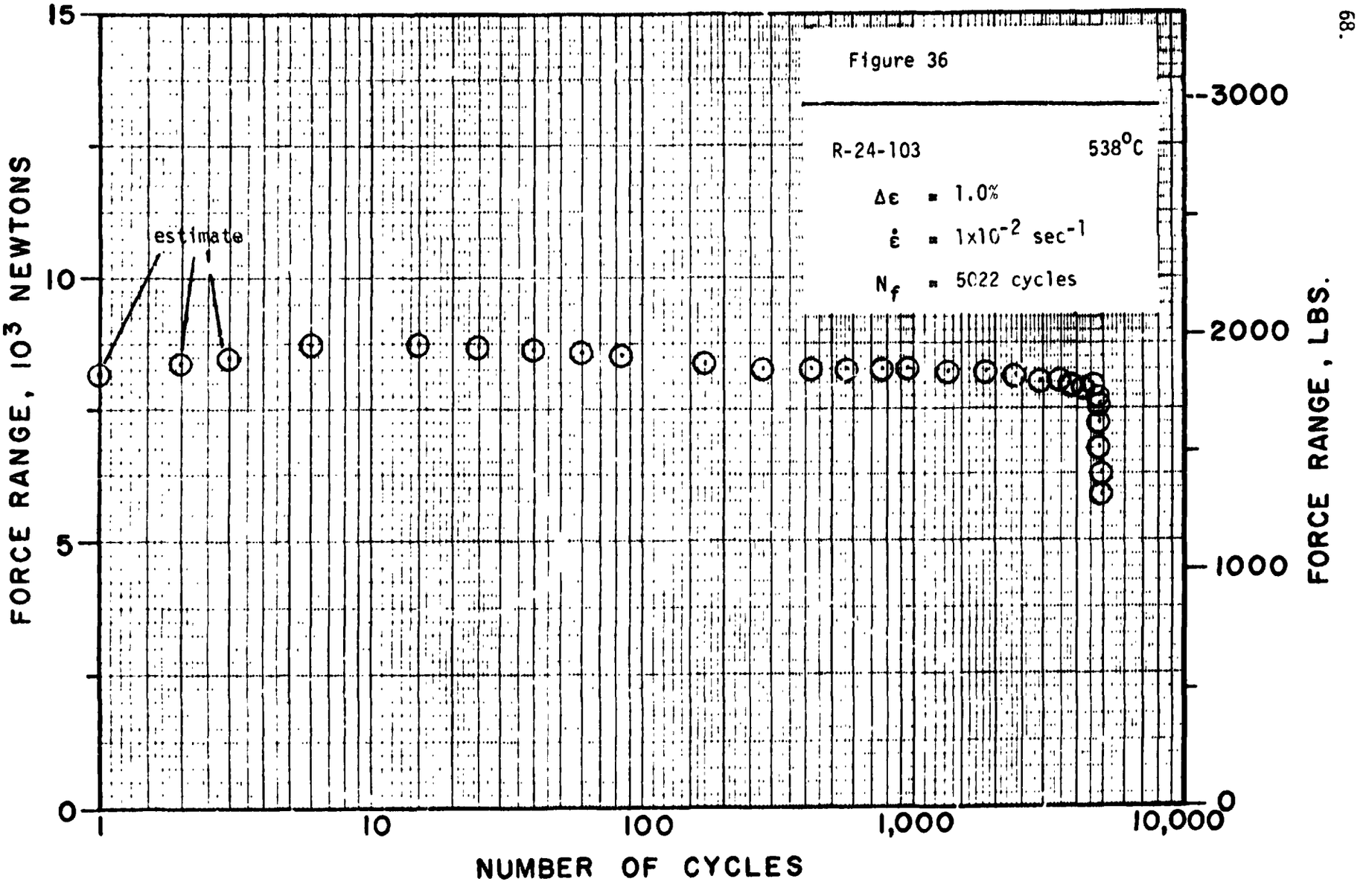
Figure 36
R-24-103
538°C
Δε = 1.0%
ε̇ = 1x10⁻² sec⁻¹
N_f = 5022 cycles
estimate
FORCE RANGE, 10³ NEWTONS
FORCE RANGE, LBS.
NUMBER OF CYCLES
15
10
5
0
3000
2000
1000
0
1
10
100
1,000
10,000

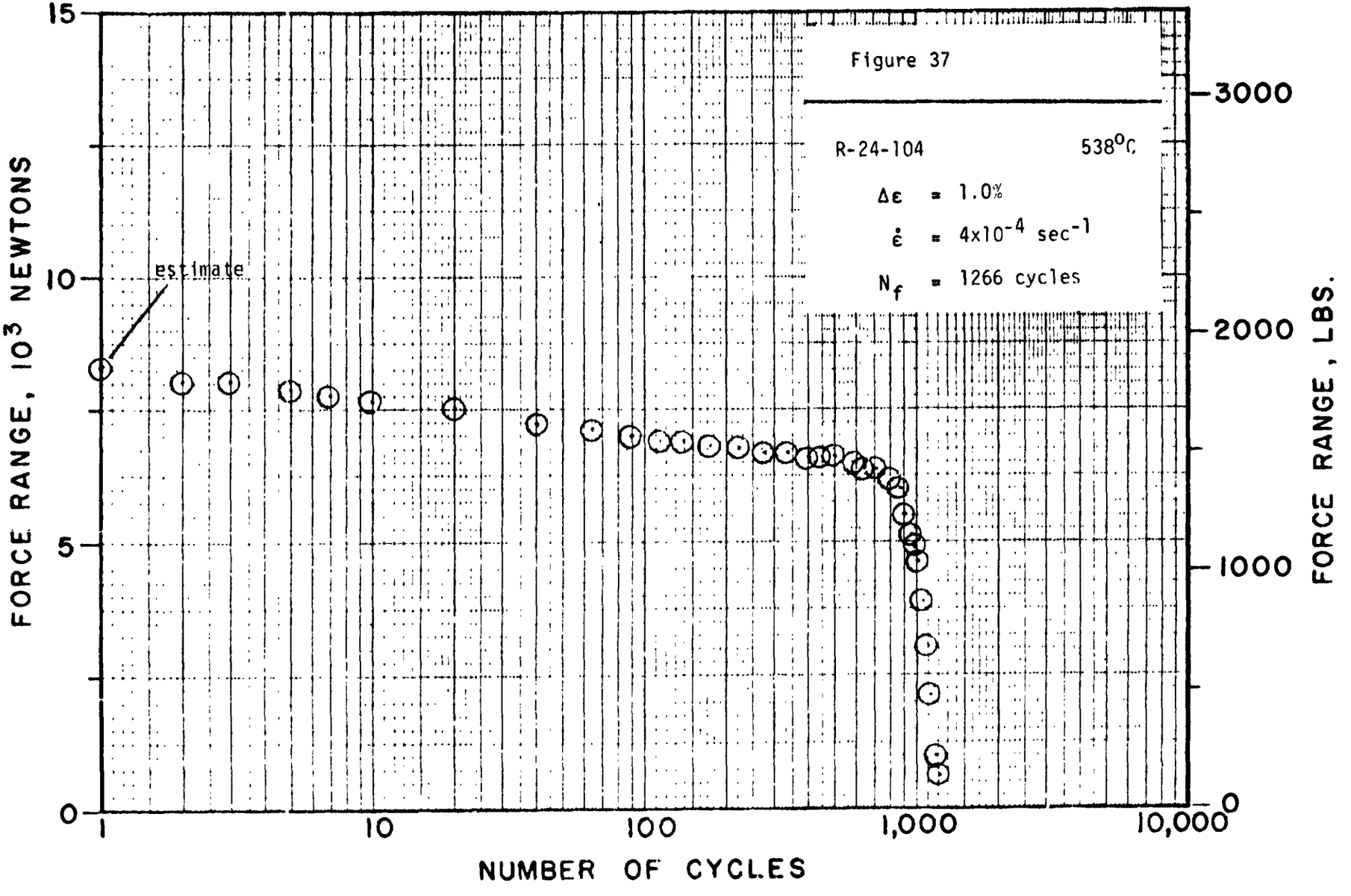
Figure 37
R-24-104
538°C
Δε = 1.0%
ε̇ = 4x10⁻⁴ sec⁻¹
N_f = 1266 cycles
estimate
FORCE RANGE, 10³ NEWTONS
FORCE RANGE, LBS.
NUMBER OF CYCLES
15
10
5
0
3000
2000
1000
0
1
10
100
1,000
10,000

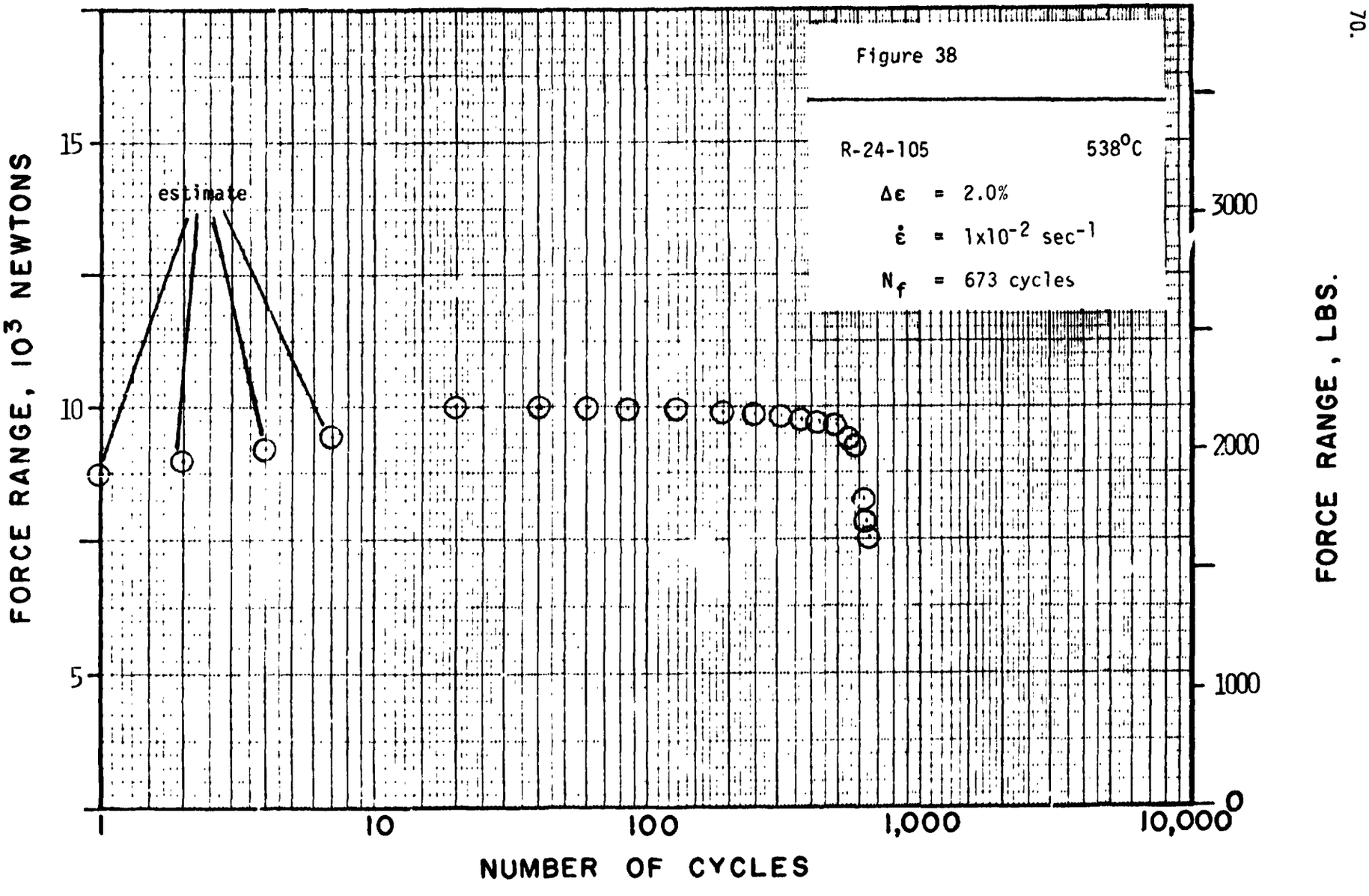
Figure 38
R-24-105
538°C
Δε = 2.0%
ε̇ = 1x10⁻² sec⁻¹
N_f = 673 cycles
estimate
FORCE RANGE, 10³ NEWTONS
15
10
5
FORCE RANGE, LBS.
3000
2000
1000
0
1
10
100
1,000
10,000
NUMBER OF CYCLES

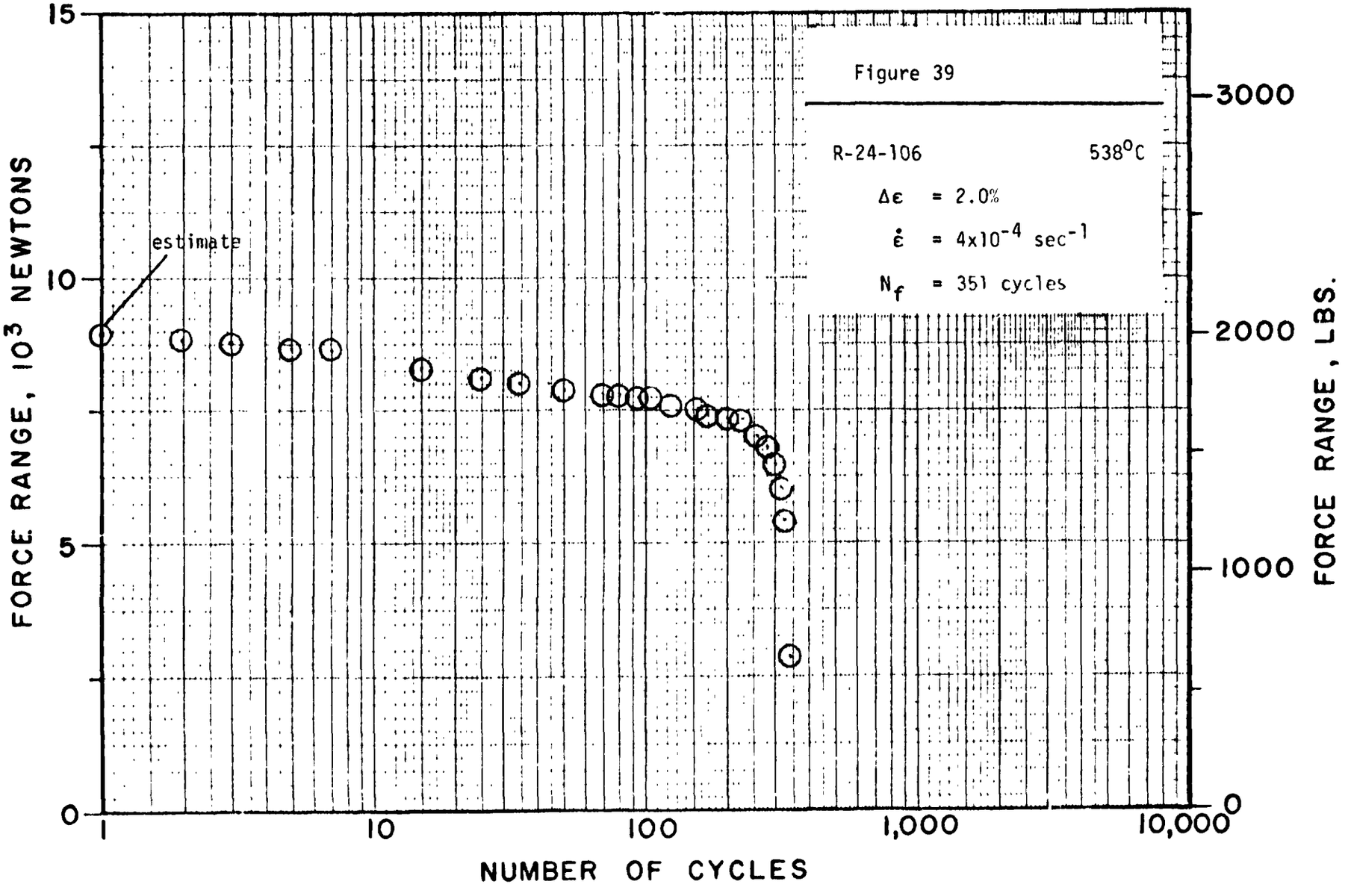
Figure 39
R-24-106
538°C
Δε = 2.0%
ε̇ = 4x10^-4 sec^-1
N_f = 351 cycles
estimate
FORCE RANGE, 10^3 NEWTONS
FORCE RANGE, LBS.
NUMBER OF CYCLES
0
5
10
15
0
1000
2000
3000
1
10
100
1,000
10,000

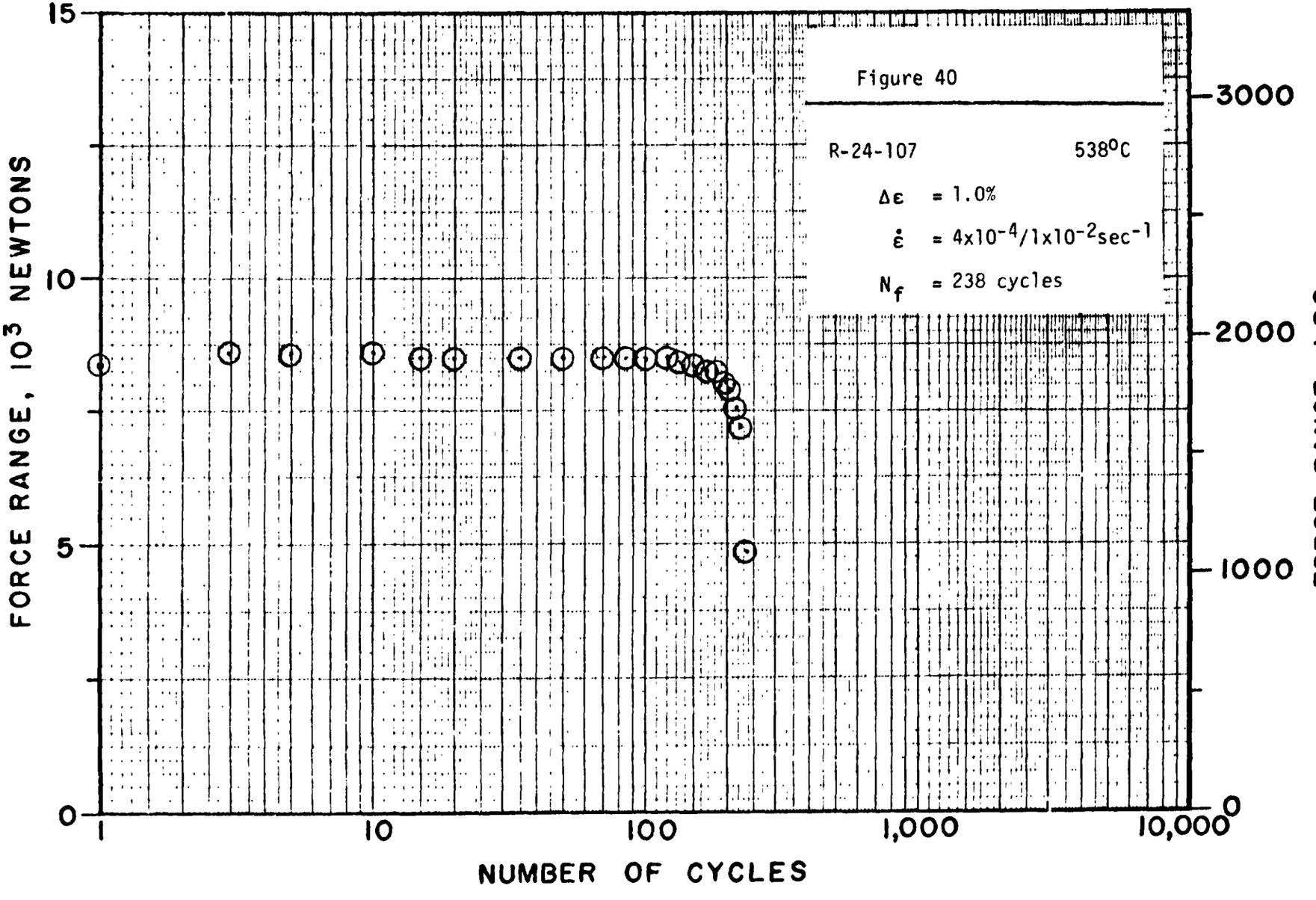
Figure 40
R-24-107
538°C
Δε = 1.0%
ε̇ = 4x10⁻⁴/1x10⁻²sec⁻¹
N_f = 238 cycles
FORCE RANGE, 10³ NEWTONS
FORCE RANGE, LBS.
NUMBER OF CYCLES
15
10
5
0
3000
2000
1000
0
1
10
100
1,000
10,000

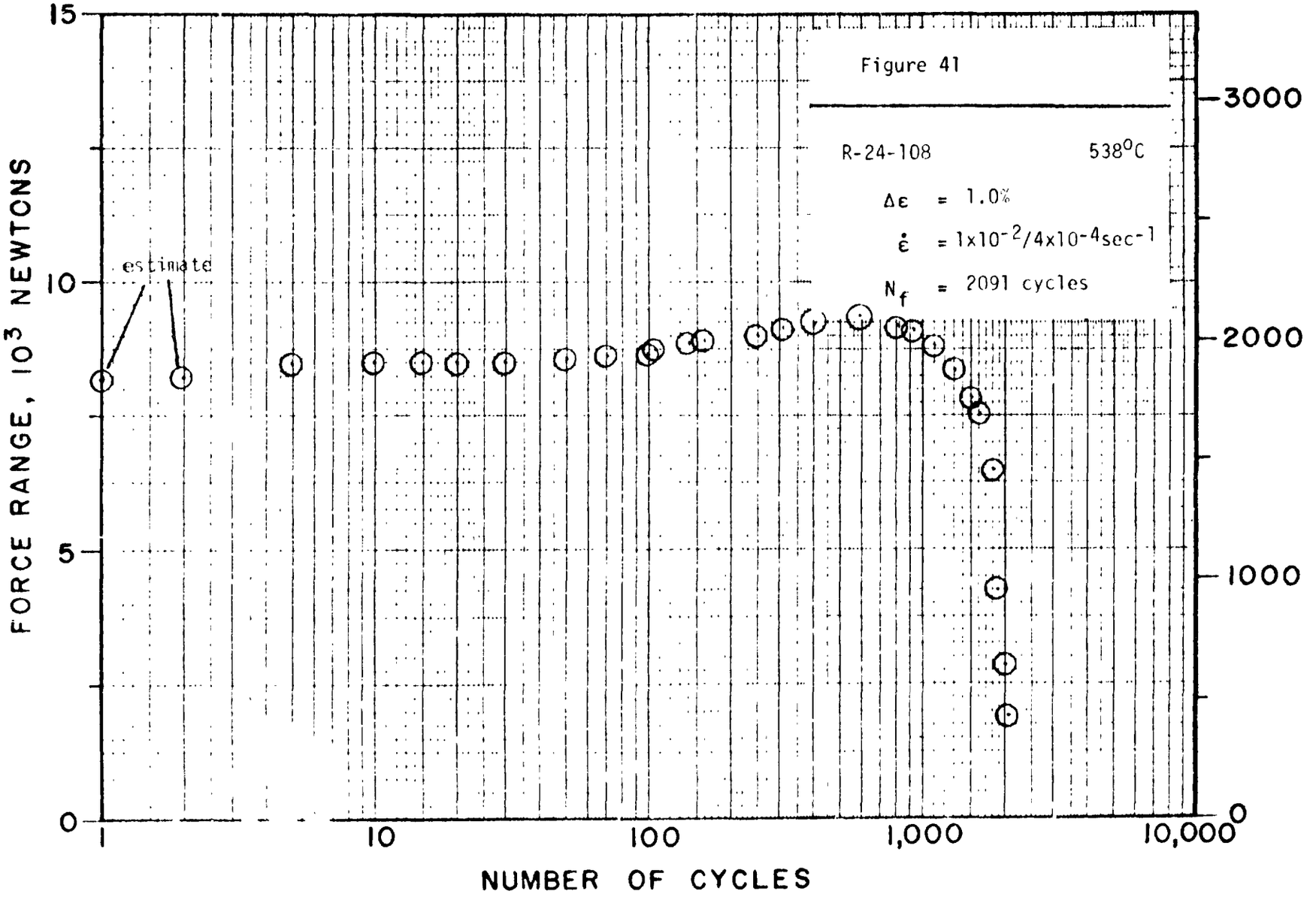
Figure 41
R-24-108
538°C
Δε = 1.0%
ε̇ = 1x10⁻²/4x10⁻⁴sec⁻¹
N_f = 2091 cycles
estimate
FORCE RANGE, 10³ NEWTONS
FORCE RANGE, LBS.
NUMBER OF CYCLES
0
5
10
15
1
10
100
1,000
10,000
0
1000
2000
3000

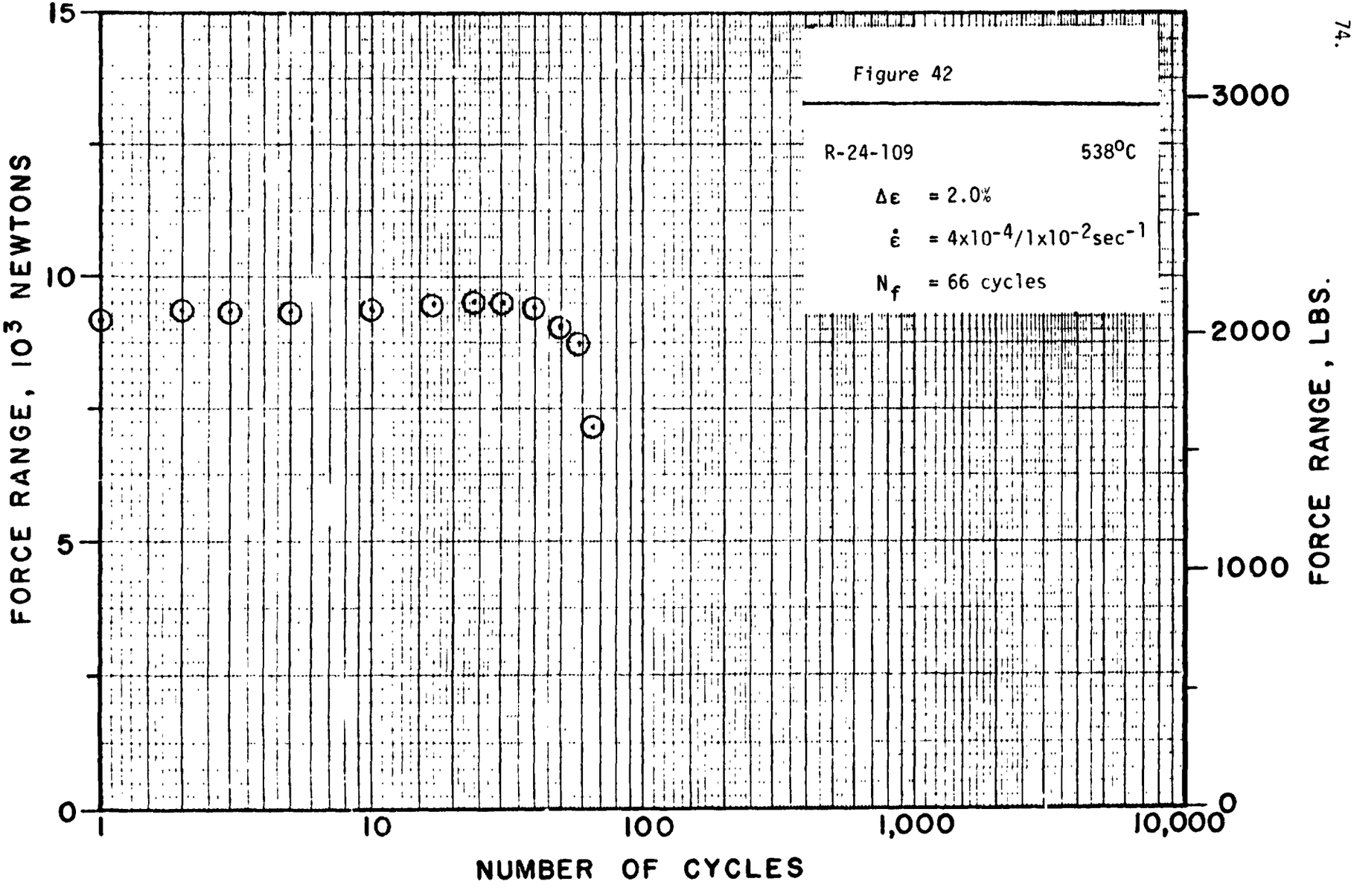
Figure 42
R-24-109
538°C
Δε = 2.0%
ε̇ = 4x10-4/1x10-2sec-1
Nf = 66 cycles
FORCE RANGE, 10³ NEWTONS
FORCE RANGE, LBS.
NUMBER OF CYCLES
15
10
5
0
3000
2000
1000
0
1
10
100
1,000
10,000

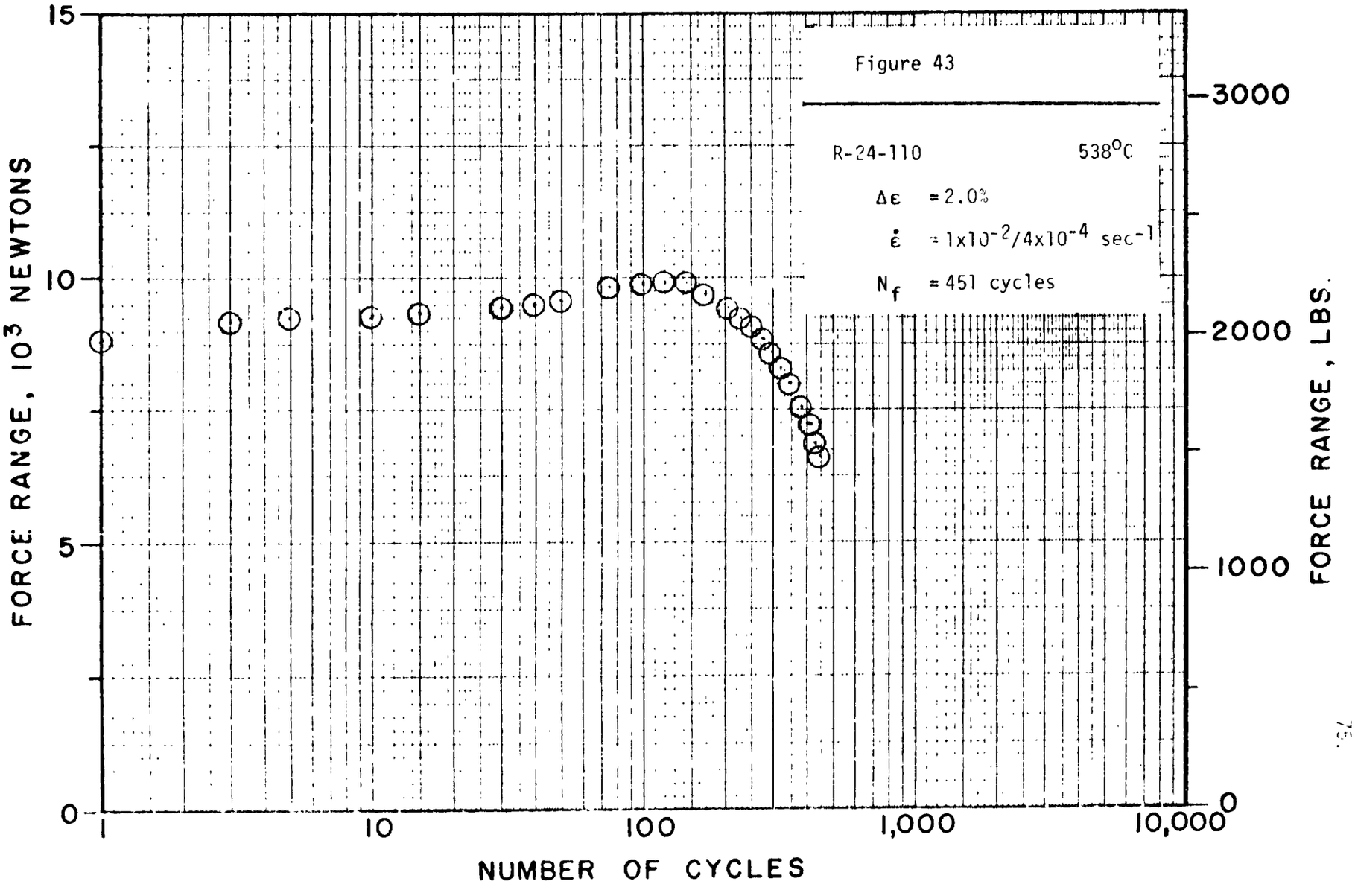
Figure 43
R-24-110
538°C
Δε = 2.0%
ε̇ = 1x10⁻²/4x10⁻⁴ sec⁻¹
N_f = 451 cycles
FORCE RANGE, 10³ NEWTONS
FORCE RANGE, LBS.
NUMBER OF CYCLES
0
5
10
15
1
10
100
1,000
10,000
0
1000
2000
3000

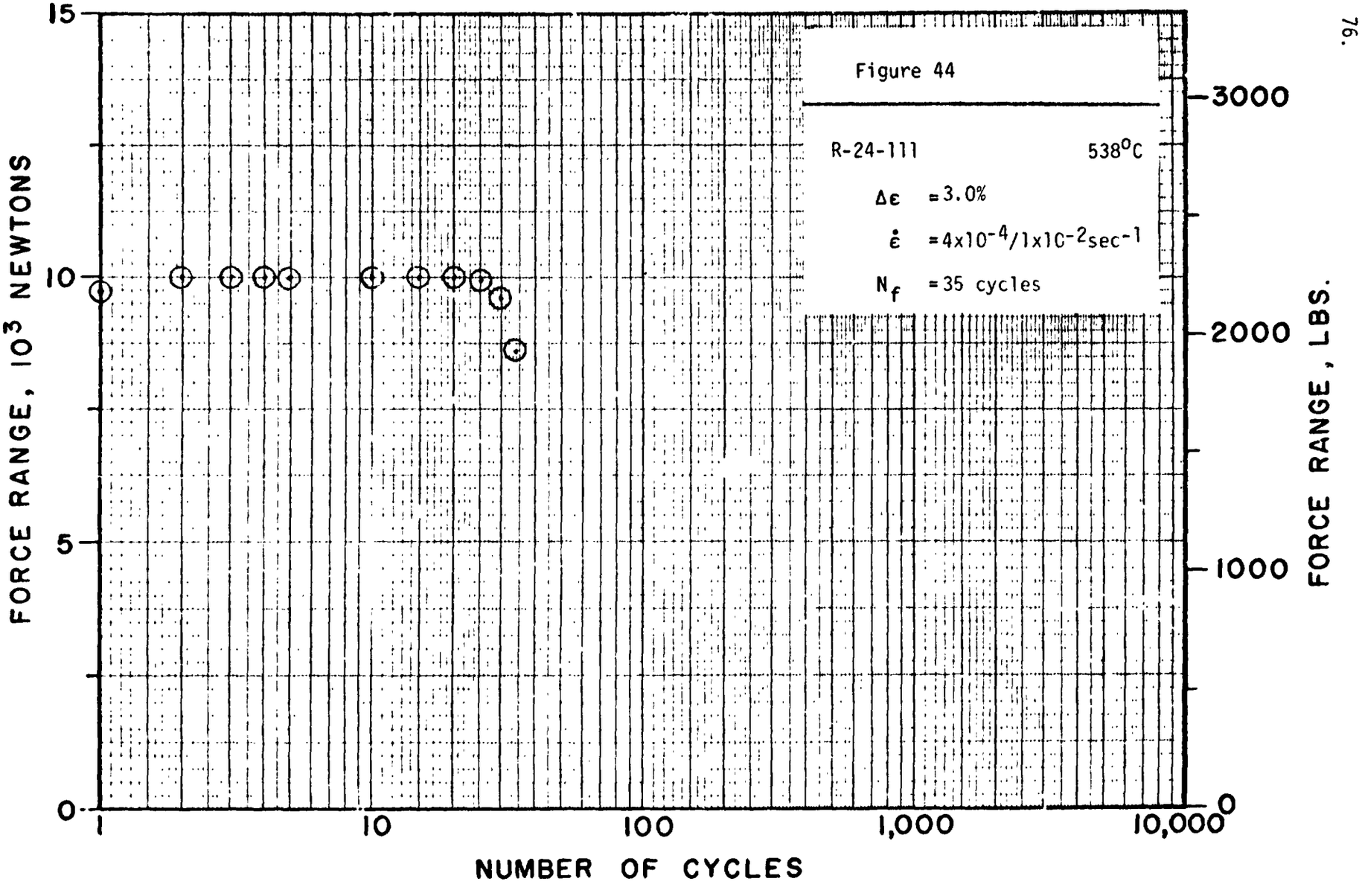
Figure 44
R-24-111
538°C
Δε =3.0%
ε̇ =4x10-4/1x10-2sec-1
Nf =35 cycles
15
10
5
0
FORCE RANGE, 10³ NEWTONS
3000
2000
1000
0
FORCE RANGE, LBS.
1
10
100
1,000
10,000
NUMBER OF CYCLES

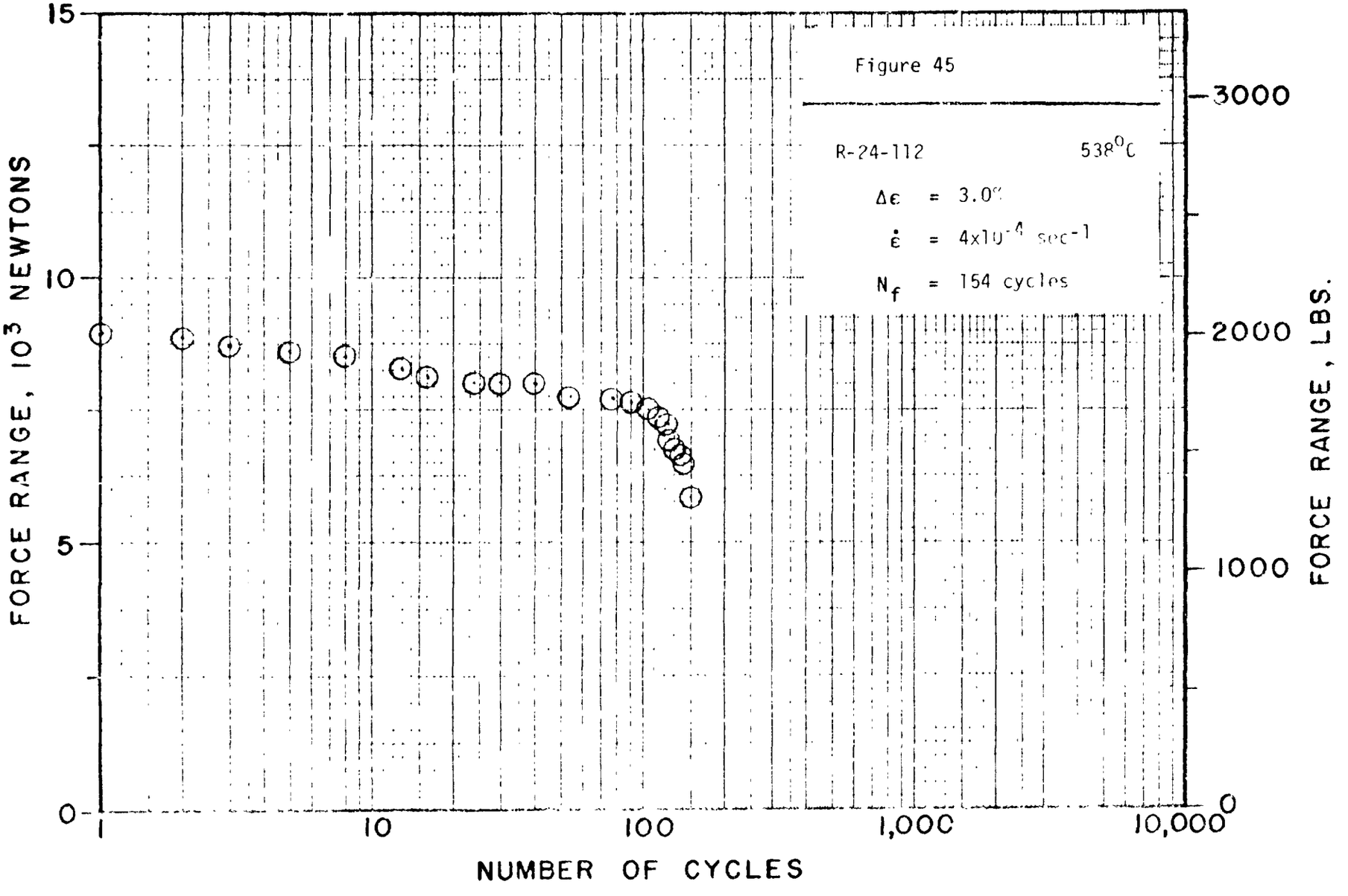
Figure 45
R-24-112
538°C
Δε = 3.0%
ε̇ = 4x10⁻⁴ sec⁻¹
N_f = 154 cycles
FORCE RANGE, 10³ NEWTONS
FORCE RANGE, LBS.
NUMBER OF CYCLES
15
10
5
0
3000
2000
1000
0
10
100
1,000
10,000

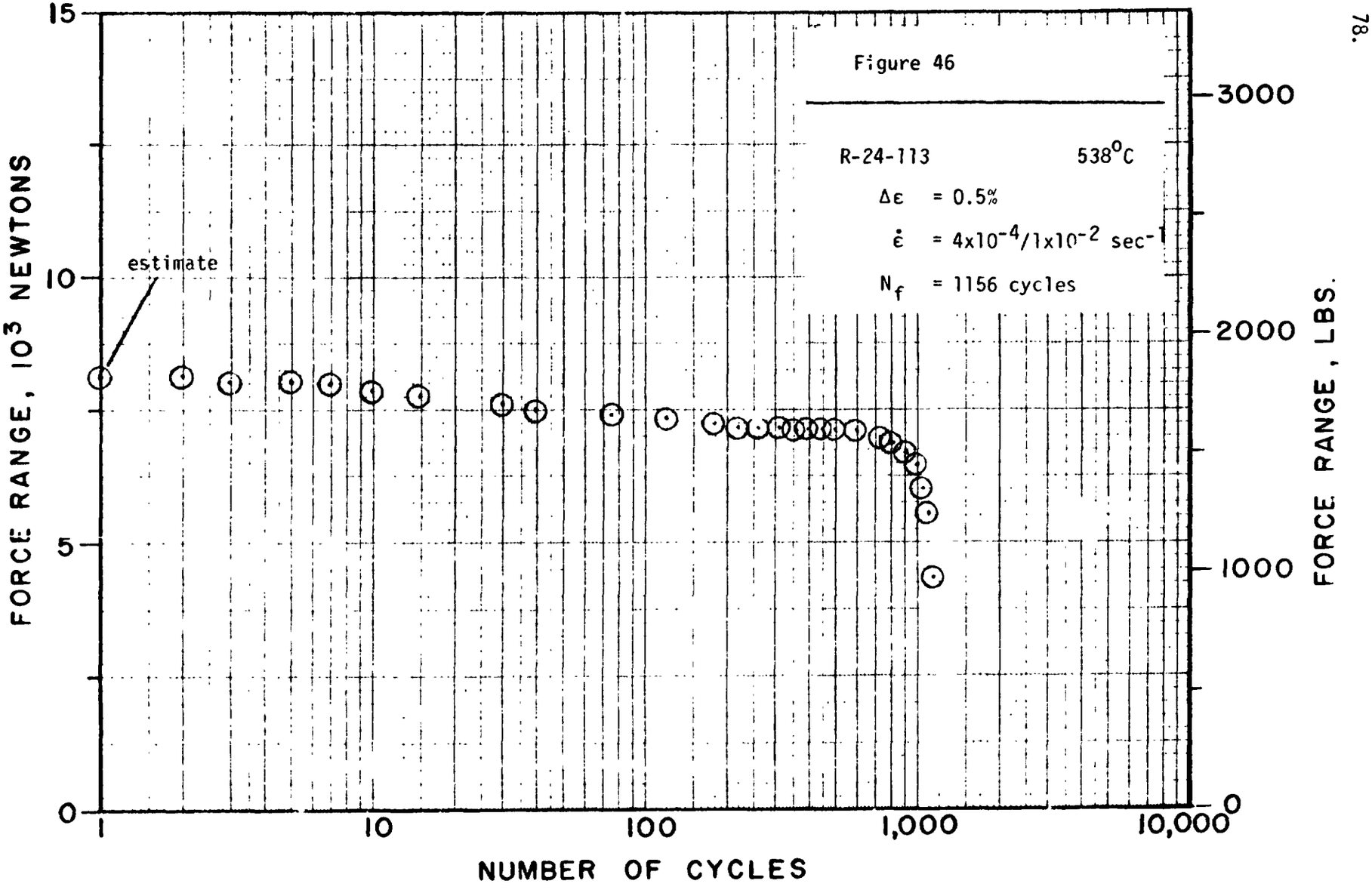
Figure 46
R-24-113
538°C
Δε = 0.5%
ε̇ = 4x10⁻⁴/1x10⁻² sec⁻¹
N_f = 1156 cycles
estimate
FORCE RANGE, 10³ NEWTONS
FORCE RANGE, LBS.
NUMBER OF CYCLES
15
10
5
0
3000
2000
1000
0
1
10
100
1,000
10,000

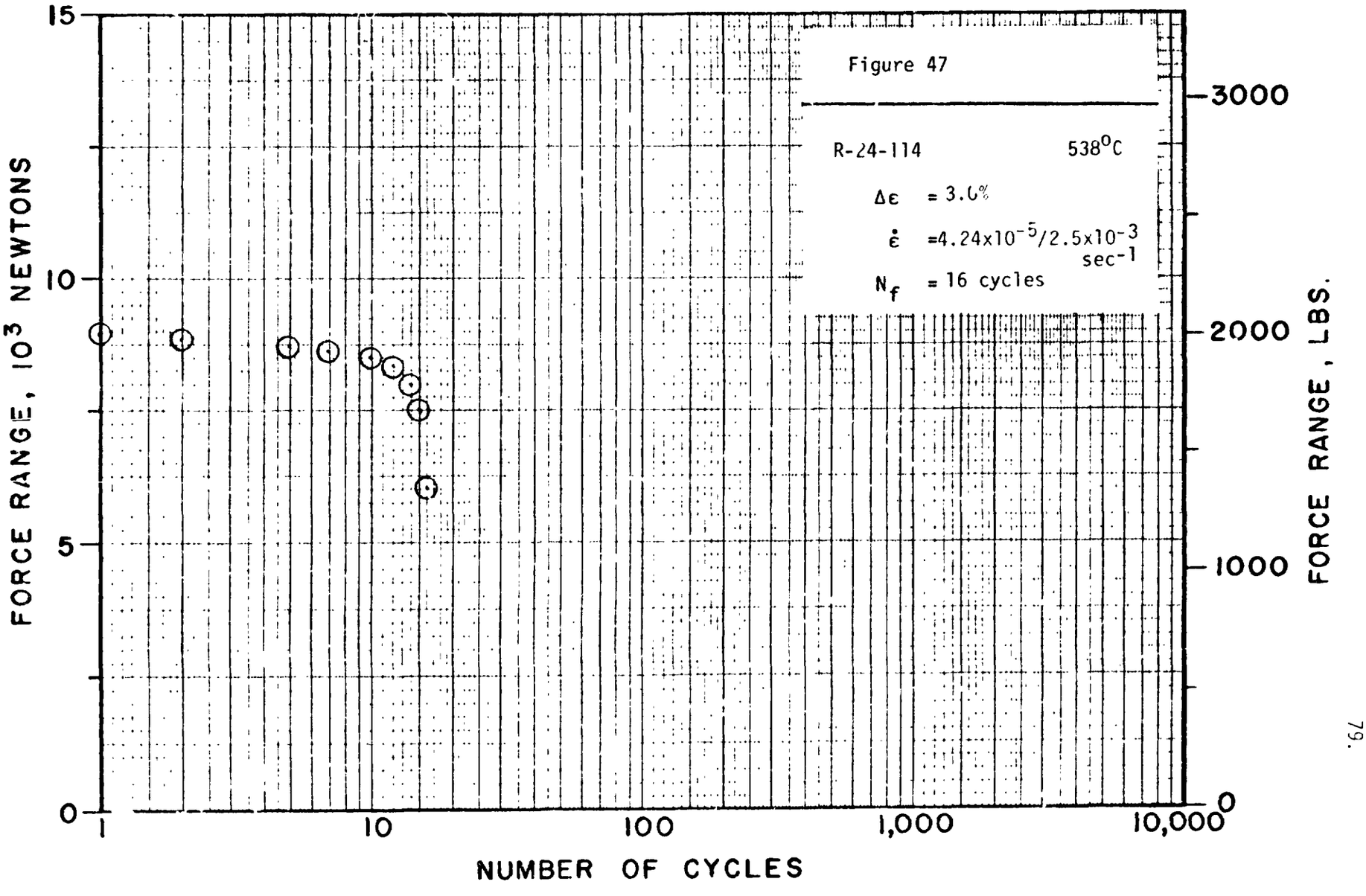
Figure 47
R-24-114
538°C
Δε = 3.0%
ε̇ =4.24x10⁻⁵/2.5x10⁻³ sec⁻¹
N_f = 16 cycles
FORCE RANGE, 10³ NEWTONS
FORCE RANGE, LBS.
NUMBER OF CYCLES
0
5
10
15
1
10
100
1,000
10,000
0
1000
2000
3000

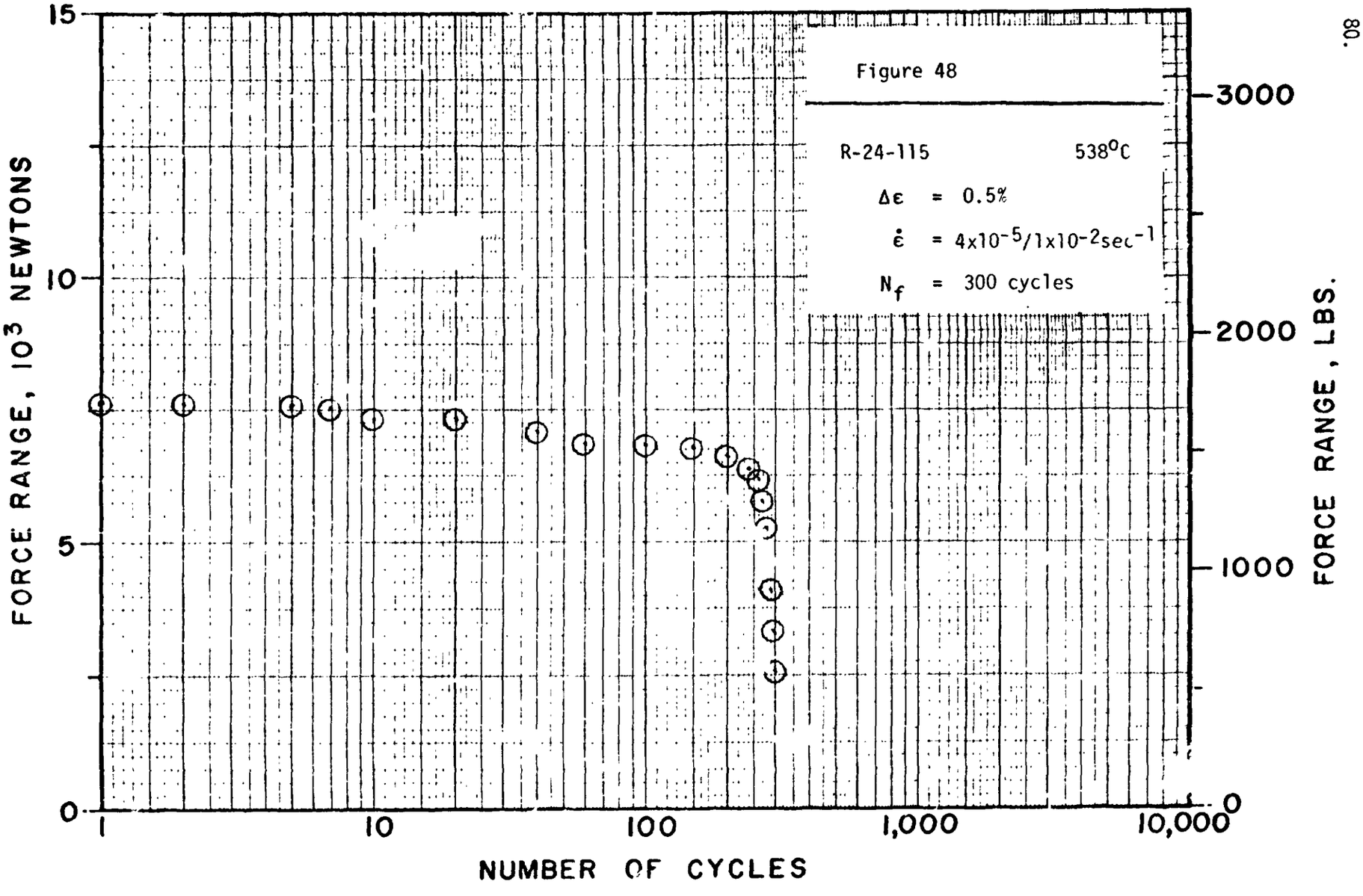
Figure 48
R-24-115
538°C
Δε = 0.5%
ε̇ = 4x10-5/1x10-2sec-1
Nf = 300 cycles
FORCE RANGE, 10³ NEWTONS
FORCE RANGE, LBS.
NUMBER OF CYCLES
15
10
5
0
3000
2000
1000
0
1
10
100
1,000
10,000

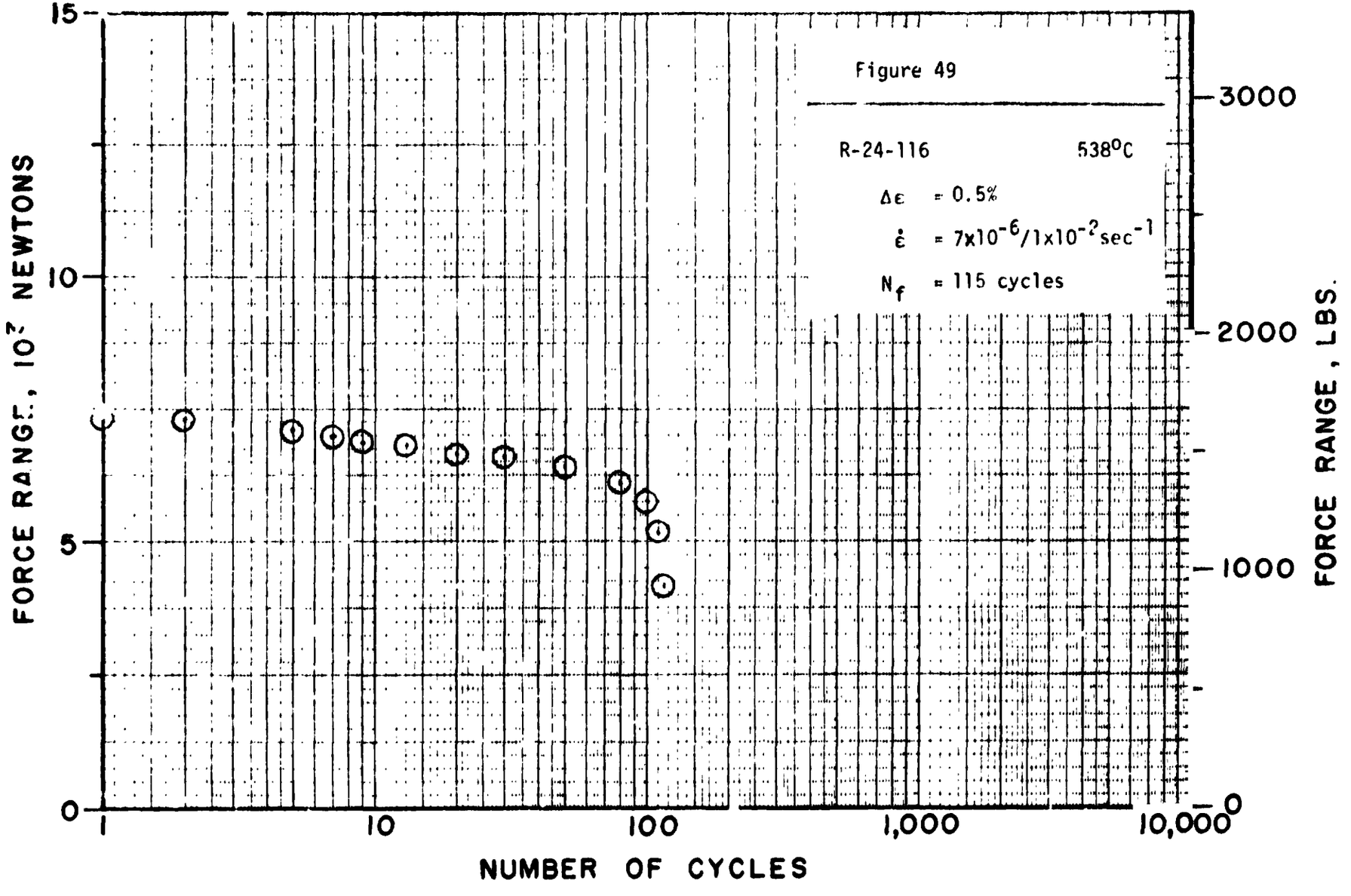
Figure 49
R-24-116
538°C
Δε = 0.5%
ε̇ = 7x10⁻⁶/1x10⁻²sec⁻¹
N_f = 115 cycles
FORCE RANGE, 10² NEWTONS
FORCE RANGE, LBS.
NUMBER OF CYCLES
15
10
5
0
3000
2000
1000
0
1
10
100
1,000
10,000

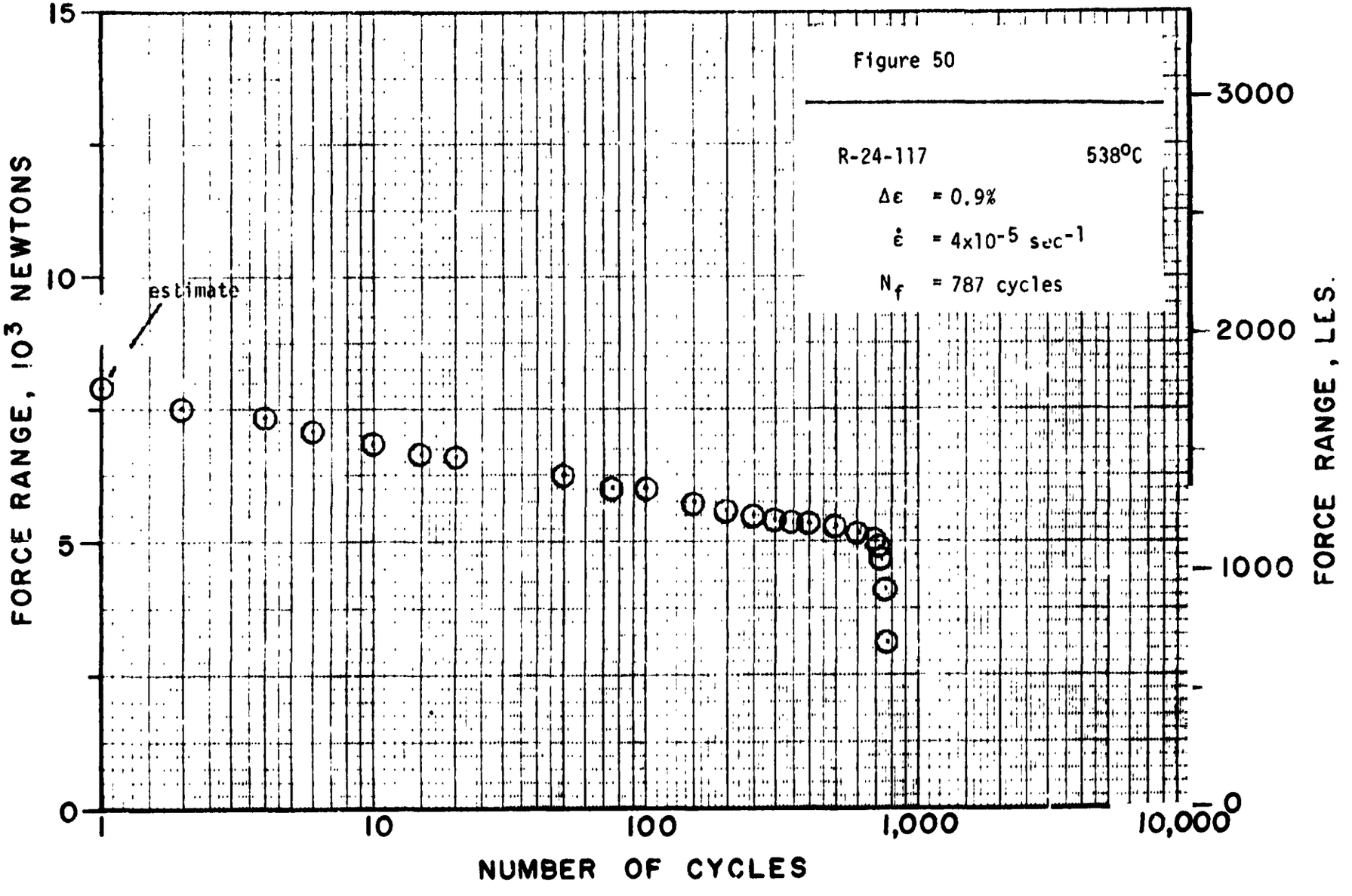
Figure 50
R-24-117
538°C
Δε = 0.9%
ε̇ = 4x10-5 sec-1
Nf = 787 cycles
estimate
FORCE RANGE, 10³ NEWTONS
FORCE RANGE, LES.
NUMBER OF CYCLES
15
10
5
0
3000
2000
1000
0
1
10
100
1,000
10,000

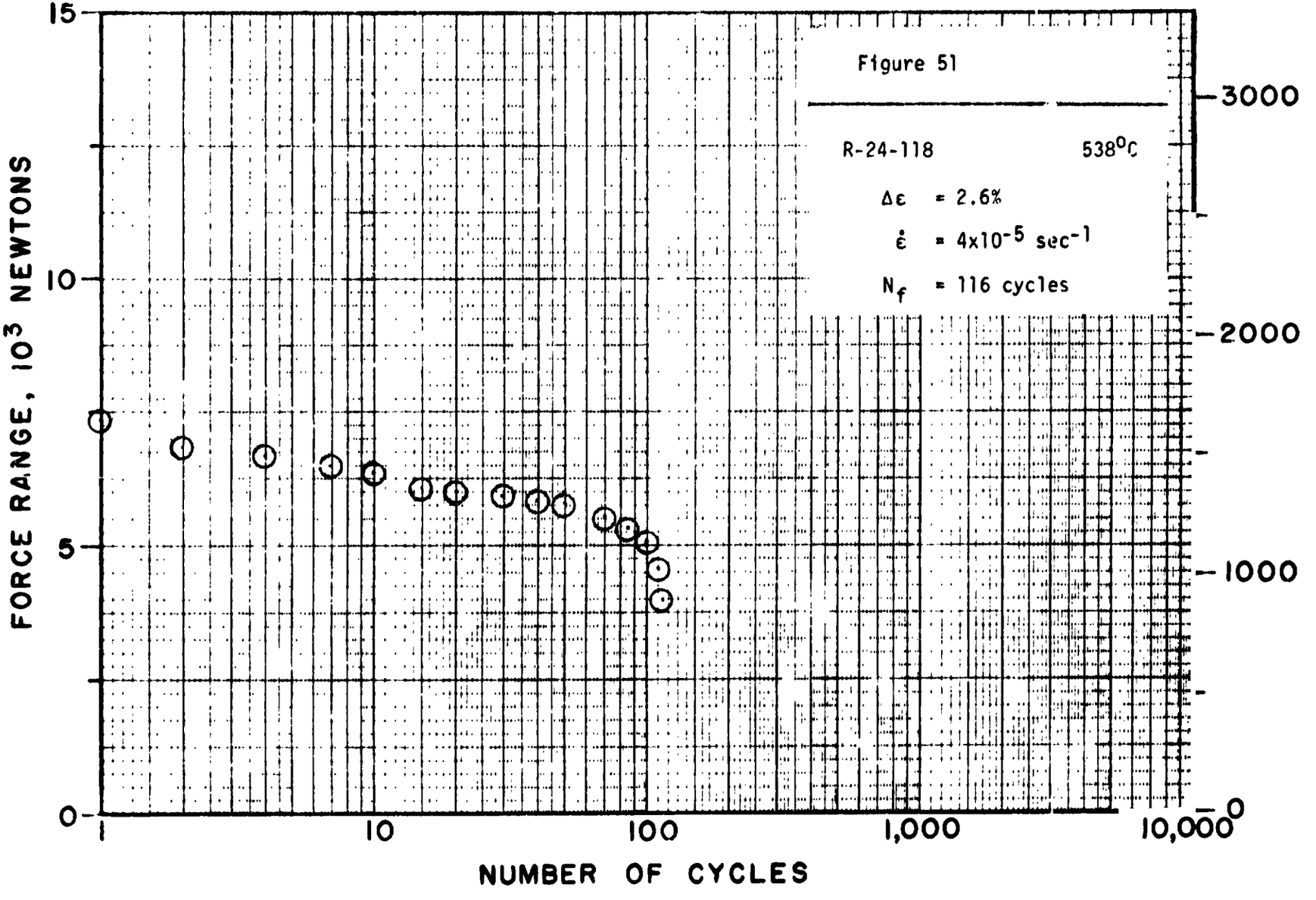
Figure 51
R-24-118
538°C
Δε = 2.6%
ε̇ = 4x10-5 sec-1
Nf = 116 cycles
FORCE RANGE, 10³ NEWTONS
FORCE RANGE, LBS.
NUMBER OF CYCLES
15
10
5
0
3000
2000
1000
0
1
10
100
1,000
10,000

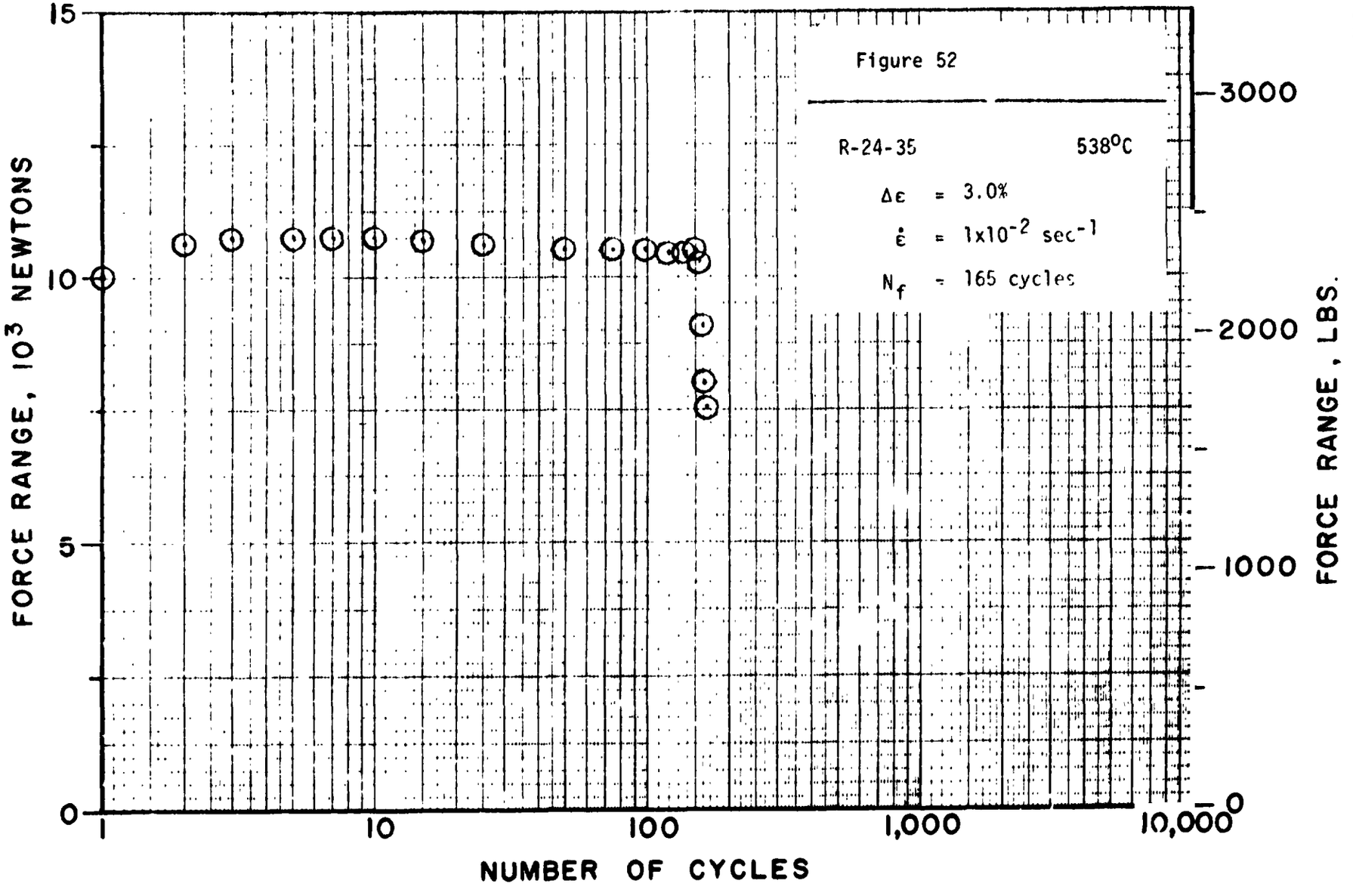
Figure 52
R-24-35
538°C
Δε = 3.0%
ε̇ = 1x10⁻² sec⁻¹
N_f = 165 cycles
FORCE RANGE, 10³ NEWTONS
FORCE RANGE, LBS.
NUMBER OF CYCLES
15
10
5
0
3000
2000
1000
0
1
10
100
1,000
10,000

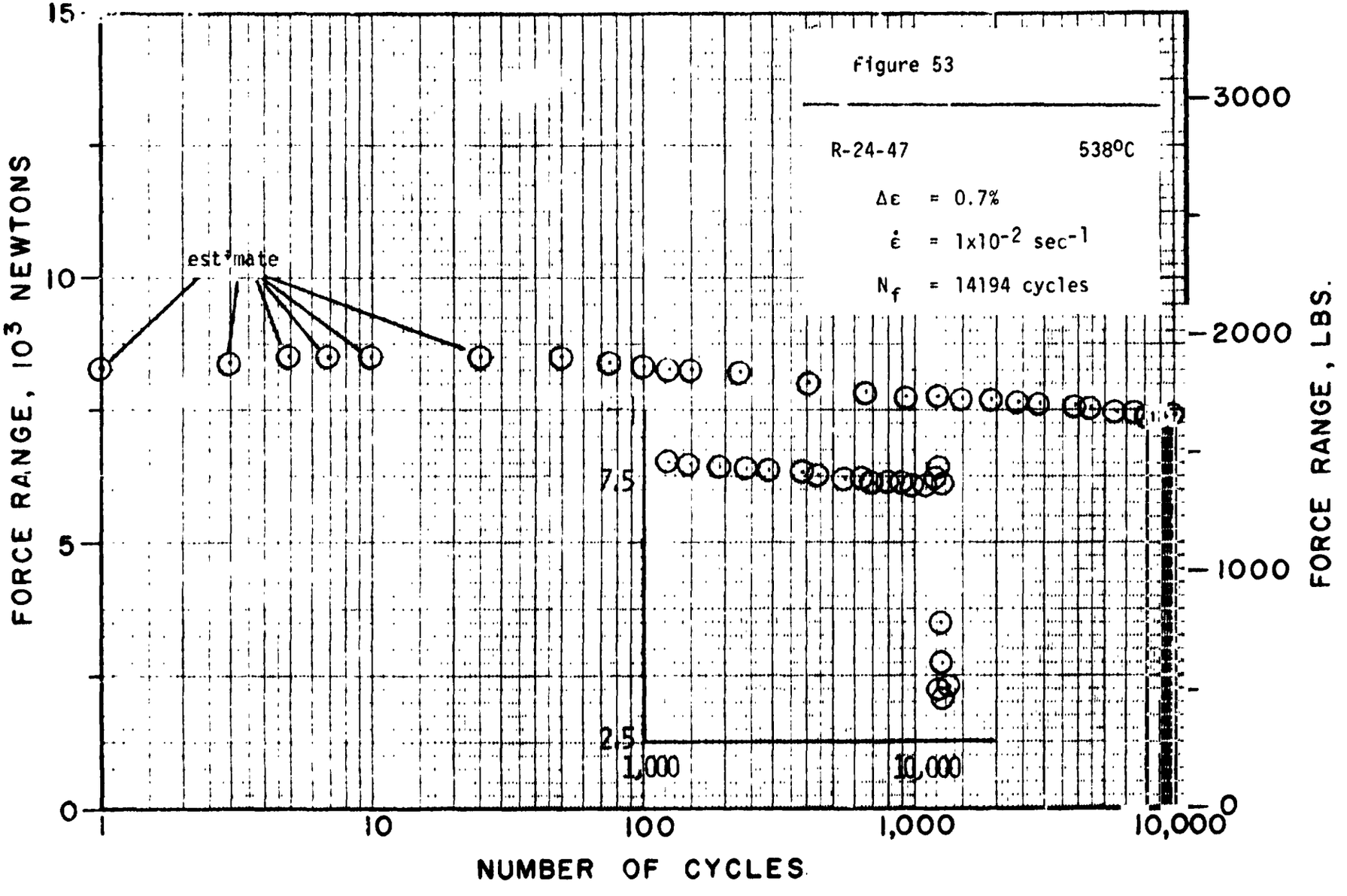
Figure 53
R-24-47
538°C
Δε = 0.7%
ε̇ = 1x10-2 sec-1
Nf = 14194 cycles
estimate
FORCE RANGE, 10³ NEWTONS
FORCE RANGE, LBS.
NUMBER OF CYCLES
15
10
5
0
3000
2000
1000
0
1
10
100
1,000
10,000
7.5
2.5
1,000
10,000

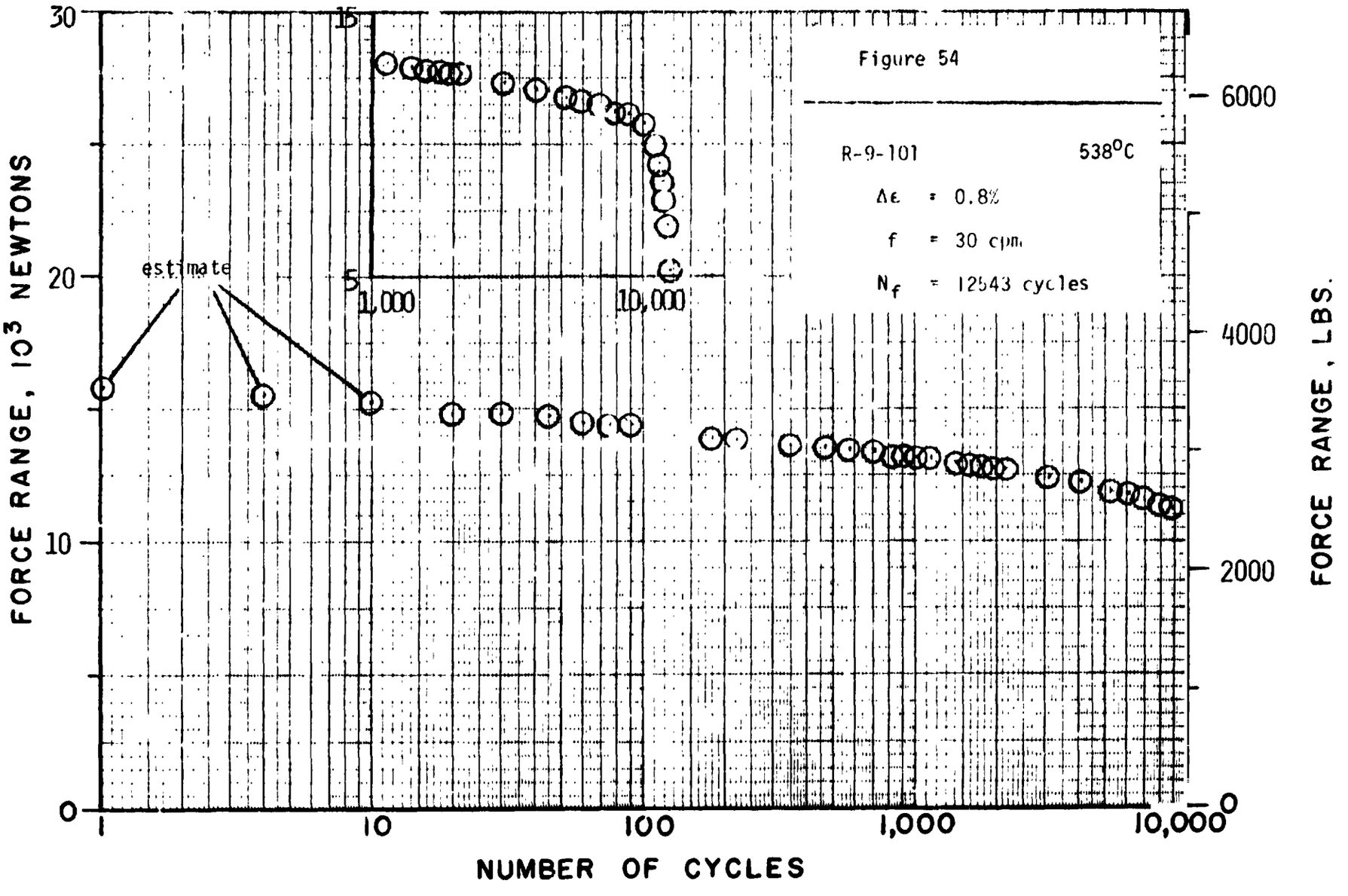
Figure 54
R-9-101
538°C
Δε = 0.8%
f = 30 cpm
N_f = 12543 cycles
estimate
FORCE RANGE, 10^3 NEWTONS
FORCE RANGE, LBS.
NUMBER OF CYCLES
30
20
10
0
6000
4000
2000
0
1
10
100
1,000
10,000
15
5
1,000
10,000

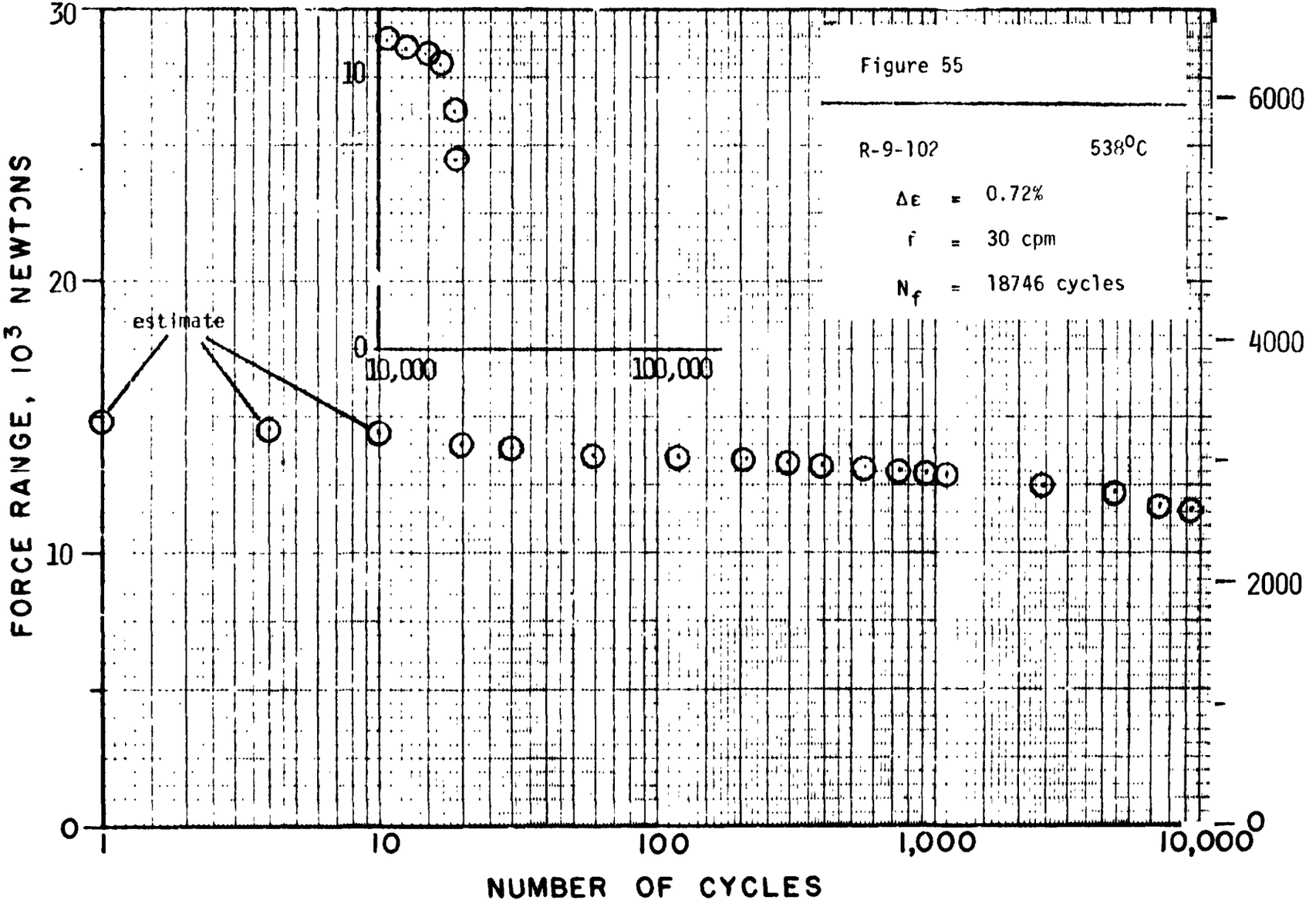
Figure 55
R-9-102
538°C
Δε = 0.72%
f = 30 cpm
N_f = 18746 cycles
estimate
FORCE RANGE, 10^3 NEWTONS
FORCE RANGE, LBS
NUMBER OF CYCLES
0
10
20
30
1
10
100
1,000
10,000
2000
4000
6000
10,000
100,000

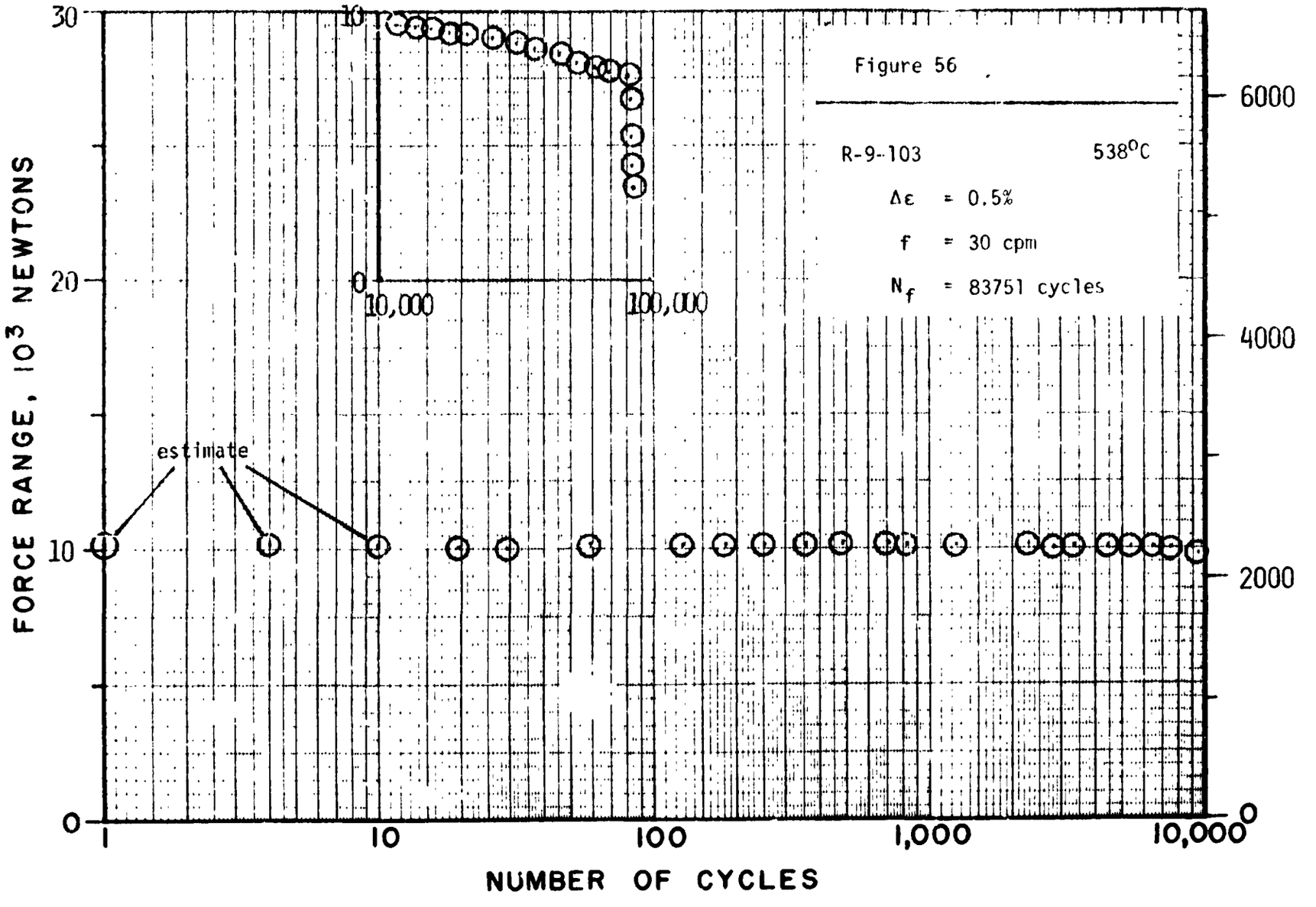
Figure 56
R-9-103
538°C
Δε = 0.5%
f = 30 cpm
N_f = 83751 cycles
10
0
10,000
100,000
estimate
30
20
10
0
FORCE RANGE, 10^3 NEWTONS
6000
4000
2000
0
FORCE RANGE, LBS.
1
10
100
1,000
10,000
NUMBER OF CYCLES

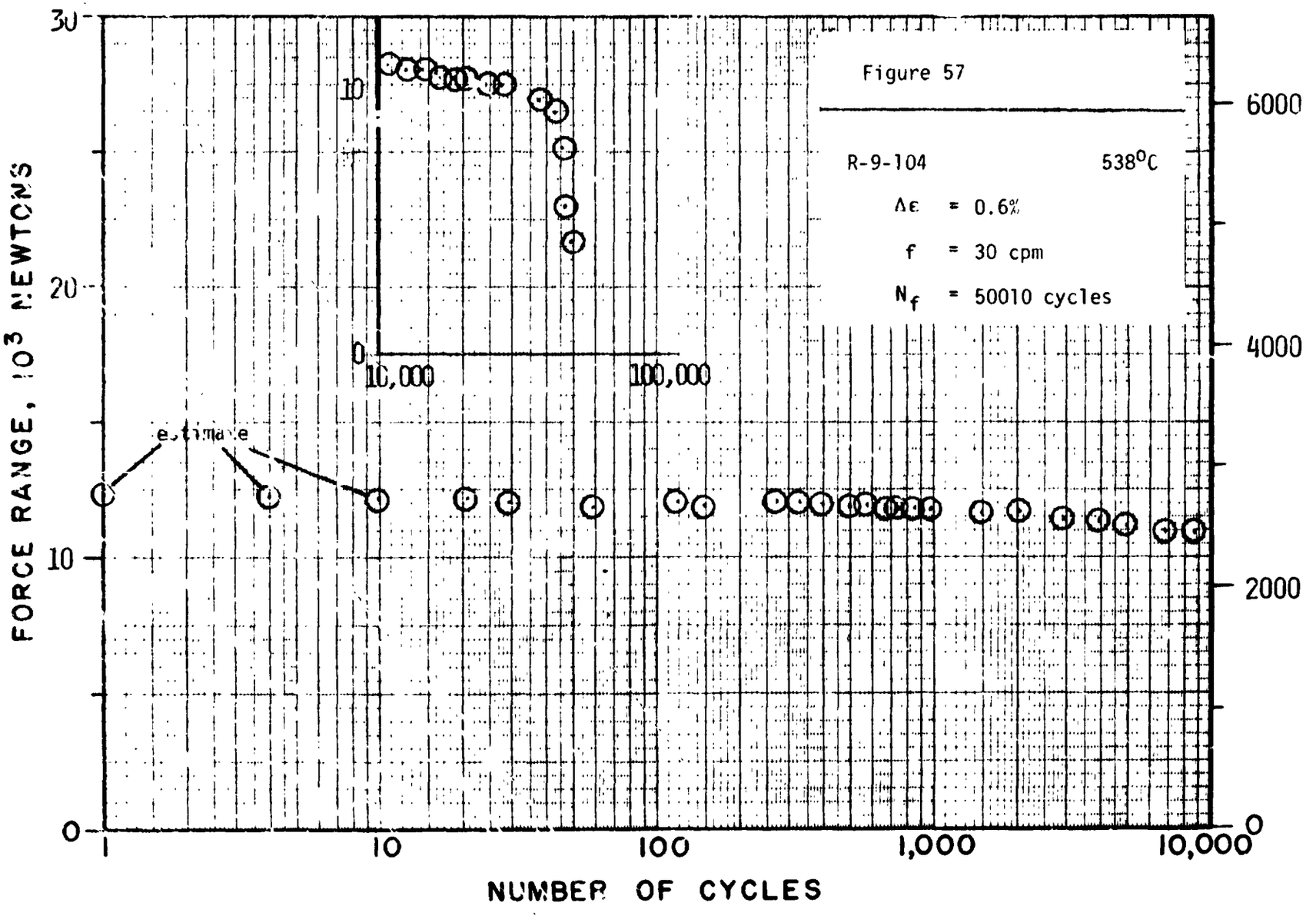
Figure 57
R-9-104
538°C
Δε = 0.6%
f = 30 cpm
N_f = 50010 cycles
estimate
10
0
10,000
100,000
30
20
10
0
FORCE RANGE, 10^3 NEWTONS
6000
4000
2000
0
FORCE RANGE, LBS.
1
10
100
1,000
10,000
NUMBER OF CYCLES

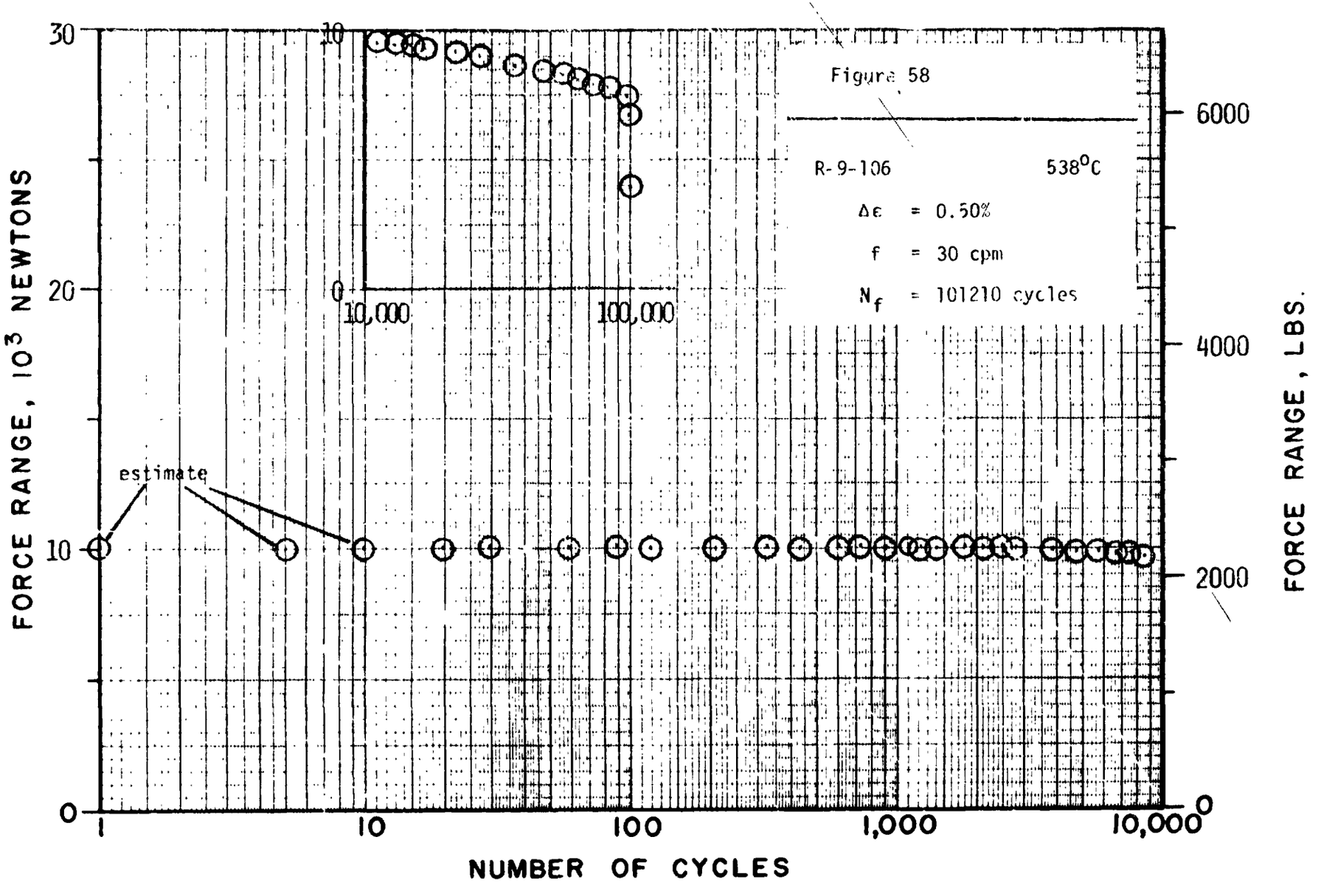
Figure 58
R-9-106
538°C
Δε = 0.50%
f = 30 cpm
N_f = 101210 cycles
10
0
10,000
100,000
estimate
30
20
10
0
1
10
100
1,000
10,000
NUMBER OF CYCLES
FORCE RANGE, 10^3 NEWTONS
6000
4000
2000
0
FORCE RANGE, LBS.

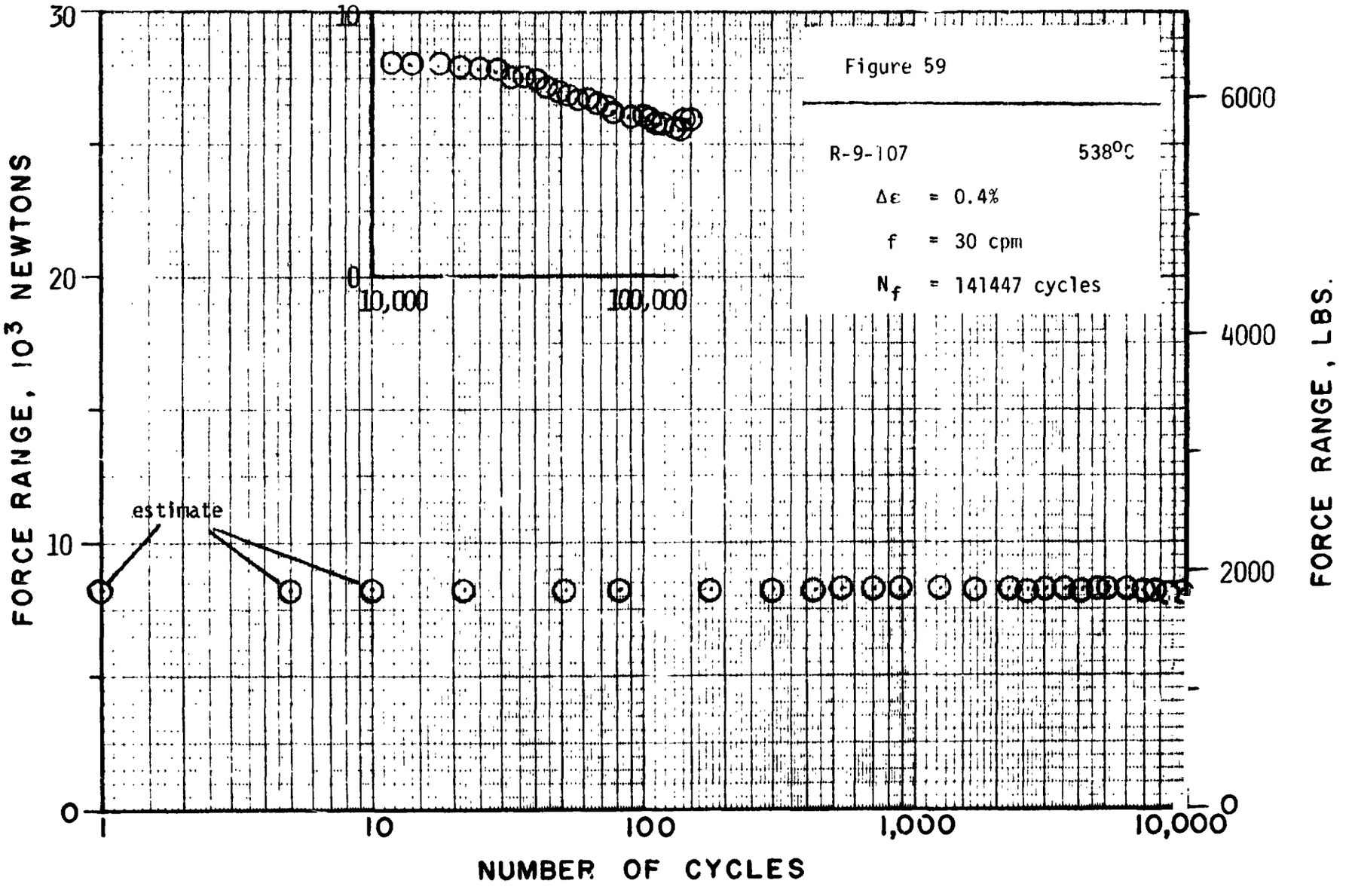
Figure 59
R-9-107
538°C
Δε = 0.4%
f = 30 cpm
N_f = 141447 cycles
10
0
10,000
100,000
estimate
30
20
10
0
1
10
100
1,000
10,000
NUMBER OF CYCLES
FORCE RANGE, 10^3 NEWTONS
6000
4000
2000
0
FORCE RANGE, LBS.

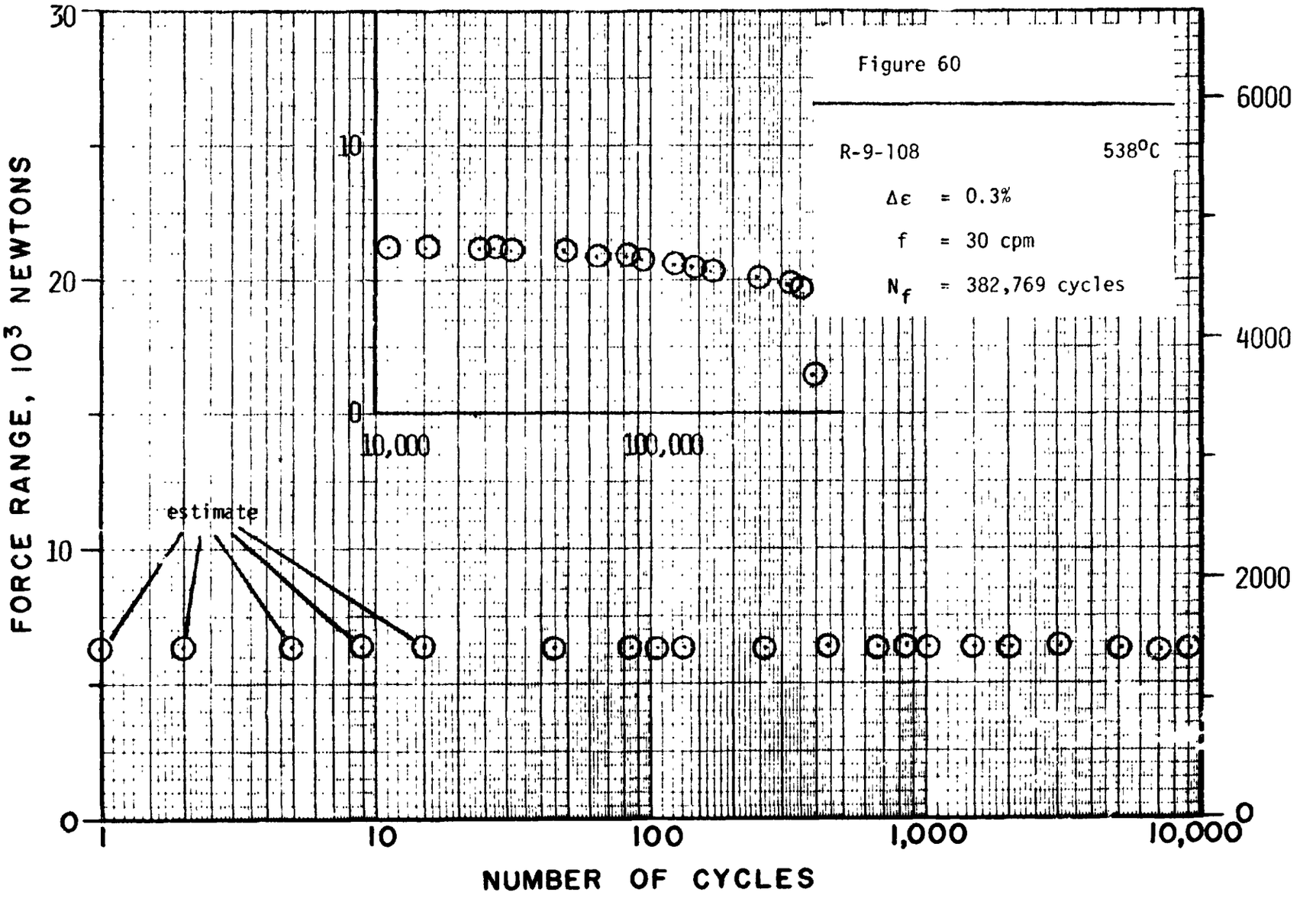
Figure 60
R-9-108
538°C
Δε = 0.3%
f = 30 cpm
N_f = 382,769 cycles
estimate
FORCE RANGE, 10^3 NEWTONS
FORCE RANGE, LBS.
NUMBER OF CYCLES
30
20
10
0
6000
4000
2000
0
1
10
100
1,000
10,000
10
0
10,000
100,000

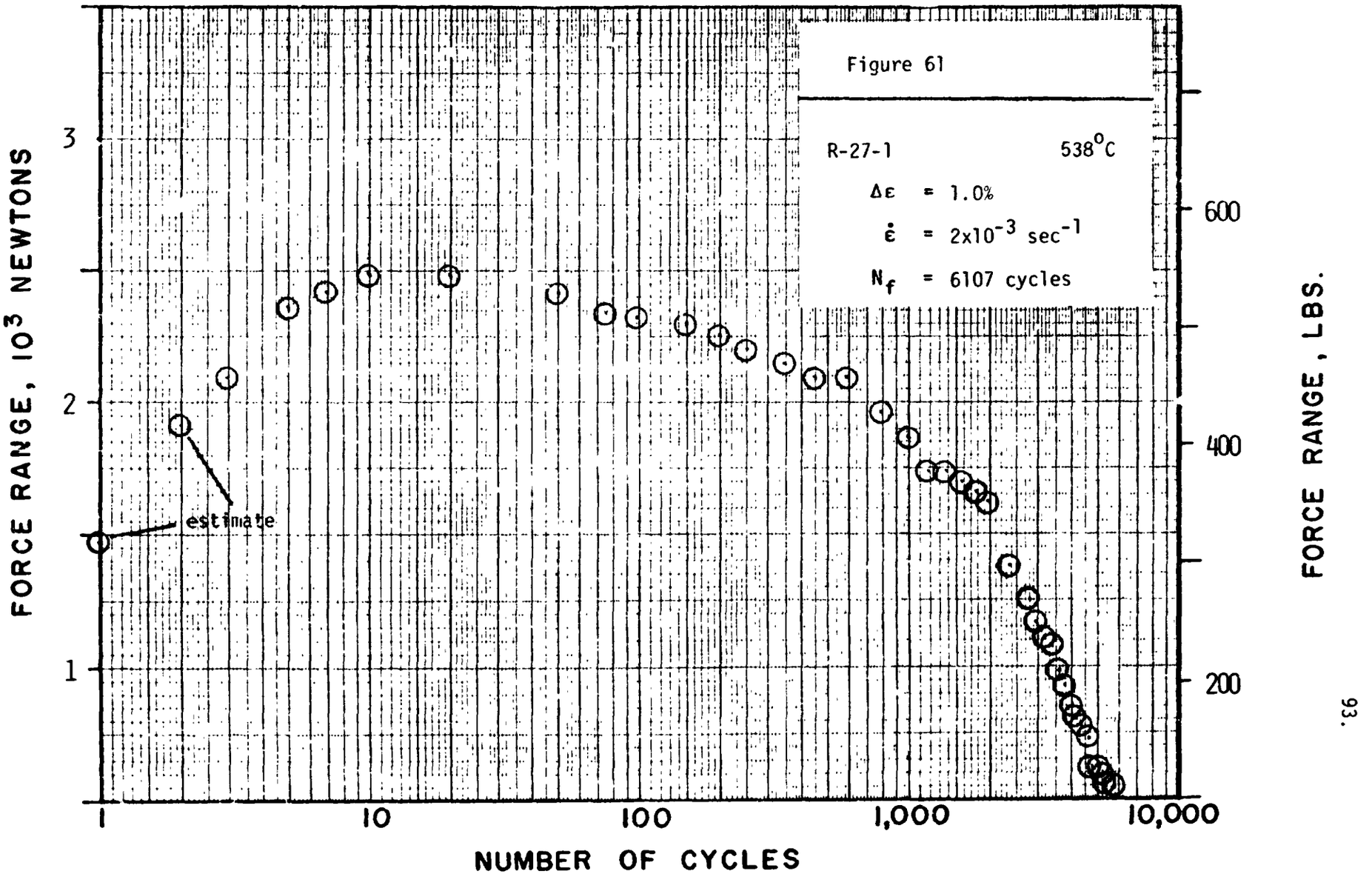
Figure 61
R-27-1
538°C
Δε = 1.0%
ε̇ = 2x10⁻³ sec⁻¹
N_f = 6107 cycles
estimate
FORCE RANGE, 10³ NEWTONS
FORCE RANGE, LBS.
NUMBER OF CYCLES
1
2
3
200
400
600
1
10
100
1,000
10,000

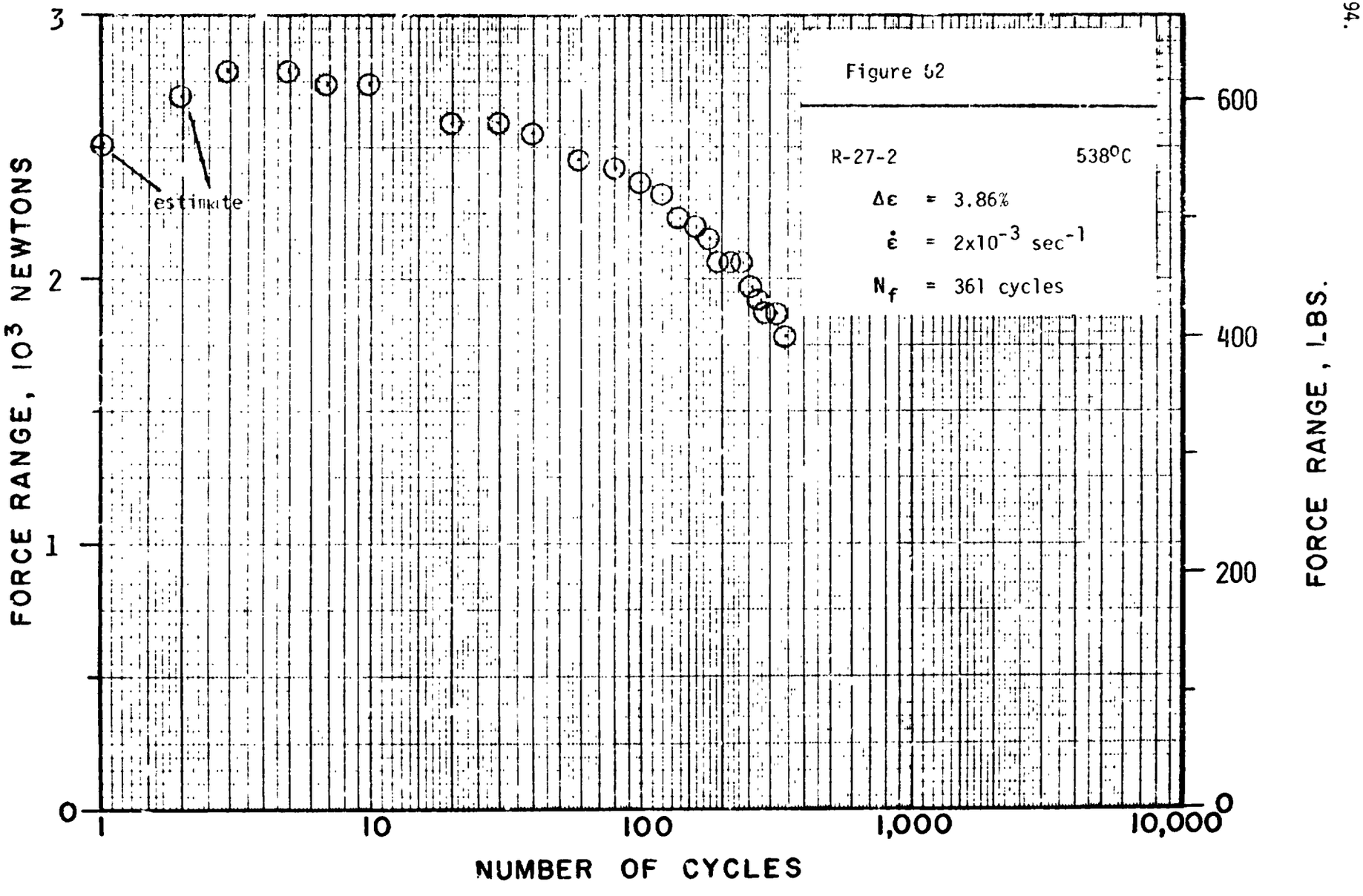
Figure 52
R-27-2
538°C
Δε = 3.86%
ε̇ = 2x10^-3 sec^-1
N_f = 361 cycles
estimate
FORCE RANGE, 10^3 NEWTONS
FORCE RANGE, LBS.
NUMBER OF CYCLES
0
1
2
3
1
10
100
1,000
10,000
0
200
400
600

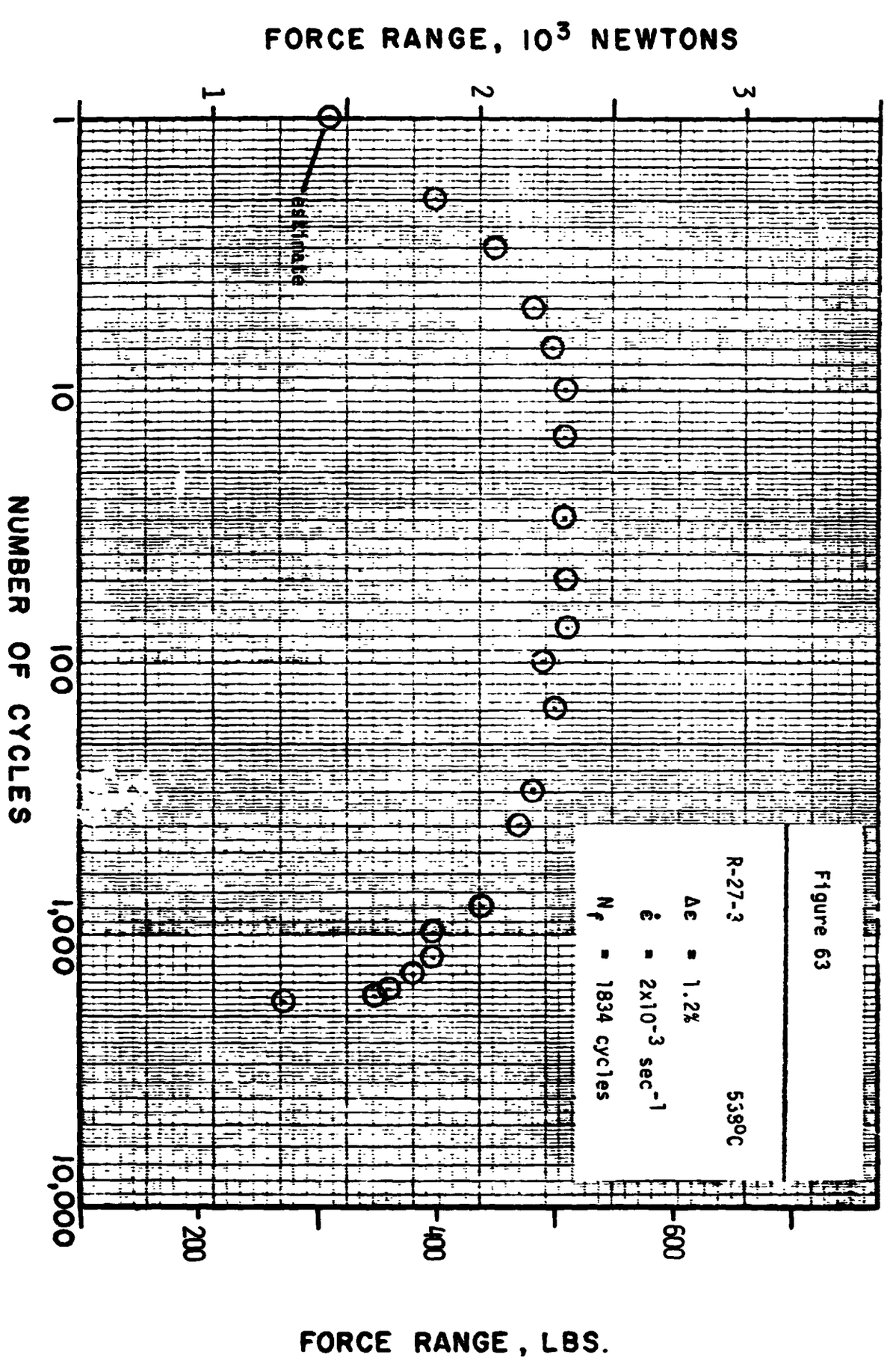
FORCE RANGE, 10^3 NEWTONS
1
2
3
estimate
10
100
1,000
10,000
NUMBER OF CYCLES
200
400
600
FORCE RANGE, LBS.
Figure 63
R-27-3
539°C
$\Delta\varepsilon$ = 1.2%
$\dot{\varepsilon}$ = 2×10^{-3} sec^{-1}
N_f = 1834 cycles

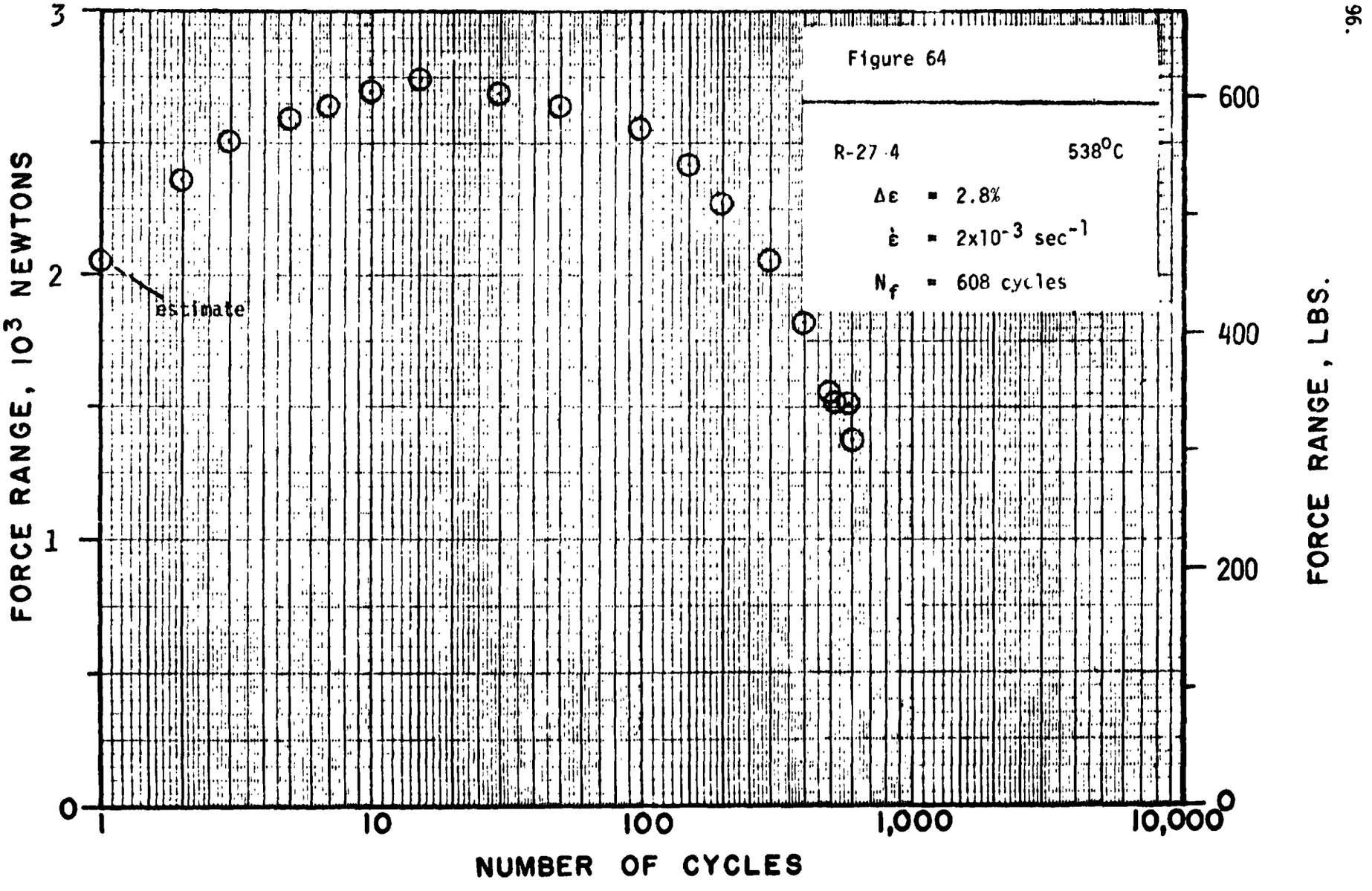
Figure 64
R-27-4
538°C
Δε = 2.8%
ε̇ = 2x10⁻³ sec⁻¹
N_f = 608 cycles
estimate
FORCE RANGE, 10³ NEWTONS
FORCE RANGE, LBS.
NUMBER OF CYCLES
0
1
2
3
200
400
600
1
10
100
1,000
10,000

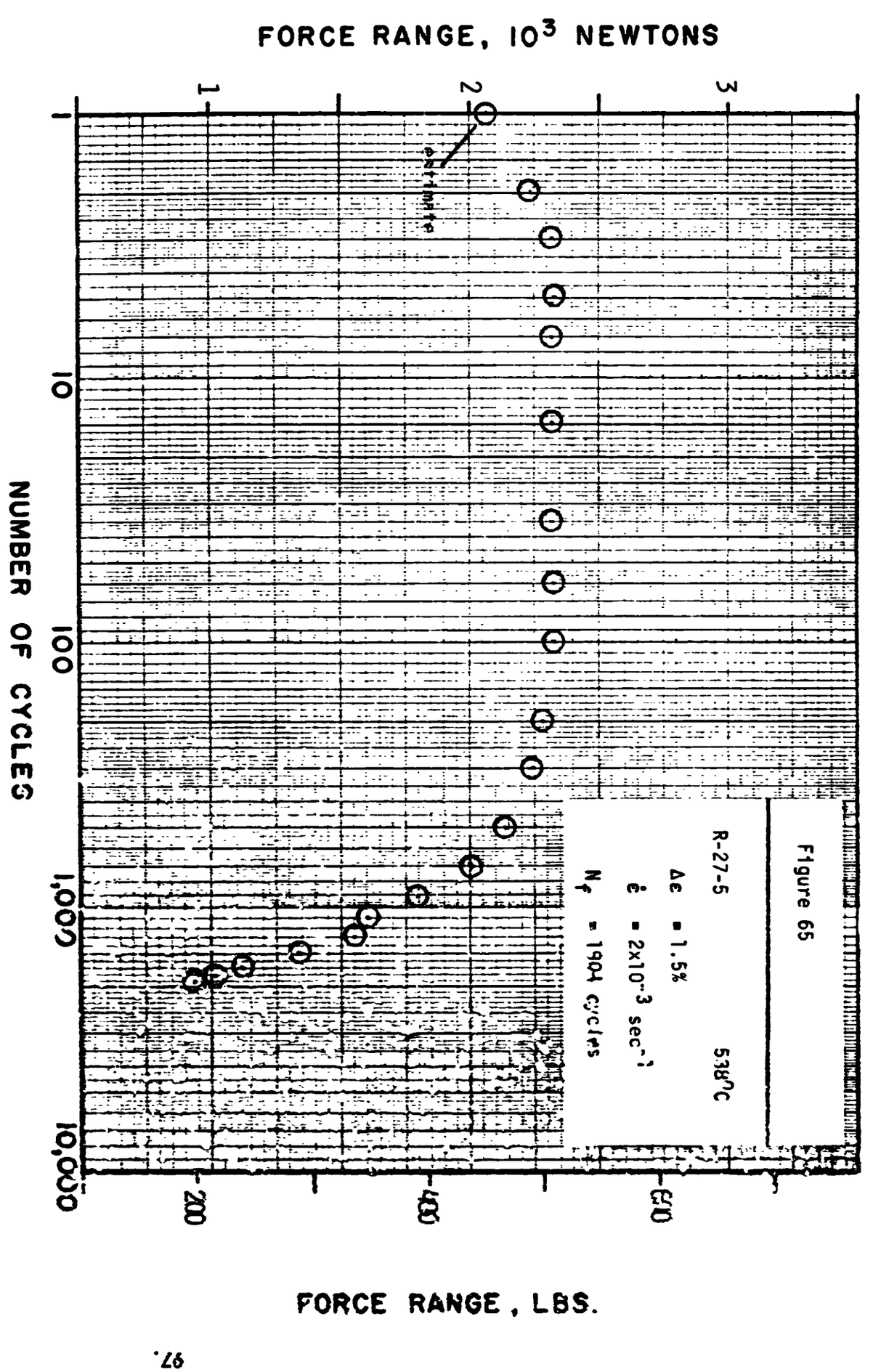
FORCE RANGE, 10^3 NEWTONS
1
2
3
estimate
NUMBER OF CYCLES
1
10
100
1,000
10,000
200
400
600
FORCE RANGE, LBS.
Figure 65
R-27-5
538°C
$\Delta\varepsilon$ = 1.5%
$\dot{\varepsilon}$ = 2×10^{-3} sec^{-1}
N_f = 1904 cycles

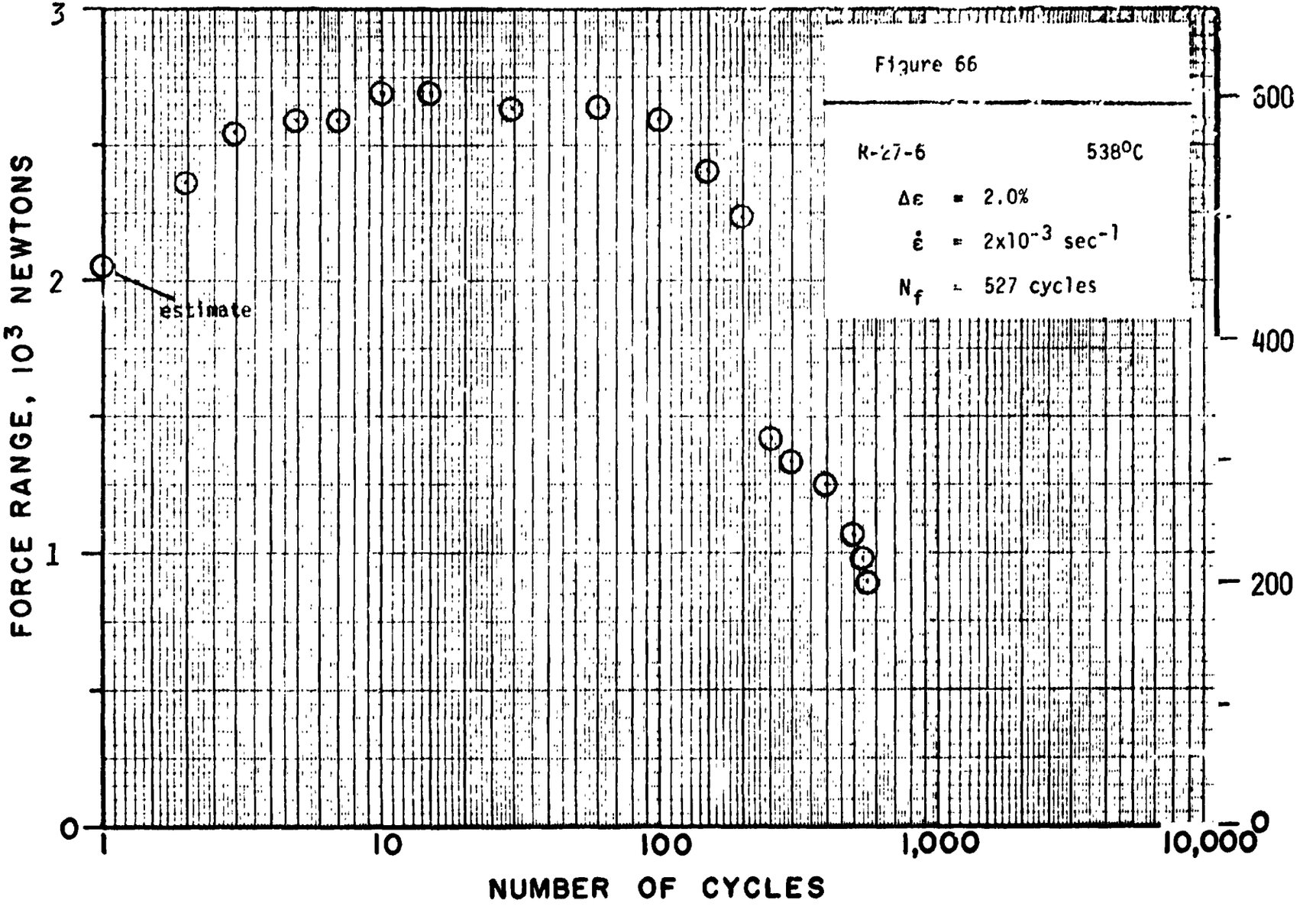
Figure 66
R-27-6
538°C
Δε = 2.0%
ε̇ = 2x10⁻³ sec⁻¹
N_f = 527 cycles
estimate
FORCE RANGE, 10³ NEWTONS
FORCE RANGE, LBS.
NUMBER OF CYCLES
0
1
2
3
600
400
200
0
1
10
100
1,000
10,000

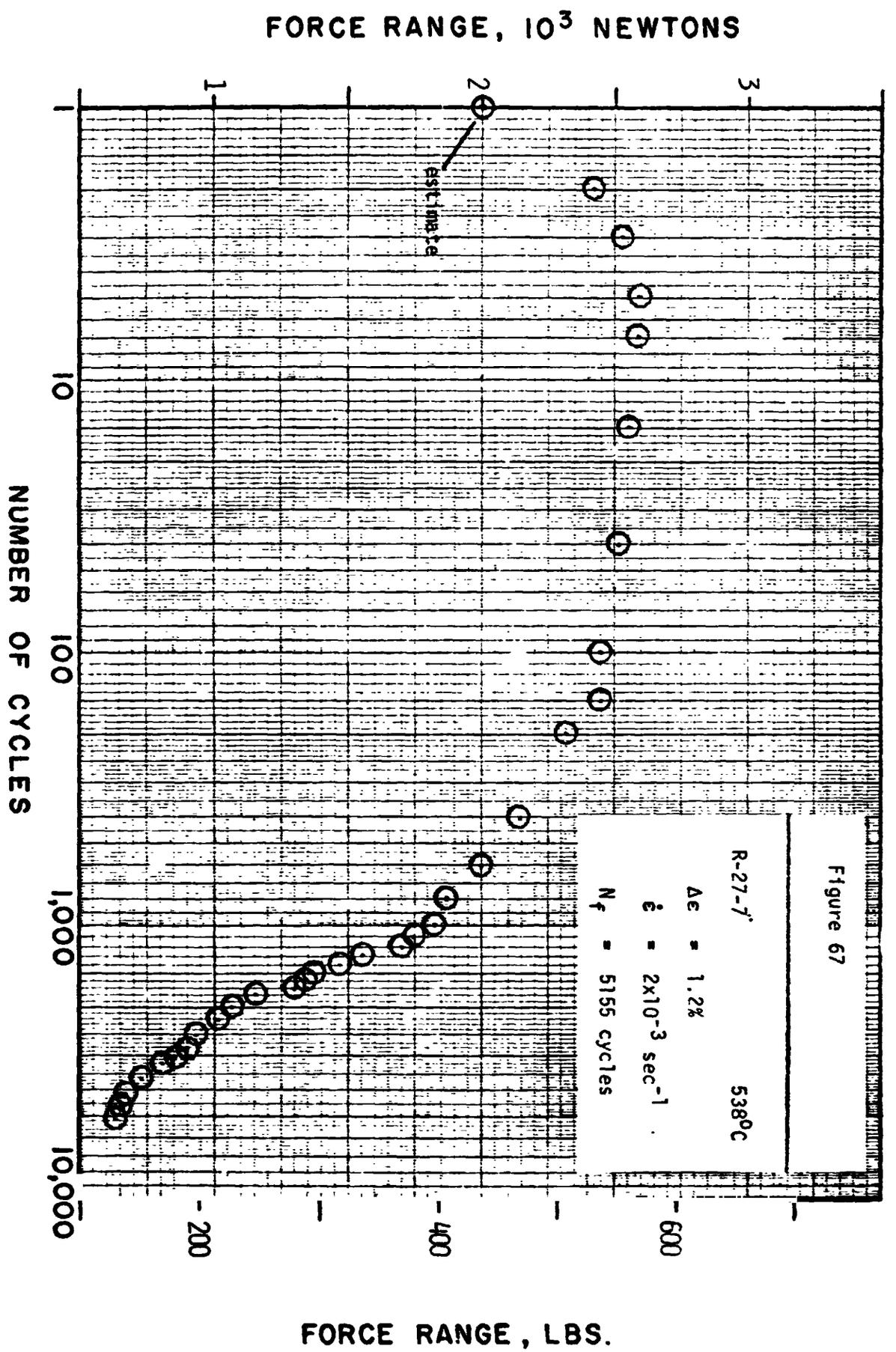
FORCE RANGE, 10^3 NEWTONS
1
2
3
estimate
10
100
1,000
10,000
NUMBER OF CYCLES
200
400
600
FORCE RANGE, LBS.
Figure 67
R-27-7'
538°C
$\Delta\varepsilon$ = 1.2%
$\dot{\varepsilon}$ = 2×10^{-3} sec^{-1}
N_f = 5155 cycles

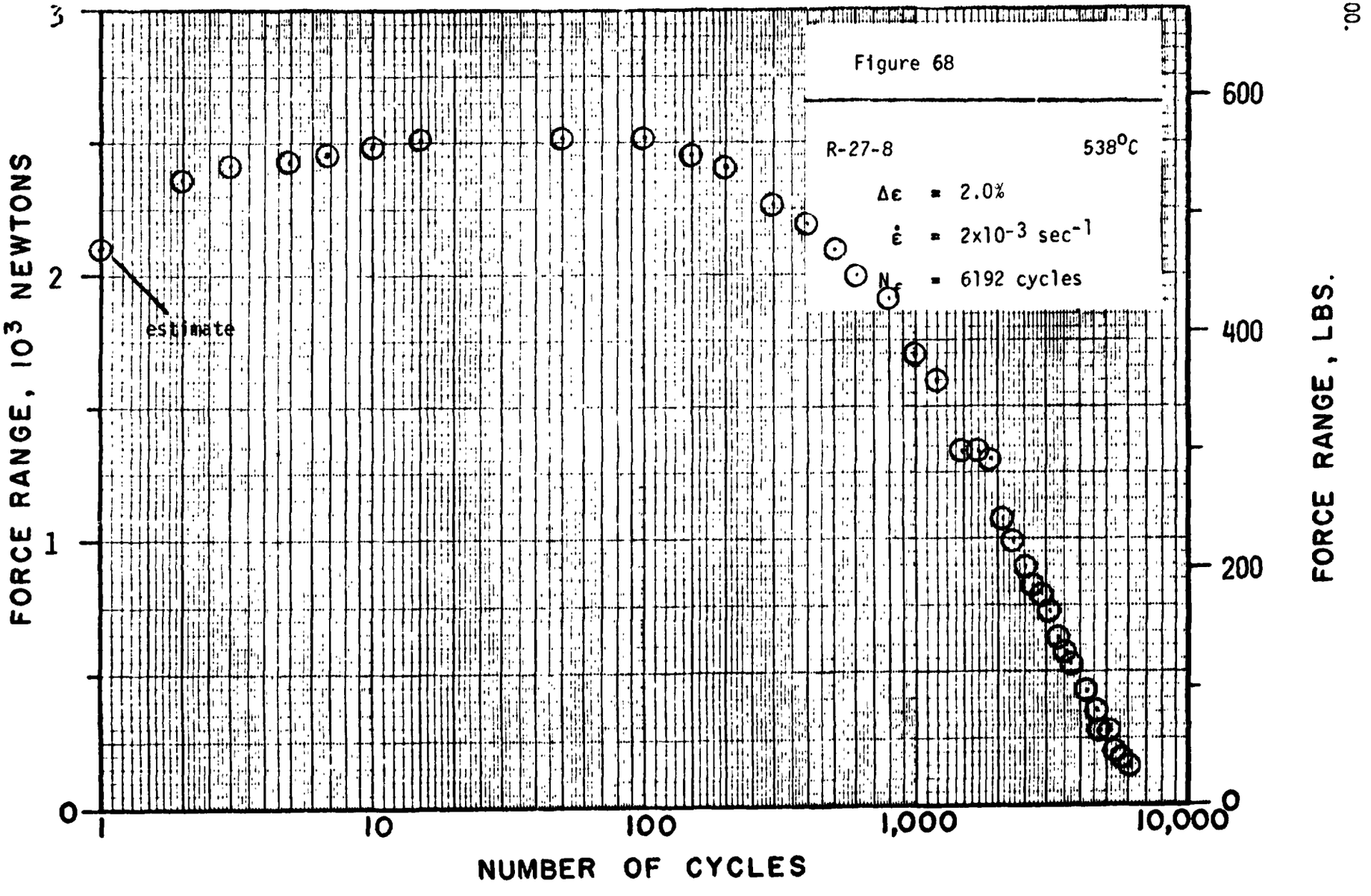
Figure 68
R-27-8
538°C
Δε = 2.0%
ε̇ = 2x10-3 sec-1
Nf = 6192 cycles
estimate
FORCE RANGE, 10³ NEWTONS
FORCE RANGE, LBS.
NUMBER OF CYCLES
0
1
2
3
200
400
600
1
10
100
1,000
10,000

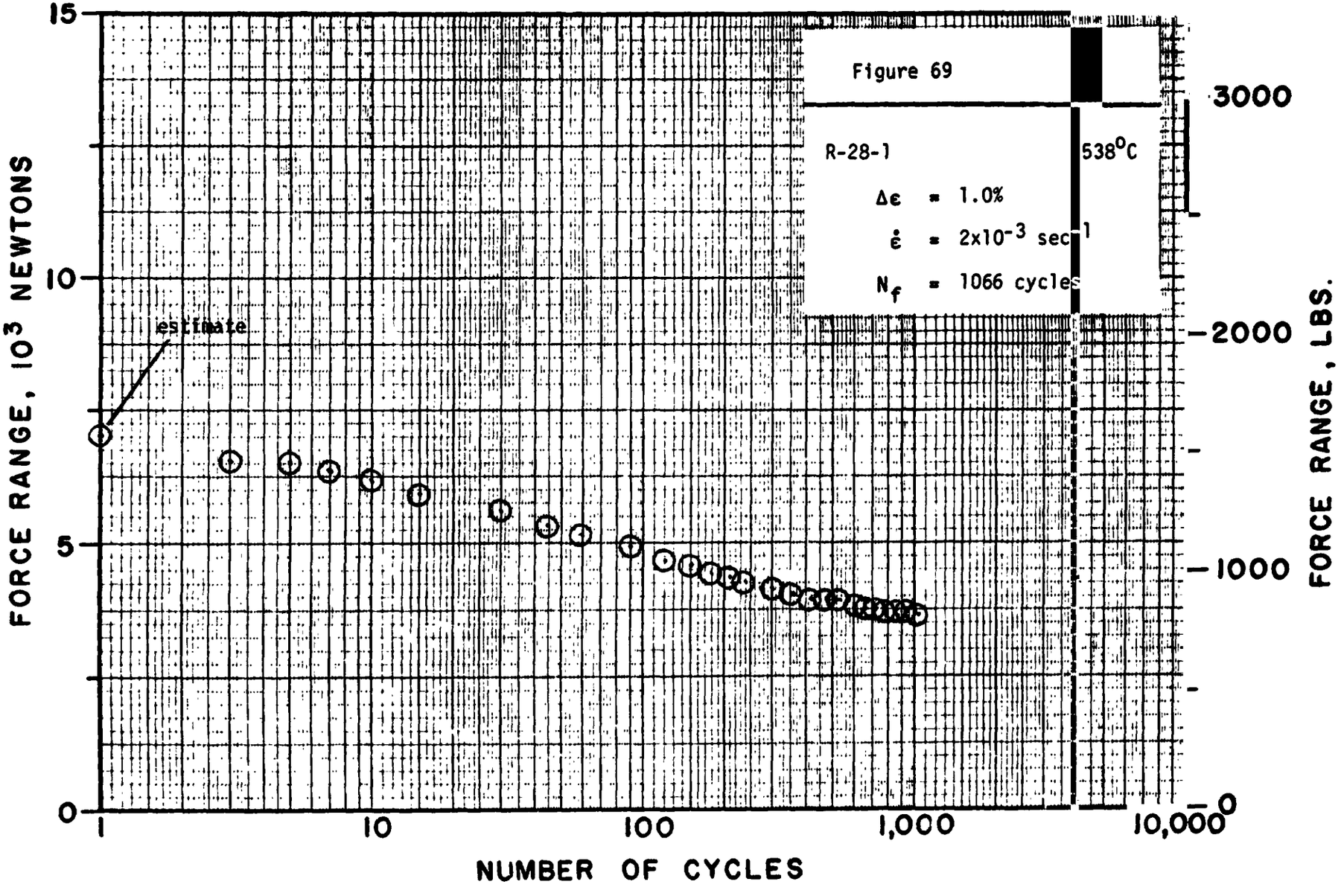
Figure 69
R-28-1
538°C
Δε = 1.0%
ε̇ = 2x10⁻³ sec⁻¹
N_f = 1066 cycles
estimate
FORCE RANGE, 10³ NEWTONS
FORCE RANGE, LBS.
NUMBER OF CYCLES
0
5
10
15
1
10
100
1,000
10,000
0
1000
2000
3000

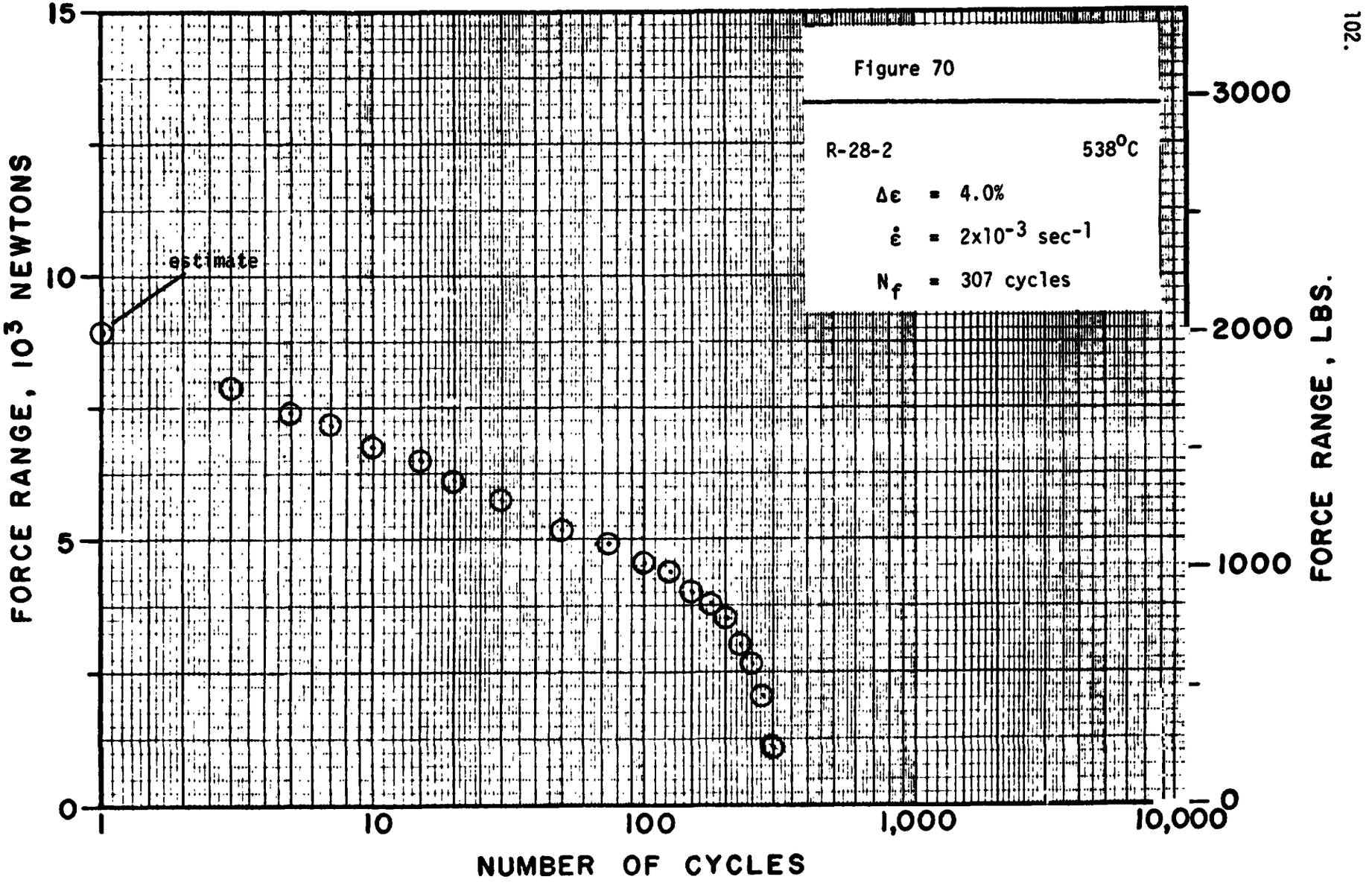
Figure 70
R-28-2
538°C
Δε = 4.0%
ε̇ = 2x10⁻³ sec⁻¹
N_f = 307 cycles
estimate
FORCE RANGE, 10³ NEWTONS
FORCE RANGE, LBS.
NUMBER OF CYCLES
15
10
5
0
3000
2000
1000
0
1
10
100
1,000
10,000

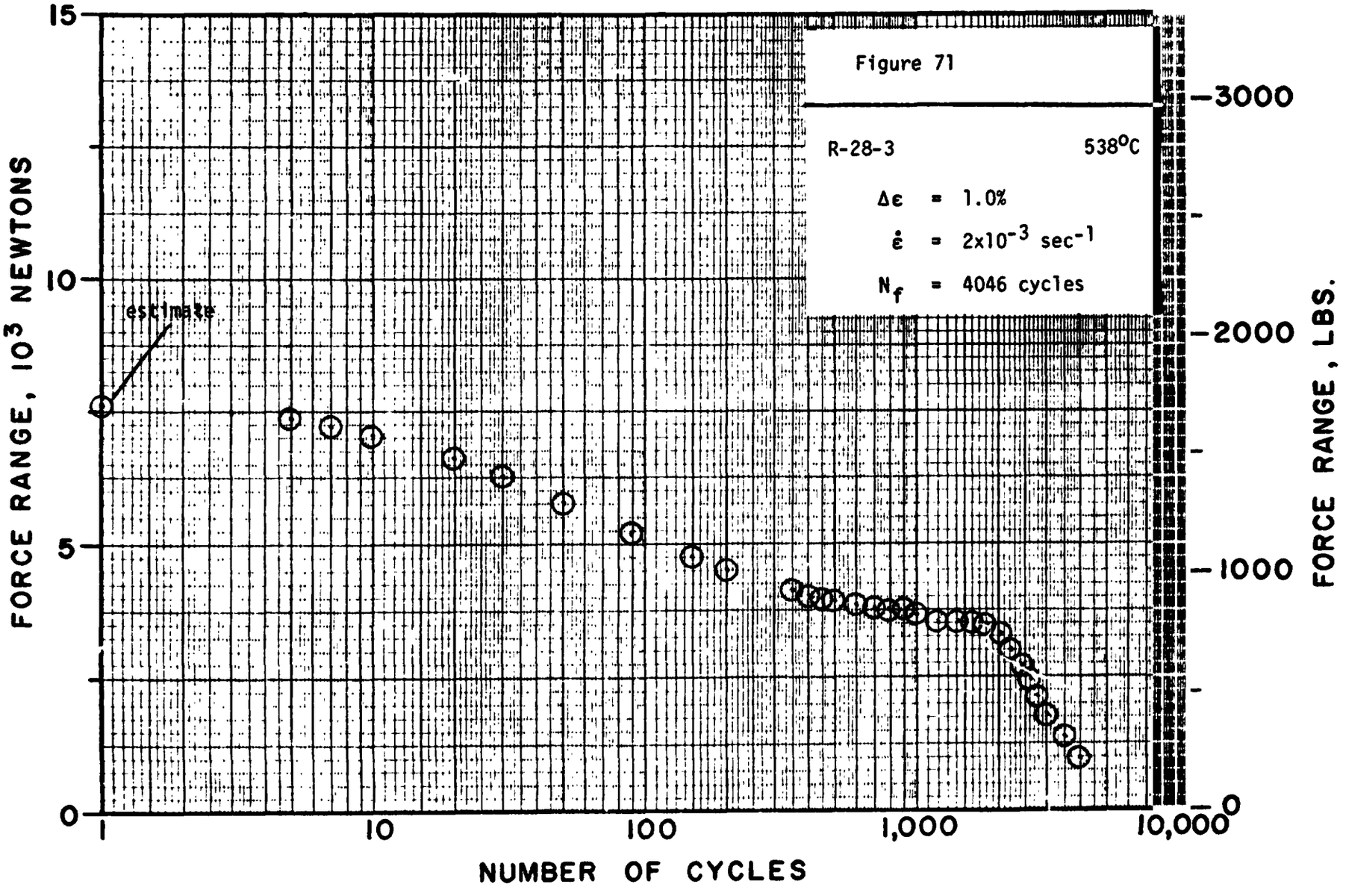
Figure 71
R-28-3
538°C
Δε = 1.0%
ε̇ = 2x10⁻³ sec⁻¹
N_f = 4046 cycles
estimate
15
10
5
0
FORCE RANGE, 10³ NEWTONS
3000
2000
1000
0
FORCE RANGE, LBS.
1
10
100
1,000
10,000
NUMBER OF CYCLES

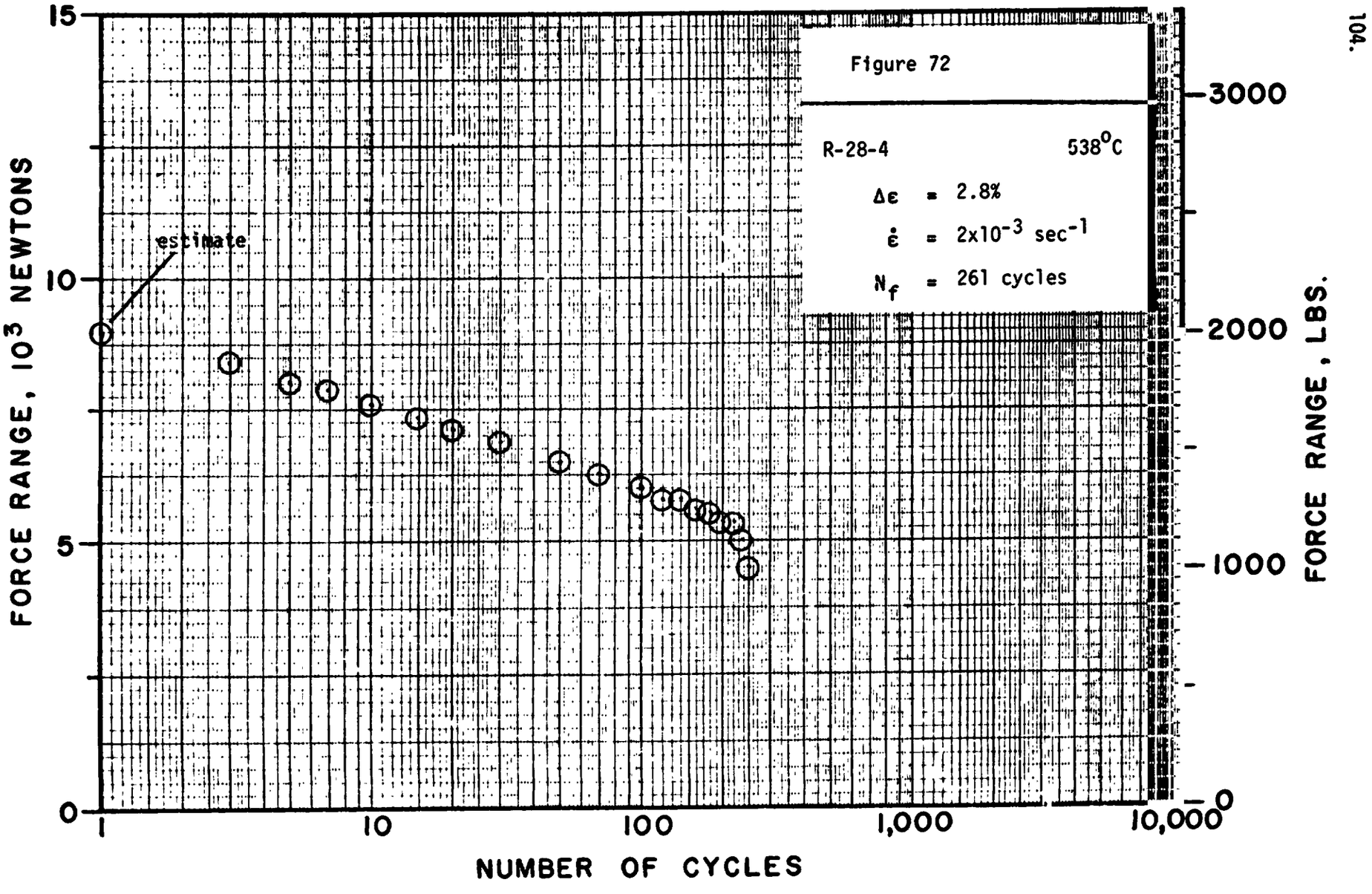
Figure 72
R-28-4
538°C
Δε = 2.8%
ε̇ = 2x10⁻³ sec⁻¹
N_f = 261 cycles
estimate
FORCE RANGE, 10³ NEWTONS
FORCE RANGE, LBS.
NUMBER OF CYCLES
15
10
5
0
3000
2000
1000
0
1
10
100
1,000
10,000

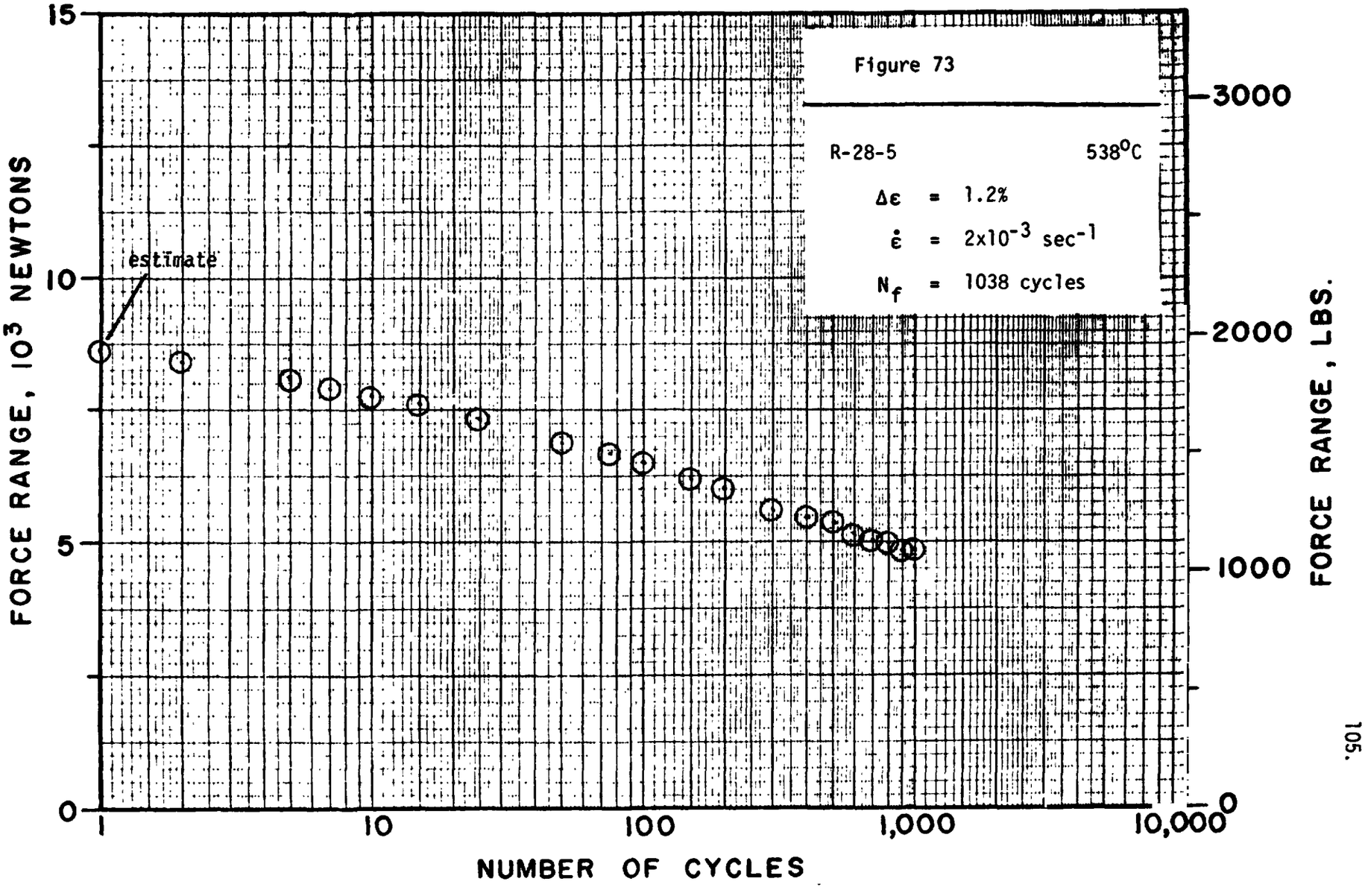
Figure 73
R-28-5
538°C
Δε = 1.2%
ε̇ = 2x10⁻³ sec⁻¹
N_f = 1038 cycles
estimate
FORCE RANGE, 10³ NEWTONS
FORCE RANGE, LBS.
NUMBER OF CYCLES
15
10
5
0
3000
2000
1000
0
1
10
100
1,000
10,000

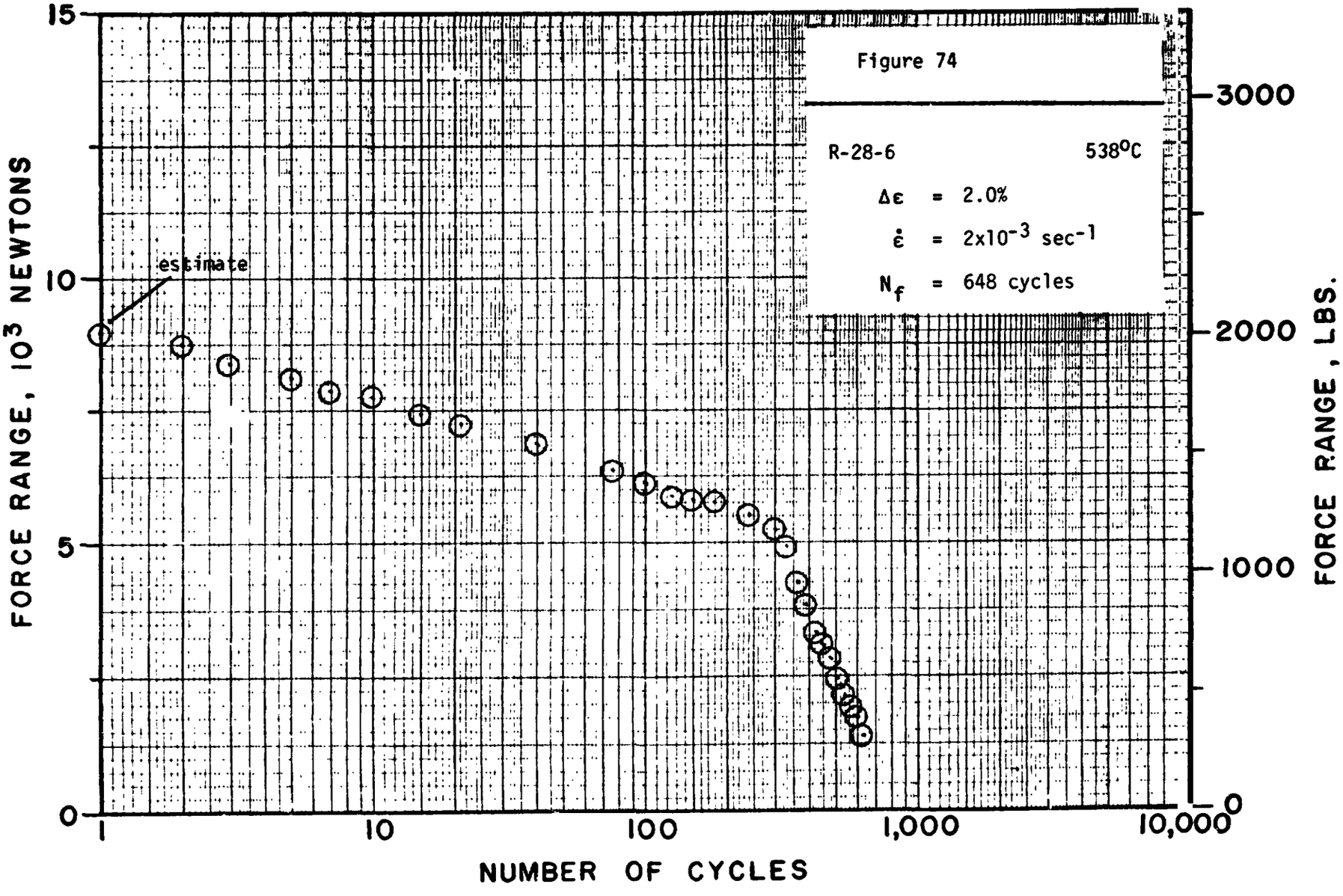
Figure 74
R-28-6
538°C
Δε = 2.0%
ε̇ = 2x10⁻³ sec⁻¹
N_f = 648 cycles
estimate
FORCE RANGE, 10³ NEWTONS
FORCE RANGE, LBS.
NUMBER OF CYCLES
0
5
10
15
0
1000
2000
3000
1
10
100
1,000
10,000

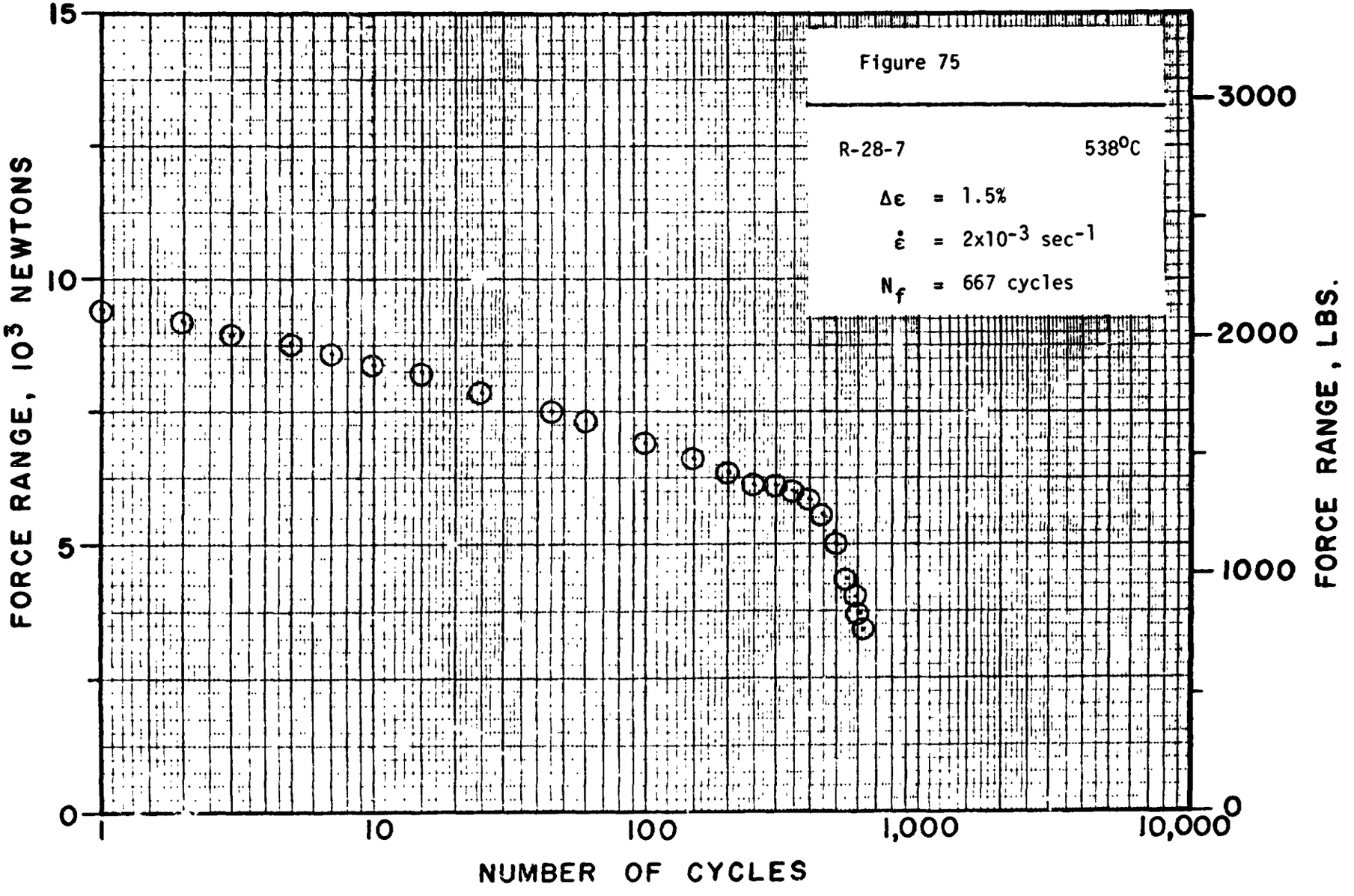
Figure 75
R-28-7
538°C
Δε = 1.5%
ε̇ = 2x10-3 sec-1
Nf = 667 cycles
FORCE RANGE, 10³ NEWTONS
FORCE RANGE, LBS.
NUMBER OF CYCLES
15
10
5
0
3000
2000
1000
0
1
10
100
1,000
10,000

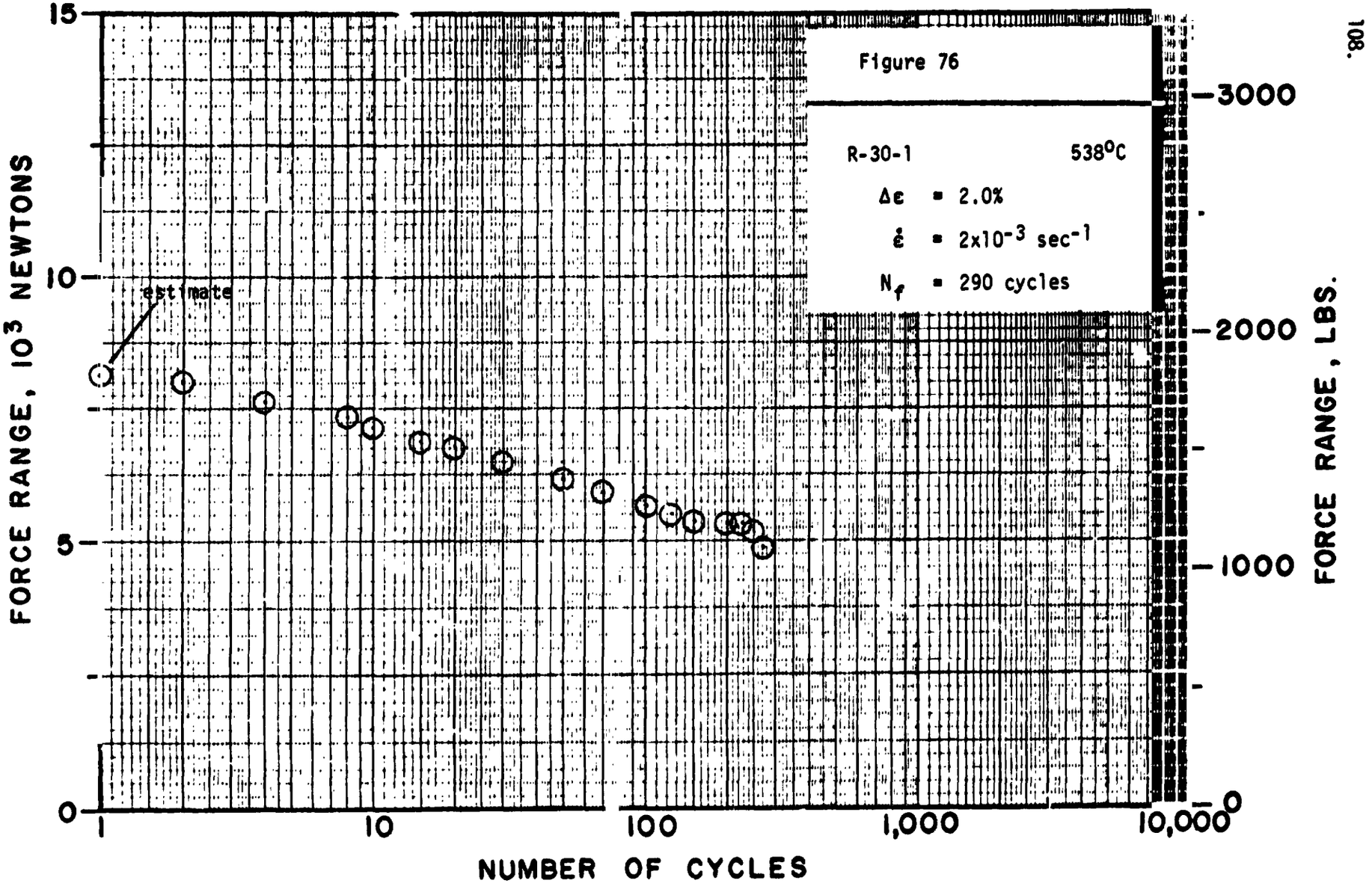
Figure 76
R-30-1
538°C
Δε = 2.0%
ε̇ = 2x10⁻³ sec⁻¹
N_f = 290 cycles
estimate
FORCE RANGE, 10³ NEWTONS
FORCE RANGE, LBS.
NUMBER OF CYCLES
15
10
5
0
3000
2000
1000
0
1
10
100
1,000
10,000

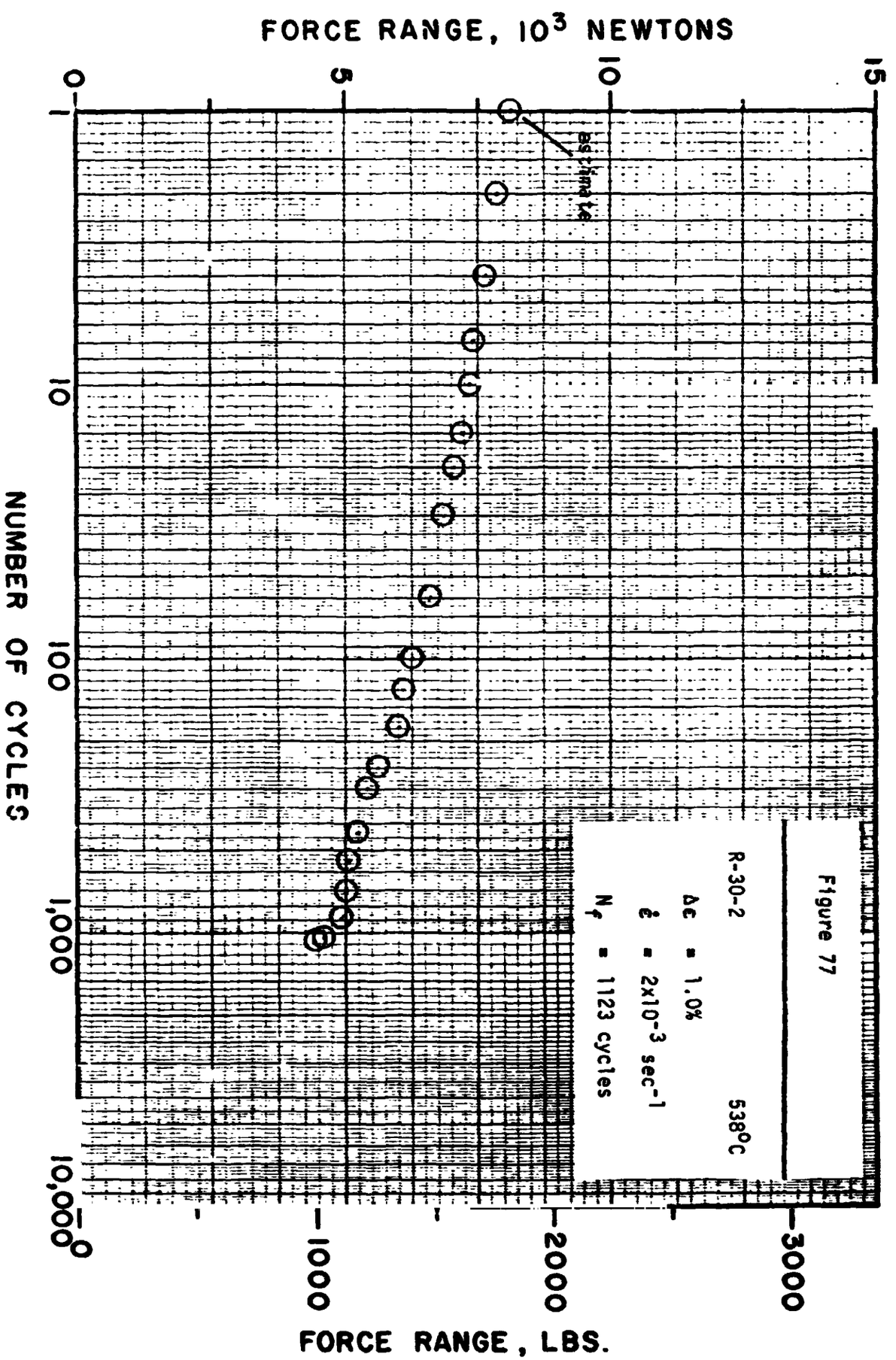
FORCE RANGE, 10^3 NEWTONS
0
5
10
15
estimate
NUMBER OF CYCLES
1
10
100
1,000
10,000
R-30-2
538°C
Δε = 1.0%
ε̇ = 2x10⁻³ sec⁻¹
N_f = 1123 cycles
Figure 77
1000
2000
3000
FORCE RANGE, LBS.

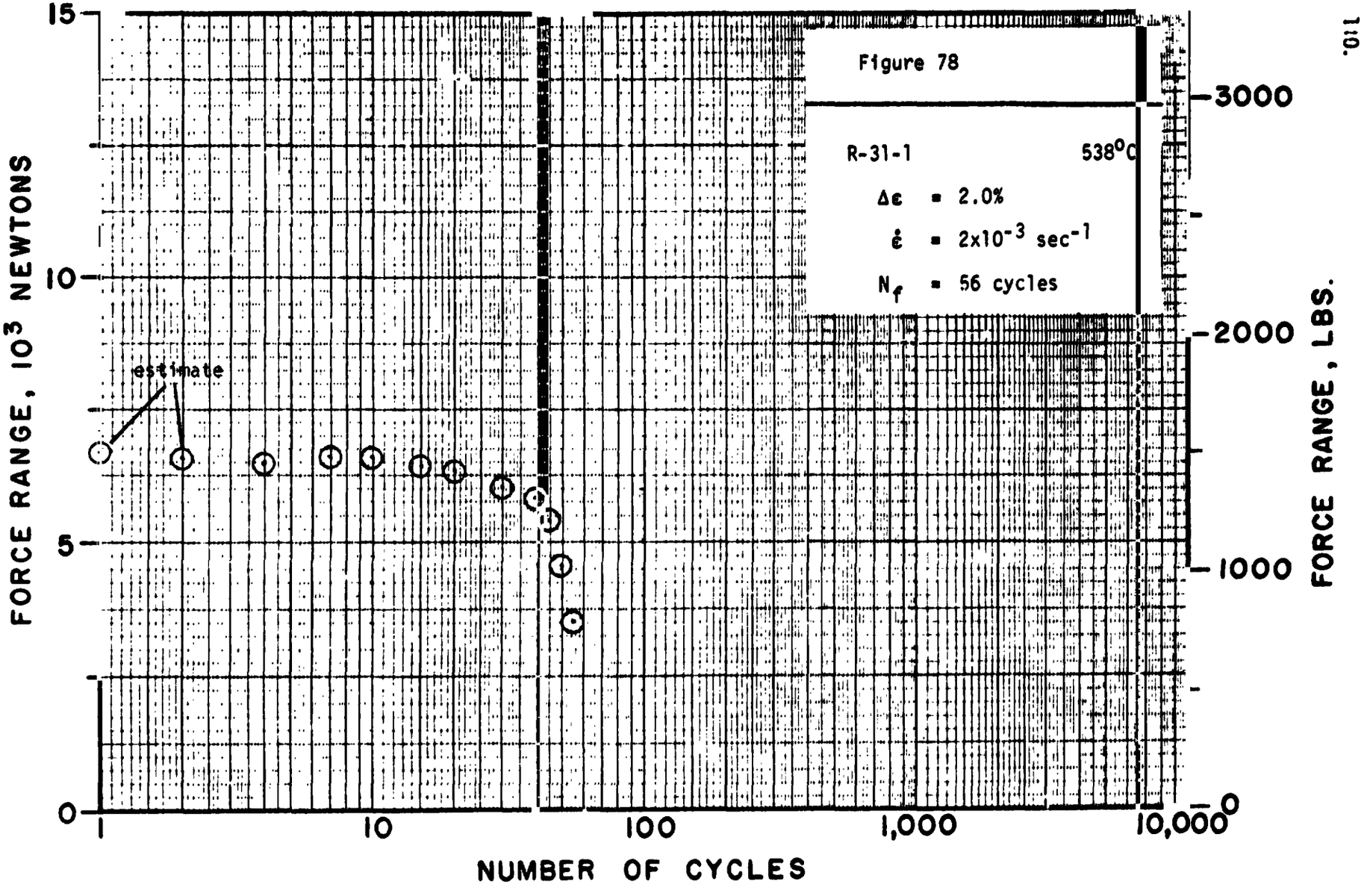
Figure 78
R-31-1
538°C
Δε = 2.0%
ε̇ = 2x10⁻³ sec⁻¹
N_f = 56 cycles
estimate
FORCE RANGE, 10³ NEWTONS
FORCE RANGE, LBS.
NUMBER OF CYCLES
15
10
5
0
3000
2000
1000
0
1
10
100
1,000
10,000

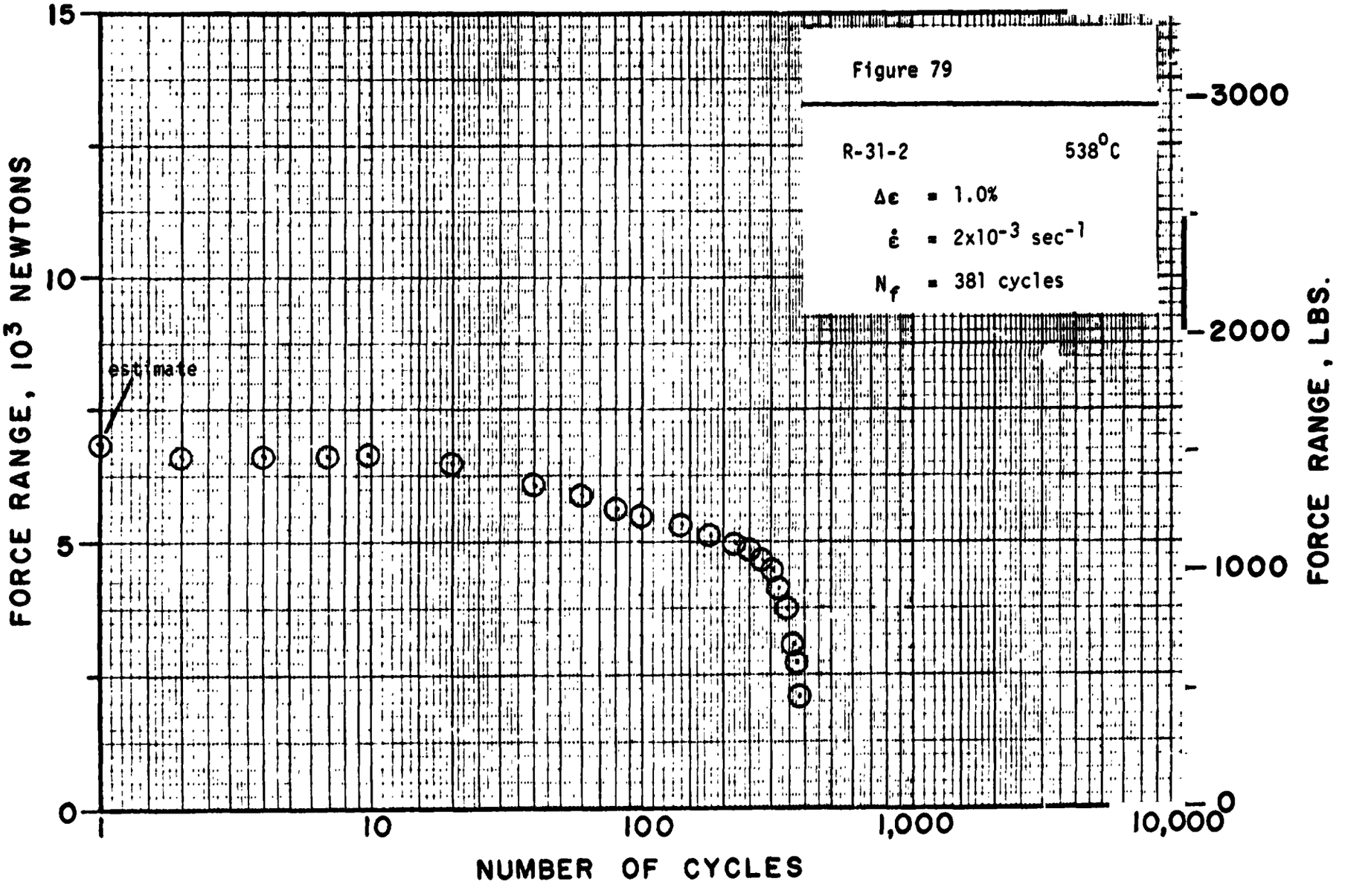
Figure 79
R-31-2
538°C
Δε = 1.0%
ε̇ = 2x10⁻³ sec⁻¹
N_f = 381 cycles
estimate
FORCE RANGE, 10³ NEWTONS
FORCE RANGE, LBS.
NUMBER OF CYCLES
15
10
5
0
3000
2000
1000
0
1
10
100
1,000
10,000

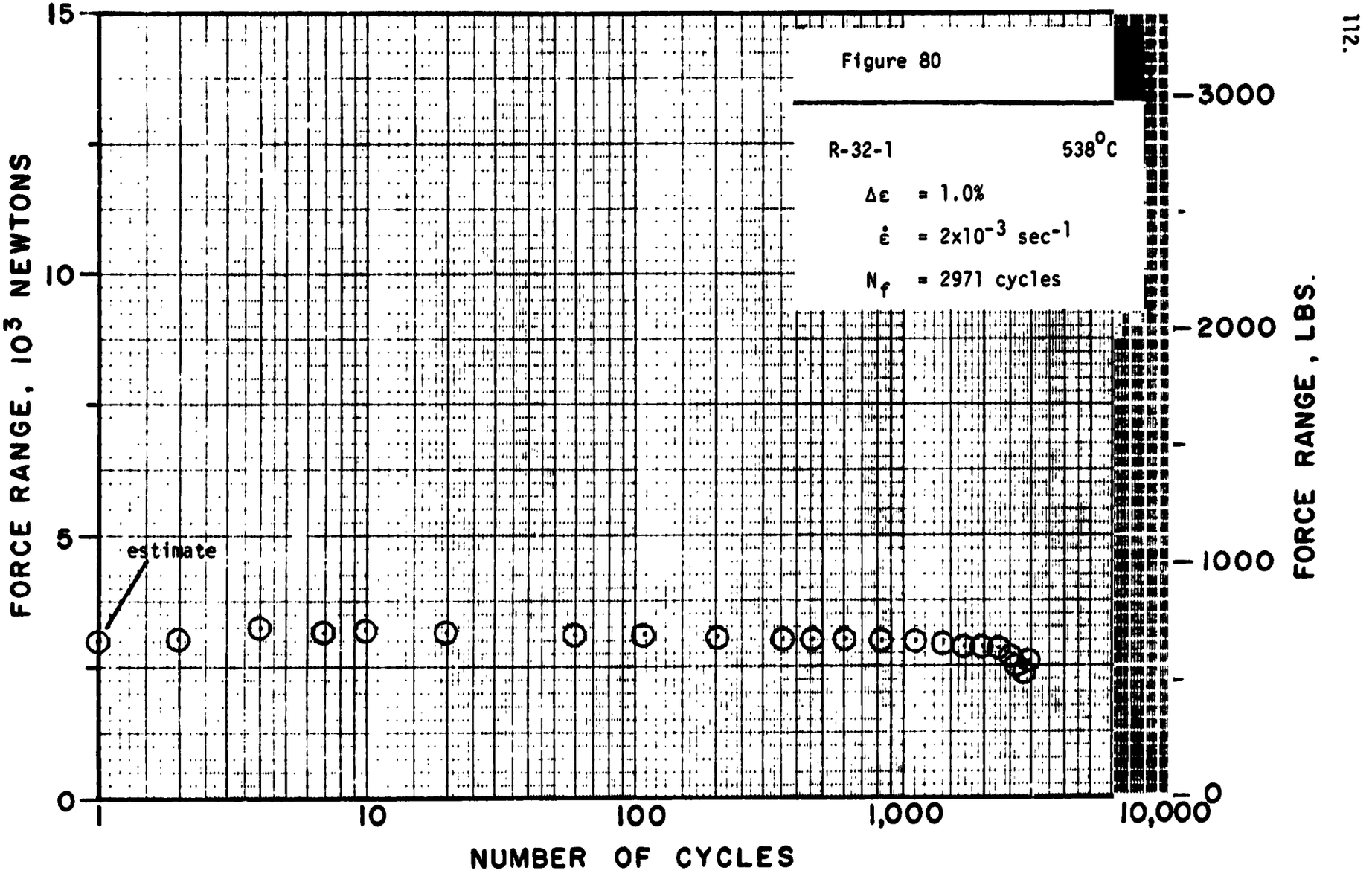
Figure 80
R-32-1
538°C
Δε = 1.0%
ε̇ = 2x10⁻³ sec⁻¹
N_f = 2971 cycles
estimate
FORCE RANGE, 10³ NEWTONS
FORCE RANGE, LBS.
NUMBER OF CYCLES
0
5
10
15
1
10
100
1,000
10,000
0
1000
2000
3000

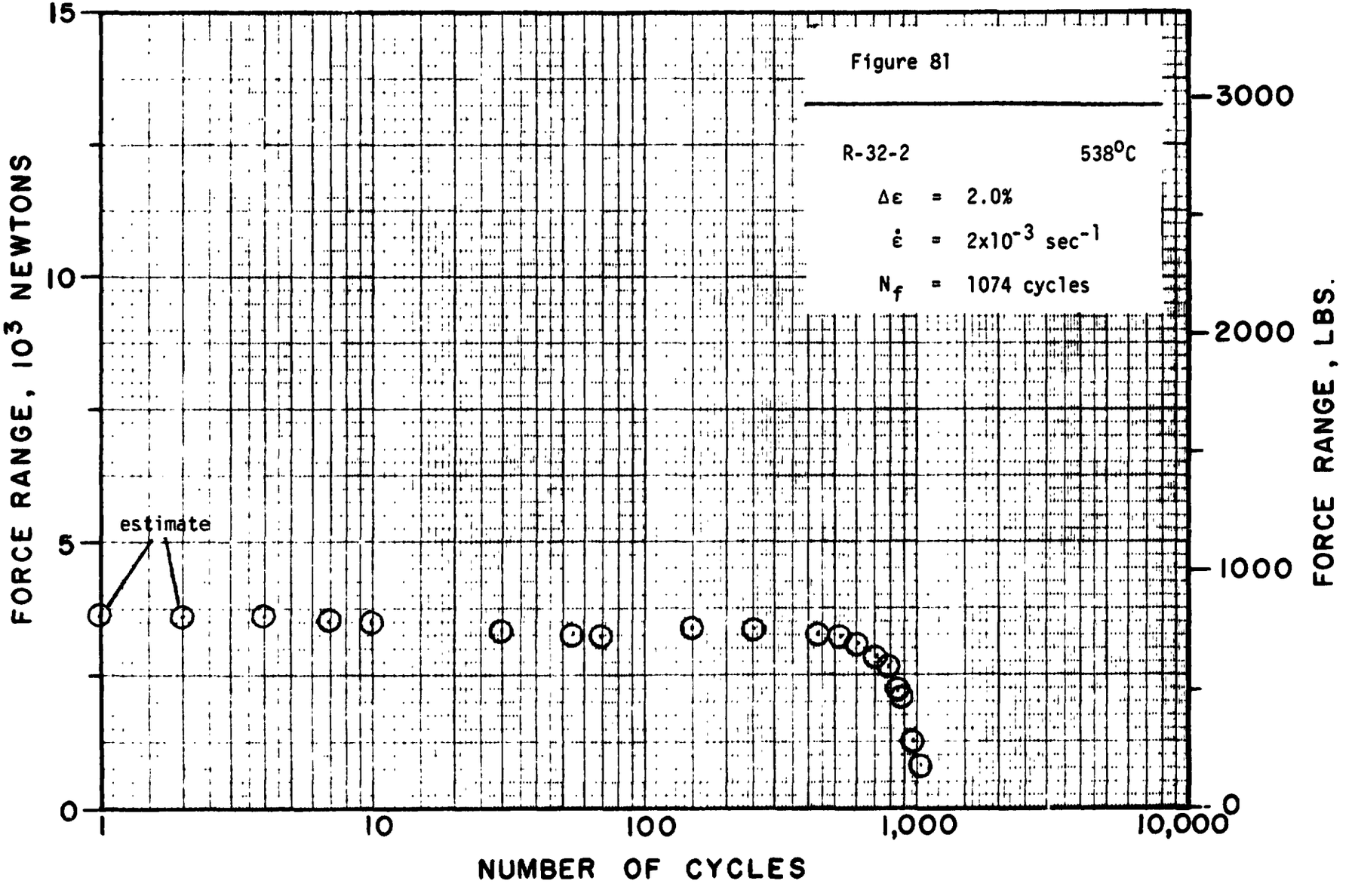
Figure 81
R-32-2
538°C
Δε = 2.0%
ε̇ = 2x10⁻³ sec⁻¹
N_f = 1074 cycles
estimate
FORCE RANGE, 10³ NEWTONS
FORCE RANGE, LBS.
NUMBER OF CYCLES
15
10
5
0
3000
2000
1000
0
1
10
100
1,000
10,000

PART VI - TYPICAL HYSTERESIS LOOPS FOR LOW-CYCLE FATIGUE TESTS

A typical hysteresis loop for each test is presented in this section. It was the intent here to show the cyclic stress-strain behavior near half-life but in many cases no hysteresis loops were recorded in the immediate vicinity of $N_f/2$. In these instances the hysteresis loop selected for reporting was the one closest to half-life and usually in the region prior to $N_f/2$. The particular cycle used in such plots is recorded in the figure along with the temperature, strain range and cycles to failure. The sequence of presentation is the same as that observed in Part V of this report.

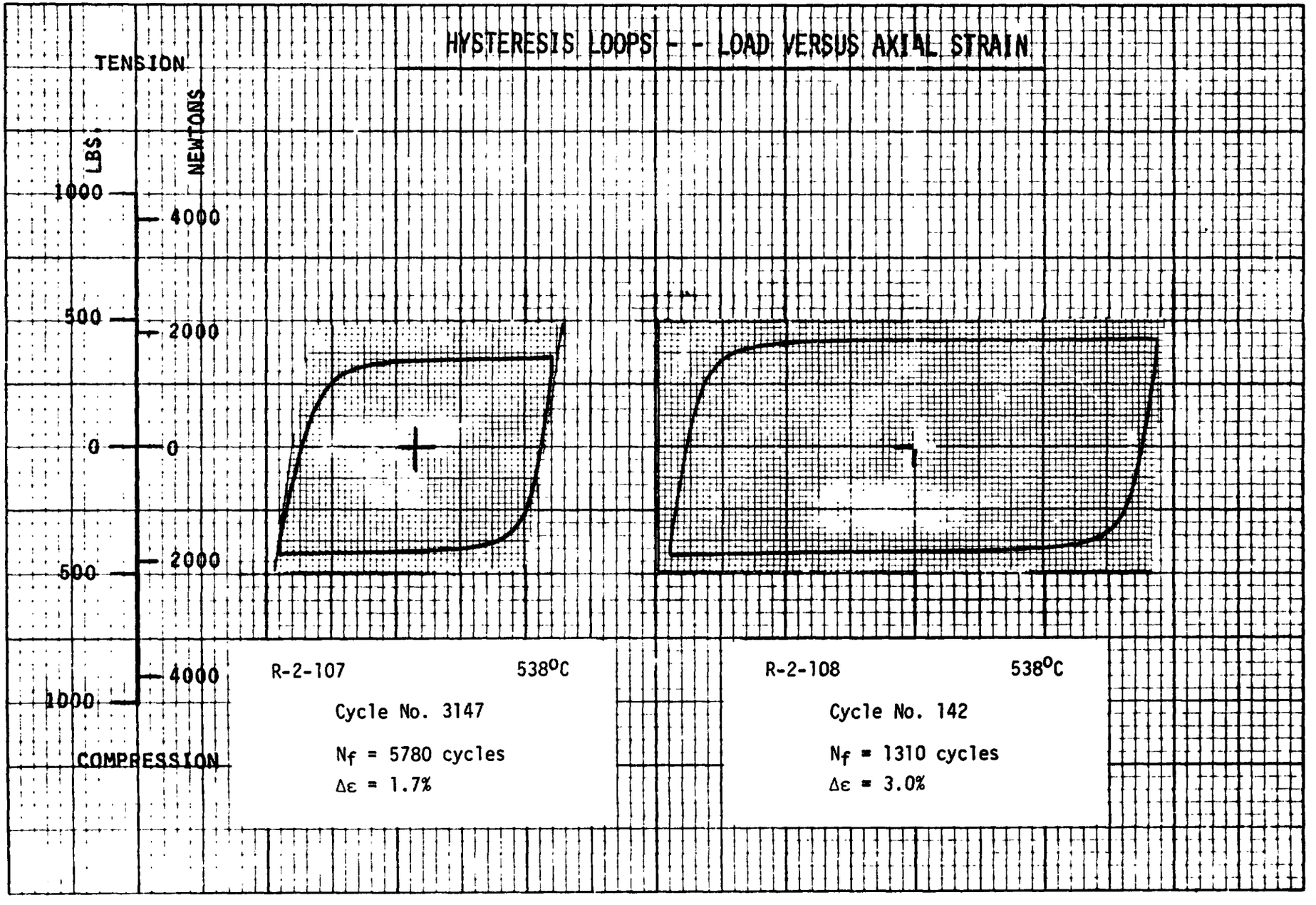
HYSTERESIS LOOPS - - LOAD VERSUS AXIAL STRAIN
TENSION
LBS.
NEWTONS
1000
4000
500
2000
0
0
500
2000
4000
1000
COMPRESSION
R-2-107
538°C
Cycle No. 3147
N_f = 5780 cycles
$\Delta\varepsilon$ = 1.7%
R-2-108
538°C
Cycle No. 142
N_f = 1310 cycles
$\Delta\varepsilon$ = 3.0%

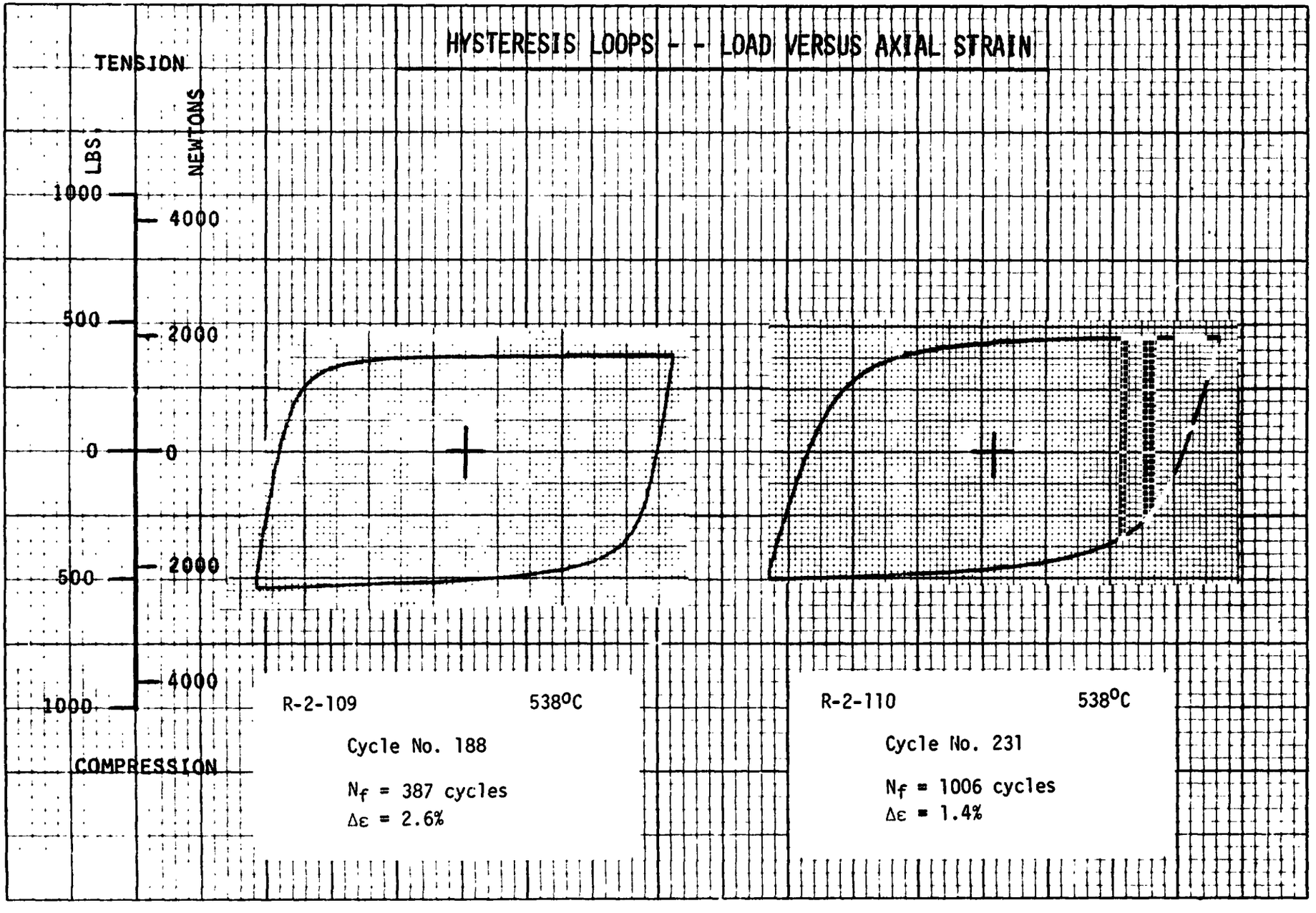
HYSTERESIS LOOPS - - LOAD VERSUS AXIAL STRAIN
TENSION
LBS
NEWTONS
1000
4000
500
2000
0
0
500
2000
1000
4000
COMPRESSION
R-2-109
538°C
Cycle No. 188
N_f = 387 cycles
$\Delta\varepsilon$ = 2.6%
R-2-110
538°C
Cycle No. 231
N_f = 1006 cycles
$\Delta\varepsilon$ = 1.4%

Page intentionally left blank

Page intentionally left blank

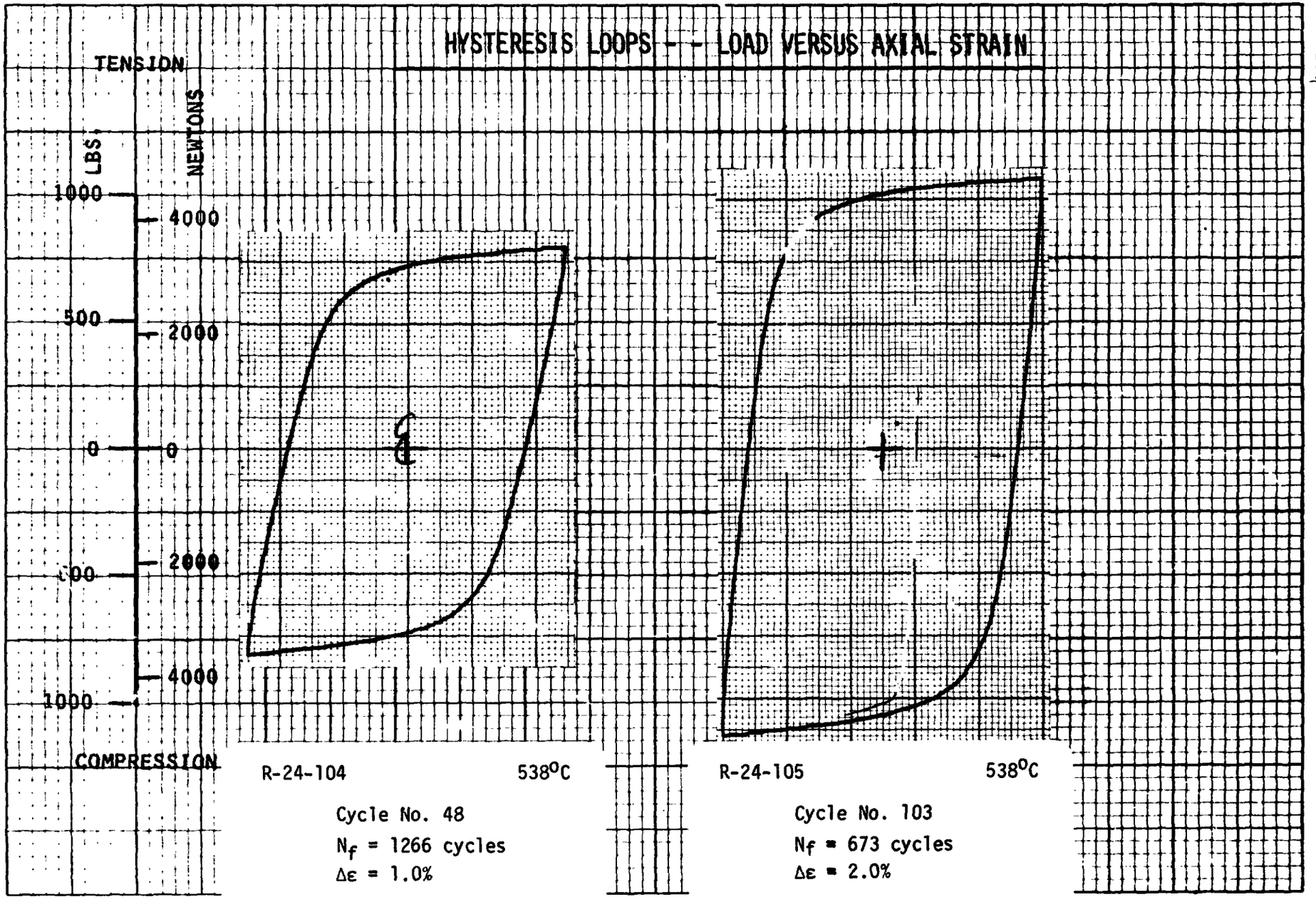
HYSTERESIS LOOPS - - LOAD VERSUS AXIAL STRAIN
TENSION
LBS.
NEWTONS
1000
4000
500
2000
0
0
2000
4000
1000
COMPRESSION
R-24-104
538°C
Cycle No. 48
N_f = 1266 cycles
$\Delta\varepsilon$ = 1.0%
R-24-105
538°C
Cycle No. 103
N_f = 673 cycles
$\Delta\varepsilon$ = 2.0%

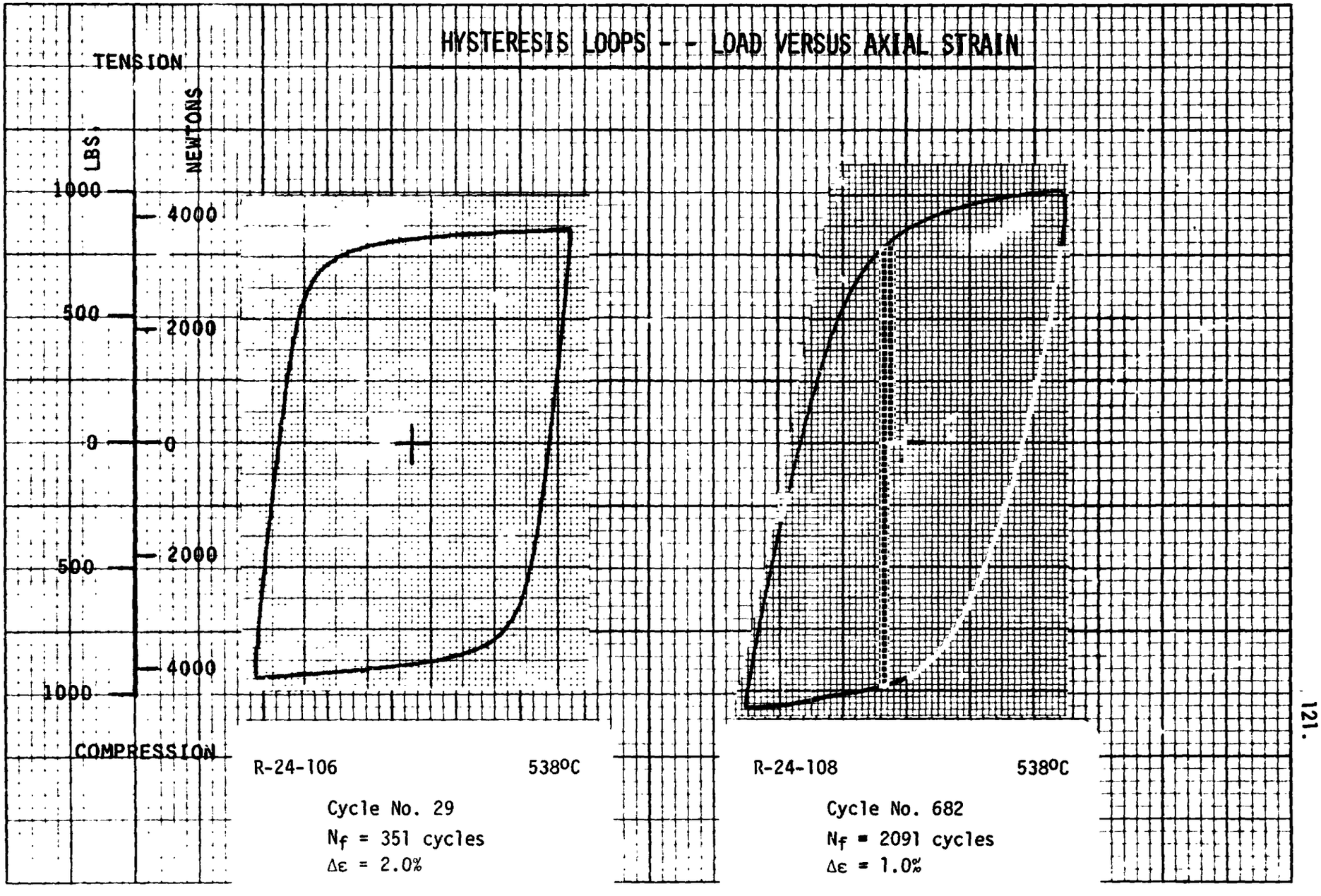
HYSTERESIS LOOPS - - LOAD VERSUS AXIAL STRAIN
TENSION
LBS.
NEWTONS
1000
4000
500
2000
0
0
500
2000
1000
4000
COMPRESSION
R-24-106
538°C
Cycle No. 29
N_f = 351 cycles
$\Delta\varepsilon$ = 2.0%
R-24-108
538°C
Cycle No. 682
N_f = 2091 cycles
$\Delta\varepsilon$ = 1.0%

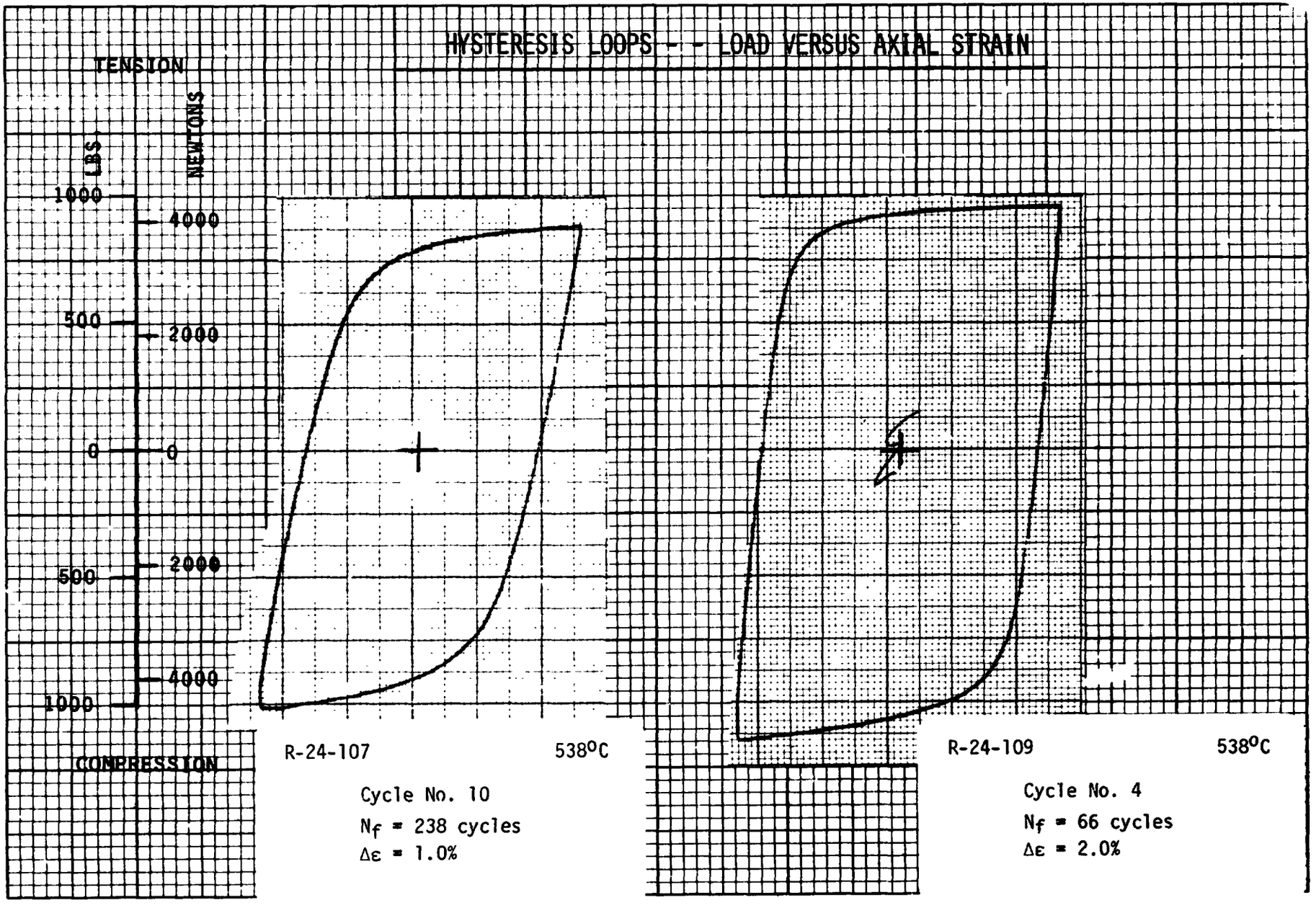
HYSTERESIS LOOPS - - LOAD VERSUS AXIAL STRAIN
TENSION
LBS.
NEWTONS
1000
4000
500
2000
0
0
500
2000
4000
1000
COMPRESSION
R-24-107
538°C
Cycle No. 10
N_f = 238 cycles
$\Delta\varepsilon$ = 1.0%
R-24-109
538°C
Cycle No. 4
N_f = 66 cycles
$\Delta\varepsilon$ = 2.0%

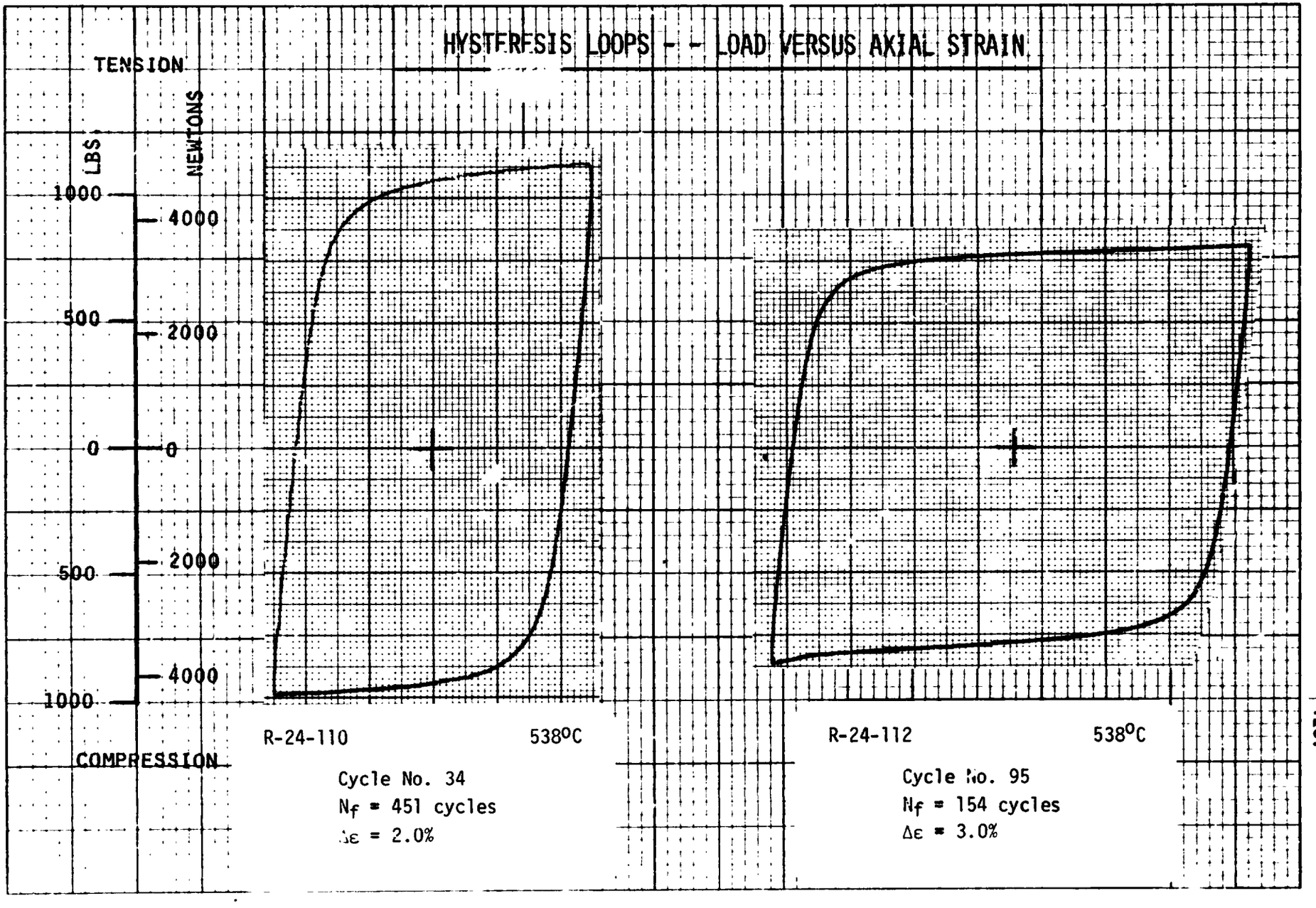
HYSTERESIS LOOPS - - LOAD VERSUS AXIAL STRAIN
TENSION
LBS.
NEWTONS
1000
4000
500
2000
0
0
500
2000
4000
1000
COMPRESSION
R-24-110
538°C
Cycle No. 34
N_f = 451 cycles
Δε = 2.0%
R-24-112
538°C
Cycle No. 95
N_f = 154 cycles
Δε = 3.0%

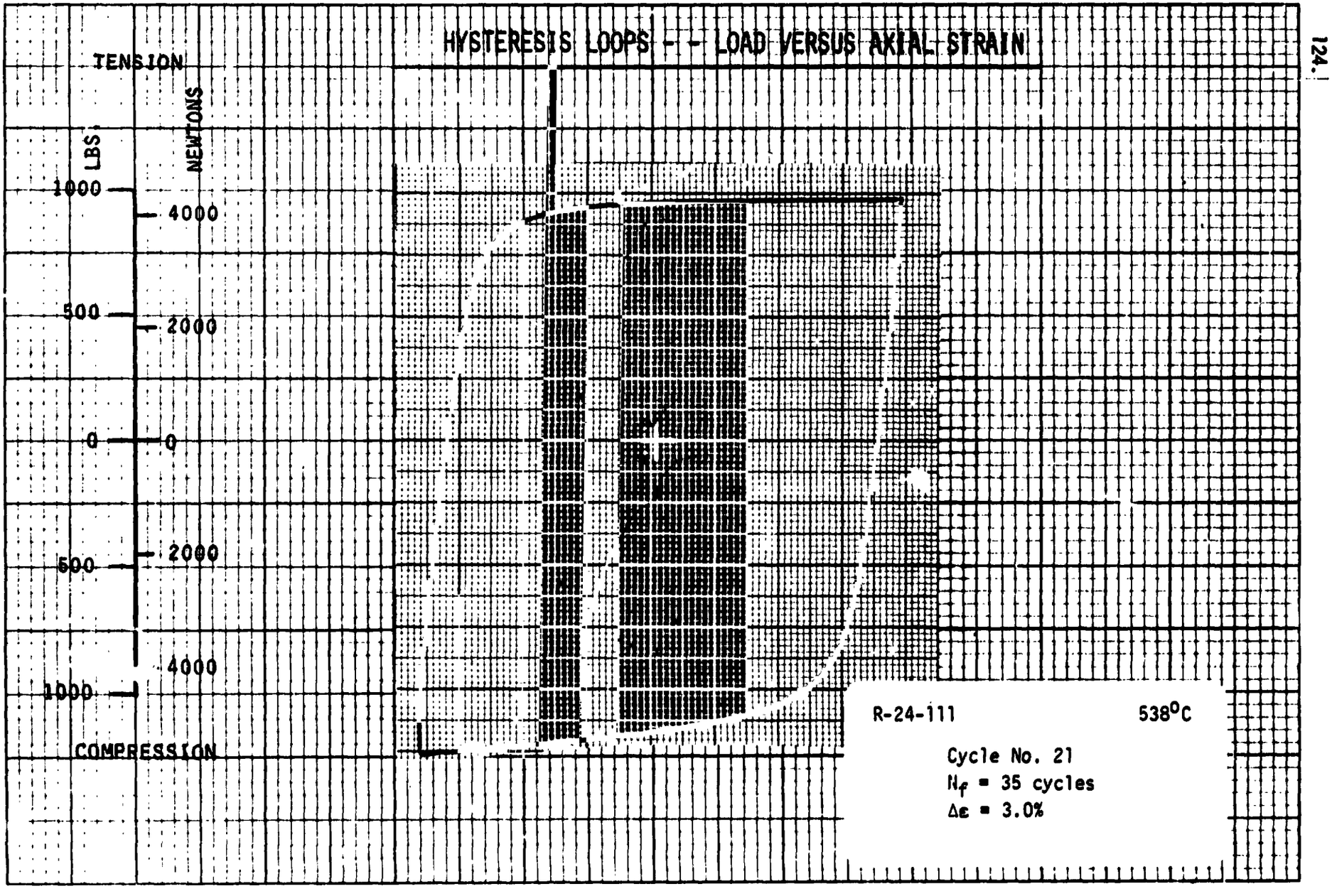
HYSTERESIS LOOPS - - LOAD VERSUS AXIAL STRAIN
TENSION
LBS
NEWTONS
1000
4000
500
2000
0
0
500
2000
4000
1000
COMPRESSION
R-24-111
538°C
Cycle No. 21
N_f = 35 cycles
$\Delta\varepsilon$ = 3.0%

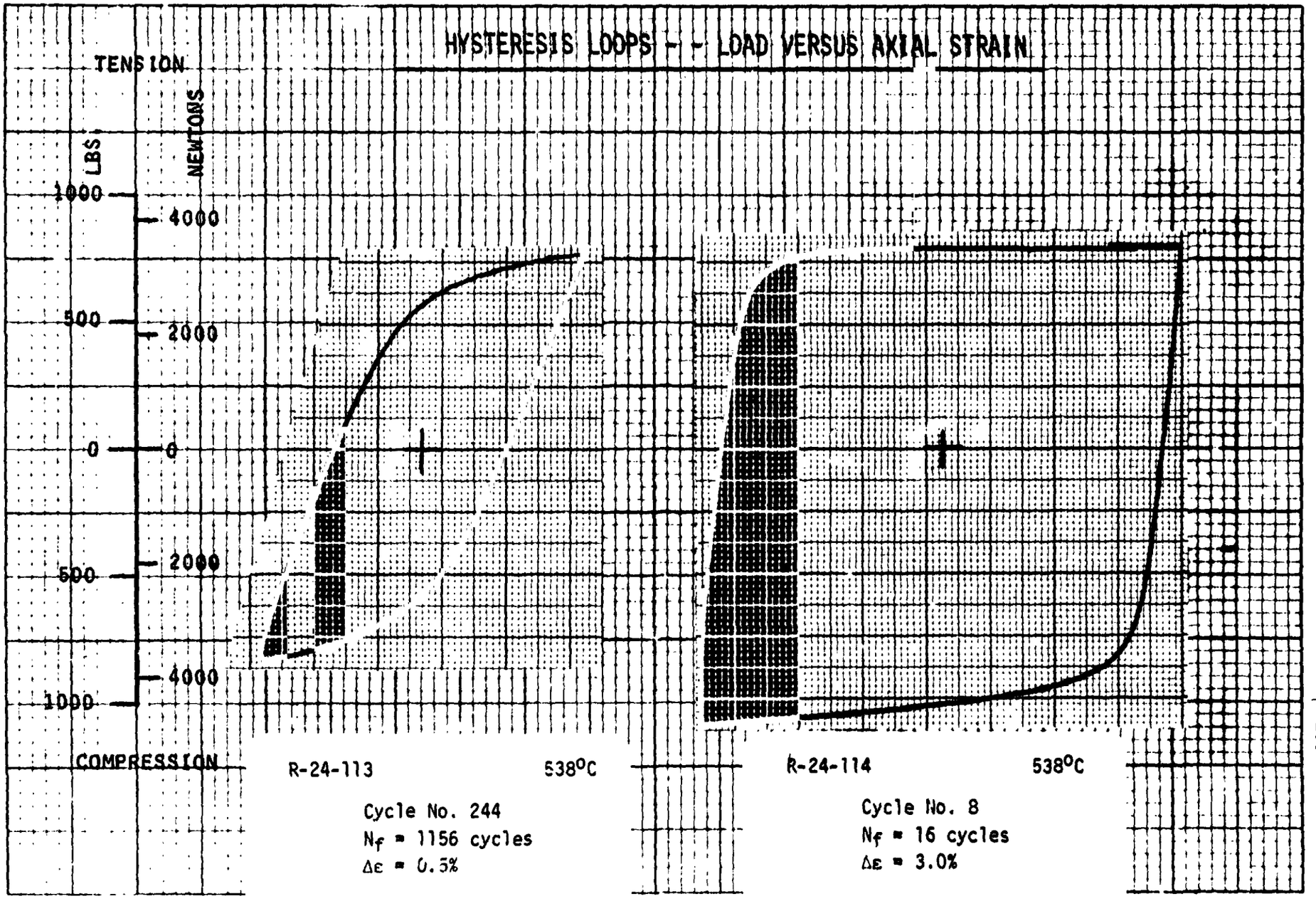
HYSTERESIS LOOPS - - LOAD VERSUS AXIAL STRAIN
TENSION
LBS
NEWTONS
1000
4000
500
2000
0
0
500
2000
1000
4000
COMPRESSION
R-24-113
538°C
Cycle No. 244
N_f = 1156 cycles
$\Delta\varepsilon$ = 0.5%
R-24-114
538°C
Cycle No. 8
N_f = 16 cycles
$\Delta\varepsilon$ = 3.0%

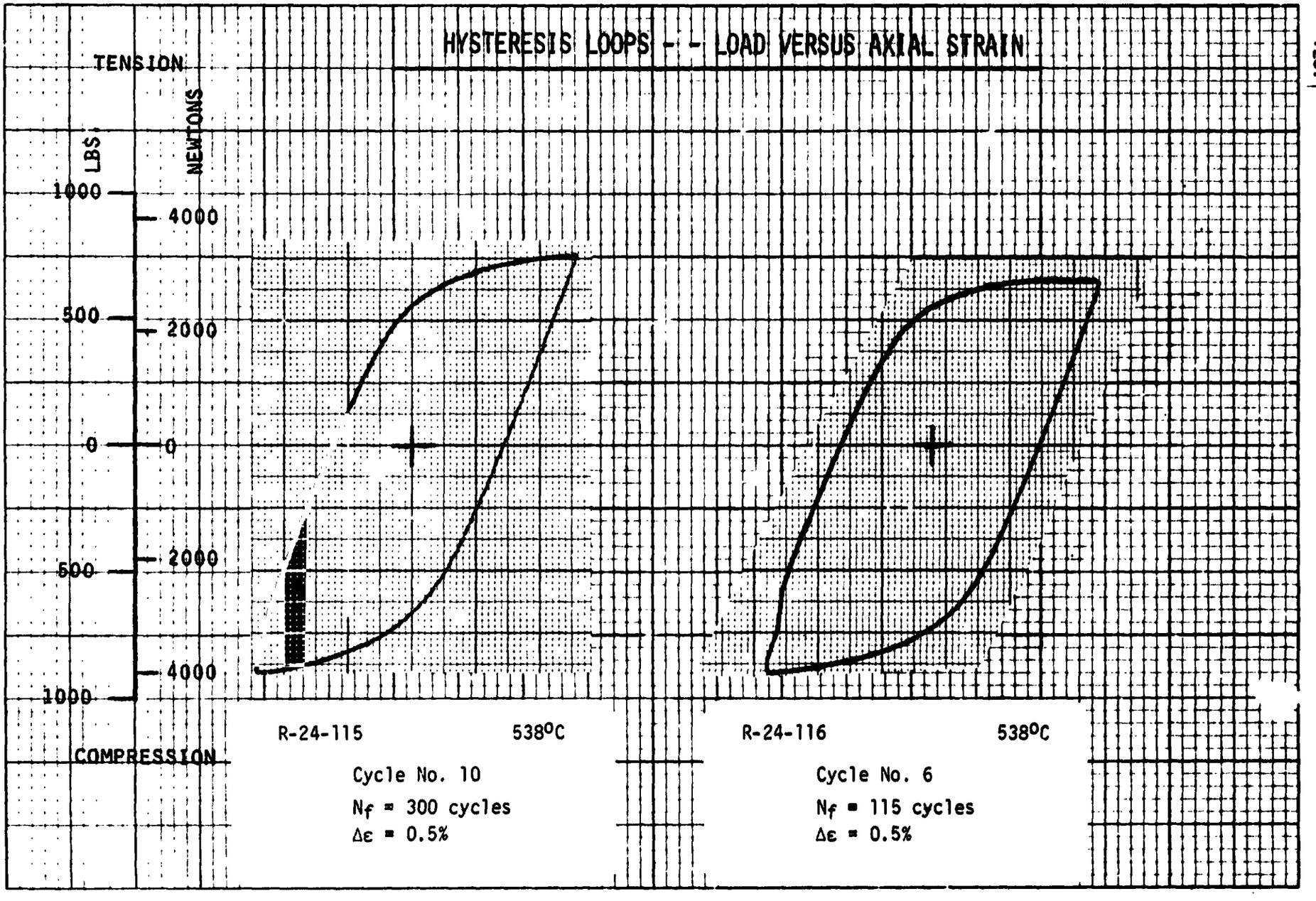
HYSTERESIS LOOPS - - LOAD VERSUS AXIAL STRAIN
TENSION
LBS
NEWTONS
1000
4000
500
2000
0
0
500
2000
4000
1000
COMPRESSION
R-24-115
538°C
Cycle No. 10
N_f = 300 cycles
$\Delta\varepsilon$ = 0.5%
R-24-116
538°C
Cycle No. 6
N_f = 115 cycles
$\Delta\varepsilon$ = 0.5%

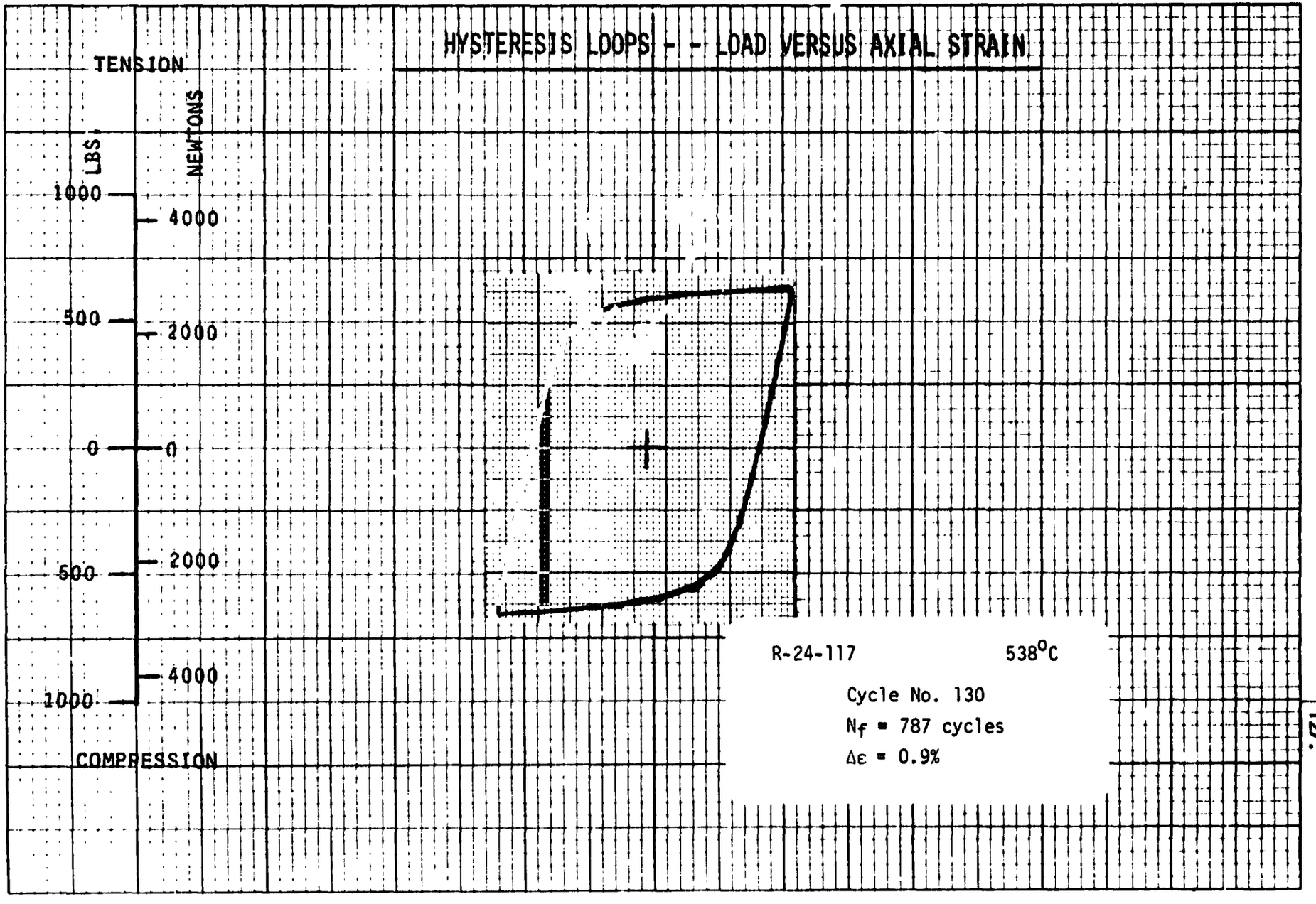
HYSTERESIS LOOPS - - LOAD VERSUS AXIAL STRAIN
TENSION
LBS.
NEWTONS
1000
4000
500
2000
0
0
500
2000
4000
1000
COMPRESSION
R-24-117
538°C
Cycle No. 130
N_f = 787 cycles
$\Delta\varepsilon$ = 0.9%

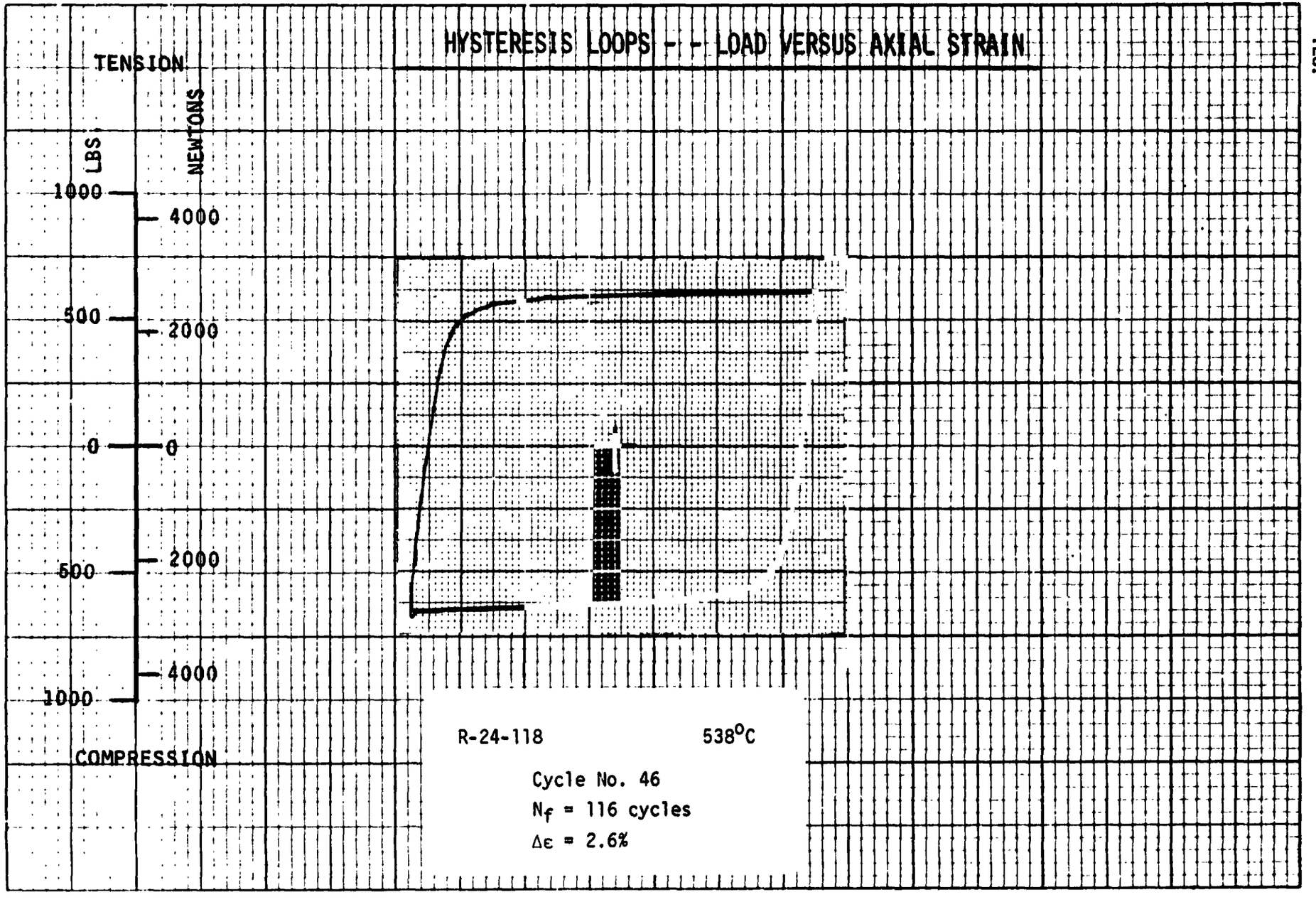
HYSTERESIS LOOPS - - LOAD VERSUS AXIAL STRAIN
TENSION
LBS.
NEWTONS
1000
4000
500
2000
0
0
500
2000
1000
4000
COMPRESSION
R-24-118
538°C
Cycle No. 46
N_f = 116 cycles
$\Delta\varepsilon$ = 2.6%

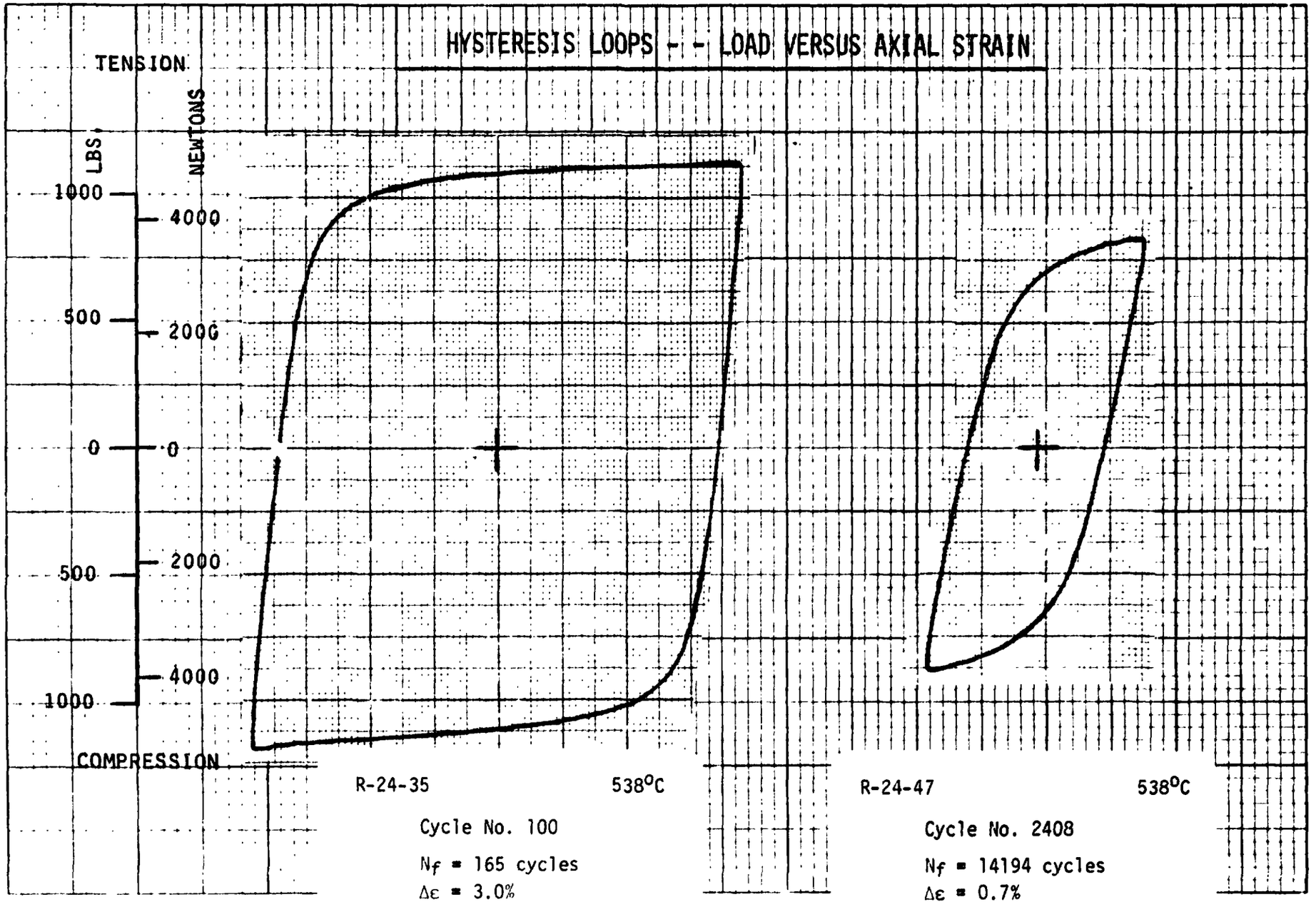
HYSTERESIS LOOPS - - LOAD VERSUS AXIAL STRAIN
TENSION
LBS
NEWTONS
1000
4000
500
2000
0
0
500
2000
4000
1000
COMPRESSION
R-24-35
538°C
Cycle No. 100
N_f = 165 cycles
$\Delta\varepsilon$ = 3.0%
R-24-47
538°C
Cycle No. 2408
N_f = 14194 cycles
$\Delta\varepsilon$ = 0.7%

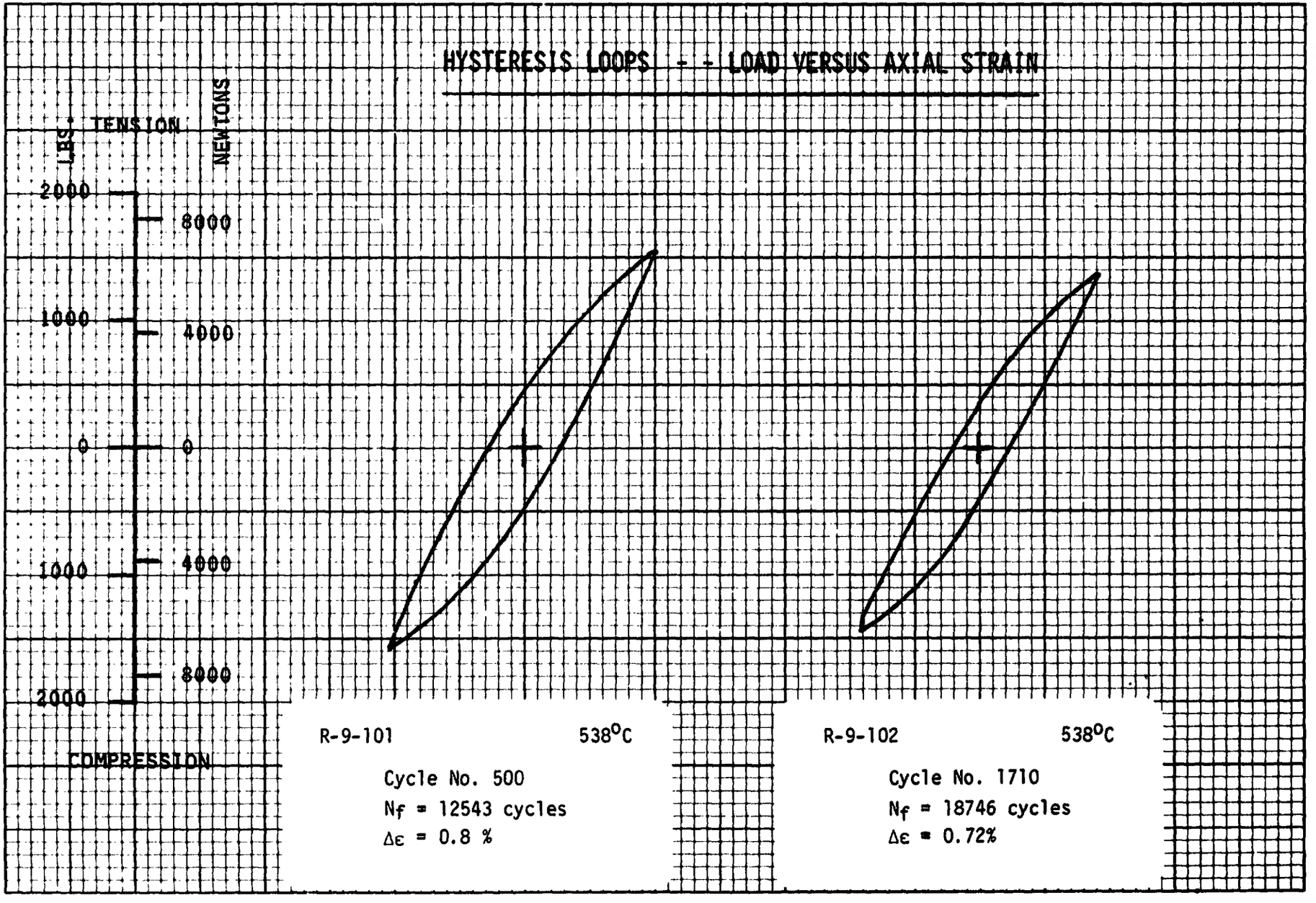
HYSTERESIS LOOPS - - LOAD VERSUS AXIAL STRAIN
LBS
TENSION
NEWTONS
2000
8000
1000
4000
0
0
1000
4000
8000
2000
COMPRESSION
R-9-101
538°C
Cycle No. 500
Nf = 12543 cycles
Δε = 0.8 %
R-9-102
538°C
Cycle No. 1710
Nf = 18746 cycles
Δε = 0.72%

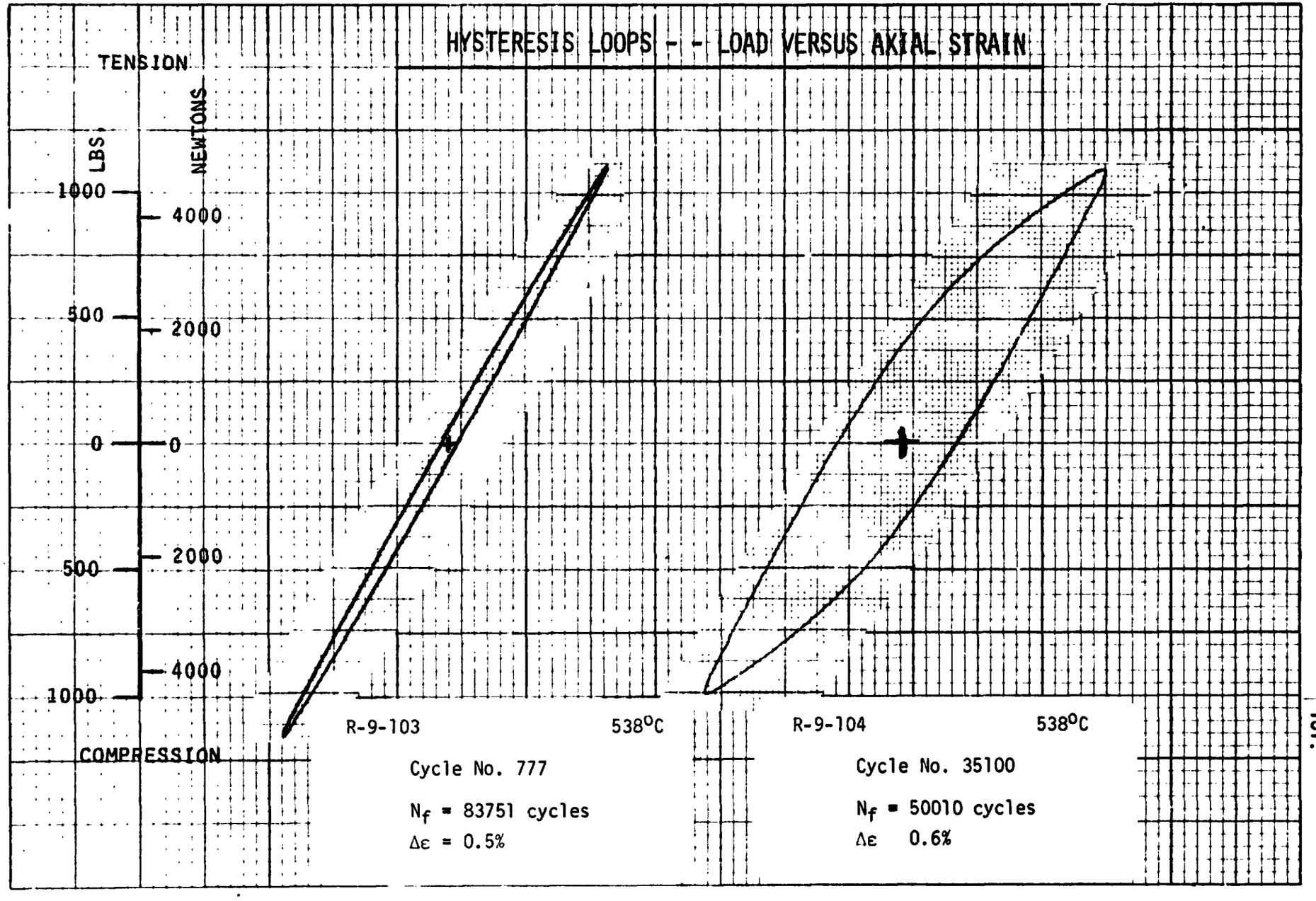
HYSTERESIS LOOPS - - LOAD VERSUS AXIAL STRAIN
TENSION
LBS.
NEWTONS
1000
4000
500
2000
0
0
500
2000
4000
1000
COMPRESSION
R-9-103
538°C
Cycle No. 777
N_f = 83751 cycles
$\Delta\varepsilon$ = 0.5%
R-9-104
538°C
Cycle No. 35100
N_f = 50010 cycles
$\Delta\varepsilon$ 0.6%

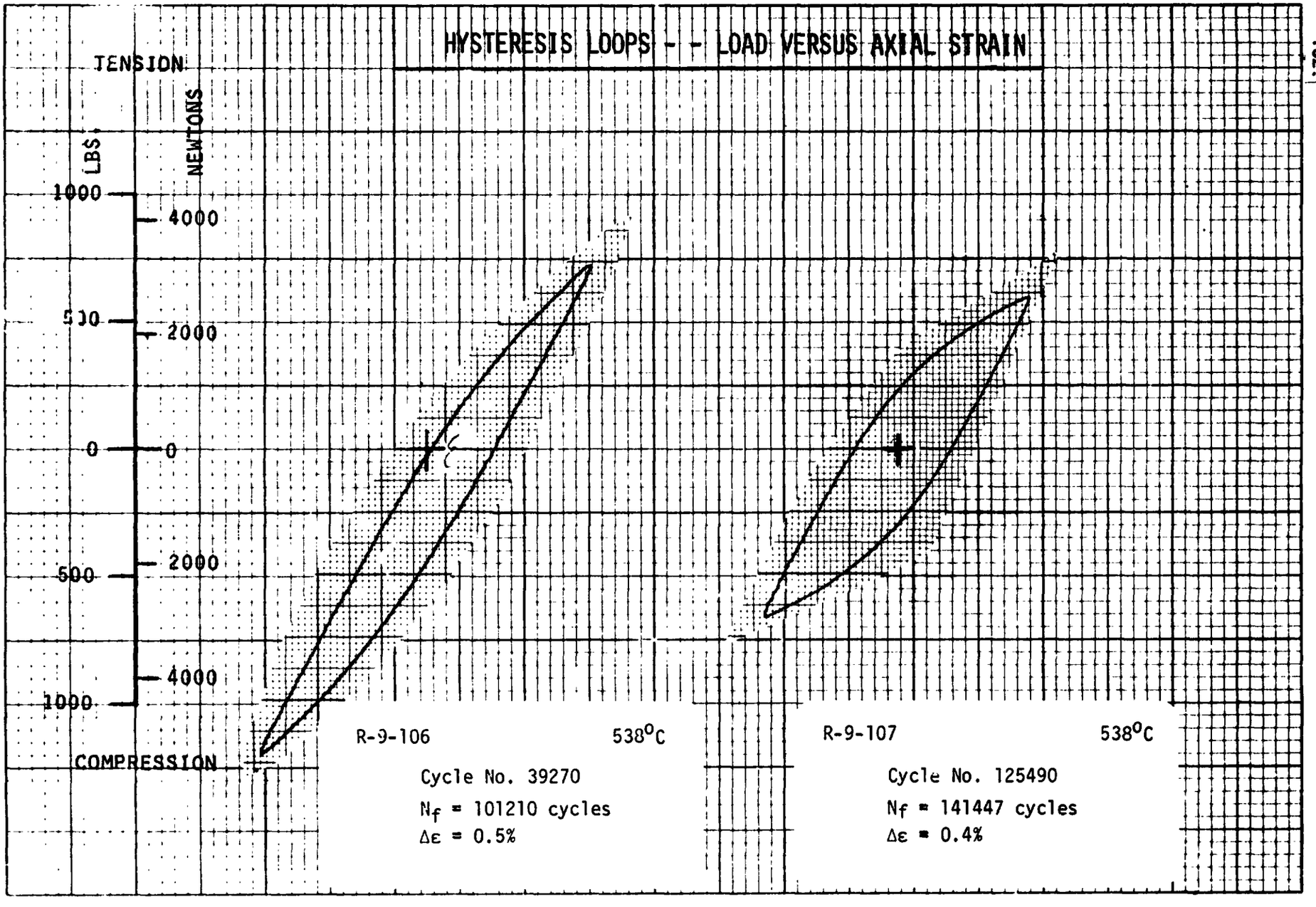
HYSTERESIS LOOPS - - LOAD VERSUS AXIAL STRAIN
TENSION
LBS.
NEWTONS
1000
4000
500
2000
0
0
500
2000
1000
4000
COMPRESSION
R-9-106
538°C
Cycle No. 39270
Nf = 101210 cycles
Δε = 0.5%
R-9-107
538°C
Cycle No. 125490
Nf = 141447 cycles
Δε = 0.4%

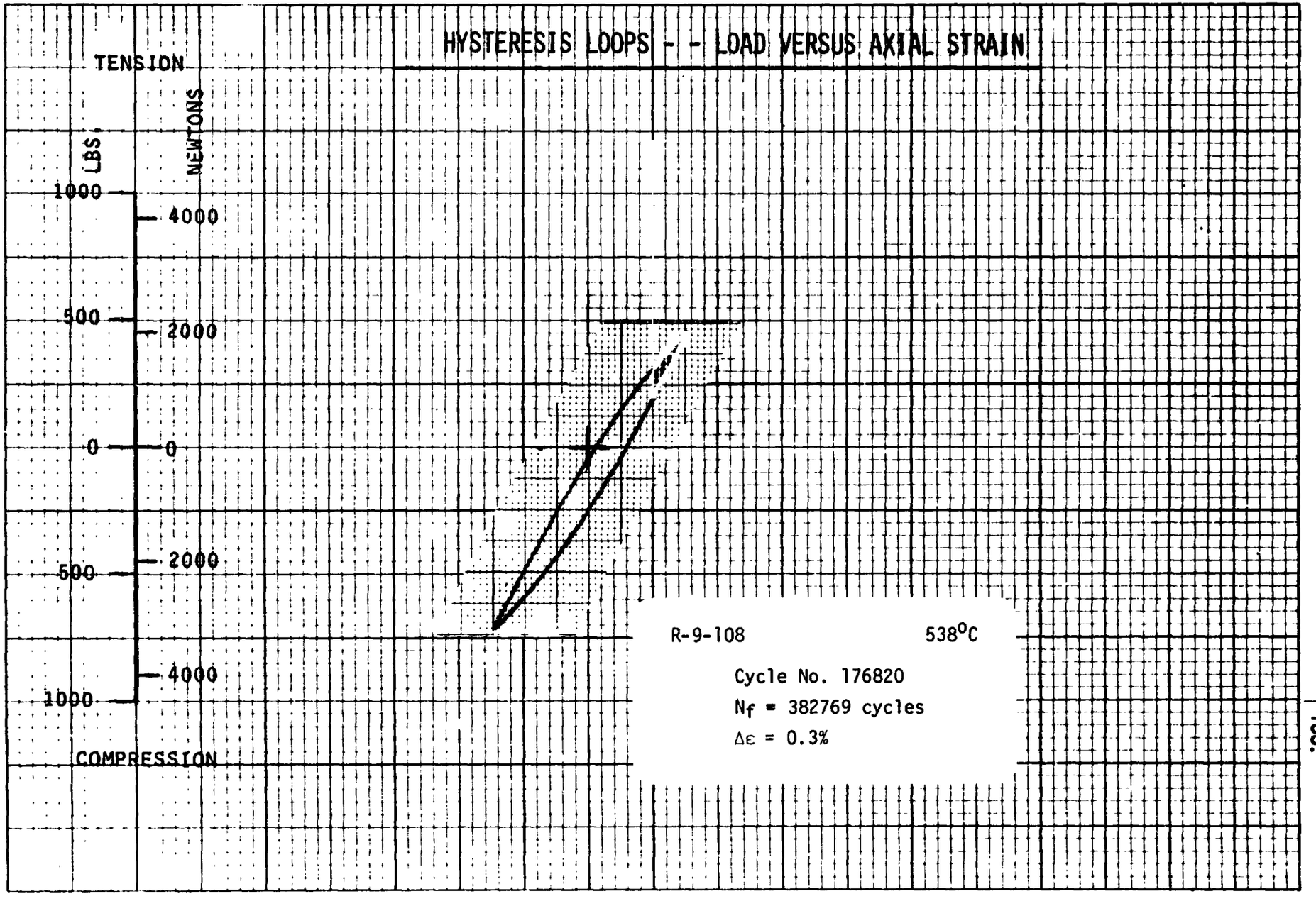
HYSTERESIS LOOPS - - LOAD VERSUS AXIAL STRAIN
TENSION
LBS
NEWTONS
1000
4000
500
2000
0
0
500
2000
4000
1000
COMPRESSION
R-9-108
538°C
Cycle No. 176820
N_f = 382769 cycles
$\Delta\varepsilon$ = 0.3%

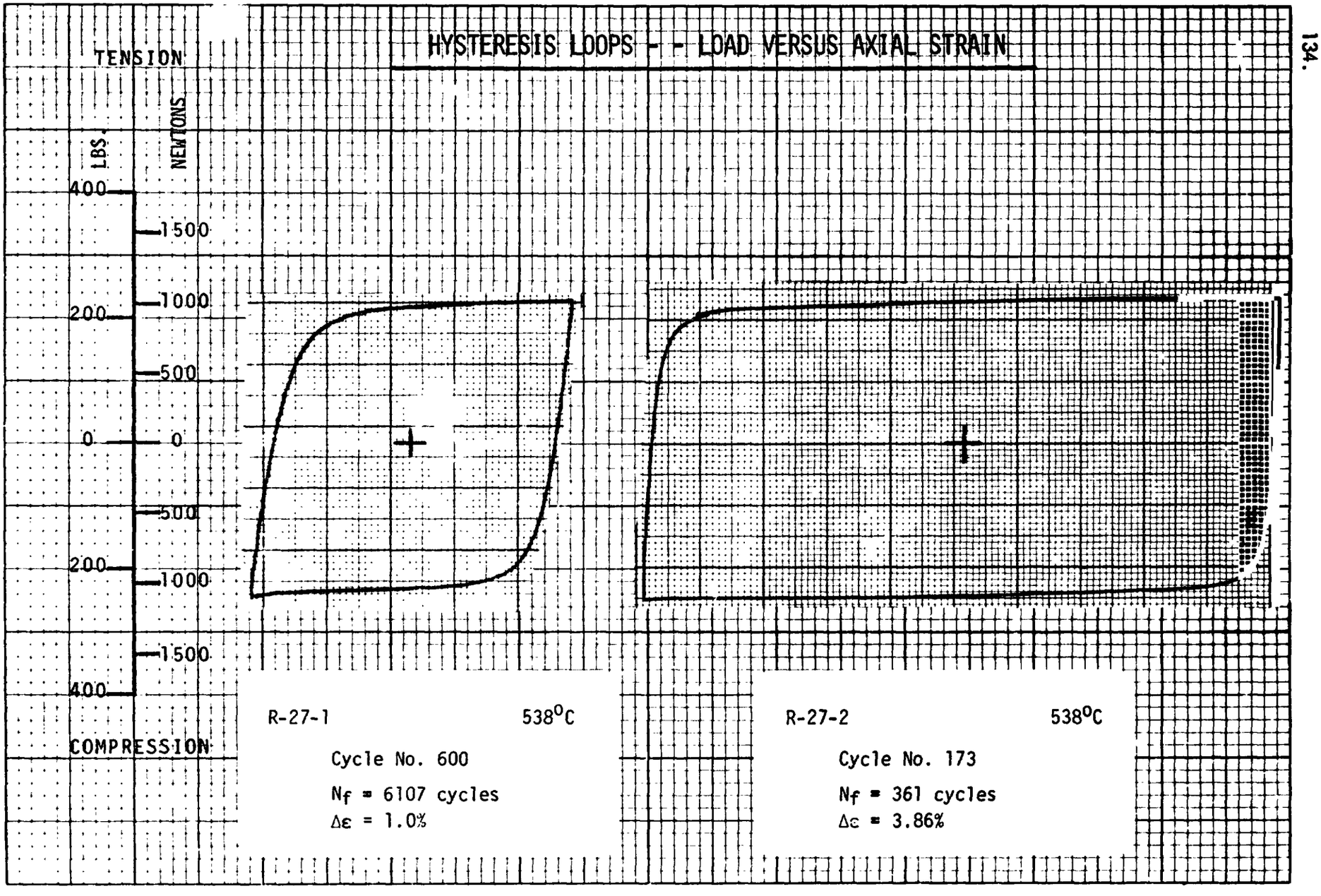
HYSTERESIS LOOPS - - LOAD VERSUS AXIAL STRAIN
TENSION
LBS.
NEWTONS
400
1500
200
1000
500
0
0
500
200
1000
1500
400
COMPRESSION
R-27-1
538°C
Cycle No. 600
Nf = 6107 cycles
Δε = 1.0%
R-27-2
538°C
Cycle No. 173
Nf = 361 cycles
Δε = 3.86%

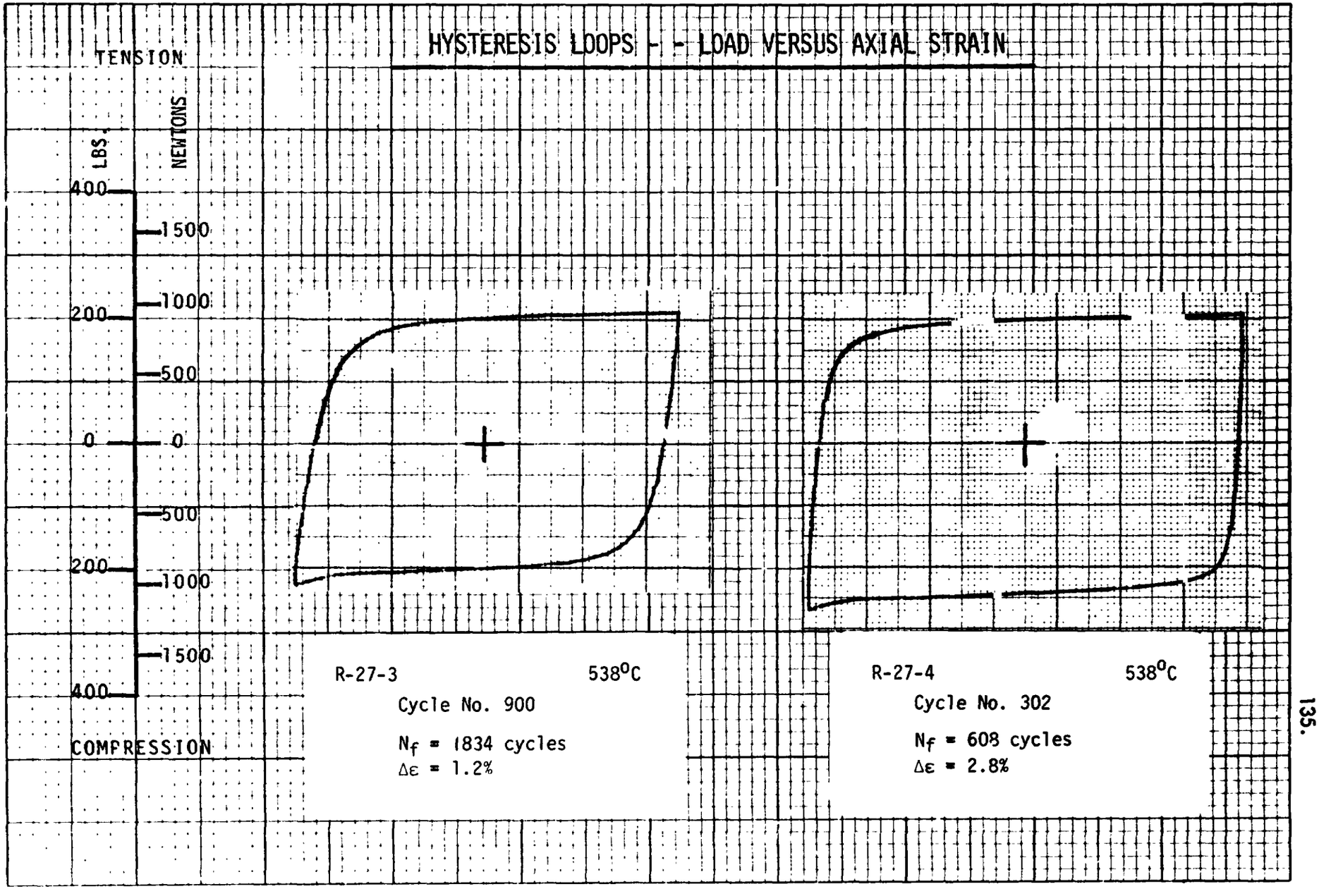
HYSTERESIS LOOPS - - LOAD VERSUS AXIAL STRAIN
TENSION
LBS.
NEWTONS
400
1500
200
1000
500
0
0
500
200
1000
1500
400
COMPRESSION
R-27-3
538°C
Cycle No. 900
N_f = 1834 cycles
$\Delta\varepsilon$ = 1.2%
R-27-4
538°C
Cycle No. 302
N_f = 608 cycles
$\Delta\varepsilon$ = 2.8%

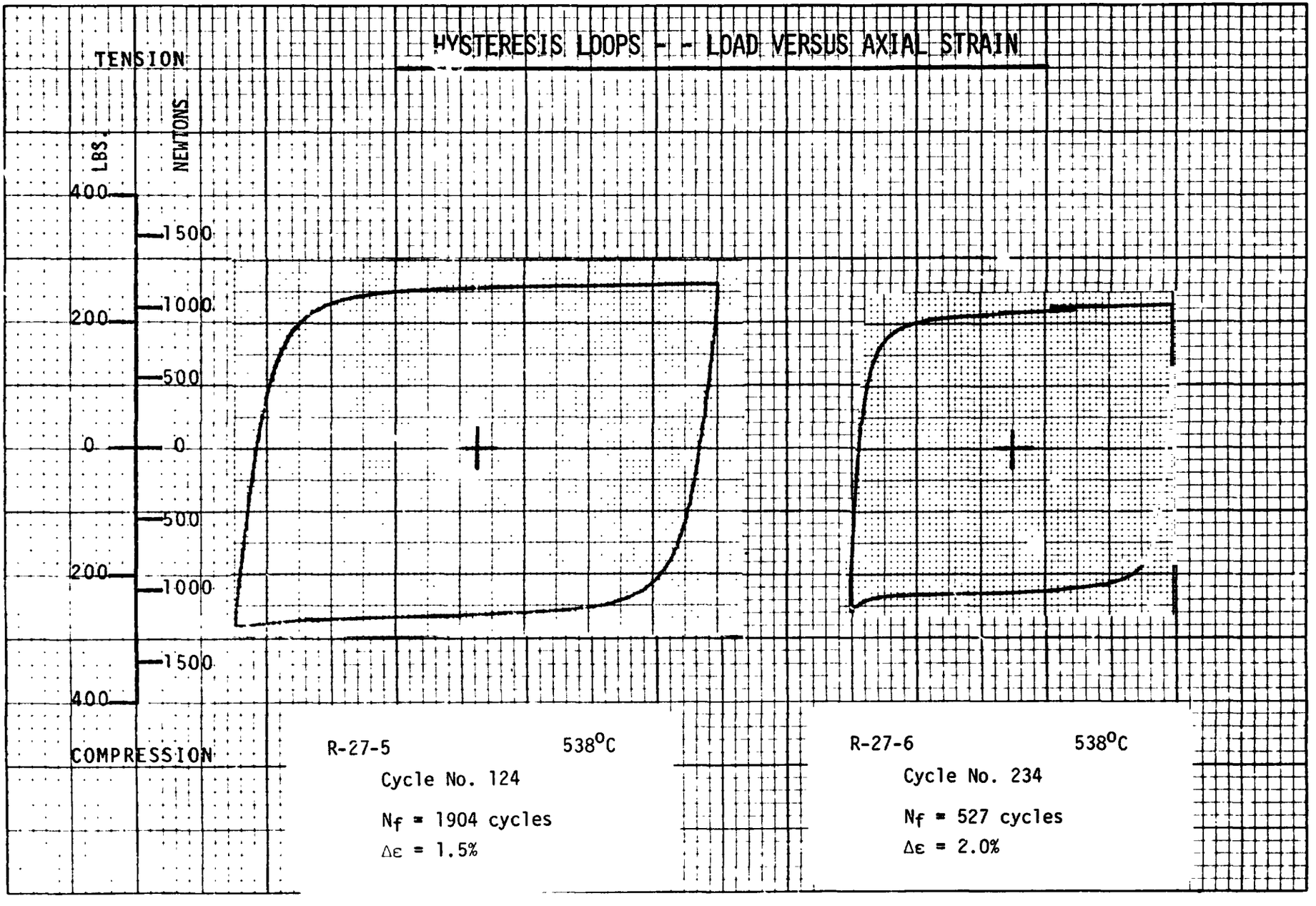
HYSTERESIS LOOPS - - LOAD VERSUS AXIAL STRAIN
TENSION
LBS.
NEWTONS
400
1500
200
1000
500
0
0
500
200
1000
1500
400
COMPRESSION
R-27-5
538°C
Cycle No. 124
Nf = 1904 cycles
Δε = 1.5%
R-27-6
538°C
Cycle No. 234
Nf = 527 cycles
Δε = 2.0%

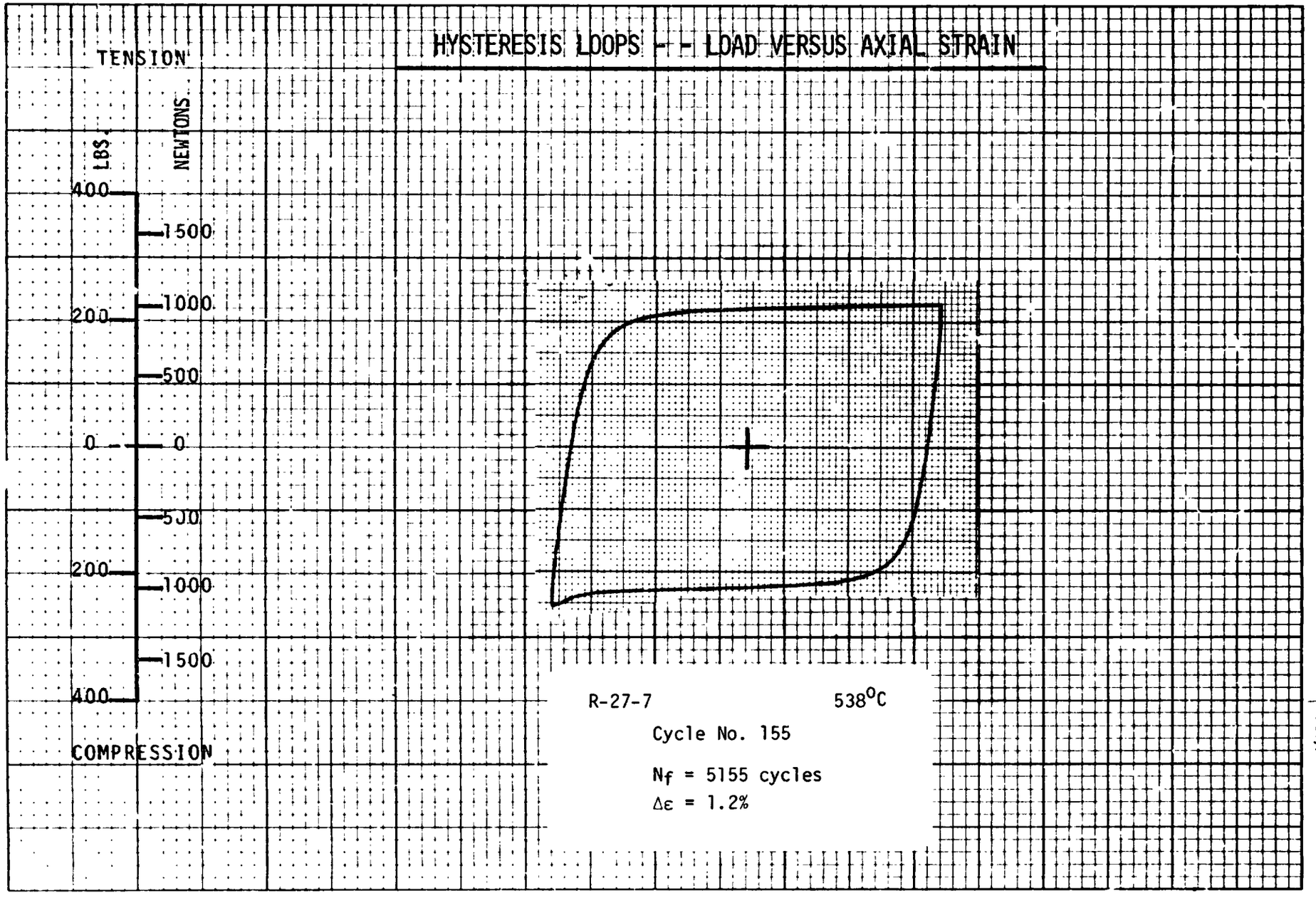
HYSTERESIS LOOPS -- LOAD VERSUS AXIAL STRAIN
TENSION
LBS
NEWTONS
400
1500
200
1000
500
0
0
500
200
1000
1500
400
COMPRESSION
R-27-7
538°C
Cycle No. 155
N_f = 5155 cycles
$\Delta\varepsilon$ = 1.2%

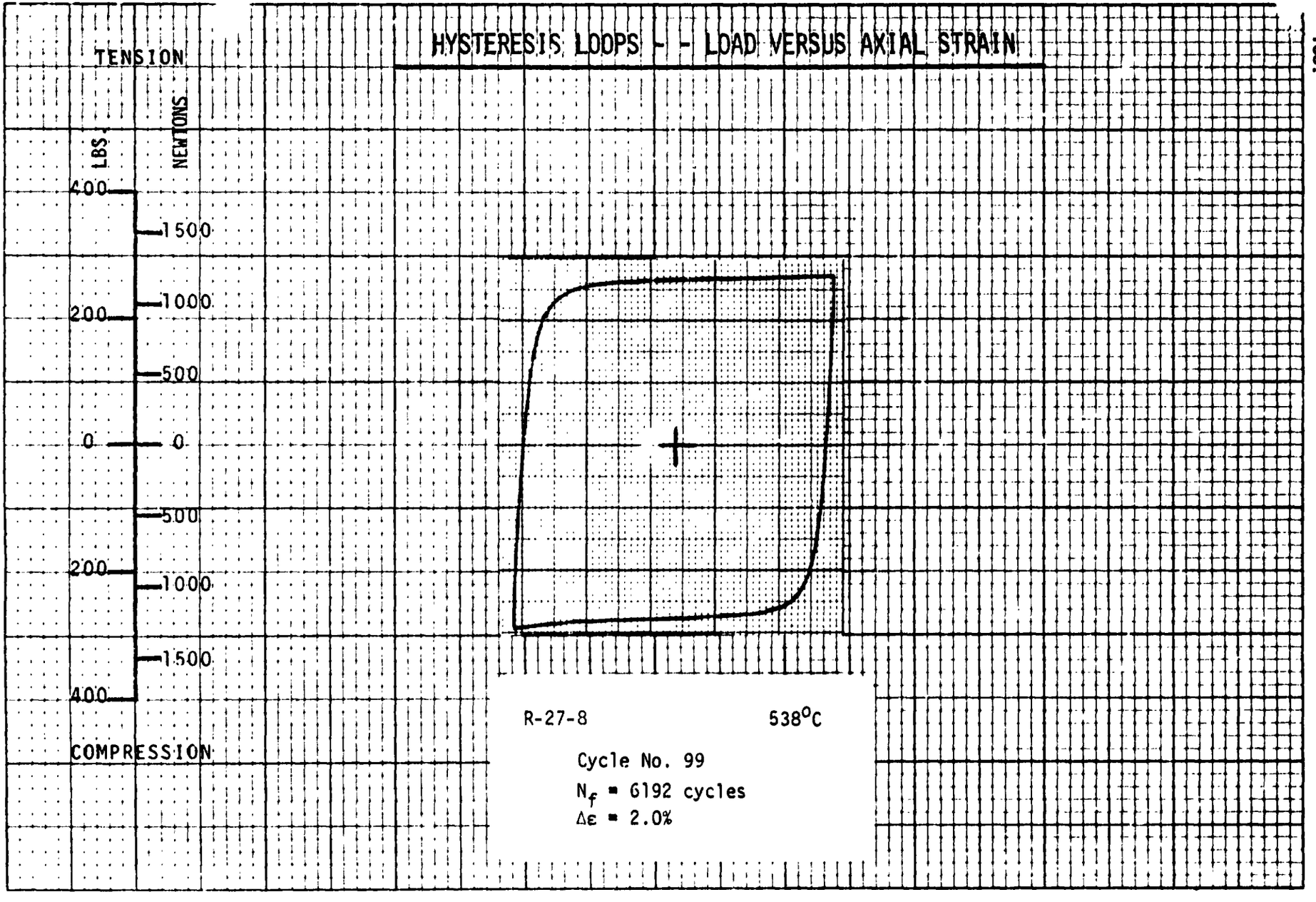
HYSTERESIS LOOPS - - LOAD VERSUS AXIAL STRAIN
TENSION
LBS.
NEWTONS
400
1500
200
1000
500
0
0
500
200
1000
1500
400
COMPRESSION
R-27-8
538°C
Cycle No. 99
N_f = 6192 cycles
$\Delta\varepsilon$ = 2.0%

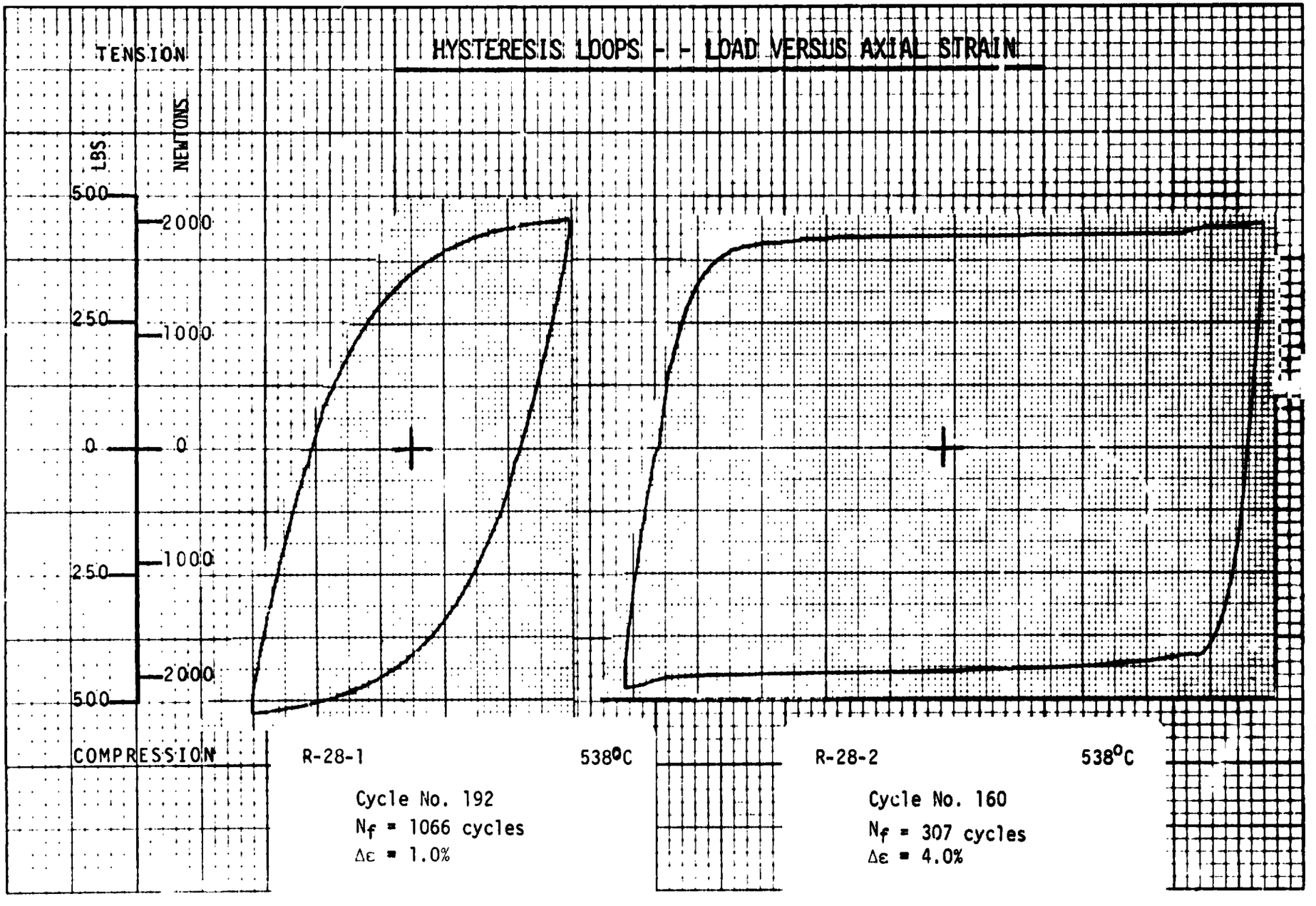
HYSTERESIS LOOPS - - LOAD VERSUS AXIAL STRAIN
TENSION
LBS
NEWTONS
500
2000
250
1000
0
0
250
1000
2000
500
COMPRESSION
R-28-1
538°C
Cycle No. 192
N_f = 1066 cycles
$\Delta\varepsilon$ = 1.0%
R-28-2
538°C
Cycle No. 160
N_f = 307 cycles
$\Delta\varepsilon$ = 4.0%

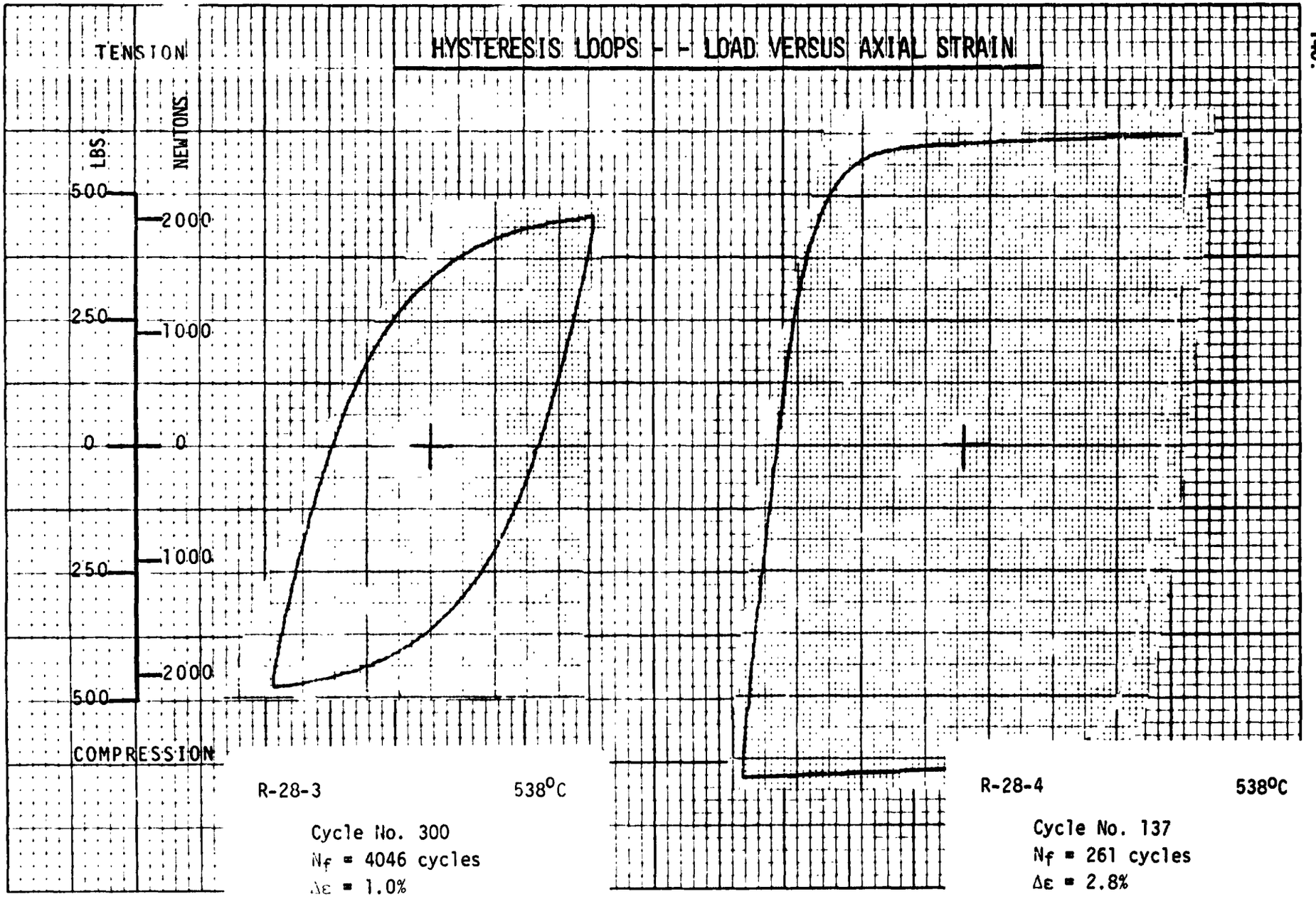
HYSTERESIS LOOPS - - LOAD VERSUS AXIAL STRAIN
TENSION
LBS
NEWTONS
500
2000
250
1000
0
0
250
1000
2000
500
COMPRESSION
R-28-3
538°C
Cycle No. 300
N_f = 4046 cycles
$\Delta\varepsilon$ = 1.0%
R-28-4
538°C
Cycle No. 137
N_f = 261 cycles
$\Delta\varepsilon$ = 2.8%

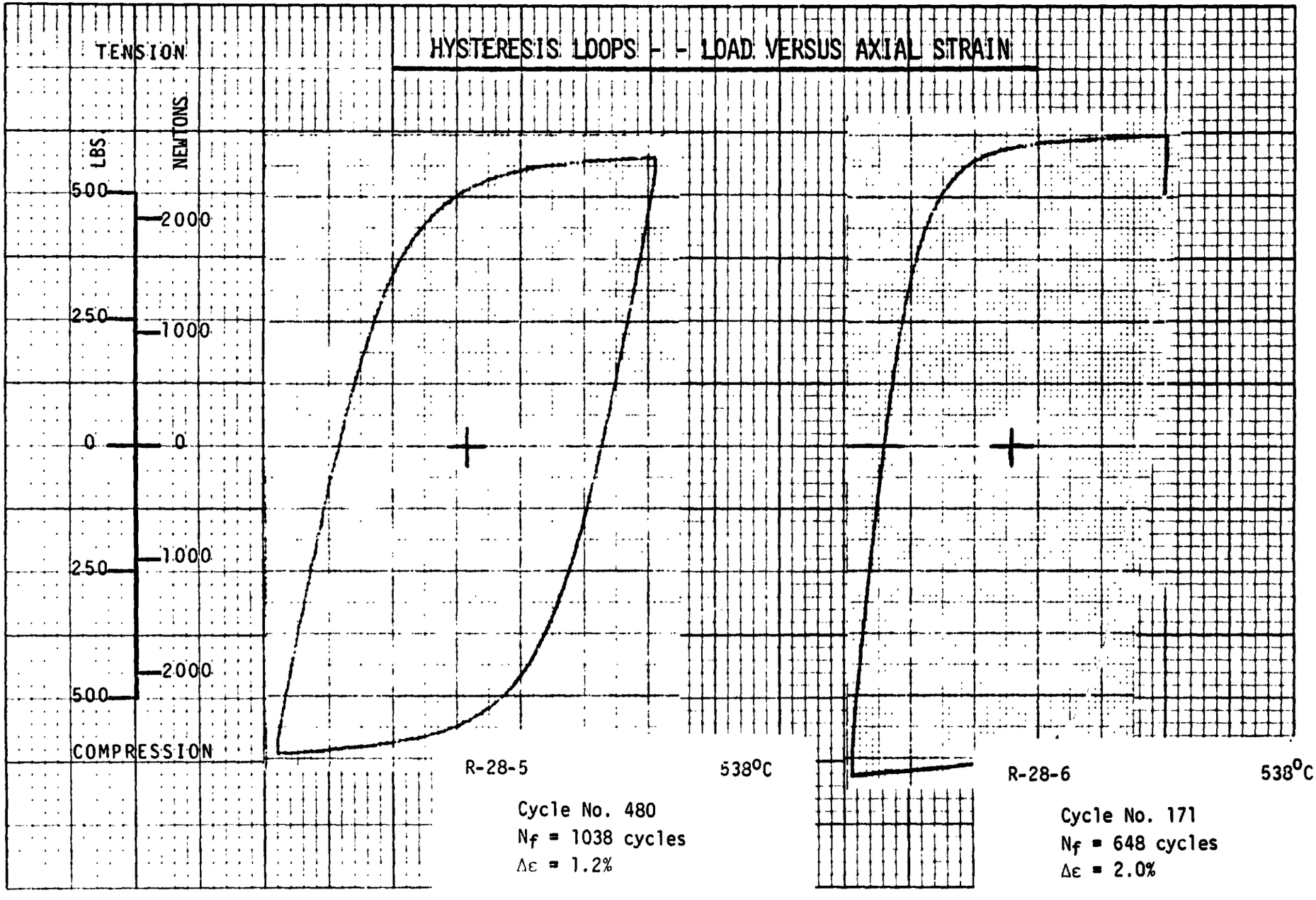
HYSTERESIS LOOPS - - LOAD VERSUS AXIAL STRAIN
TENSION
LBS
NEWTONS
500
2000
250
1000
0
0
250
1000
2000
500
COMPRESSION
R-28-5
538°C
Cycle No. 480
N_f = 1038 cycles
$\Delta\varepsilon$ = 1.2%
R-28-6
538°C
Cycle No. 171
N_f = 648 cycles
$\Delta\varepsilon$ = 2.0%

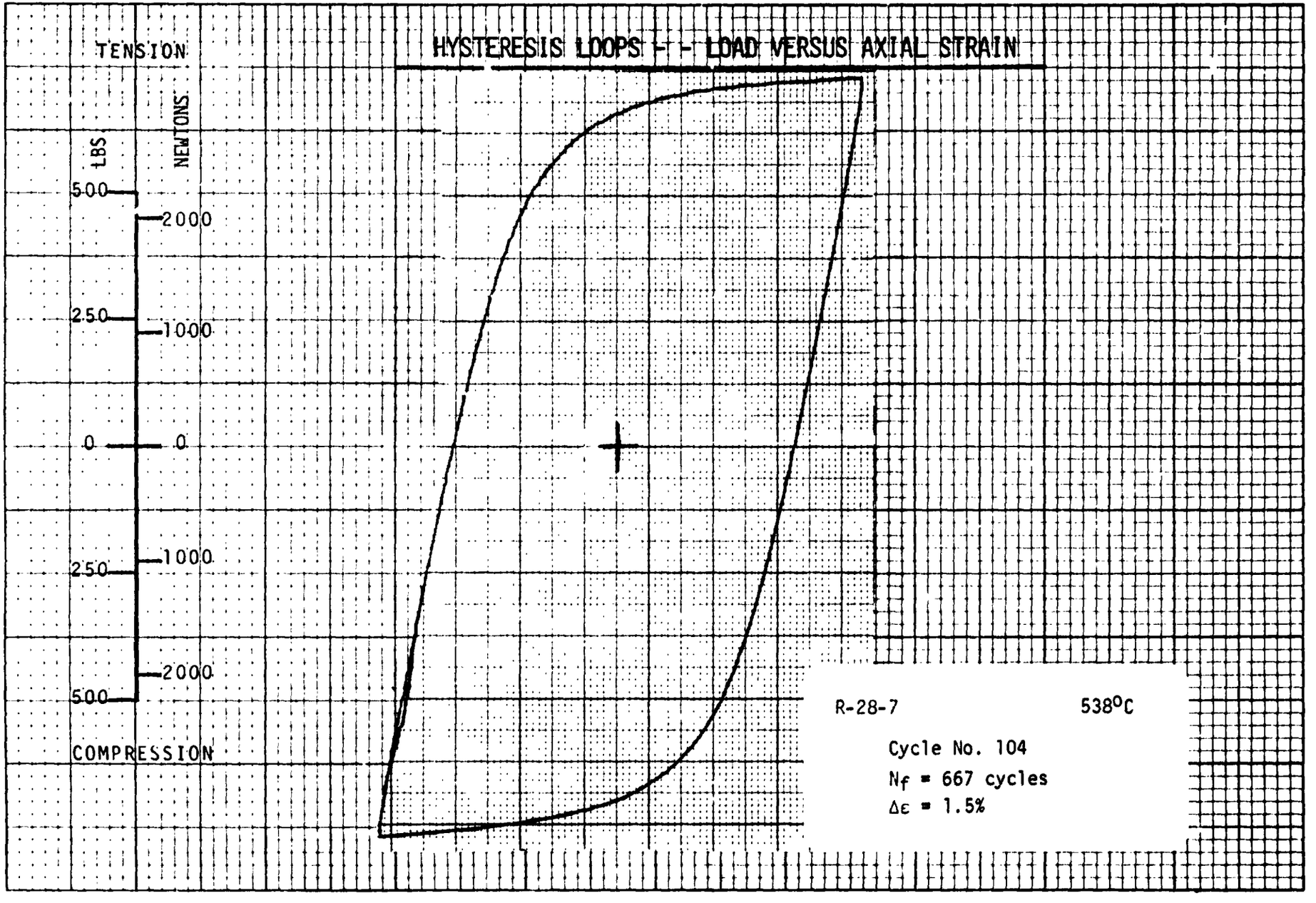
HYSTERESIS LOOPS -- LOAD VERSUS AXIAL STRAIN
TENSION
LBS
NEWTONS
500
2000
250
1000
0
0
250
1000
2000
500
COMPRESSION
R-28-7
538°C
Cycle No. 104
N_f = 667 cycles
$\Delta\varepsilon$ = 1.5%

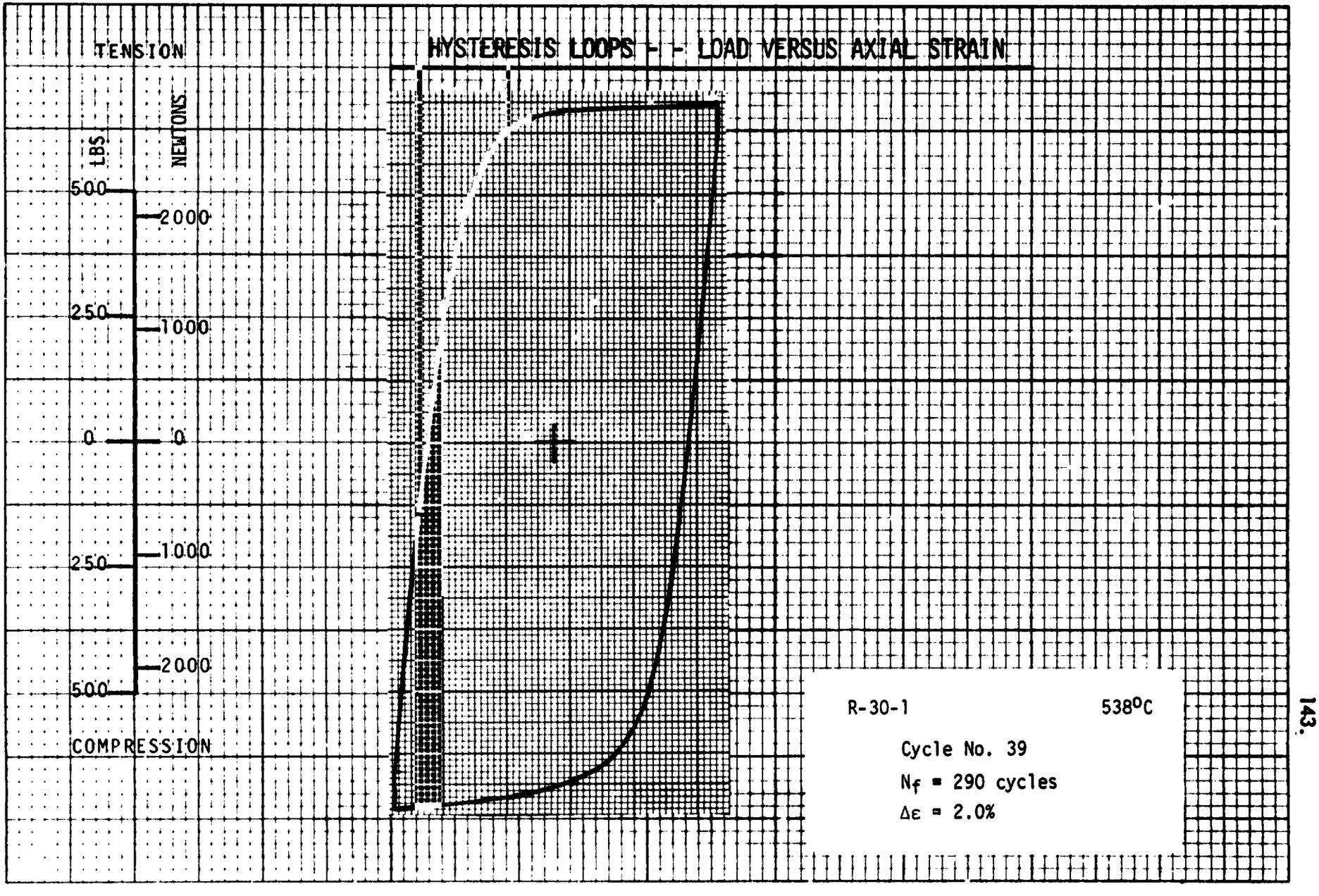
HYSTERESIS LOOPS - - LOAD VERSUS AXIAL STRAIN
TENSION
LBS
NEWTONS
500
2000
250
1000
0
0
250
1000
2000
500
COMPRESSION
R-30-1
538°C
Cycle No. 39
N_f = 290 cycles
$\Delta\varepsilon$ = 2.0%

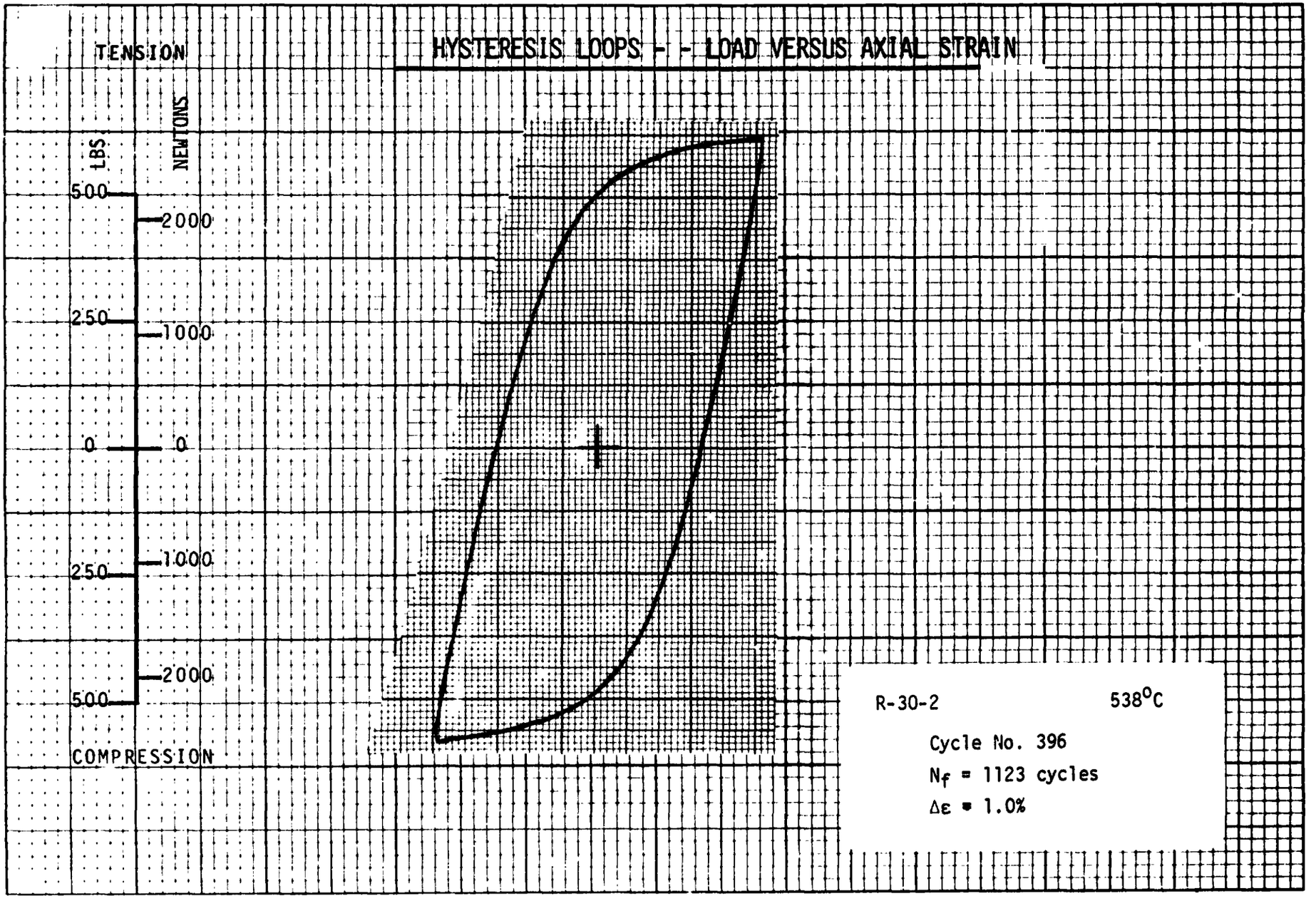
HYSTERESIS LOOPS - - LOAD VERSUS AXIAL STRAIN
TENSION
LBS
NEWTONS
500
2000
250
1000
0
0
250
1000
2000
500
COMPRESSION
R-30-2
538°C
Cycle No. 396
N_f = 1123 cycles
$\Delta\varepsilon$ = 1.0%

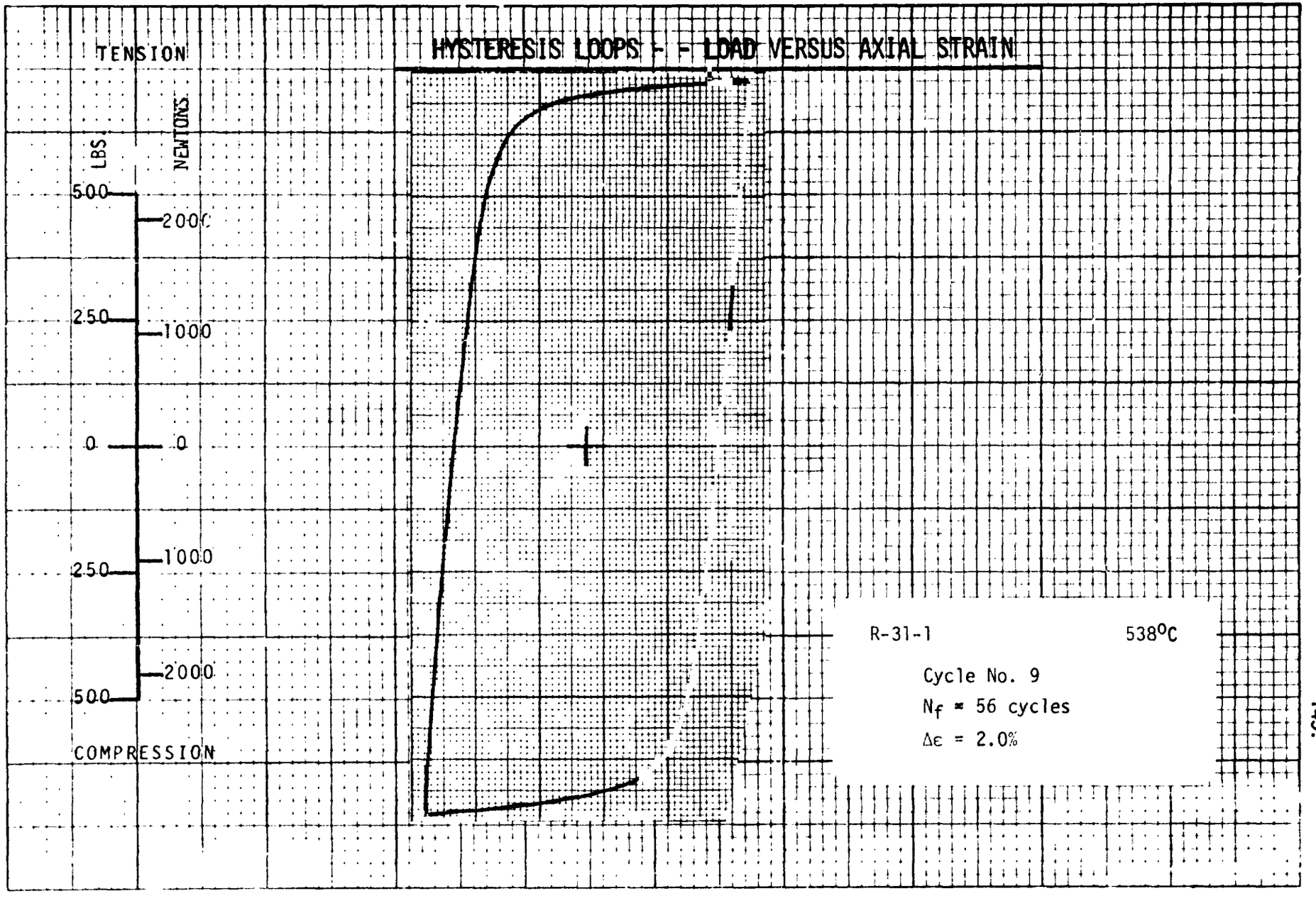
HYSTERESIS LOOPS - - LOAD VERSUS AXIAL STRAIN
TENSION
LBS.
NEWTONS
500
2000
250
1000
0
0
250
1000
2000
500
COMPRESSION
R-31-1
538°C
Cycle No. 9
N_f = 56 cycles
$\Delta\varepsilon$ = 2.0%

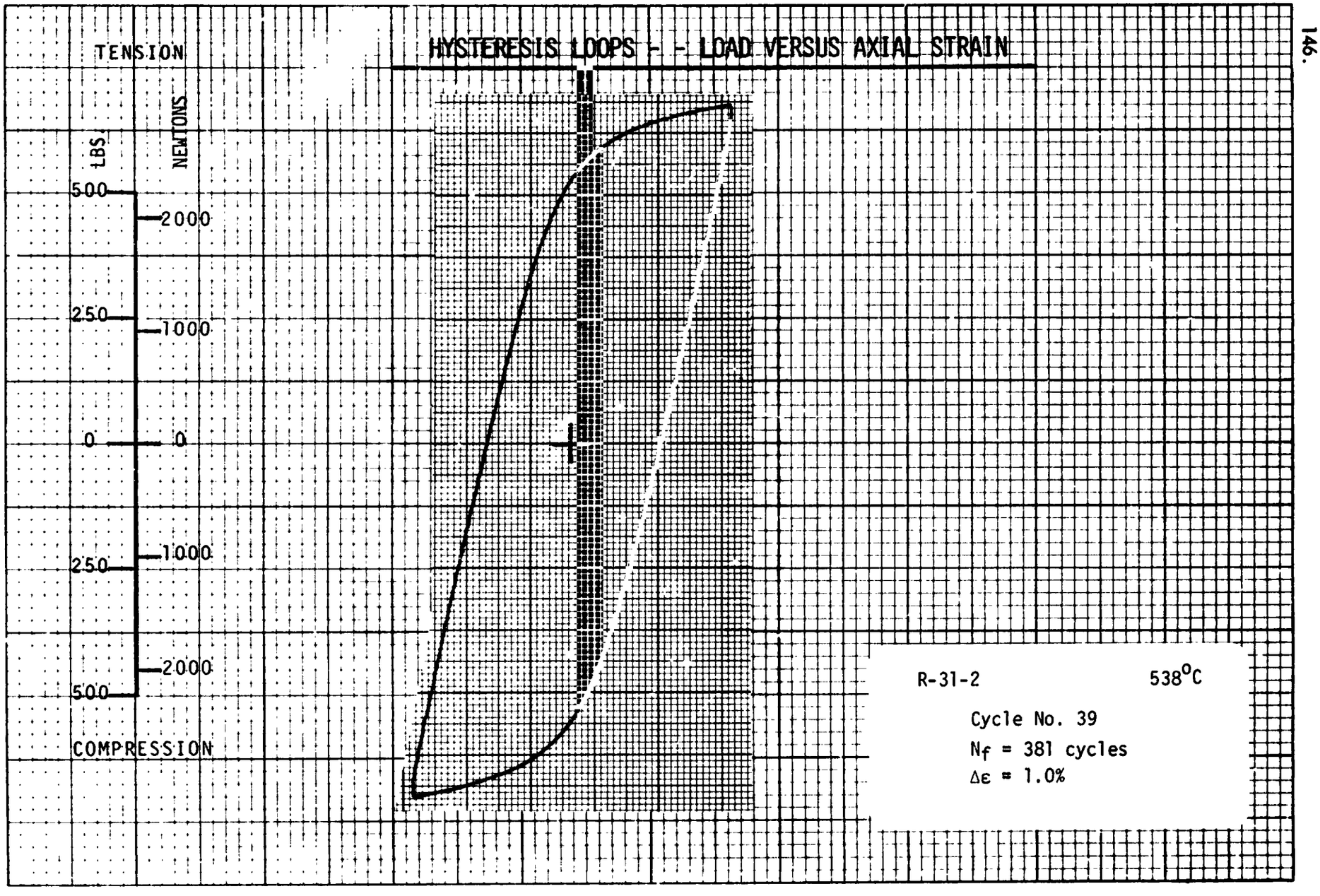
HYSTERESIS LOOPS - - LOAD VERSUS AXIAL STRAIN
TENSION
LBS.
NEWTONS
500
2000
250
1000
0
0
250
1000
2000
500
COMPRESSION
R-31-2
538°C
Cycle No. 39
N_f = 381 cycles
$\Delta\varepsilon$ = 1.0%

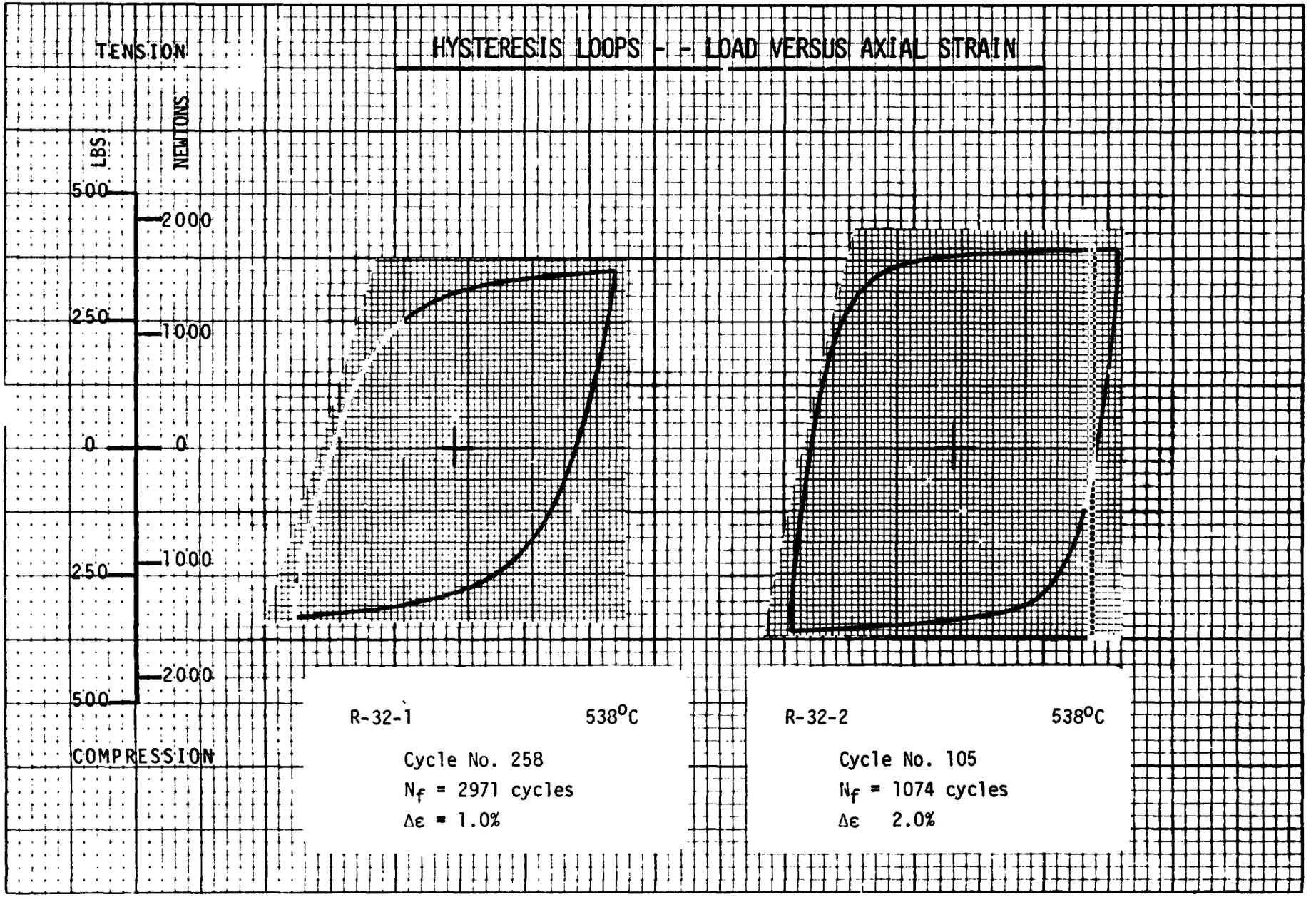
HYSTERESIS LOOPS - - LOAD VERSUS AXIAL STRAIN
TENSION
LBS
NEWTONS
500
2000
250
1000
0
0
250
1000
2000
500
COMPRESSION
R-32-1
538°C
Cycle No. 258
N_f = 2971 cycles
$\Delta\varepsilon$ = 1.0%
R-32-2
538°C
Cycle No. 105
N_f = 1074 cycles
$\Delta\varepsilon$ 2.0%

PART VII - VALUES OF N_5 AND N_f FOR LOW-CYCLE FATIGUE TESTS OF SECTION IV (all tests in argon at 538°C)

For each test, values of N_5, the cycles to a five percent load range drop, and N_f, cycles to complete specimen separation, are compared. Some interpretation of N_5 had to be made in those instances where cyclic softening was exhibited. In these situations the plot of load range versus cycles on semi-logarithmic coordinates indicated a gradual decrease in the load range as cycling progressed and it was not possible to identify a stabilized load range for calculating a five percent reduction. The special interpretation adopted for these cases involved the selection of that point on the load range plot where a change in curvature first began to appear as the load range began to decrease rapidly as failure approached. A five percent drop from this load range value was then used to establish the value for N_5. In a few cases no value of N_5 is reported due either to the fact that the specimen failed before a five percent load range reduction was reached or,because of the orientation of the crack with respect to the extensometer tips, the load range actually increased slightly near the failure point.

Values of N_5 and N_f for all Tests

(N_5 is the number of cycles to a five percent load range drop and N_f is the number of cycles to complete separation of the specimen)

Specimen Number	Total Strain Range, %	Strain Rate, sec^{-1}	N_5 cycles	N_f cycles
		AMZIRC Copper, ½ Hard		
R-2-107	1.7	$2x10^{-3}$	5400	5780
R-2-108	3.0	$2x10^{-3}$	1200	1310
R-2-111	2.6	$1x10^{-2}/4x10^{-4}$	-	1314
R-2-112	1.4	$1x10^{-2}/4x10^{-4}$	-	3239
R-2-109	2.6	$4x10^{-4}/1x10^{-2}$	340	387
R-2-110	1.4	$4x10^{-4}/1x10^{-2}$	900	1006
		NARloy Z		
R-24-101	1.0	$2x10^{-3}$	1700	1948
R-24-102	2.0	$2x10^{-3}$	450	535
R-24-105	1.0	$1x10^{-2}$	4500	5022
R-24-47	0.7	$1x10^{-2}$	12000	14194
R-24-105	2.0	$1x10^{-2}$	600	673
R-24-35	3.0	$1x10^{-2}$	160	165
R-24-104	1.0	$4x10^{-4}$	900	1266
R-24-106	2.0	$4x10^{-4}$	320	351
R-24-112	3.0	$4x10^{-4}$	130	154
R-24-117	0.9	$4x10^{-5}$	740	787
R-24-118	2.6	$4x10^{-5}$	100	116
R-24-108	1.0	$1x10^{-2}/4x10^{-4}$	1500	2091
R-24-110	2.0	$1x10^{-2}/4x10^{-4}$	200	451
R-24-107	1.0	$4x10^{-4}/1x10^{-2}$	220	238
R-24-109	2.0	$4x10^{-4}/1x10^{-2}$	60	66
R-24-111	3.0	$4x10^{-4}/1x10^{-2}$	30	35
R-24-113	0.5	$4x10^{-4}/1x10^{-2}$	1000	1156
R-24-115	0.5	$4x10^{-5}/1x10^{-2}$	260	300
R-24-114	3.0	$4x10^{-5}/1x10^{-2}$	15	16
R-24-116	0.5	$7x10^{-6}/1x10^{-2}$	105	115
		Zr-Cr-Mg Copper		
R-9-101	0.80	30 cpm	11500	12543
R-9-102	0.72	30 cpm	18000	18746
R-9-103	0.50	30 cpm	82000	83751
R-9-104	0.60	30 cpm	45000	50010
R-9-106	0.50	30 cpm	100000	101210
R-9-107	0.40	30 cpm	-	141447
R-9-108	0.30	30 cpm	360000	382769

Values of N_5 and N_f for all Tests - continued

Specimen Number	Total Strain Range, %	Strain Rate, sec^{-1}	N_5 cycles	N_f cycles
		Experimental Copper Alloy		
R-27-1	1.0	$2x10^{-3}$	600	6107
R-27-2	3.86	↓	15	361
R-27-3	1.2	↓	300	1834
R-27-4	2.8	↓	80	608
R-27-5	1.5	↓	400	1904
R-27-6	2.0	↓	100	577
R-27-7	1.2	↓	80	5155
R-27-8	2.0	↓	200	6192
		Experimental Silver Alloy		
R-28-1	1.0	$2x10^{-3}$	-	1066
R-28-2	4.0	↓	250	307
R-28-3	1.0	↓	2400	4046
R-28-4	2.8	↓	240	261
R-28-5	1.2	↓	-	1038
R-28-6	2.0	↓	360	648
R-28-7	1.5	↓	520	667
R-30-1	2.0	↓	280	290
R-30-2	1.0	↓	1050	1123
R-31-1	2.0	↓	48	56
R-31-2	1.0	↓	300	381
R-32-1	1.0	↓	2500	2971
R-32-2	2.0	↓	600	1074

V - CONCLUSIONS

Low-cycle fatigue tests of ½ Hard ANZIRC Copper and NARloy Z were performed in argon at 538°C to generate the type of data required in the determination of partitioned strainrange versus life relationships. It was found that both of these materials exhibited very high creep rates at the conditions imposed so that it was not possible to employ strain rates high enough to completely eliminate the creep component in the type of strain cycling employed. For this reason an indirect approach to the identification of the PP and CC components of inelastic strain was adopted. Fatigue life data at various strain rates were analyzed and an evaluation of the saturation fatigue life in both the high and low strain rate regimes led to the desired PP and CC information. This evaluation enabled the PP and CC lines to be positioned and then special fatigue tests involving slow-fast and fast-slow cycling were employed to yield CP and PC information to enable these partitioned strainrange lines to be defined.

Dimensional instability (barrelling) was observed in the tests of the R-2 alloy and for this reason the partitioned strainrange versus life relationships for this material should be viewed as tentative and some slight repositioning might be necessary as more data become available. These plots are, however, of immediate use in approximating fatigue results. For example, estimates of hold-time behavior have been obtained that are in reasonable agreement with experimental observations.

Slow-fast ($4x10^{-4}/1x10^{-2}$ sec^{-1}) cycling of the R-24 material at 538°C was found to be much more detrimental than fast-slow cycling. It was also noted that continued reduction in the fatigue life was obtained as the slow strain rate in the slow-fast cycling was reduced from $4x10^{-4}$ sec^{-1} to $4x10^{-5}$ sec^{-1} and then to $7x10^{-6}$ sec^{-1}. Partitioned strainrange versus life relationships for the R-24 alloy were shown to give excellent estimates of the slow-fast cycling fatigue life.

An interesting correlation was identified for the R-24 data obtained in the slow-fast and fast-slow tests. A linear relationship was obtained in a logarithmic plot of the tensile stress component versus the total tension-going time ($N_f \, \Delta\varepsilon/\dot{\varepsilon}_t$). The line defined by the fast-slow and slow-fast data was also shown to provide an excellent representation of continuous cycling fatigue data for strain rates from $1x10^{-2}$ sec^{-1} to $4x10^{-5}$ sec^{-1}. In addition, the previously reported hold-time data were in accord with this relation when the average tensile stress was used for the hold period.

Strain controlled fatigue data for Zr-Cr-Mg Copper alloy (R-9) were obtained in argon at 538°C using a frequency of 30 cpm and strain ranges from 0.80% to 0.30%. These results provide a smooth extension of the fatigue curve reported previously for this material in the strain range regime from 0.9% to 3.0%. This study has extended the fatigue curve for this material to about 400,000 cycles.

An experimental copper alloy (electroformed copper), R-27, and an experimental silver alloy (pure silver containing 0.5% zirconium), R-28, were evaluated in short-term tensile and low-cycle fatigue tests. These studies showed that at 538°C the yield and ultimate strengths of the R-27 alloy were comparable to those of a previously reported electroformed copper (R-10) but the ductility of the R-27 alloy was much higher than that of the R-10 composition. Fatigue values for the two alloys (R-27 and R-10) were comparable

with slightly higher fatigue resistance being exhibited by the R-27 material. For the R-28 alloy the high temperature yield and ultimate strengths were significantly higher than those reported previously for pure silver (R-8 alloy). The ductility of the R-28 composition at 538°C was about one-half of that exhibited by pure silver and the fatigue life for R-28 was just slightly below that previously reported for R-8.

The effect of three different heat treatments on the tensile and fatigue properties of R-28 was investigated. A 1-hour solution anneal of R-28 at 899°C followed by a water quench led to a sizeable reduction in ductility without having a significant effect on the yield and ultimate strengths. The fatigue life was noticeably reduced below the R-28 values. A 2-hour aging treatment of R-28 at 593°C led to a substantial reduction in the yield and ultimate strengths at 538°C, an increase in high temperature ductility but essentially no change in the fatigue life.

VI - REFERENCES

1. Hirschberg, M.H. and Halford, G.R.: Use of Strainrange Partitioning to Predict High-Temperature Low-Cycle Fatigue Life. NASA TN D-8072, 1976.

2. Manson, S.S.: The Challenge to Unify Treatment of High Temperature Fatigue - A Partisan Proposal Based on Strainrange Partitioning. STP 520, ASTM, 1973. pp. 744-755.

3. Conway, J.B., Berling, J.T. and Stentz, R.H.: Strain Rate and Holdtime Saturation in Low-Cycle Fatigue: Design Parameter Plots. STP 520, ASTM, 1973. pp. 637-647.

4. Manson, S.S., Halford, G.R. and Nachtigall, A.J.: Separation of the Strain Components for Use in Strainrange Partitioning. Advances in Design for Elevated Temperature Environment, ASME, 1975. pp. 17-28.